Doctoral School in Environmental Engineering

Two-phase modelling of debris flow over composite topography: theoretical and numerical aspects

Daniel Zugliani

UNIVERSITÀ DEGLI STUDI DI TRENTO
Dipartimento di Ingegneria Civile e Ambientale

2015

Doctoral thesis in **Environmental Engineering,** 27^{th} **cycle**
Department of Civil, Environmental and Mechanical Engineering,
University of Trento
Academic year 2013/2014
Supervisor: **Prof. Giorgio Rosatti, DICAM, University of Trento**

University of Trento
Trento, Italy
28^{th} April, 2015

Acknowledgments

First and foremost, I offer my gratitude to my supervisor, Prof. Giorgio Rosatti, who has supported me with his knowledge and patience. In addition, I thank Nadia Zorzi for her help in the writing process and Giulia Graregnani for her support during the enrollment and the first year of my PhD.

Particular thanks and gratitude go to my parents and friends for their support during all these years.

Contents

List of Figures

List of Tables

Summary

In the mountain territory the majority of the population and of the productive activities are concentrated in the proximity of torrents or over alluvial fans. Here, when intense rainfall occurs, debris flow or hyper-concentrated flow events can produce serious problems to the population with possible casualties. On the other hand, the majority of these problems could be overcome with accurate hazard mapping, disaster prevention planning and mitigation structures (e.g. silt check dams, paved channels, weirs ...). Good and reliable mathematical and numerical models, able to accurately describe these phenomena are therefore necessary.
Debris flows and hyper-concentrated flows can be adequately represented by means of a mixture of a fluid (usually water) and a solid phase (granular sediment, e.g. sand, gravel ...), flowing over complex and composite topography. Complex topography is related to complicated bed elevation variety inasmuch as there are slopes, channels, human artifacts and so on. On the other hand, topography is composite because every type of flow can encounter two different bed behaviors: the mobile bed and the fixed bed. In the first case, mass can be exchanged between the bed and the flow, so the bottom elevation can change in time. In the second case (fixed bed case), this mass transfer is inhibited, due to the presence of a rigid bottom, such as bedrock or concrete, and the bottom cannot change in time. The first objective of the work presented in this thesis concerns the development of a new type of hyperbolic mathematical model for free-surface two-phase hyper-concentrated flows able to describe in a single way the fixed bed, the mobile bed and also the transition between them. The second objective, strictly connected with the first, is the development of a numerical scheme that implements this mathematical model in an accurate and efficient way.

In the framework of finite-volume methods with Godunov approach, the fluxes are evaluated solving a Riemann Problem (RP). A RP is an initial value problem related to a set of PDEs equations wherein, in a certain point, there is a discontinuity separating different left and right initial constant states. However, if the topography is composite, a new type of Riemann problem, called Composite Riemann Problem (CRP), occurs. In a CRP, not only the initial constant states, but also the relevant PDEs systems change across the discontinuity. This additional complexity makes the general solution of the CRP quite challenging to obtain.

The first part of the work is devoted to the derivation of the PDEs systems describing the fixed- and mobile-bed behaviors. Starting from the 3D discrete equations valid for each phase (continuous fluid and solid granular) and using suitable average processes the 3D continuous equations (continuous fluid and solid) are obtained. Introducing the shallow water approximation and performing the depth average process, the 2D fully two-phase models for free-surface flow over fixed- and mobile-bed are derived. The isokinetic approximation, which states the equality between the velocity of the solid phase and the liquid phase, is then used, ending up with the so-called two-phase isokinetic models. Finally, an exhaustive comparison between the fixed- and the mobile-bed fully two-phase models, the two-phase isokinetic models and others models proposed in the literature is presented.

The second part of the work concerns the definition and, mainly, the solution of the CRP from a mathematical point of view. Firstly, a general strategy for the CRP solution is developed. It allows to couple different hyperbolic systems that are physically compatible (e.g. fixed-bed with mobile-bed systems, free-surface flow with pressurized flow), also if they have a different number of equations. The resulting CRP solution is composed of a single PDEs system, called Composite PDEs system, whose properties, under some assumptions, degenerate to the properties of the original PDEs systems. The general strategy is developed using the simplest 1D isokinetic models for the fixed bed and the mobile bed (i.e. PDEs systems valid only for low concentration). Coherently with the generality of the CRP solution method, the low concentration constraint is then relaxed, ending up with a Composite PDEs system describing also high concentrated flows.

From the numerical point of view, all the developed Composite systems are integrated using the finite-volume method with Godunov fluxes. These fluxes are evaluated using three different approximated Riemann solvers: the Generalized Roe solver, the LHLL solver and the Universal Osher solver. All the solvers are analyzed and an exhaustive comparison between them is performed, highlighting pros and cons. The schemes are second order accurate in space and time, and this has been achieved by means of the MUSCL approach. Finally numerical schemes have been parallelized using OpenMP standard.

All the models are then tested comparing analytical and numerical solutions. The results are satisfactory, with an accurate agreement between the two solutions in the majority of the physically-based test cases. There is only some small issue when the simulations are performed in a few resonant cases. However, these problems arise in not realistic situations, so it is impossible to encounter them in real situations. Also a realistic application is presented (i.e. the evolution of a trench over partially paved channel), proving the capabilities of both the mathematical approach and the numerical scheme.

Part I

Derivation and eigenstructure analysis of the two-phase flow equations over fixed and mobile bed

Chapter 1

Continuum formulations for liquid-granular mixture flows

From a physical point of view, a liquid-granular flow is a gravity-driven movement of a mixture composed by a granular phase, usually sand or gravel, and by a fluid phase surrounding the solid one. The problem can be faced with the use of an appropriate set of three-dimensional partial differential equations that describe the interstitial fluid and an equation of motion for the center of mass each single particle. The variables related to a specific phase of the mixture are therefore defined *only* in the space actually occupied by the phase itself. However, this approach has a practical problem: when we approach real scale phenomena, the number of equations needed to describe all the particles in a debris flow or hyperconcentrated flow becomes larger and larger producing an unmanageable system. A possible solution is switching to a continuum description of the liquid-granular mixture. With this type of formulation, unlike before, a generic variable related to one phase (both fluid and solid) is defined in *every* point of the mixture flow domain, even where a phase does not actually occupy the space. The definition of such variables is possible only by means of appropriated average.
This approach was used in the works of Zhang and Prosperetti [67, 68] where the authors use a statistical ensemble average, and the works of Anderson and Jackson [5] and Jackson [35, 36] where a volume average is used.
Another possible approach is use, as starting point, a continuum descrip-

tion of both the fluid and the solid constituent. Although, as said before, a mixture is the sum of fluid and solid components, the continuum description of this mixture is not obtained simply adding together the equations for the fluid and solid phases described as continuum, but an indicator function must be introduced in order to recognize which phase occupy a certain point of the space. The introduction of the indicator function leads to a discrete definition of the variables, so an appropriate average process (e.g. ensemble or volume) has to be used in order to obtain a continuum formulations for the liquid-granular mixture. Among this class of derivation we cite the works of Drew [21], Hill [32] and Joseph and Lundgren [38].

In this Chapter we analyze the approaches presented in the literature in order to have a clear understand of the terms involved in the three dimensional differential equations that describe the liquid-granular mixture flows. Moreover a unified approach has been presented, since, different approaches produce slightly different partial differential equations. In particular, we focus our attention on first approach in Section 1.1 where the ensemble average is presented, and in Section 1.2 where the volume average is described. The second approach is briefly introduced in Section 1.3, while in Section 1.4 a comparison between the different approaches is presented with the definition of an unified model. Finally, in Section 1.5 some aspects related to the closure of the problem are introduced.

1.1 Ensemble average for continuous fluid phase and discrete particles

Given a set of measurements regarding a debris flow or an hyperconcentrated flow with certain macroscopic conditions (e.g. flow depth, fluid and solid discharge), the microscopic characteristics, measured during each realization, are different from one to each other. As for the turbulence, the study of the pointwise properties for this type of flow is based on the use of the ensemble average.

The ensemble averaging process for the motion equations of a liquid-granular mixture was derived by Zhang and Prosperetti [67, 68]. The authors

use, as starting point, the equation of motion of a set of spherical particles of radius r surrounded by an inviscid [67] or a viscous fluid [68]. In the follow only the main aspect of the derivation are presented, while we refer to the original article for the complete derivation.

1.1.1 Definitions

A configuration C^N of a mixture flow is defined by a number N of spherical particles of radius r, with instantaneous position $\mathbf{y}^\alpha$ and velocity $\mathbf{w}^\alpha$ (with $\alpha = 1 \dots N$), and a fluid which surrounds the particles (see Figure 1.1 for an overview of a configuration C^N). It is possible to define the indicator

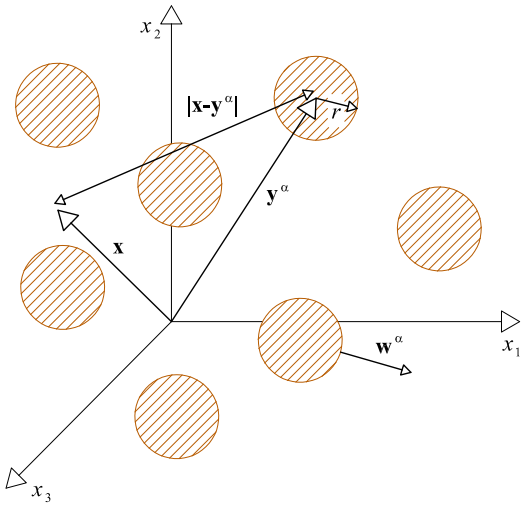

Figure 1.1: Sketch of the configuration C^N with the reference system.

function for the fluid phase associated to the configuration C^N as

$$\chi_F(\mathbf{x}; C^N) = \begin{cases} 1 & \text{if } \mathbf{x} \text{ is in the fluid phase} \\ 0 & \text{otherwise} \end{cases} \tag{1.1}$$

while the indicator function for the solid phase, due to impenetrability of the two phases, is

$$\chi_S(\mathbf{x}; C^N) = 1 - \chi_F(\mathbf{x}; C^N) \tag{1.2}$$

Introducing the Heaviside step function defined as

$$H(x) = \begin{cases} 0 & \text{if } x < 0 \\ 1 & \text{if } x \geq 0 \end{cases} \tag{1.3}$$

the indicator function for the solid phase can be written as

$$\chi_S(\mathbf{x}; C^N) = \sum_{\alpha=1}^{N} H\left(r - |\mathbf{x} - \mathbf{y}^\alpha|\right) \tag{1.4}$$

where $(r - |\mathbf{x} - \mathbf{y}^\alpha|)$ is positive only when the point $\mathbf{x}$ is inside the particle α located at $\mathbf{y}^\alpha$.

Using this indicator function it is possible to define the volume fractions (also know as volumetric concentration) for the solid phase as

$$c(\mathbf{x}, t) = \frac{1}{N!} \int \chi_S(\mathbf{x}; C^N) P(C^N; t)\ dC^N \tag{1.5}$$

where $P(C^N; t)$ is the probability density function associated to the configuration C^N and normalized as

$$\int P\left(C^N; t\right)\ dC^N = N!$$

where the integral is performed all over the configurations. It is also possible to define the reduced one-particle density function as

$$P\left(\mathbf{y}, \mathbf{w}; t\right) = P\left(1; t\right) = \frac{1}{(N-1)!} \int P\left(C^N; t\right)\ dC^{N-1} \tag{1.6}$$

where the integral is performed all over the possible degrees of freedom of the system except for the ones associated to particle 1.
With this definition and remembering the definition of the solid indicator function, the solid concentration can be defined as

$$c(\mathbf{x}, t) = \int_{|\mathbf{x}-\mathbf{y}| \leq r} \int P(\mathbf{y}, \mathbf{w}; t)\ d^3w\ d^3y \tag{1.7}$$

where now the integral is performed only over the space (d^3y) and velocity (d^3w) associated to the particles. For the fluid phase, instead, the volume concentration is defined as

$$\beta(\mathbf{x}, t) = \frac{1}{N!} \int \chi_F(\mathbf{x}; C^N) P(C^N; t)\ dC^N$$

Since the sum of the indicator function is one, the two concentration are correlated by

$$\beta = 1 - c \tag{1.8}$$

The ensemble average of a generic local quantity $f_F(\mathbf{x}, t; C^N)$ related to the fluid phase, at position $\mathbf{x}$, time t, given the configuration C^N, is defined as

$$\langle f_F \rangle (\mathbf{x}, t) = \frac{1}{N!} \frac{1}{\beta} \int f_F(\mathbf{x}, t; C^N) \chi_F(\mathbf{x}; C^N) P(C^N; t) \, dC^N \tag{1.9}$$

This definition has the advantage that is defined in *every* point of the mixture domain, but it has the disadvantage that the integral and the derivative is not commutative due to the discontinuity of the indicator function $\chi_F(\mathbf{x}; C^N)$.

Performing some algebraic manipulations, it is possible to evaluate the ensemble average of the time and spatial derivative of $f_F(\mathbf{x}, t)$ (we refer to the original articles for the full mathematical manipulation needed) obtaining

$$\left\langle \frac{\partial}{\partial t} f_F \right\rangle = \frac{1}{\beta} \left(\frac{\partial}{\partial t} \beta \langle f_F \rangle + \oint_s \int \mathbf{w} \cdot \hat{\mathbf{n}} \langle f_F \rangle_1 P(1; t) \, d^3 w \, dS_y \right) \tag{1.10}$$

$$\left\langle \frac{\partial}{\partial x_i} f_F \right\rangle = \frac{1}{\beta} \left(\frac{\partial}{\partial x_i} \beta \langle f_F \rangle - \oint_s \int \hat{\mathbf{n}} \langle f_F \rangle_1 P(1; t) \, d^3 w \, dS_y \right) \tag{1.11}$$

where $\hat{\mathbf{n}}$ is the normal unit vector oriented outward from the particle, S_y is the surface of the particle and $\langle f_F \rangle_1$ is the ensemble average of the function f_F where the position and velocity of one particle is a priori defined. These two equations will be fundamental when, in the next Sections, we apply the ensemble average process to the motion equations for the fluid phase.

For a quantity associated to the solid particles as a whole (like center of mass velocity, momentum, ...) it is more useful to introduce a different indicator function describing the particle as a point

$$\chi_S(\mathbf{x}; C^N) = \upsilon \sum_{\alpha=1}^{N} \delta \left(\mathbf{x} - \mathbf{y}^\alpha \right) \tag{1.12}$$

where υ is the constant volume of one particle and δ is the Dirac delta function defined as

$$\delta(x) = \frac{\partial H(x)}{\partial x} = \begin{cases} 0 & \text{if} \quad x \neq 0 \\ \infty & \text{if} \quad x = 0 \end{cases} \tag{1.13}$$

Given $f_S^{(\alpha)}(t; C^N)$, a quantity pertaining to the particle α as a whole in the configuration C^N at time t, its ensemble average, over all configurations

in which one particle is located in the point $\mathbf{x}$, is

$$\langle f_S(\mathbf{x},t)\rangle = \frac{1}{n(\mathbf{x},t)} \int f_S^{(1)}\,(t;1)\,P(1,t)\;d^3w \tag{1.14}$$

where n is the particle number density

$$\begin{aligned} n(\mathbf{x},t) &= \int P(1;t)\;d^3w \\ &= \int P(\mathbf{x},\mathbf{w};t)\;d^3w \end{aligned} \tag{1.15}$$

Expanding equation (1.7) in Taylor series around $\mathbf{x}$ (this is possible since the averaged quantity changes slowly at the scale of particle) and using equation (1.15), a more common definition of the solid concentration is obtained

$$\begin{aligned} c(\mathbf{x},t) &= \upsilon n(\mathbf{x},t) + O\left(\frac{r^2}{L^2}\right) \\ &\simeq \upsilon n(\mathbf{x},t) \end{aligned} \tag{1.16}$$

where L is a characteristic length scale of the flow field variation.

The ensemble average of total time derivative of the property $f_S(\mathbf{x},t)$, associated to the center of mass of a particle, can be written, after some mathematical manipulation (see the original papers for the complete derivation), as

$$\left\langle \frac{d}{dt} f_S \right\rangle = \frac{1}{n}\left(\frac{\partial}{\partial t}\left(n\,\langle f_S\rangle\right) + \frac{\partial}{\partial x_i}\left(n\,\langle f_S w_i\rangle\right)\right) \tag{1.17}$$

We highlight that, for a f_S related to a particle as a whole, so the particle is a points, a Lagrangian approach has to be used. However, when the average process is applied, the averaged function $\langle f_S\rangle$ is define all over the space, so an Eulerian approach can be used. Equation (1.17) defines this passage from a Lagrangian approach to an Eulerian one.

Equation (1.17) is, as equations (1.10) and (1.11) for the fluid phase, the key point for the ensemble average process applied to the equations of motion for the solid particles.

1.1.2 Fluid phase equations

The local equation for the mass conservation of the incompressible fluid phase, valid, as written before, only when the fluid is present, is

$$\frac{\partial}{\partial x_i}\left(u_i^F\right) = 0 \tag{1.18}$$

where $\mathbf{u}^F$ is the fluid velocity. Applying the average process to the equation the result is

$$\left\langle \frac{\partial}{\partial x_i}\left(u_i^F\right) \right\rangle = 0 \tag{1.19}$$

This equation is not useful, inasmuch it is defined over all the mixture domain due to the average process, but it is not expressed in term of average functions. However using equations (1.10), (1.11) and the kinematic boundary condition that states the impenetrability of the solid and fluid phase

$$\mathbf{w} \cdot \hat{\mathbf{n}} = \mathbf{u}^F \cdot \hat{\mathbf{n}} \tag{1.20}$$

the resulting expression is

$$\frac{\partial}{\partial t}\left(\beta\right) + \frac{\partial}{\partial x_i}\left(\beta \left\langle u_i^F \right\rangle\right) = 0 \tag{1.21}$$

where now only the average variables of the flow compare in the equation.

The local momentum balance for the incompressible fluid phase, with constant density ρ_F, is

$$\rho_F \frac{\partial}{\partial t}\left(u_j^F\right) + \rho_F \frac{\partial}{\partial x_i}\left(u_i^F u_j^F\right) = \frac{\partial}{\partial x_i} T_{ij}^F + \rho_F g_j \tag{1.22}$$

where $\mathbf{T}^F$ is the local fluid stress tensor and $\mathbf{g}$ is the gravity force.

In order to obtain the averaged momentum equation, the procedure is similar to the one used for the continuity equations, ending up with

$$\rho_F \frac{\partial}{\partial t}\left(\beta \left\langle u_j^F \right\rangle\right) + \rho_F \frac{\partial}{\partial x_i}\left(\beta \left\langle u_i^F u_j^F \right\rangle\right) = \beta \left\langle \frac{\partial}{\partial x_i} T_{ij}^F \right\rangle + \rho_F \beta g_j \tag{1.23}$$

However, in this equation some terms are not expressed using average variables (e.g. in the second derivative the average is applied to $u_i^F u_j^F$ and not

separately to the functions u_i^F and u_j^F) so same mathematical manipulation is needed. At the end this expression becomes

$$\rho_F \frac{\partial}{\partial t}\left(\beta \left\langle u_j^F \right\rangle\right) + \rho_F \frac{\partial}{\partial x_i}\left(\beta \left\langle u_i^F \right\rangle \left\langle u_j^F \right\rangle\right) = \rho_F \frac{\partial}{\partial x_i}\left(\beta R_{ij}^F\right) + \\ + \frac{\partial}{\partial x_i}\left(\beta \left\langle T_{ij}^F \right\rangle\right) - F_{F-S,j}^{zp} + \rho_F \beta g_j \quad (1.24)$$

where R_{ij}^F is the ij component of the stress tensor $\mathbf{R}^F = -\left\langle \left(\left\langle \mathbf{u}^F \right\rangle - \mathbf{u}^F\right)^2 \right\rangle$ composed by the Reynold like terms (the ensemble average of the square of the difference between the ensemble average fluid velocity and the local fluid velocity) and $F_{F-S,j}^{zp}$ is the j-th component of the interphase forces between fluid and particles $\mathbf{F}_{F-S}^{zp}$ defined as

$$\mathbf{F}_{F-S}^{zp} = \oint_s \int P\left(\mathbf{y}, \mathbf{w}; t\right) \left\langle \mathbf{T}^F \right\rangle_1 \left(\mathbf{x}, t; 1\right) \cdot \hat{\mathbf{n}} \; d^3w \; dS_y \quad (1.25)$$

1.1.3 Solid phase equations

Using $f_S = 1$ in equation (1.17) it is possible to derive the conservation of the particle density number n

$$\frac{\partial}{\partial t}\left(n\right) + \frac{\partial}{\partial x_i}\left(n \left\langle w_i \right\rangle\right) = 0 \quad (1.26)$$

and, using the definition of the solid concentration (1.16) the final result is

$$\frac{\partial}{\partial t}\left(c\right) + \frac{\partial}{\partial x_i}\left(c \left\langle w_i \right\rangle\right) = 0 \quad (1.27)$$

remembering that the volume v of a particle does not change in time and space.

The equation of motion of one particle moving, with other particles, in a viscous fluid is

$$m\frac{d}{dt}\left(\mathbf{w}\right) = \mathbf{F}_C + m\mathbf{g} + \oint_s \mathbf{T}^F\left(\mathbf{z}, t; N\right) \cdot \hat{\mathbf{n}} \; dS_z \quad (1.28)$$

where m is the particle constant mass, $\mathbf{F}_C$ is force due to the collision with the other particles and the integral represents the normal forces exerted by the

fluid phase on the surface of the particle s. Applying the ensemble average process to this expression and using equation (1.17), the averaged momentum equation for the solid phase is obtained

$$\frac{\partial}{\partial t}\left(nm\left\langle w_j\right\rangle\right)+\frac{\partial}{\partial x_i}\left(nm\left\langle w_i w_j\right\rangle\right)=\left\langle \mathbf{F}_C\right\rangle+m\mathbf{g}+ \\ +\frac{1}{n}\int P\left(\mathbf{x},\mathbf{w};t\right)\oint_s\left\langle \mathbf{T}^F\right\rangle_1\left(\mathbf{z},t;1\right)\cdot\hat{\mathbf{n}}\;dS_z\;d^3w \quad (1.29)$$

As for the fluid momentum equation, same mathematical manipulation are needed in order to express all the terms using only average variable, ending up with

$$\rho_S\frac{\partial}{\partial t}\left(c\left\langle w_j\right\rangle\right)+\rho_S\frac{\partial}{\partial x_i}\left(c\left\langle w_i\right\rangle\;\left\langle w_j\right\rangle\right)=\rho_S\frac{\partial}{\partial x_i}\left(cR_{ij}^S\right)+F_{S-F,j}^{zp}+ \\ +n\left\langle F_{C,j}\right\rangle+\rho_S c g_j \quad (1.30)$$

where $\left\langle F_{C,j}\right\rangle$ is the j-th component of the average collisional force $\mathbf{F}_C$, R_{ij}^S is the ij component of the stress tensor $\mathbf{R}^S=-\left\langle\left(\left\langle\mathbf{w}\right\rangle-\mathbf{w}\right)^2\right\rangle$ composed by the Reynolds like stress produced by the average process, $F_{S-F,j}^{zp}$ is the j-th component of the interphase forces between solid and fluid phases $\mathbf{F}_{S-F}^{zp}$ defined as

$$\mathbf{F}_{S-F}^{zp}=\int P\left(\mathbf{x},\mathbf{w};t\right)\oint_s\left\langle \mathbf{T}^F\right\rangle_1\left(\mathbf{z},t;1\right)\cdot\hat{\mathbf{n}}\;dS_z\;d^3w \quad (1.31)$$

and ρ_S is the constant solid density

$$\rho_S=\frac{m}{v} \quad (1.32)$$

1.1.4 Final set of ensembe averaged equations for conitnuum liquid-granular mixture flow

The final set of equations describing a liquid-granular mixture flows in a continuum formulation derived using the ensemble average is composed by

equations (1.21), (1.24), (1.27) and (1.30) that reads

$$\begin{cases} \dfrac{\partial \beta}{\partial t} + \nabla \cdot (\beta \mathbf{u}_f) = 0 \\ \rho_f \left(\dfrac{\partial}{\partial t} (\beta \mathbf{u}_f) + \nabla \cdot (\beta \mathbf{u}_f \mathbf{u}_f) \right) = \rho_f \nabla \cdot \left(\beta \mathbf{R}^F \right) + \nabla \cdot \left(\beta \mathbf{T}^F \right) + \\ \qquad\qquad -\mathbf{F}^{zp}_{F-S} + \beta \rho_f \mathbf{g} \\ \dfrac{\partial c}{\partial t} + \nabla \cdot (c \mathbf{w}) = 0 \\ \rho_s \left(\dfrac{\partial}{\partial t} (c \mathbf{w}) + \nabla \cdot (c \mathbf{w} \mathbf{w}) \right) = \rho_S \nabla \cdot \left(c \mathbf{R}^S \right) + n \mathbf{F}_C \\ \qquad\qquad +\mathbf{F}^{zp}_{S-F} + c \rho_s \mathbf{g} \end{cases} \tag{1.33}$$

where, for shake of clarity, we neglect the average symbol.

1.2 Volume average for continuous fluid phase and discrete particles

The volume average is performed averaging a quantity over a volume in which there are fluid and particles. This Section is a short review of the works of Anderson and Jackson [5] and Jackson [35, 36]. The authors start from the local differential equations of motion for the fluid phase and the equation of motion for the center of mass of a single particle surrounded by a viscous fluid (as for the ensemble average presented in Section 1.1). Here we present only the basic aspect of the volume average process, while for more exhaustive information about the derivation we refer the reader to the original works.

1.2.1 Definitions

The generic volume average of a function $f(\mathbf{x}, t)$ over a sphere of volume V is define as

$$\langle f \rangle (\mathbf{x}, t) = \frac{1}{V} \int_V f(\mathbf{y}, t) \, dV_y \tag{1.34}$$

where dV_y is the element of volume near $\mathbf{y}$

However, if in the volume there are two or more phases (see Figure 1.2 for a sketch of the problem), it is possible to introduce a weighting function $g\left(|\mathbf{x}-\mathbf{y}|\right)$ in order to define the volume average of the generic function as

$$\langle f \rangle (\mathbf{x}, t) = \int_{V(t)} f(\mathbf{y}, t) g\left(|\mathbf{x}-\mathbf{y}|\right) \, dV_y \tag{1.35}$$

where $V(t)$ is the whole volume occupied by the phases that can change in time.

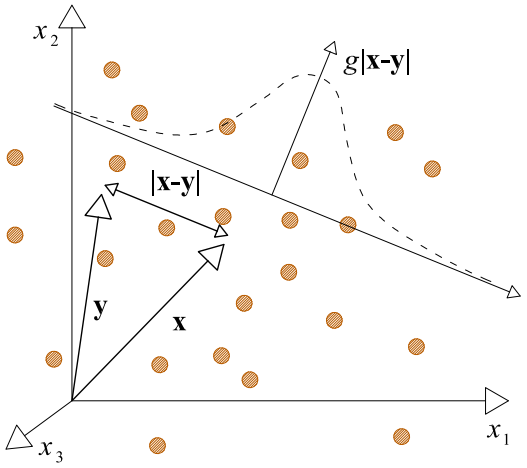

Figure 1.2: Sketch of the variable involved in the volume average with the reference system.

The weighting function is a generic function that has the following property:

- it is normalized to one

$$\int_{V(t)} g\left(|\mathbf{x}-\mathbf{y}|\right) \, dV_y = 1$$

- it is positive defined;
- it is monotone decreasing function of $r = |\mathbf{x}-\mathbf{y}|$;
- it goes to zero when r approach the infinity.

An example of this kind of weighting function is a Gaussian function centered in $\mathbf{x}$

For a two phase flow it is possible to divide the total volume $V(t)$ into the fluid one ($V_F(t)$) and the solid one ($V_S(t)$). The average process over these two volumes produce the definition of the fluid and the solid volume fraction

$$\beta(\mathbf{x},t) = \int_{V_F(t)} g\left(|\mathbf{x}-\mathbf{y}|\right)\ dV_y \tag{1.36}$$

$$c(\mathbf{x},t) = \int_{V_S(t)} g\left(|\mathbf{x}-\mathbf{y}|\right)\ dV_y \tag{1.37}$$

and, since $V_F + V_F = V$, the relation between the two volume fractions follows straightforwardly

$$\beta + c = 1$$

However, since the solid volume is composed of $N(t)$ particles of volume υ, the solid volume fraction can be also written as

$$c(\mathbf{x},t) = \sum_{\alpha=1}^{N(t)} \int_{\upsilon} g\left(|\mathbf{x}-\mathbf{y}|\right)\ dV_y \tag{1.38}$$

The particle number density $n(\mathbf{x},t)$ is defined as

$$n(\mathbf{x},t) = \sum_{\alpha=1}^{N(t)} g\left(|\mathbf{x}-\ \mathbf{y}_\alpha|\right) \tag{1.39}$$

and it is possible to obtain a realtion with the concentration $c(\mathbf{x},t)$ via

$$n(\mathbf{x},t) \simeq \frac{c(\mathbf{x},t)}{\upsilon} \tag{1.40}$$

where the order of approximation is $O\left(\frac{r^2}{L^2}\right)$.

The average of a generic function related the fluid phase $f_F(\mathbf{x},t)$ is defined as

$$\langle f_F \rangle(\mathbf{x},t) = \frac{1}{\beta(\mathbf{x},t)} \int_{V_f(t)} f_F(\mathbf{y},t) g\left(|\mathbf{x}-\mathbf{y}|\right)\ dV_y \tag{1.41}$$

and in a similar way it is possible to define the average of a function regarding the solid phase $f_S(\mathbf{x}, t)$

$$\langle f_S \rangle (\mathbf{x}, t) = \frac{1}{c(\mathbf{x}, t)} \int_{V_S(t)} f_S(\mathbf{y}, t) g\left(|\mathbf{x} - \mathbf{y}|\right) \, dV_y \tag{1.42}$$

Nevertheless there are some function $f_P(\mathbf{x}_P, t)$ defined for a particle as a whole (e.g. the center of mass velocity, the angular momentum, ...) for which it is more convenient to use the average based on the particle number

$$\langle f_P \rangle (\mathbf{x}, t) = \frac{1}{n(\mathbf{x}, t)} \sum_{\alpha=1}^{N(t)} f_P(\mathbf{y}_\alpha, t) g\left(|\mathbf{x} - \mathbf{y}_\alpha|\right) \tag{1.43}$$

where $\mathbf{y}_\alpha$ is the center of the α-th particle.

With some mathematical manipulation (we refer the reader to the original works for the complete derivation), the volume averaged of the time and space derivatives of a function $f_F(\mathbf{x}, t)$ related to the fluid phase are

$$\left\langle \frac{\partial}{\partial t} f_F \right\rangle = \frac{1}{\beta} \left(\frac{\partial}{\partial t} \left(\beta \langle f_F \rangle \right) + \sum_{\alpha=1}^{N(t)} \oint_{s^\alpha} f_F(\mathbf{y}, t) g\left(|\mathbf{x} - \mathbf{y}|\right) \mathbf{w}^\alpha \cdot \hat{\mathbf{n}}^\alpha \, dS_y \right) \tag{1.44}$$

where $\mathbf{w}^\alpha$ and $\hat{\mathbf{n}}^\alpha$ are the velocity and the normal outward vector of the α-th particle respectively, and the integral is performed all over the surface s^α of each particle, and

$$\left\langle \frac{\partial}{\partial x_i} f_F \right\rangle = \frac{1}{\beta} \left(\frac{\partial}{\partial x_i} \left(\beta \langle f_F \rangle \right) - \sum_{\alpha=1}^{N(t)} \oint_{s^\alpha} f_F(\mathbf{y}, t) g\left(|\mathbf{x} - \mathbf{y}|\right) \hat{n}_i^\alpha \, dS_y \right) \tag{1.45}$$

where $\hat{n}_i^\alpha$ is the i-th component of $\hat{\mathbf{n}}^\alpha$. The volume average of the total time derivative for a function f_P regarding the particles as a whole is instead

$$\left\langle \frac{d}{dt} f_P \right\rangle = \frac{1}{n} \left[\frac{\partial}{\partial t} \left(n \langle f_P \rangle \right) + \frac{\partial}{\partial x_i} \sum_{\alpha=1}^{N(t)} f_P(\mathbf{y}_\alpha, t) w_i^\alpha g\left(|\mathbf{x} - \mathbf{y}_\alpha|\right) \right] \tag{1.46}$$

We recall, as for the ensemble average, that this expression allows the switch between the Lagrangian approach used when we describe the particles as points, to an Eulerian approach that is necessary when we deal with the continuum liquid-granular mixture.

1.2.2 Fluid phase equations

Like in the ensemble average, the main objective of this Section (and also the next one) is to derive the averaged equations of motion for the fluid (and solid) phase, constituting the mixture, expressed in term of the average variables that are defined everywhere in the mixture domain.

The averaged mass equation for the incompressible fluid phase is derived, as for the ensemble average, starting from the local equation (1.18). The equation is then averaged over the fluid volume using the definition written in the previous Section. The result is

$$\frac{\partial}{\partial t}\left(\beta\right) + \frac{\partial}{\partial x_i}\left(\beta \left\langle u_i^F \right\rangle\right) = 0 \tag{1.47}$$

In the same way, starting from the equation (1.22), it is possible to derive the following averaged fluid momentum equation

$$\rho_F \frac{\partial}{\partial t}\left(\beta \left\langle u_j^F \right\rangle\right) + \rho_F \frac{\partial}{\partial x_i}\left(\beta \left\langle u_i^F u_j^F \right\rangle\right) = \beta \left\langle \frac{\partial}{\partial x_i} T_{ij}^F \right\rangle + \rho_F \beta g_j$$

and with some mathematical manipulation this equation becomes

$$\rho_F \frac{\partial}{\partial t}\left(\beta \left\langle u_j^F \right\rangle\right) + \rho_F \frac{\partial}{\partial x_i}\left(\beta \left\langle u_i^F \right\rangle \left\langle u_j^F \right\rangle\right) = \rho_F \frac{\partial}{\partial x_i}\left(\beta R_{ij}^F\right) + \\ + \frac{\partial}{\partial x_i}\left(\beta \left\langle T_{ij}^F \right\rangle\right) - F_{F-S,j} + \rho_F \beta g_j \tag{1.48}$$

where R_{ij}^F is the ij component of the stress tensor $\mathbf{R}^F = -\left\langle \left(\left\langle \mathbf{u}^F \right\rangle - \mathbf{u}^F \right)^2 \right\rangle$ composed by the Reynolds like stress produced by the average process and $F_{F-S,j}$ is the j-th component of the interphase forces between fluid and particles $\mathbf{F}_{F-S}$ defined as

$$\mathbf{F}_{F-S} = \sum_{\alpha=1}^{N} \oint_{s^\alpha} \mathbf{T}^F\left(\mathbf{y}, t\right) \cdot \hat{\mathbf{n}}^\alpha g\left(\left|\mathbf{x} - \mathbf{y}\right|\right) \, dS_y \tag{1.49}$$

1.2.3 Solid phase equations

Starting from the equation (1.28), describing the motion for a single particle immersed in a viscous fluid with other particles, and applying the volume

average process, it is possible to derive the averaged momentum equation for the solid phase

$$\rho_S \frac{\partial}{\partial t}\left(n\left\langle w_j\right\rangle\right) + \rho_S \frac{\partial}{\partial x_i}\left(n\left\langle w_j w_i\right\rangle\right) = \frac{n}{\upsilon}\left\langle F_{C,j}\right\rangle + \rho_S n g_j + \\ + \left(\sum_{\alpha=1}^{N} g\left(\left|\mathbf{x}-\mathbf{y}_\alpha\right|\right) \oint_{s^\alpha} \mathbf{T}^F \cdot \hat{\mathbf{n}}^\alpha \, dS_y\right)_j \quad (1.50)$$

where $\langle F_{C,j}\rangle$ is the j-th component of the averaged collisonal force $\mathbf{F}_C$. With some mathematical manipulation, introducing $\mathbf{R}^S = -\left\langle\left(\langle\mathbf{w}\rangle - \mathbf{w}\right)^2\right\rangle$ and remembering that $c = n\upsilon$, the final momentum equation for the solid phase is

$$\rho_S \frac{\partial}{\partial t}\left(c\left\langle w_j\right\rangle\right) + \rho_S \frac{\partial}{\partial x_i}\left(c\left\langle w_i\right\rangle\left\langle w_j\right\rangle\right) = \rho_S \frac{\partial}{\partial x_i}\left(cR_{ij}^S\right) + F_{S-F,j} + \\ + n\left\langle F_{C,j}\right\rangle + \rho_S c g_j \quad (1.51)$$

where $F_{S-F,j}$ is the j-th component of the the interphase force exerted by the solid particles on fluid $\mathbf{F}_{S-F}$ defined as

$$\mathbf{F}_{S-F} = \sum_{\alpha=1}^{N} g\left(\left|\mathbf{x}-\mathbf{y}_\alpha\right|\right) \oint_{s^\alpha} \mathbf{T}^F\left(\mathbf{y},t\right) \cdot \hat{\mathbf{n}}^\alpha \, dS_y \quad (1.52)$$

The conservation of the particle number density is derived from equation (1.46) imposing $f_P = 1$ in equation (1.46) ending up with

$$\frac{\partial}{\partial t}\left(n\right) + \frac{\partial}{\partial x_i}\left(n\left\langle w_i\right\rangle\right) = 0 \quad (1.53)$$

Using the definition of n, the conservation of solid mass is then obtained

$$\frac{\partial}{\partial t}\left(c\right) + \frac{\partial}{\partial x_i}\left(c\left\langle w_i\right\rangle\right) = 0 \quad (1.54)$$

1.2.4 Final set of volume averaged equations for continuum liquid-granular mixture flow

The final set of equations describing a liquid-granular mixture flows in a continuum formulation derived using the volume average is composed by

equations (1.47), (1.48), (1.54) and (1.51) that reads

$$\begin{cases} \dfrac{\partial \beta}{\partial t} + \nabla \cdot (\beta \mathbf{u}_f) = 0 \\ \rho_f \left(\dfrac{\partial}{\partial t} (\beta \mathbf{u}_f) + \nabla \cdot (\beta \mathbf{u}_f \mathbf{u}_f) \right) = \rho_f \nabla \cdot \left(\beta \mathbf{R}^F \right) + \nabla \cdot \left(\beta \mathbf{T}^F \right) + \\ \qquad\qquad -\mathbf{F}_{F-S} + \beta \rho_f \mathbf{g} \\ \dfrac{\partial c}{\partial t} + \nabla \cdot (c \mathbf{w}) = 0 \\ \rho_s \left(\dfrac{\partial}{\partial t} (c \mathbf{w}) + \nabla \cdot (c \mathbf{w} \mathbf{w}) \right) = \rho_S \nabla \cdot \left(c \mathbf{R}^S \right) + n \mathbf{F}_C + \\ \qquad\qquad +\mathbf{F}_{S-F} + c \rho_s \mathbf{g} \end{cases} \tag{1.55}$$

where, for shake of clarity as in the ensemble average, we neglect the average symbol.

1.3 Average approaches for continuous fluid and solid phase

The second class of approaches present in the literature uses, as said before, a continuous description of both the fluid and the solid constituent as starting point. Although a mixture is the sum of fluid and solid components, the continuum description of this mixture is not obtained simply adding together the equations for the fluid and solid phases described as continuum, but an indicator function must be introduced in order to recognize which phase occupy a certain point of the space. The introduction of the indicator function leads to a discrete definition of the variables, so an appropriate average process (e.g. ensemble or volume) has to be used in order to obtain a continuum formulations for the liquid-granular mixture. Among this class, we briefly summarize here the works of Drew [21], Hill [32] and Joseph and Lundgren [38].

In the work of Drew [21] a review of different average processes (time, space, ensemble, ...) is introduced highlighting some property they must have. Then the derivation of the partial differential equations for the continuum formulation of a liquid-granular mixture flow is presented using a general

average process. With some mathematical manipulation these equations can be written as

$$\begin{cases} \dfrac{\partial \beta}{\partial t} + \nabla \cdot (\beta \langle \mathbf{u}_f \rangle) = 0 \\ \rho_f \left(\dfrac{\partial}{\partial t} (\beta \langle \mathbf{u}_f \rangle) + \nabla \cdot (\beta \langle \mathbf{u}_f \rangle \langle \mathbf{u}_f \rangle) \right) = \nabla \cdot \left(\beta \mathbf{R}^F \right) + \nabla \cdot \left(\beta \left\langle \mathbf{T}^F \right\rangle \right) + \\ \qquad + \left(\mathbf{M}_f^d + \left\langle p^F \right\rangle \nabla \beta \right) + \beta \rho_f \mathbf{g} \\ \dfrac{\partial c}{\partial t} + \nabla \cdot (c \langle \mathbf{u}_s \rangle) = 0 \\ \rho_s \left(\dfrac{\partial}{\partial t} (c \langle \mathbf{u}_s \rangle) + \nabla \cdot (c \langle \mathbf{u}_s \rangle \langle \mathbf{u}_s \rangle) \right) = \nabla \cdot \left(c \mathbf{R}^S \right) + \nabla \cdot \left(c \left\langle \mathbf{T}^S \right\rangle \right) + \\ \qquad - \left(\mathbf{M}_f^d + \left\langle p^F \right\rangle \nabla \beta \right) + c \rho_s \mathbf{g} \end{cases} \tag{1.56}$$

where the first two equations are the fluid mass and momentum balance, while the last two are the balances of the solid phase. In these equations the solid phase velocity is $\mathbf{u}_s$, the fluid stress tensor is decomposed in a deviatoric part $\bar{\tau}^F$ and an pressure p^F

$$\mathbf{T}^F = \bar{\tau}^F - p^F \mathbf{I} \tag{1.57}$$

where $\mathbf{I}$ is the identity matrix. Similar decomposition is applied to the solid stress tensor, but following the paper, the solid pressure p^S can be further decomposed in fluid pressure plus a collisional pressure due to the interaction between the particles

$$\mathbf{T}^S = \bar{\tau}^S - \left(p^F + p^{co} \right) \mathbf{I} \tag{1.58}$$

Terms $\mathbf{M}_f^d + \left\langle p^F \right\rangle \nabla \beta$ includes all the interphase forces (drag, buoyancy, virtual mass effect, ...). In particular we highlight the presence of the gradient of the fluid phase concentration, though this term is not exactly a gradient, but only a way to identify the surfaces of the solid particles. We do not write here the explicit expression of $\mathbf{M}_f^d$ due to the complexity of the terms and it is also not relevant for the rest of the discussion.

Hill, in his work [32], follow the dissertation of Drew using a generic average, but he introduces a weighted decomposition for the fluid and solid

pressure terms at the interface between the two phases. In this way the final set of equations is

$$\begin{cases} \dfrac{\partial \beta}{\partial t} + \nabla \cdot (\beta \langle \mathbf{u}_f \rangle) = 0 \\ \rho_f \left(\dfrac{\partial}{\partial t} (\beta \langle \mathbf{u}_f \rangle) + \nabla \cdot (\beta \langle \mathbf{u}_f \rangle \langle \mathbf{u}_f \rangle) \right) = \nabla \cdot \left(\beta \mathbf{R}^F \right) + \nabla \cdot \left(\beta \left\langle \mathbf{T}^F \right\rangle \right) + \\ \qquad + \left(\mathbf{M}_f + \left\langle p^F \right\rangle \nabla \beta \right) + \beta \rho_f \mathbf{g} \\ \dfrac{\partial c}{\partial t} + \nabla \cdot (c \langle \mathbf{u}_s \rangle) = 0 \\ \rho_s \left(\dfrac{\partial}{\partial t} (c \langle \mathbf{u}_s \rangle) + \nabla \cdot (c \langle \mathbf{u}_s \rangle \langle \mathbf{u}_s \rangle) \right) = \nabla \cdot \left(c \mathbf{R}^S \right) + \nabla \cdot \left(c \left\langle \mathbf{T}^S \right\rangle \right) + \\ \qquad - \left(\mathbf{M}_f - \left\langle p^S \right\rangle \nabla c \right) + c \rho_s \mathbf{g} \end{cases} \tag{1.59}$$

where the only difference with the one obtained by Drew (1.56) is in the terms related to the interphase forces that now are $\mathbf{M}_f$ plus the terms $\left\langle p^F \right\rangle \nabla \beta$ for the fluid phase and $\langle p^s \rangle \nabla c$ for the solid one. $\mathbf{M}_f$, in this case, contains all the interphase forces plus the Reynolds like terms derived from the decomposition used. Also in this case we do not show the explicit expression of $\mathbf{M}_f$ for the same reason as before.

The last average system that we report here is the one proposed by Joseph and Lundgren [38] obtained by te use of an ensemble average. The equations that they derive are the following

$$\begin{cases} \dfrac{\partial \beta}{\partial t} + \nabla \cdot (\beta \langle \mathbf{u}_f \rangle) = 0 \\ \rho_f \left(\dfrac{\partial}{\partial t} (\beta \langle \mathbf{u}_f \rangle) + \nabla \cdot (\beta \langle \mathbf{u}_f \rangle \langle \mathbf{u}_f \rangle) \right) = \nabla \cdot \left(\beta \mathbf{R}^F_* \right) + \nabla \cdot \left(\beta \left\langle \mathbf{T}^F \right\rangle \right) + \\ \qquad - \langle \delta_S \mathbf{t} \rangle + \beta \rho_f \mathbf{g} \\ \dfrac{\partial c}{\partial t} + \nabla \cdot (c \langle \mathbf{u}_s \rangle) = 0 \\ \rho_s \left(\dfrac{\partial}{\partial t} (c \langle \mathbf{u}_s \rangle) + \nabla \cdot (c \langle \mathbf{u}_s \rangle \langle \mathbf{u}_s \rangle) \right) = \nabla \cdot \left(c \mathbf{R}^S_* \right) + \nabla \cdot \left(c \left\langle \mathbf{T}^S \right\rangle \right) + \\ \qquad + \langle \delta_S \mathbf{t} \rangle + c \rho_s \mathbf{g} \end{cases} \tag{1.60}$$

where $\mathbf{R}^F_*$ and $\mathbf{R}^S_*$ are a the Reynolds like stresses due to the averaging process, while $\langle \delta_S \mathbf{t} \rangle$ represents all the normal interphase forces acting on

the solid particles. The Reynold stresses presented in this work are slightly different from the previous ones since they include also the indicator function used during the average process.

1.4 Comparison of the 3D continuum liquid-granular systems

In order to going on with the derivation of the two dimensional shallow flow equations for the two-phase flow over fixed and mobile bed presented in the next Chapters, it is necessary to define an unified model that represent all the systems presented in the previous Sections since they are slightly different from each other. For this purpose a comparison between the proposed systems is necessary. For sake of clarity, from now on we neglect the symbols of the average.

First of all we say something about the velocity $\mathbf{u}_s$ of the particle compared with the velocity $\mathbf{w}$ of the center of mass used in Sections 1.1 and 1.2. Following the works of Zhang and Prosperetti [67, 68] and Jackson [36, 35] the velocity $\mathbf{u}_s$ can be expanded in Taylor series as

$$\mathbf{u}_s = \mathbf{w} + \frac{r^2}{L^2} f(\mathbf{\Omega}) + O\left(\frac{r^4}{L^4}\right)$$

where $f(\mathbf{\Omega})$ is a function concerning the angular velocity of the particles. With the same order of approximation $O\left(\frac{r^2}{L^2}\right)$ used in the previous Sections, the two velocity are equal

$$\mathbf{u}_s \simeq \mathbf{w} \tag{1.61}$$

so, without adding errors, a switch between them is possible.

With this approximation, the sets of averaged equations (1.33) derived

Section 1.1 are

$$\begin{cases} \dfrac{\partial \beta}{\partial t} + \nabla \cdot (\beta \mathbf{u}_f) = 0 \\ \rho_f \left(\dfrac{\partial}{\partial t} (\beta \mathbf{u}_f) + \nabla \cdot (\beta \mathbf{u}_f \mathbf{u}_f) \right) = \rho_f \nabla \cdot \left(\beta \mathbf{R}^F \right) + \nabla \cdot \left(\beta \mathbf{T}^F \right) + \\ \qquad\qquad -\mathbf{F}^{zp}_{F-S} + \beta \rho_f \mathbf{g} \\ \dfrac{\partial c}{\partial t} + \nabla \cdot (c \mathbf{u}_s) = 0 \\ \rho_s \left(\dfrac{\partial}{\partial t} (c \mathbf{u}_s) + \nabla \cdot (c \mathbf{u}_s \mathbf{u}_s) \right) = \rho_S \nabla \cdot \left(c \mathbf{R}^S \right) + n \mathbf{F}_C + \\ \qquad\qquad +\mathbf{F}^{zp}_{S-F} + c \rho_s \mathbf{g} \end{cases} \tag{1.62}$$

With the same approximation for the solid velocity, the volume averaged equations (1.55) derived in Section 1.2 constitute the following system

$$\begin{cases} \dfrac{\partial \beta}{\partial t} + \nabla \cdot (\beta \mathbf{u}_f) = 0 \\ \rho_f \left(\dfrac{\partial}{\partial t} (\beta \mathbf{u}_f) + \nabla \cdot (\beta \mathbf{u}_f \mathbf{u}_f) \right) = \rho_f \nabla \cdot \left(\beta \mathbf{R}^F \right) + \nabla \cdot \left(\beta \mathbf{T}^F \right) + \\ \qquad\qquad -\mathbf{F}_{F-S} + \beta \rho_f \mathbf{g} \\ \dfrac{\partial c}{\partial t} + \nabla \cdot (c \mathbf{u}_s) = 0 \\ \rho_s \left(\dfrac{\partial}{\partial t} (c \mathbf{u}_s) + \nabla \cdot (c \mathbf{u}_s \mathbf{u}_s) \right) = \rho_S \nabla \cdot \left(c \mathbf{R}^S \right) + n \mathbf{F}_C + \\ \qquad\qquad +\mathbf{F}_{S-F} + c \rho_s \mathbf{g} \end{cases} \tag{1.63}$$

Now it is possible to compare the systems describing the three dimensional two-phase flow for liquid-granular mixture with a continuum formulation obtained with the different average procedures.

The equations describing the fluid and solid mass conservation, i.e. the first and the third equation in systems (1.56), (1.59), (1.60), (1.62) and (1.63), are equal in all the approaches. The differences between the different approaches arise when we consider the momentum equations.
A general structure for these systems can be found looking at the mixture theory (see the work of Truesdell [65] for more details) used to model multiphase systems with the principles of continuum mechanics generalized to

several interpenetrable continua. The set of equations for this theory is

$$\begin{cases} \dfrac{\partial \beta}{\partial t} + \nabla \cdot (\beta \mathbf{u}_f) = 0 \\ \rho_f \left(\dfrac{\partial}{\partial t} (\beta \mathbf{u}_f) + \nabla \cdot (\beta \mathbf{u}_f \mathbf{u}_f) \right) = \nabla \cdot \mathbf{T}^F - \mathbf{F}_{F-S} + \beta \rho_f \mathbf{g} \\ \dfrac{\partial c}{\partial t} + \nabla \cdot (c \mathbf{u}_s) = 0 \\ \rho_s \left(\dfrac{\partial}{\partial t} (c \mathbf{u}_s) + \nabla \cdot (c \mathbf{u}_s \mathbf{u}_s) \right) = \nabla \cdot \mathbf{T}^S + \mathbf{F}_{F-S} + c \rho_s \mathbf{g} \end{cases} \tag{1.64}$$

Analyzing the momentum equations it is possible to highlight some terms. On the left side there are the advection terms, while on the right one there are the stress terms ($\mathbf{T}^F$ and $\mathbf{T}^S$), the interphase forces ($\mathbf{F}_{F-S}$) that are, due to the action-reaction law, equal for the equation of both phases but with an opposite sign, and the gravity force ($\mathbf{g}$). All the systems derived in this Chapter can be reduced in this form regrouping some terms.
First of all we can look at the left side of the momentum equations, underling that for all the proposed systems the advection terms are equal. Moving to the right hand side, one of the common terms in all the systems are the gravity and the interphase forces. Regrading this last term, the expressions are slightly different from one approach to the other, but their physical meaning is the same, so we classify therm as interphase forces. The last class is the stress terms that in systems (1.64) are presented in a divergence form. Looking at systems (1.62), (1.63), (1.56), (1.59) and (1.60) a divergence form of some tensors are present on the right hand side. Since the divergence is a linear operator it is possible to sum up these terms obtaining a single divergence. E.g. in system (1.60) it is possible to sum, in the solid momentum phase, the terms $c\mathbf{R}^S_*$ and $c\mathbf{T}^S$.

Using this classification all the terms in the momentum equations for the systems (1.56), (1.59) and (1.60) are classified. However, for systems (1.62) and (1.63), there is one more term outside the classification. This term is the collisional forces exerted between the particles ($n\mathbf{F}_C$). However, following the kinetic theory of gases, that is widely used in the granular flow field (we refer to the works of Jenkins and Savage [37], Savage [59], Reif [50] and Chapman and Cowling [17]), it is possible to rewrite it as a divergence of a collisional

stress tensor

$$n\mathbf{F}_C = \nabla \cdot \mathbf{T}^{Coll} \tag{1.65}$$

In this way, since the collisional forces are the divergence of the tensor $\mathbf{T}^{Coll}$, it is possible to insert also this term into the generic solid stress tensor $\mathbf{T}^S$.

Since all the systems presented in the Chapter have the same general structure, we can assume, as unified model for the remainder of the thesis, the system derived from the mixture theory (1.64), without loss of generality.

1.5 Closure relations

Here we present only some aspects of the closure relation needed for the $3D$ equations for the continuum formulation of fluid-granular mixture flow, since lots of terms will be neglected in the following Chapters due to some suitable simplifications that will be introduced later on.

The system of equations (1.64) is composed of eight equations (two mass conservations, three momentum balances for the fluid phase and three momentum balances for the solid one) with 22 unknowns. The unknowns are: the solid concentration c (the fluid one β is not an unknown since equation (1.8) establishes a relation with the solid concentration), the three components of solid velocities $\mathbf{u}_s$, the three components of the fluid velocities $\mathbf{u}_f$, the three components of interphase forces $\mathbf{F}_{F-S}$ and the components of the fluid and solid stress tensor (the unknown components for each tensor are six). Since the number of unknowns is larger than the number of equations, it is necessary to use some closure relations.

The first terms that we analyze are the stress tensors. A generic tensor can be decompose in an isotropic part plus a deviatoric one. In this way the stress tensors $\mathbf{T}^i$ (where the superscript i refers to the phases involved: f for fluid phase and s for solid one) is decomposed in isotropic pressure $p^i\mathbf{I}$ and in tangential stresses (the deviatoric part) $\overline{\tau}^i$ as

$$\mathbf{T}^i = -p^i\mathbf{I} + \overline{\tau}^i \tag{1.66}$$

where $\mathbf{I}$ is the identity matrix. These decomposition introduces two additional unknown: the solid an fluid pressure (p^s and p^f), however the introduction of them allows some important considerations that will be presented in the next Chapter where the shallow flow approximation is introduced.

The second important term that need attention is the interphase forces vector $\mathbf{F}_{F-S}$. From a physical point of view, this term is composed of all the forces that the fluid and the solid phases exchange each other. They are essentially the buoyancy (since there are solid particles immersed in a fluid) and the drag effect (due to possible differences of velocity between the phases). Other forces could also be introduced (e.g. the virtual added mass) but they are smaller than the first two, so we neglected them. Following the works of Armanini [7, 8] and Jackson [36], the interphase force can be decomposed as

$$F_i^{F-S} = c\frac{\partial}{\partial x_j}T_{ij}^f + F_i^D \tag{1.67}$$

where F_i^D is the i-th component of the drag vector force $\mathbf{F}^D$, and using equation (1.66) it becomes

$$F_i^{F-S} = -c\frac{\partial}{\partial x_i}p^f + c\frac{\partial}{\partial x_j}\tau_{ij}^f + F_i^D \tag{1.68}$$

The drag force is a function of the difference between fluid and solid velocity, the net area of the particles and the density of the fluid phase

$$\mathbf{F}^D \propto r^2\rho_f\left(\mathbf{u}_f - \mathbf{u}_S\right)^2 \tag{1.69}$$

In this way the interphase force is no more unknown since it is a function of the other unknowns of the problem.

Using equations (1.66), (1.68) and remembering that $\beta = 1 - c$, the set

of equations (1.64) that describe a two phase flow becomes

$$\begin{cases} \dfrac{\partial}{\partial t}(1-c) + \nabla \cdot ((1-c)\,\mathbf{u}_f) = 0 \\ \rho_f \left(\dfrac{\partial}{\partial t}((1-c)\,\mathbf{u}_f) + \nabla \cdot ((1-c)\,\mathbf{u}_f \mathbf{u}_f) \right) = -(1-c)\,\nabla p^f + \\ \qquad\qquad + (1-c)\,\nabla \cdot \bar{\tau}^F - \mathbf{F}^D + (1-c)\,\rho_f \mathbf{g} \\ \dfrac{\partial c}{\partial t} + \nabla \cdot (c\mathbf{u}_s) = 0 \\ \rho_s \left(\dfrac{\partial}{\partial t}(c\mathbf{u}_s) + \nabla \cdot (c\mathbf{u}_s \mathbf{u}_s) \right) = -\nabla p^s - c\nabla p^f + \nabla \cdot \bar{\tau}^S + \\ \qquad\qquad + c\nabla \cdot \bar{\tau}^f + \mathbf{F}^D + c\rho_s \mathbf{g} \end{cases} \tag{1.70}$$

This is the system that we are going to use in the following Chapters, where the derivation of the two dimensional shallow flow models is developed.

Chapter 2

The shallow flow approximation

The thee dimensional continuum equations derived in Chapter 1 compose a system that is particularly complicated and, as written in Section 1.5, requires lots of closure relations not always available in the literature. Since in a debris flow the planar scale is commonly larger than the vertical one, it is possible to introduce the shallow flow approximation which is widely used in the field of free-surface flow when this difference between the spatial scales is present. The use of the shallow flow simplification allows us to reduce the complexity of the original set of equations obtaining a simplified three dimensional system of partial differential equations which will be depth integrated later on.

The Chapter is structured as follow: in Section 2.1 we focus our attention on the characteristic scales of a debris flow, then in the Section 2.2 the momentum equations along the normal directions are simplified, while in Section 2.3 we simplify the momentum equations in the planar directions. Finally, in Section 2.4, some consideration about the number of closure relations needed is presented.

2.1 Debris flow characteristic scales

With shallow flow (SF) we define a free-surface flow where the vertical scale H is small if compared with the planar scale L

$$H \ll L \tag{2.1}$$

The first step, for the introduction of the shallow flow approximation, is the definition of the reference system. The choice, widely used in the derivation of the SF models, is to define the reference system (x_1, x_2, x_3) with the 1^{st} and 2^{nd} direction parallel to the bottom (the planar axis), while the 3^{rd} one is perpendicular to it (normal direction) (see Figure 2.1).

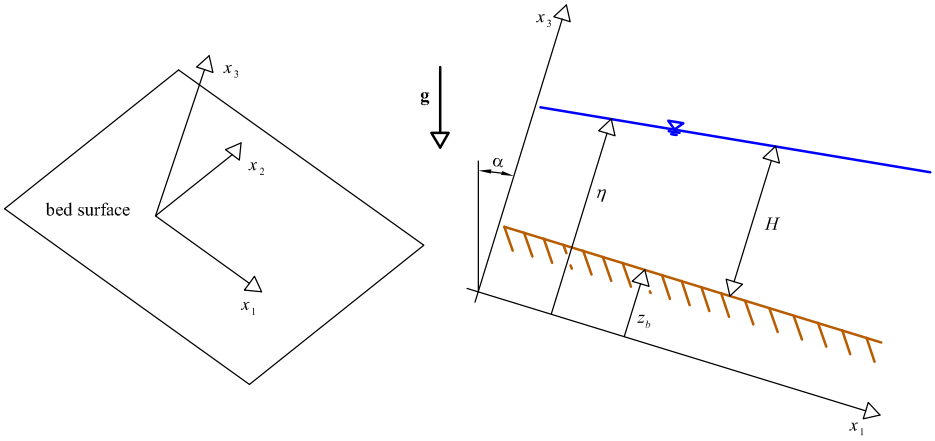

Figure 2.1: Sketch of the reference system and the angle of inclination α respect the gravity force.

Usually a debris flow happens in small basins with an area of less than 5 km^2 (see for example [44]), and has a planar extension of about hundreds of meters, while the the vertical one is of the order of meters. With these considerations a debris flow can be defined as a shallow flow. As said before, in order to going on with the simplification of the equations of motion, it is necessary to understand the orders of magnitude of the variables involved in the problem (some information can be found in [34], [60], [69] and [56]). In the follow we present a list of all these variables with their characteristic scale and order of magnitude.

- Planar direction x_1 and x_2 is about hundreds of meter and the characteristic scale is L

$$L \sim 10^2 \ m \tag{2.2}$$

- Normal direction x_3 is meters with scale H

$$H \sim 10^0 \ m \tag{2.3}$$

- Longitudinal solid (u_1^s, u_2^s) and fluid velocities (u_1^f, u_2^f) have scale U and their order of magnitude is few meters per second

$$U \sim 10^0 \ m/s \tag{2.4}$$

  We use the same velocity scale for both solid and fluid phases since in an uniform flow the two velocities are similar.

- Solid (c) and liquid (β) volumetric concentrations assume different values. Usually a debris flow flow has concentration of about $0.3 \div 0.5$, so the characteristic scale is

$$C \sim 10^{-1} \tag{2.5}$$

  on the contrary, the liquid concentration, since $\beta = 1 - c$, is about $0.5 \div 0.7$ so the same order of magnitude can be used

$$\mathcal{B} \sim 10^{-1} \tag{2.6}$$

  Of course the concentration of a debris flow could be larger, reaching the maximum value of around 0.65 that is the maximum concentration of the solid fraction in the bed, however here we are speaking of order of magnitude, so this approximation cold be reasonable if we look at the average over a flow event.

- Density of fluid phase ρ_f, that usually is water or water with silt, is about $1000 \div 1500 \ kg/m^3$ while the density of the solid phase ρ_s is about $2600 \ kg/m^3$. The order of magnitude of the density is therefore

$$\rho \sim 10^3 \ kg/m^3 \tag{2.7}$$

- Gravity force **g** that must be decomposed along x_3 and along x_1 and x_2. Defining α as the angle between the gravity vector an the normal to the bed (see Figure 2.1 for a sketch), the two components of the gravity are $g_3 = g\cos\alpha$ and $g_1 = g_2 = g\sin\alpha$ where g is the module of the gravity force with a characteristic scale

  $$G \sim 10^1 \ m/s^2$$

  The angle α assumes different value along the path of the debris flow, ranging from 0° up to 20° and over in the triggering area. However, since we are speaking of order of magnitude we can assume an average value along the debris flow path of about $8°\div10°$. With these definitions the two characteristic scales needed are respectively for gravity force normal to the bed and for the tangential one:

  $$G_N \sim 10^1 \ m/s^2 \tag{2.8}$$
  $$G_T \sim 10^{-1} \ m/s^2 \tag{2.9}$$

- The fluid pressure p^f could be assumed as hydrostatic obtaining, as order of magnitude

  $$P^f = \rho G_N H \sim 10^4 \ Pa \tag{2.10}$$

- The components of the tangential fluid stresses τ_{ij}^f with $i, j = 1, 2, 3$ can be estimated using empirical relation derived for the uniform flow such as the Gaukler-Stickler relation (see [6] for more details on this formulation)

  $$\tau_0 = \frac{\rho g u^2}{k_s^2 h^{1/3}}$$

  where k_s is the Stickler coefficient with a magnitude of $10^1 \ m^{1/3}s^{-1}$, h is the flow depth and u is the flow velocity. With this relation the order of magnitude for the components of the tangential fluid stresses is

  $$T^f \sim 10^2 \ Pa \tag{2.11}$$

- The solid pressure p^s can be assumed hydrostatic like the fluid one. The difference, respect to the fluid pressure, is that now we introduce the solid concentration in order to take into account the fact that not all the volume is occupied by the solid phase.

$$P^s = \rho C G_N H \sim 10^3 \ Pa \tag{2.12}$$

  Of course it is an approximation since the solid pressure, as the solid stress tensor, takes into account also the presence of the collision between the particles.

- The order of magnitude for the components of solid stress tensor τ^s_{ij} with $i, j = 1, 2, 3$ can be estimated following the works of Armanini [8, 7] and Armanini *et al.* [11] where the kinetic gas theory is applied to the liquid-granular flows. Omitting all the formulation, due to its complexity and length, the final result is

$$T^s \sim 10^1 \ Pa \tag{2.13}$$

Among these variables are missing the time and the vertical fluid and solid velocities. In order to evaluate their orders of magnitude, it is necessary to use the first and the third equations of system (1.70) that represent the mass balances for the fluid and solid phases

$$\frac{\partial}{\partial t}\beta + \frac{\partial}{\partial x_1}\beta u_1^f + \frac{\partial}{\partial x_2}\beta u_2^f + \frac{\partial}{\partial x_3}\beta u_3^f = 0 \tag{2.14}$$

$$\frac{\partial}{\partial t}c + \frac{\partial}{\partial x_1}c u_1^s + \frac{\partial}{\partial x_2}c u_2^s + \frac{\partial}{\partial x_3}c u_3^s = 0 \tag{2.15}$$

The order of magnitude of one term for each equations, using the previous characteristic scales, is

$$\frac{\partial}{\partial x_2}\beta u_2^f \rightsquigarrow \frac{\mathcal{B}U}{L} \sim 10^{-3} \ s^{-1} \tag{2.16}$$

and

$$\frac{\partial}{\partial x_2}c u_2^s \rightsquigarrow \frac{CU}{L} = 10^{-3} \ s^{-1} \tag{2.17}$$

Since all the terms involved in the mass balance have the same order of magnitude, it is possible to write the following relations

$$\frac{\mathcal{B}}{T} = \frac{\mathcal{B}V}{H} = \frac{\mathcal{B}U}{L} \sim 10^{-3}\ s^{-1} \tag{2.18}$$

and

$$\frac{C}{T} = \frac{CV}{H} = \frac{CU}{L} \sim 10^{-3}\ s^{-1} \tag{2.19}$$

where T is the characteristic time scale and V is the fluid and solid normal velocity scale. From these expressions it is possible to evaluate the order of magnitude for the solid and liquid vertical velocity (u_3^s and u_3^f)

$$V = \frac{H}{L}U \sim 10^{-2}\ m/s \tag{2.20}$$

and for the time scale T

$$T = \frac{L}{U} = \frac{H}{V} \sim 10^{2}\ s \tag{2.21}$$

The last term missing is the drag force $\mathbf{F}^D$. As specified in equation (1.69) in Section 1.5, the drag force is a function of the difference between solid and fluid velocities, the area of the particles and the fluid density

$$F_i^D \propto r^2 \left(u_i^f - u_i^s\right)^2 \rho_f \qquad i = 1, 2, 3 \tag{2.22}$$

In order to understand the order of magnitude of the these forces, we assume that the radius of the particles is about $10^{-1}\ m$, while the maximum difference between the two velocity is reached when the solid particles are stationary and the fluid is moving (this happens in the triggering and deposition area where the debris flow starts and stops) so $\left(u_i^f - u_i^s\right)^2 \sim \left(u_i^f\right)^2$ with $i = 1, 2, 3$. With these assumption the order of magnitude for the drag force on direction $i = 1, 2$ is

$$F_T^D \sim 10^{1}\ N \tag{2.23}$$

while for the normal direction $i = 3$ becomes

$$F_N^D \sim 10^{-3}\ N \tag{2.24}$$

We want to highlight that this is only an order of magnitude for the drag force valid in the triggering and deposition area where the solid velocity is null. Instead, when the uniform flow is developed the fluid and solid velocities have the same order of magnitude, so the drag force becomes negligible. Since we are speaking about the orders of magnitude, we can assume that the drag force values obtained are also the same when we refer to a unit volume, so we can use them inside the momentum equations.

An estimation of the magnitude of all the variables present into the three dimensional equations for a continuum fluid-granular mixture flow derived in Chapter 1 are presented, so it is possible to evaluate which terms into these equations can be neglected under the shallow flow approximation.

2.2 Simplification of the momentum equations on the normal direction

The first equation we analyze is the momentum balance for the fluid phase along the normal direction that is the second equation of system (1.70). Expanding all the terms, the equation reads

$$\begin{aligned}\frac{\partial}{\partial t}\beta u_3^f + \frac{\partial}{\partial x_1}\beta u_1^f u_3^f + \frac{\partial}{\partial x_2}\beta u_2^f u_3^f + \frac{\partial}{\partial x_3}\beta u_3^f u_3^f = \\ = -\frac{\beta}{\rho_f}\frac{\partial}{\partial x_3}p^f + \frac{\beta}{\rho_f}\frac{\partial}{\partial x_1}\tau_{13}^f + \frac{\beta}{\rho_f}\frac{\partial}{\partial x_2}\tau_{23}^f + \frac{\beta}{\rho_f}\frac{\partial}{\partial x_3}\tau_{33}^f - \frac{F_3^D}{\rho_f} + \beta g_3\end{aligned} \tag{2.25}$$

Using the characteristic scales derived in Section 2.1, the orders of magnitude for each terms of the equation are (we neglect the unit of measure since now

all the terms are expressed in m/s^2)

$$\begin{aligned}
&\frac{\partial}{\partial t}\beta u_3^f \rightsquigarrow \frac{\mathcal{B}V}{T} = 10^{-1} && ; \quad \frac{\partial}{\partial x_1}\beta u_1^f u_3^f \rightsquigarrow \frac{\mathcal{B}UV}{L} = 10^{-5} \\
&\frac{\partial}{\partial x_2}\beta u_2^f u_3^f \rightsquigarrow \frac{\mathcal{B}UV}{L} = 10^{-5} && ; \quad \frac{\partial}{\partial x_3}\beta u_3^f u_3^f \rightsquigarrow \frac{\mathcal{B}V^2}{H} = 10^{-5} \\
&\frac{\beta}{\rho_f}\frac{\partial}{\partial x_3}p^f \rightsquigarrow \frac{\mathcal{B}P^f}{\rho H} = 10^{0} && ; \quad \frac{\beta}{\rho_f}\frac{\partial}{\partial x_1}\tau_{13}^f \rightsquigarrow \frac{\mathcal{B}T^f}{\rho L} = 10^{-4} \\
&\frac{\beta}{\rho_f}\frac{\partial}{\partial x_2}\tau_{23}^f \rightsquigarrow \frac{\mathcal{B}T^f}{\rho L} = 10^{-4} && ; \quad \frac{\beta}{\rho_f}\frac{\partial}{\partial x_3}\tau_{33}^f \rightsquigarrow \frac{\mathcal{B}T^f}{\rho H} = 10^{-2} \\
&\frac{F_3^D}{\rho_f} \rightsquigarrow \frac{F_N^D}{\rho} = 10^{-6} && ; \quad \beta g_3 \rightsquigarrow \epsilon G_N = 10^{0}
\end{aligned}$$

Taking into account only the terms with the highest order of magnitude (so 10^0) the fluid momentum equation in the normal direction becomes

$$-\frac{\beta}{\rho_f}\frac{\partial}{\partial x_3}p^f + \beta g_3 = 0 \tag{2.26}$$

which, simplifying β, becomes

$$\frac{\partial}{\partial x_3}p^f = \rho_f g_3 \tag{2.27}$$

The starting solid phase momentum equation along the normal direction is the fourth equation in system (1.70) that reads

$$\begin{aligned}
&\frac{\partial}{\partial t}cu_3^s + \frac{\partial}{\partial x_1}cu_1^s u_3^s + \frac{\partial}{\partial x_2}cu_2^s u_3^s + \frac{\partial}{\partial x_3}cu_3^s u_3^s = \\
&= \frac{F_3^D}{\rho_s} + cg_3 + \frac{1}{\rho_s}\left(-\frac{\partial}{\partial x_3}p^s - c\frac{\partial}{\partial x_3}p^f + \frac{\partial}{\partial x_1}\tau_{13}^s + \frac{\partial}{\partial x_2}\tau_{23}^s + \right. \\
&\qquad \left. + \frac{\partial}{\partial x_3}\tau_{33}^s + c\frac{\partial}{\partial x_1}\tau_{13}^f + c\frac{\partial}{\partial x_2}\tau_{23}^f + c\frac{\partial}{\partial x_3}\tau_{33}^f\right)
\end{aligned} \tag{2.28}$$

Following the same procedure as for the fluid phase, the order of magnitude

of the different terms into this equation are

$$\begin{array}{lll}
\dfrac{\partial}{\partial t}cu_3^s \rightsquigarrow \dfrac{CV}{T} = 10^{-1} & ; & \dfrac{\partial}{\partial x_1}cu_1^s u_3^s \rightsquigarrow \dfrac{CUV}{L} = 10^{-5} \\
\dfrac{\partial}{\partial x_2}cu_2^s u_3^s \rightsquigarrow \dfrac{CUV}{L} = 10^{-5} & ; & \dfrac{\partial}{\partial x_3}cu_3^s u_3^s \rightsquigarrow \dfrac{CV^2}{H} = 10^{-5} \\
\dfrac{1}{\rho_s}\dfrac{\partial}{\partial x_3}p^s \rightsquigarrow \dfrac{P^s}{\rho H} = 10^{0} & ; & \dfrac{1}{\rho_s}\dfrac{\partial}{\partial x_1}\tau_{13}^s \rightsquigarrow \dfrac{T^s}{\rho L} = 10^{-4} \\
\dfrac{1}{\rho_s}\dfrac{\partial}{\partial x_2}\tau_{23}^s \rightsquigarrow \frac{T^s}{\rho L} = 10^{-4} & ; & \dfrac{1}{\rho_s}\dfrac{\partial}{\partial x_3}\tau_{33}^s \rightsquigarrow \dfrac{T^s}{\rho H} = 10^{-2} \\
\dfrac{c}{\rho_s}\dfrac{\partial}{\partial x_3}p^f \rightsquigarrow \dfrac{CP^f}{\rho H} = 10^{0} & ; & \dfrac{c}{\rho_s}\dfrac{\partial}{\partial x_1}\tau_{13}^f \rightsquigarrow \dfrac{CT^f}{\rho L} = 10^{-4} \\
\dfrac{c}{\rho_s}\dfrac{\partial}{\partial x_2}\tau_{23}^f \rightsquigarrow \dfrac{CT^f}{\rho L} = 10^{-4} & ; & \dfrac{c}{\rho_s}\dfrac{\partial}{\partial x_3}\tau_{33}^f \rightsquigarrow \dfrac{CT^f}{\rho H} = 10^{-2} \\
\dfrac{F_3^D}{\rho_s} \rightsquigarrow \dfrac{F_N^D}{\rho} = 10^{-6} & ; & cg_3 \rightsquigarrow CG_N = 10^{0}
\end{array}$$

Using only the first order of approximation, so neglecting all the term with a magnitude less than 10^0, the solid momentum equation along the x_3 direction reduce to

$$\frac{\partial}{\partial x_3}p^s + c\frac{\partial}{\partial x_3}p^f = c\rho_s g_3 \tag{2.29}$$

The normal derivative of both solid and liquid pressures appears in this equation. However, using equation (2.27) that describe the normal derivative of the fluid pressure, equation (2.29) becomes

$$\begin{aligned}
\frac{\partial}{\partial x_3}p^s &= c\left(\rho_s - \rho_f\right) g_3 \\
&= c\rho' g_3
\end{aligned} \tag{2.30}$$

and represent the vertical variation of the solid pressure, where $\rho' = (\rho_s - \rho_f)$ is the submerged solid density.

Equations (2.27) and (2.30) constitute the shallow flow momentum equations for a two-phase flow along the normal direction and in Chapter 3 we will demonstrate that the integration of these equations produce the well known linear pressure distributions for both phases.

2.3 Simplification of the momentum equations on the planar direction

The momentum equation in the plane x_1, x_2 for the fluid phase derived in Section 1.4 is

$$\frac{\partial}{\partial t}\beta u_i^f + \frac{\partial}{\partial x_1}\beta u_1^f u_i^f + \frac{\partial}{\partial x_2}\beta u_2^f u_i^f + \frac{\partial}{\partial x_3}\beta u_3^f u_i^f = \\ = -\frac{\beta}{\rho_f}\frac{\partial}{\partial x_i}p^f + \frac{\beta}{\rho_f}\frac{\partial}{\partial x_1}\tau_{1i}^f + \frac{\beta}{\rho_f}\frac{\partial}{\partial x_2}\tau_{2i}^f + \frac{\beta}{\rho_f}\frac{\partial}{\partial x_3}\tau_{3i}^f - \frac{F_i^D}{\rho_f} + \beta g_i \quad (2.31)$$

where $i = 1, 2$.

The order of magnitude of each terms in this equation, using $i = 1$, are the same than using $i = 2$ since these two directions are, up to now, interchangeable. The magnitude of these terms are the following

$$\frac{\partial}{\partial t}\beta u_i^f \rightsquigarrow \frac{\mathcal{B}U}{T} = 10^{-3} \quad ; \quad \frac{\partial}{\partial x_1}\beta u_1^f u_i^f \rightsquigarrow \frac{\mathcal{B}U^2}{L} = 10^{-3}$$
$$\frac{\partial}{\partial x_2}\beta u_2^f u_i^f \rightsquigarrow \frac{\mathcal{B}U^2}{L} = 10^{-3} \quad ; \quad \frac{\partial}{\partial x_3}\beta u_3^f u_i^f \rightsquigarrow \frac{\mathcal{B}UV}{H} = 10^{-3}$$
$$\frac{\beta}{\rho_f}\frac{\partial}{\partial x_i}p^f \rightsquigarrow \frac{\mathcal{B}P^f}{\rho L} = 10^{-2} \quad ; \quad \frac{\beta}{\rho_f}\frac{\partial}{\partial x_1}\tau_{1i}^f \rightsquigarrow \frac{\mathcal{B}T^f}{\rho L} = 10^{-4}$$
$$\frac{\beta}{\rho_f}\frac{\partial}{\partial x_2}\tau_{2i}^f \rightsquigarrow \frac{\mathcal{B}T^f}{\rho L} = 10^{-4} \quad ; \quad \frac{\beta}{\rho_f}\frac{\partial}{\partial x_3}\tau_{3i}^f \rightsquigarrow \frac{\mathcal{B}T^f}{\rho H} = 10^{-2}$$
$$\frac{F_i^D}{\rho_f} \rightsquigarrow \frac{F_T^D}{\rho} = 10^{-2} \quad ; \quad \beta g_i \rightsquigarrow \mathcal{B}G_T = 10^{-2}$$

Taking into account only the leading terms (so the ones with magnitude of 10^{-2}) the resulting equation describe only permanent flow where no time variation is allowed. We remember that, as said in Section 2.1, that in a permanent flow the drag term is smaller, so it is negligible. Since we want to study phenomena with a time variation in the plane, we need to take into account also the term with an order of 10^{-3}. With this approximation it is possible to neglect the terms related to the tangential stresses τ_{1i}^f and τ_{2i}^f as commonly happens in the shallow flow models. With all these considerations the final fluid momentum equation for directions x_1 and x_2, under the shallow

flow approximation, for a two-phase flow is

$$\frac{\partial}{\partial t}\beta u_i^f + \frac{\partial}{\partial x_1}\beta u_1^f u_i^f + \frac{\partial}{\partial x_2}\beta u_2^f u_i^f + \frac{\partial}{\partial x_3}\beta u_3^f u_i^f = \\ = -\frac{\beta}{\rho_f}\frac{\partial}{\partial x_i}p^f + \frac{\beta}{\rho_f}\frac{\partial}{\partial x_3}\tau_{3i}^f - \frac{F_i^D}{\rho_f} + \beta g_i \quad (2.32)$$

with $i = 1, 2$.

Moving now on the solid momentum equation for the axis x_1 and x_2, the relevant equation, derived in Section 1.4, is

$$\frac{\partial}{\partial t}cu_i^s + \frac{\partial}{\partial x_1}cu_1^s u_i^s + \frac{\partial}{\partial x_2}cu_2^s u_i^s + \frac{\partial}{\partial x_3}cu_3^s u_i^s = \\ = \frac{F_i^D}{\rho s} + cg_i + \frac{1}{\rho_s}\left(-\frac{\partial}{\partial x_i}p^s - c\frac{\partial}{\partial x_i}p^f + \frac{\partial}{\partial x_1}\tau_{1i}^s + \frac{\partial}{\partial x_2}\tau_{2i}^s + \right. \\ \left. + \frac{\partial}{\partial x_3}\tau_{3i}^s + c\frac{\partial}{\partial x_1}\tau_{1i}^f + c\frac{\partial}{\partial x_2}\tau_{2i}^f + c\frac{\partial}{\partial x_3}\tau_{3i}^f\right) \quad (2.33)$$

for $i = 1, 2$. Using the same procedure as for the fluid momentum equation, the following order of magnitude terms are obtained

$$\begin{array}{lll}
\frac{\partial}{\partial t}cu_i^s \rightsquigarrow \frac{CU}{T} = 10^{-3} & ; & \frac{\partial}{\partial x_1}cu_1^s u_i^s \rightsquigarrow \frac{CU^2}{L} = 10^{-3} \\
\frac{\partial}{\partial x_2}cu_2^s u_i^s \rightsquigarrow \frac{CU^2}{L} = 10^{-3} & ; & \frac{\partial}{\partial x_3}cu_3^s u_i^s \rightsquigarrow \frac{CUV}{H} = 10^{-3} \\
\frac{1}{\rho_s}\frac{\partial}{\partial x_i}p^s \rightsquigarrow \frac{P^s}{\rho L} = 10^{-2} & ; & \frac{1}{\rho_s}\frac{\partial}{\partial x_1}\tau_{1i}^s \rightsquigarrow \frac{T^s}{\rho L} = 10^{-4} \\
\frac{1}{\rho_s}\frac{\partial}{\partial x_2}\tau_{2i}^s \rightsquigarrow \frac{T^s}{\rho L} = 10^{-4} & ; & \frac{1}{\rho_s}\frac{\partial}{\partial x_3}\tau_{3i}^s \rightsquigarrow \frac{T^s}{\rho H} = 10^{-2} \\
\frac{c}{\rho_s}\frac{\partial}{\partial x_i}p^f \rightsquigarrow \frac{CP^f}{\rho L} = 10^{-2} & ; & \frac{c}{\rho_s}\frac{\partial}{\partial x_1}\tau_{1i}^f \rightsquigarrow \frac{CT^f}{\rho L} = 10^{-4} \\
\frac{c}{\rho_s}\frac{\partial}{\partial x_2}\tau_{2i}^f \rightsquigarrow \frac{CT^f}{\rho L} = 10^{-4} & ; & \frac{c}{\rho_s}\frac{\partial}{\partial x_3}\tau_{3i}^f \rightsquigarrow \frac{CT^f}{\rho H} = 10^{-2} \\
\frac{F_i^D}{\rho_s} \rightsquigarrow \frac{F_T^D}{\rho} = 10^{-2} & ; & cg_i \rightsquigarrow CG_T = 10^{-2}
\end{array}$$

Taking into account only the first order terms (10^{-2}) the equation describe, as for the fluid one, a permanent flow, so it is necessary to use also the second order terms (10^{-3}). With these assumptions we neglect only the fluid and

solid tangential stresses $\tau_{i1}^{f,s}$ and $\tau_{i2}^{f,s}$. The final shallow flow solid momentum equation along the x_1 and x_2 direction for a two-phase flow is then

$$\frac{\partial}{\partial t}cu_i^s + \frac{\partial}{\partial x_1}cu_1^s u_i^s + \frac{\partial}{\partial x_2}cu_2^s u_i^s + \frac{\partial}{\partial x_3}cu_3^s u_i^s = \frac{F_i^D}{\rho s} + cg_i + \\ + \frac{1}{\rho_s}\left(-\frac{\partial}{\partial x_i}p^s - c\frac{\partial}{\partial x_i}p^f + \frac{\partial}{\partial x_3}\tau_{3i}^s + c\frac{\partial}{\partial x_3}\tau_{3i}^f\right) \quad (2.34)$$

with $i = 1, 2$.

2.4 Number of closure relations needed

The final set of the three dimensional equations that describes a debris flow or hyperconcentrated flow, under the hypothesis of shallow flow, is composed by eight partial differential equations: the continuity equations for the fluid phase (2.14) and for the solid phase (2.15), the two momentum equations (2.27) and (2.30) along the normal direction x_3, the momentum equations for the fluid (2.32) phase and for the solid (2.34) phase on the plain x_1, x_2

$$\begin{cases} \dfrac{\partial}{\partial t}\beta + \dfrac{\partial}{\partial x_1}\beta u_1^f + \dfrac{\partial}{\partial x_2}\beta u_2^f + \dfrac{\partial}{\partial x_3}\beta u_3^f = 0 \\ \dfrac{\partial}{\partial t}c + \dfrac{\partial}{\partial x_1}cu_1^s + \dfrac{\partial}{\partial x_2}cu_2^s + \dfrac{\partial}{\partial x_3}cu_3^s = 0 \\ \dfrac{\partial}{\partial x_3}p^f = \rho_f g_3 \\ \dfrac{\partial}{\partial x_3}p^s = c\rho' g_3 \\ \dfrac{\partial}{\partial t}\beta u_i^f + \dfrac{\partial}{\partial x_j}\beta u_i^f u_j^f = -\dfrac{\beta}{\rho_f}\dfrac{\partial}{\partial x_i}p^f + \dfrac{\beta}{\rho_f}\dfrac{\partial}{\partial x_3}\tau_{3i}^f - \dfrac{F_i^D}{\rho_f} + \beta g_i \\ \dfrac{\partial}{\partial t}cu_i^s + \dfrac{\partial}{\partial x_j}cu_i^s u_j^s = \dfrac{1}{\rho_s}\left(-\dfrac{\partial}{\partial x_i}p^s - c\dfrac{\partial}{\partial x_i}p^f + \dfrac{\partial}{\partial x_3}\tau_{3i}^s + c\dfrac{\partial}{\partial x_3}\tau_{3i}^f\right) + \\ \qquad\qquad + \dfrac{F_i^D}{\rho s} + cg_i \end{cases} \quad (2.35)$$

with $i = 1, 2$ and $j = 1, 2, 3$.

Looking at the unknowns, they are the fluid and solid velocities in the three directions (u_i^f and u_i^s with $i = 1, 2, 3$), the solid volume concentration

(c), the solid and liquid pressures (p^s and p^f) and the stress tensor elements τ_{31} and τ_{32} for the fluid and solid phases. The last two unknowns are the drag forces F_1^D and F_2^D. In total the number of unknowns are now 15, while the equations are only eight. The introduction of seven closure relations are needed, however, as done in Section 1.5, here we do not specify any of them, since in the next Chapter we integrate these equations along the normal direction and then we introduce some other simplifications that reduce drastically the unknowns number.

Chapter 3

Two-dimensional modelling

Frequently, in real cases, debris flow phenomena have the horizontal spatial extension much bigger than the vertical dimension. As said in Chapter 2, this characteristic allows the introduction of the shallow flow approximation that simplifies the three dimensional equation of motion derived in Chapter 1. Nevertheless, as specified in Section 2.4, a three dimensional shallow flow model needs a lot of closure relations still not available in the literature. However for many practical use, e.g. the realization of hazard map, disaster prevention plan and mitigation structures or the study of the morphology of rivers and creeks, the vertical structure of the flow (i.e. the vertical profile of concentration, velocity, pressure, ...) is not so important compared to the planar one. For this reason it is convenient to introduce a two dimensional depth integrated shallow flow approach, widely used in the field of free-surface flow applications where only the depth-averaged values of the flow variables are present.

The switch from a $3D$ shallow flow (SF) model to a $2D$ depth averaged model is performed depth integrating the equations of motion (2.35) derived in Chapter 2. The depth integration is performed along the normal to the bottom direction between the bottom and the free surface. The choice of the normal direction reflect what it was done in the derivation of the SF equations in Chapter 2. Therefore, using the same reference system, the depth integration is consistent with the SF approximation. The integrated equations are then expressed in terms of depth average quantities (in a similar

way as for the derivation of the 3D continuum equations for fluid-granular mixture described in Chapter 1). With this procedure, in this Chapter we derive the *fully* two-phase, two dimensional depth averaged models for mobile and fixed bed. The distinction between the two models is necessary since, as we explain better later on, the bed elevation in the first model can change in time due to exchange of solid and liquid mass between the flow field and the bed itself. On the contrary, in the fixed bed model the bed elevation is fixed in time since the mass exchange is hindered due to the presence, for example, of a bedrock surface or a paved channel. The derivation of both models is necessary inasmuch the main objective of the thesis is to study the transition between fixed and mobile bed.

In this Chapter, we also introduce the *isokinetic* approximations, in which the solid and fluid velocities are equal, deriving the so called isokinetic mobile and fixed models. This approximation is necessary for the simplification the two-dimensional fully two-phase models since, as we explain better later on, they are quite complicated and lots of closure relations are needed. Indeed in the literature there are still not complete and reliable closure relations valid for debris flow.

During the derivation of all these models we assume that fluid and solid phases are present in all the flow field, so we disregard all the extreme cases, e.g. the plug flow (see [40] for a classification of the different cases of flow).

The Chapter is structured as follow: in Chapter 3.1 the two dimensional depth integrated equations of motion for the mobile bed are derived, while Chapter 3.2 is devoted derivation of the depth integrated equations for the fixed bed system. The isokinetic approximation is introduce in Chapter 3.3 and finally a short literature review of two-dimensional SF models is presented in Chapter 3.4 with a comparison with the models we derived.

3.1 Fully two-phase free-surface mobile bed system

The two-phase, free-surface phenomena with mobile bed are characterized by the presence of two distinct surfaces of separation between the mixture

(composed by fluid and solid phase) an the surrounding environment, where these surfaces change in time. The first one describes the free-surface and separates the flow from the air above. The other one separates the flow from the static bed where no flow is present (velocities of fluid and solid phase are null). Once these surfaces are defined, appropriated boundary conditions can be set on them and definite integration of the shallow flow equations derived in Chapter 2 can be done, obtaining the mobile bed system.

3.1.1 Boundary conditions

The first step for the depth integration of the equations, is the definition of the appropriate boundary conditions that have to be applied on the separation surfaces. In the follow they are explained in details.

Free surface conditions

Mathematically, the free-surface η can be expressed as

$$\eta(x_1, x_2, t) = z_b(x_1, x_2, t) + H(x_1, x_2, t)$$

where z_b is the bed elevation and H is the flow depth (see Figure 3.1 for a sketch of the variables). It is useful to introduce the function ψ defined as

$$\psi(x_1, x_2, x_3, t) = \eta(x_1, x_2, t) - x_3 = 0$$

where x_3 is the normal direction. We highlight that ψ is a function of the space x_i and time t. Since the function ψ is identically zero, also the total time derivative is null

$$\frac{d\psi}{dt} = \frac{\partial \eta}{\partial t} + u_1^{int}\frac{\partial \eta}{\partial x_1} + u_2^{int}\frac{\partial \eta}{\partial x_2} - u_3^{int} = 0 \tag{3.1}$$

in which u_j^{int} is the j-th component of the velocity of the interface.

On this surface, since no penetration or detachment of the three different phases (air, solid and fluid) occurs, the interface, the solid ($\mathbf{u}^s$) and the fluid ($\mathbf{u}^f$) velocities are the same

$$\mathbf{u}^{int} = \left[\mathbf{u}^s\right]_\eta = \left[\mathbf{u}^f\right]_\eta \tag{3.2}$$

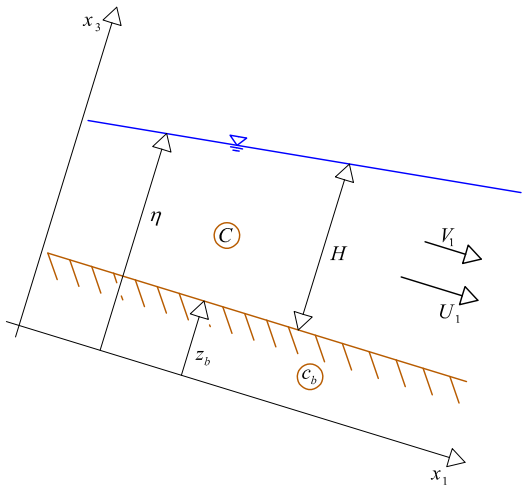

Figure 3.1: Sketch of the main variables of the problem.

In this way two distinct kinematic boundary conditions are obtained

$$\frac{\partial \eta}{\partial t} + \left[u_1^f\right]_\eta \frac{\partial \eta}{\partial x_1} + \left[u_2^f\right]_\eta \frac{\partial \eta}{\partial x_2} - \left[u_3^f\right]_\eta = 0 \tag{3.3}$$

$$\frac{\partial \eta}{\partial t} + [u_1^s]_\eta \frac{\partial \eta}{\partial x_1} + [u_2^s]_\eta \frac{\partial \eta}{\partial x_2} - [u_3^s]_\eta = 0 \tag{3.4}$$

Bed surface conditions

The bottom surface $z_b(x_1, x_2, t)$ is the locus of points with null fluid and solid velocity below which, in the vertical direction, all the other points have still null fluid and solid velocity. On this surface we use, as boundary condition, the null velocities statement

$$\left[u_1^f\right]_{z_b} = \left[u_2^f\right]_{z_b} = \left[u_3^f\right]_{z_b} = 0 \tag{3.5}$$

$$[u_1^s]_{z_b} = [u_2^s]_{z_b} = [u_3^s]_{z_b} = 0 \tag{3.6}$$

The velocities, as specified in the definition of bottom surface, are null even below the bottom, since we disregard possible underground flow. Finally we want to highlight that the bottom elevation is a function of space and time, since we are speaking about mobile bed system.

Another important aspect of the bed is represented by the concentration: the solid bed concentration (the solid concentration below bottom elevation)

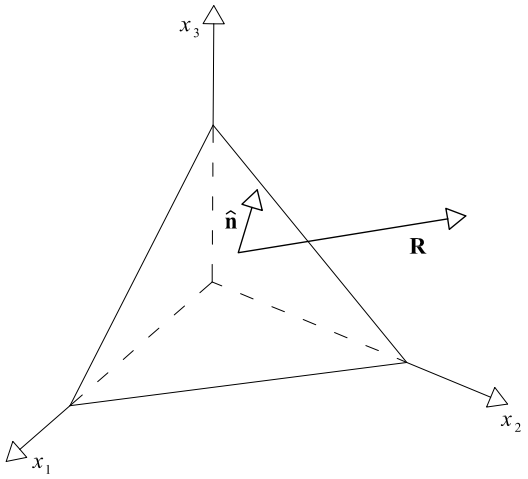

Figure 3.2: Sketch of a generic stress vector $\mathbf{R}$ applied on a surface with normal $\hat{\mathbf{n}}$.

is constant in time and space, is called c_b and depends essentially on the granulometric distribution of bed material. Usually it is about $0.6 \div 0.65$. The rest of the volume inside the bed is occupied by the interstitial fluid, so when an erosion occurs (the bed elevation decreases) a release of solid and fluid phases happens; on the contrary, when deposition occurs (the bed elevation increases) an amount of solid and liquid phase are trapped. The concentration c_b is also the limit value for the concentration inside the mixture when we are dealing with debris flows.

Shear stresses at the bottom and at the free surface

Given a stress vector $\mathbf{R}$ applied on a surface with normal $\hat{\mathbf{n}}$ (see figure 3.2 for a sketch), the component along the i-th axis can be expressed using the Chaucy's stress theorem

$$R_i = T_{1i}n_1 + T_{2i}n_2 + T_{3i}n_3 = T_{ji}n_j$$

in which n_j is the j-th component of the surface outward normal and T_{ji} is the ji element of the stress tensor $\mathbf{T}$.

Given a generic surface $\psi = 0$, the outward normal vector $\hat{n}$ is

$$\hat{\mathbf{n}} = \frac{\nabla\psi}{|\nabla\psi|}$$

and in our case, for the free surface, the normal becomes

$$\hat{\mathbf{n}}_\eta = \frac{\left(-\frac{\partial \eta}{\partial x_1}; -\frac{\partial \eta}{\partial x_2}; 1\right)}{r_\eta} \tag{3.7}$$

where

$$r_\eta = \sqrt{\left(\frac{\partial \eta}{\partial x_1}\right)^2 + \left(\frac{\partial \eta}{\partial x_2}\right)^2 + 1} \tag{3.8}$$

while for the bottom is

$$\hat{\mathbf{n}}_{z_b} = \frac{\left(-\frac{\partial z_b}{\partial x_1}; -\frac{\partial z_b}{\partial x_2}; 1\right)}{r_{z_b}} \tag{3.9}$$

in which

$$r_{z_b} = \sqrt{\left(\frac{\partial z_b}{\partial x_1}\right)^2 + \left(\frac{\partial z_b}{\partial x_2}\right)^2 + 1} \tag{3.10}$$

Using the above definitions, the projections along the x_1, x_2 directions of the stress vector, for the fluid (f) and solid (s) phases, at the bottom, are

$$\tau_{i,z_b}^{f,s} = \frac{1}{r_{z_b}} \left(- \left[\tau_{1i}^{f,s}\right]_{z_b} \frac{\partial z_b}{\partial x_1} - \left[\tau_{2i}^{f,s}\right]_{z_b} \frac{\partial z_b}{\partial x_2} + \left[\tau_{3i}^{f,s}\right]_{z_b} \right) \tag{3.11}$$

where $i = 1, 2$ while, at the free surface, they are

$$\tau_{i,\eta}^{f,s} = \frac{1}{r_\eta} \left(- \left[\tau_{1i}^{f,s}\right]_{\eta} \frac{\partial \eta}{\partial x_1} - \left[\tau_{2i}^{f,s}\right]_{\eta} \frac{\partial \eta}{\partial x_2} + \left[\tau_{3i}^{f,s}\right]_{\eta} \right) \tag{3.12}$$

where $i = 1, 2$.

Usually, in the field of debris flow and hyperconcentrated flow, the stress vectors at the free surface are negligible respect to all the other forces. This happens since these stresses are produced by the wind forces that usually are very weak respect to other forces acting inside the flow. Therefore expression (3.12) becomes null

$$\tau_{1,\eta}^{f} = \tau_{2,\eta}^{f} = 0 \tag{3.13}$$

$$\tau_{1,\eta}^{s} = \tau_{2,\eta}^{s} = 0 \tag{3.14}$$

Pressures at the free surface

Concerning the solid and liquid pressures on the free surface, we assume that they are null, since it is widely used working with relative pressure where the atmospheric one is considered as reference pressure, so

$$p_\eta^s = p_\eta^f = 0 \tag{3.15}$$

3.1.2 Continuity equations

The $3D$ shallow flow equation describing the fluid mass balance (2.14) can be expressed in the following way

$$-\frac{\partial}{\partial t}c + \frac{\partial}{\partial x_j}u_j^f - \frac{\partial}{\partial x_j}cu_j^f = 0 \tag{3.16}$$

The depth integration gives

$$-\int_{z_b(x_1,x_2,t)}^{\eta(x_1,x_2,t)} \frac{\partial}{\partial t}c \; dx_3 + \int_{z_b(x_1,x_2,t)}^{\eta(x_1,x_2,t)} \frac{\partial}{\partial x_j}u_j^f \; dx_3 - \int_{z_b(x_1,x_2,t)}^{\eta(x_1,x_2,t)} \frac{\partial}{\partial x_j}cu_j^f \; dx_3 = 0$$

where we highlight the space and time dependency of the domain integration extrema. Introducing the definition of the depth average expression for a generic quantity $f(\mathbf{x}, t)$

$$F(x_1, x_2, t) = \frac{1}{H}\int_{z_b}^{\eta} f(\mathbf{x}, t) \; dx_3 \tag{3.17}$$

where H is the mixture depth defined as

$$H = \int_{z_b}^{\eta} dx_3 = \eta - z_b \tag{3.18}$$

and, since we want to express, as said before, the terms of the equation as a depth average value, it is necessary to switch the integral with the derivatives. Because the integration extrema depend on space and time, the switch between integration and derivative can be done via the Leibniz

integration rule, obtaining

$$
\begin{aligned}
&-\left(\frac{\partial}{\partial t}\int_{z_b}^{\eta} c\ dx_3 - [c]_\eta \frac{\partial \eta}{\partial t} + [c]_{z_b}\frac{\partial z_b}{\partial t}\right) + \\
&+\left(\frac{\partial}{\partial x_1}\int_{z_b}^{\eta} u_1^f\ dx_3 - \left[u_1^f\right]_\eta \frac{\partial \eta}{\partial x_1} + \left[u_1^f\right]_{z_b}\frac{\partial z_b}{\partial x_1}\right) + \\
&+\left(\frac{\partial}{\partial x_2}\int_{z_b}^{\eta} u_2\ dx_3 - \left[u_2^f\right]_\eta \frac{\partial \eta}{\partial x_2} + \left[u_2^f\right]_{z_b}\frac{\partial z_b}{\partial x_2}\right) + \left(\left[u_3^f\right]_\eta - \left[u_3^f\right]_{z_b}\right) + \\
&-\left(\frac{\partial}{\partial x_1}\int_{z_b}^{\eta} cu_1^f\ dx_3 - \left[cu_1^f\right]_\eta \frac{\partial \eta}{\partial x_1} + \left[cu_1^f\right]_{z_b}\frac{\partial z_b}{\partial x_1}\right) + \\
&-\left(\frac{\partial}{\partial x_2}\int_{z_b}^{\eta} cu_2^f\ dx_3 - \left[cu_2^f\right]_\eta \frac{\partial \eta}{\partial x_2} + \left[cu_2^f\right]_{z_b}\frac{\partial z_b}{\partial x_2}\right) - \left(\left[cu_3^f\right]_\eta - \left[cu_3^f\right]_{z_b}\right) = 0
\end{aligned}
$$

Regrouping the different terms, the following expression is obtained

$$
\begin{aligned}
&-\frac{\partial}{\partial t}\int_{z_b}^{\eta} c\ dx_3 + \frac{\partial}{\partial x_1}\int_{z_b}^{\eta} u_1^f\ dx_3 - \frac{\partial}{\partial x_1}\int_{z_b}^{\eta} cu_1^f\ dx_3 + \frac{\partial}{\partial x_2}\int_{z_b}^{\eta} u_2^f\ dx_3 + \\
&-\frac{\partial}{\partial x_2}\int_{z_b}^{\eta} cu_2^f\ dx_3 + [c]_\eta \underbrace{\left(\frac{\partial \eta}{\partial t} + \left[u_1^f\right]_\eta \frac{\partial \eta}{\partial x_1} + \left[u_2^f\right]_\eta \frac{\partial \eta}{\partial x_2} - \left[u_3^f\right]_\eta\right)}_{I} + \\
&\underbrace{-\left(\left[u_1^f\right]_\eta \frac{\partial \eta}{\partial x_1} + \left[u_2^f\right]_\eta \frac{\partial \eta}{\partial x_2} - \left[u_3^f\right]_\eta\right)}_{II} + \\
&-[c]_{z_b}\underbrace{\left(\frac{\partial z_b}{\partial t} + \left[u_1^f\right]_{z_b}\frac{\partial z_b}{\partial x_1} + \left[u_2^f\right]_{z_b}\frac{\partial z_b}{\partial x_2} - \left[u_3^f\right]_{z_b}\right)}_{III} + \\
&\qquad\qquad + \underbrace{\left(\left[u_1^f\right]_{z_b}\frac{\partial z_b}{\partial x_1} + \left[u_2^f\right]_{z_b}\frac{\partial z_b}{\partial x_2} - \left[u_3^f\right]_{z_b}\right)}_{IV} = 0 \quad (3.19)
\end{aligned}
$$

In this expression term I is nothing but the kinematic boundary condition for the fluid phase at free surface (3.3), so it is null. Using the same boundary condition, the term II becomes

$$II = -\frac{\partial \eta}{\partial t}$$

The term III, due to the non-slip and impermeability condition at the bottom (3.5) reduces to

$$III = \frac{\partial z_b}{\partial t}$$

while, for the same reasons, the term IV is zero. Finally, remembering that at the bottom the solid concentration is constant and equal to c_b, the depth integrated equation for the mass conservation of the fluid phase becomes

$$-\frac{\partial}{\partial t}\int_{z_b}^{\eta} c\ dx_3 + \frac{\partial}{\partial x_1}\int_{z_b}^{\eta} u_1^f\ dx_3 - \frac{\partial}{\partial x_1}\int_{z_b}^{\eta} cu_1^f\ dx_3 + \frac{\partial}{\partial x_2}\int_{z_b}^{\eta} u_2^f\ dx_3 + \\ - \frac{\partial}{\partial x_2}\int_{z_b}^{\eta} cu_2^f\ dx_3 + \frac{\partial \eta}{\partial t} - c_b\frac{\partial z_b}{\partial t} = 0 \quad (3.20)$$

Using the definition of the depth average quantity (3.17) to the motion variables, the fluid phase mass conservation becomes

$$\frac{\partial}{\partial t}(1-C)\,H + (1-c_b)\frac{\partial z_b}{\partial t} + \frac{\partial}{\partial x_1}(1-\alpha_{cu_1}C)\,HU_1 + \\ + \frac{\partial}{\partial x_2}(1-\alpha_{cu_2}C)\,HU_2 = 0 \quad (3.21)$$

where C, U_1 and U_2 are the depth average solid concentration c, fluid velocities u_1^f and u_2^f respectively. Finally

$$\alpha_{cu_1} = \frac{\int_{z_b}^{\eta} cu_1^f\ dz}{CHU_1} \quad (3.22)$$

$$\alpha_{cu_2} = \frac{\int_{z_b}^{\eta} cu_2^f\ dz}{CHU_2} \quad (3.23)$$

are two corrective coefficients. These coefficients arise since we are expressing the integral of the product between two (or more) variables with a non uniform vertical profiles (in Figure 3.3 is sketched a qualitative vertical distribution of concentration and velocity) in terms of their depth average counterparts.

Moving now to the solid phase, the mass balance equation (2.15) reads

$$\frac{\partial c}{\partial t} + \frac{\partial cu_j^s}{\partial x_j} = 0$$

and following the same procedure as for the fluid phase, the depth averaged equation becomes

$$\frac{\partial}{\partial t}(CH) + c_b\frac{\partial z_b}{\partial t} + \frac{\partial}{\partial x_1}(\alpha_{cv_1}CHV_1) + \frac{\partial}{\partial x_2}(\alpha_{cv_2}CHV_2) = 0 \quad (3.24)$$

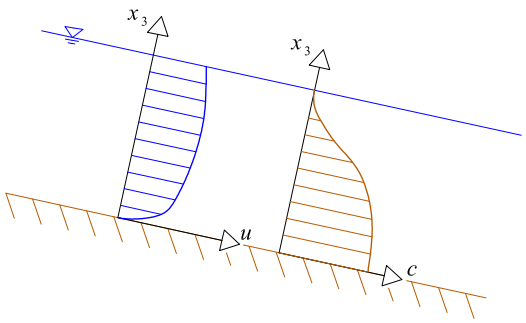

Figure 3.3: Sketch of a qualitative profile of the concentration c and velocity u along x_3 for an hyperconcentrated flow over mobile bed.

where the boundary condition expressed by equations (3.4) and (3.6) have been used. In equation (3.24) the terms V_1 and V_2 are the depth average value of solid velocities u_1^s and u_2^s respectively, while the two corrective coefficients are

$$\alpha_{cv_1} = \frac{\int_{z_b}^{\eta} c u_1^s \, dz}{CHV_1} \tag{3.25}$$

$$\alpha_{cv_2} = \frac{\int_{z_b}^{\eta} c u_2^s \, dz}{CHV_2} \tag{3.26}$$

3.1.3 Momentum equations

Pressure distributions

The momentum along x_3 for the fluid phase (2.27) reads

$$\frac{\partial p^f}{\partial x_3} = \rho_f g_3 \tag{3.27}$$

where g_3 is the component of the gravity force along the x_3 direction. Performing an indefinite integral along x_3, the results is

$$p^f(x_3) = \rho_f g_3 x_3 + K_f \tag{3.28}$$

where the constant K_f can be evaluated at free surface thanks to the boundary condition (3.15)

$$p^f(\eta) = 0 = \rho_f g_3 \eta + K_f$$

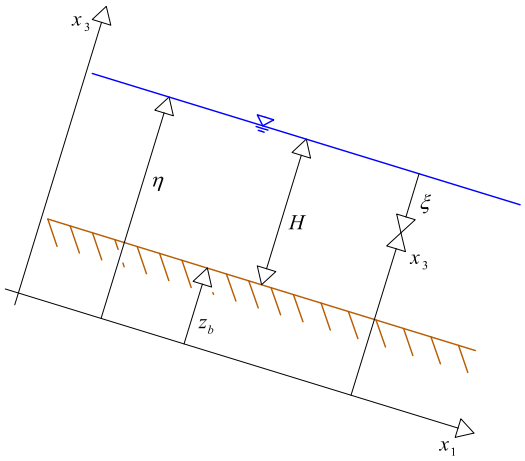

Figure 3.4: Sketch of the reference system with the direction ξ.

from which follows

$$K_f = -\rho_f g_3 \left(z_b + H\right) \tag{3.29}$$

and

$$p^f \left(x_3\right) = -\rho_f g_3 \left(z_b + H - x_3\right) \tag{3.30}$$

therefore, with the assumption of shallow flow, the fluid pressure distribution is hydrostatic, as said before and also supposed in Section 2.1.

It is useful to define the variable $\xi = \eta - x_3$ sketched in Figure 3.4 and performing the depth integration using this variable, the fluid pressure distribution becomes

$$p^f \left(\xi\right) = -\rho_f g_3 \xi \tag{3.31}$$

In a similar way it is possible to evaluate the solid pressure distribution starting from equation (2.30) that is

$$\frac{\partial}{\partial x_3} p^s = c \rho' g_3 \tag{3.32}$$

where $\rho' = \rho_s - \rho_f$ is the submerged solid density. Performing the same integration as for the fluid phase, the result is

$$p^s \left(x_3\right) = \rho' g_3 \int_0^{x_3} c \; dx_3' + K_s \tag{3.33}$$

where the constant K_s is evaluated imposing the boundary condition (3.15)

$$p^s(\eta) = 0 = \rho' g_3 \int_0^\eta c \, dx_3 + K_s$$

obtaining

$$\begin{aligned} K_s &= -\rho' g_3 \int_0^\eta c \, dx_3 = -\rho' g \left(\int_0^{z_b} c \, dx_3 + \int_{z_b}^\eta c \, dx_3 \right) \\ &= -\rho' g_3 \left(c_b z_b + CH \right) \end{aligned} \tag{3.34}$$

So the final expression for the solid pressure distribution under the hypothesis of shallow flow is

$$p^s(x_3) = -\rho' g_3 \left(c_b z_b + CH - \int_0^{x_3} c \, dx_3' \right) \tag{3.35}$$

In this expression the integral of the concentration is undefined since it is strictly depending on the concentration distribution. The solution of the integral will be discuss later on in this Section where the momentum equations in directions x_1, x_2 for the liquid phase are integrated.

As for the fluid phase, it useful to perform the integration of the solid pressure using the ξ variable, obtaining

$$p^s(\xi) = -\rho' g_3 \int_0^\xi c \, d\xi' \tag{3.36}$$

The solid and fluid pressures evaluated at the bed surface are

$$p^f\big|_{z_b} = -\rho_f g_3 H \tag{3.37}$$

$$p^s\big|_{z_b} = -\rho' g_3 CH \tag{3.38}$$

and these expressions will be useful in later on, where the depth integration of the momentum equations along x_1 and x_2, are performed.

The fluid phase momentum on the x_1, x_2 plane

The depth integral of the $3D$ SF equation for the fluid momentum along the x_1 direction derived in Section 2.3, is

$$\underbrace{\int_{z_b}^{\eta}\left(\frac{\partial}{\partial t}(1-c)u_1^f+\frac{\partial}{\partial x_j}(1-c)u_1^f u_j^f\right)\,dx_3}_{I}=$$
$$\underbrace{-\int_{z_b}^{\eta}\frac{(1-c)}{\rho_f}\frac{\partial}{\partial x_1}p^f\,dx_3}_{II}+\underbrace{\int_{z_b}^{\eta}\frac{(1-c)}{\rho_f}\frac{\partial}{\partial x_3}\tau_{31}^f\,dx_3}_{III}+\underbrace{\int_{z_b}^{\eta}\left((1-c)g_1-\frac{F_1^D}{\rho_f}\right)\,dx_3}_{IV} \tag{3.39}$$

with $j=1,2,3$. Since the momentum equation has a lot of different terms that have to be integrated, we group them in four categories that have the same integration strategy: the advective terms (I), the pressure term (II), the shear stress (III) and gravity and drag forces (IV).

Expansion of term I, using the Leibniz rule, gives

$$I=\frac{\partial}{\partial t}\int_{z_b}^{\eta}(1-c)u_1^f\,dx_3+\frac{\partial}{\partial x_1}\int_{z_b}^{\eta}(1-c)u_1^f u_1^f\,dx_3+\frac{\partial}{\partial x_2}\int_{z_b}^{\eta}(1-c)u_1^f u_2^f\,dx_3+$$
$$\underbrace{-\left[(1-c)\,u_1^f\right]_\eta\left(\frac{\partial\eta}{\partial t}+\left[u_1^f\right]_\eta\frac{\partial\eta}{\partial x_1}+\left[u_2^f\right]_\eta\frac{\partial\eta}{\partial x_2}-\left[u_3^f\right]_\eta\right)}_{a}+$$
$$\underbrace{+\left[(1-c)\,u_1^f\right]_{z_b}\left(\frac{\partial z_b}{\partial t}+\left[u_1^f\right]_{z_b}\frac{\partial z_b}{\partial x_1}+\left[u_2^f\right]_{z_b}\frac{\partial z_b}{\partial x_2}-\left[u_3^f\right]_{z_b}\right)}_{b}$$

Using the kinematic boundary condition (3.3), term a becomes null, while using the bed boundary condition (3.5) term b becomes null. The previous expression reduces now to

$$I=\frac{\partial}{\partial t}\int_{z_b}^{\eta}(1-c)u_1^f\,dx_3+\frac{\partial}{\partial x_1}\int_{z_b}^{\eta}(1-c)u_1^f u_1^f\,dx_3+\frac{\partial}{\partial x_2}\int_{z_b}^{\eta}(1-c)u_1^f u_2^f\,dx_3$$

Finally, using the definition of depth average variable (3.17) and introducing

the following corrective coefficients

$$\alpha_{cu_1u_1} = \frac{\int_{z_b}^{\eta} cu_1^f u_1^f \, dz}{CHU_1U_1} \tag{3.40}$$

$$\alpha_{cu_1u_2} = \frac{\int_{z_b}^{\eta} cu_1^f u_2^f \, dz}{CHU_1U_2} \tag{3.41}$$

the depth integration of term I becomes

$$I = \frac{\partial}{\partial t}(1-\alpha_{cu_1}C)HU_1 + \frac{\partial}{\partial x_1}(1-\alpha_{cu_1u_1}C)HU_1U_1 + \\ + \frac{\partial}{\partial x_2}(1-\alpha_{cu_1u_2}C)HU_1U_2 \tag{3.42}$$

Term II can be expanded as

$$-\frac{(1-c)}{\rho_f}\frac{\partial}{\partial x_1}p^f = \underbrace{-\frac{1}{\rho_f}\frac{\partial}{\partial x_1}p^f}_{a} + \underbrace{\frac{c}{\rho_f}\frac{\partial}{\partial x_1}p^f}_{b} \tag{3.43}$$

Integration of term a, using the Leibniz rule, gives

$$-\frac{1}{\rho_f}\int_{z_b}^{\eta}\frac{\partial}{\partial x_1}p^f \, dx_3 = -\frac{1}{\rho_f}\left(\frac{\partial}{\partial x_1}\int_{z_b}^{\eta} p^f \, dx_3 - \left[p^f\right]_{\eta}\frac{\partial \eta}{\partial x_1} + \left[p^f\right]_{z_b}\frac{\partial z_b}{\partial x_1}\right)$$

Using the hydrostatic fluid pressure distribution (3.30), the value of the pressure at the bottom (3.37) and the boundary condition at the free surface (3.15), this expression reduces to

$$-\frac{1}{\rho_f}\int_{z_b}^{\eta}\frac{\partial}{\partial x_1}p^f \, dx_3 = \frac{\partial}{\partial x_1}g_3\frac{H^2}{2} + g_3H\frac{\partial z_b}{\partial x_1} \tag{3.44}$$

However the last term of this equation is null since, for the reference system used (direction x_1 and x_2 are tangential to the bed surface) we have

$$\frac{\partial z_b}{\partial x_i} = 0 \tag{3.45}$$

for $i = 1, 2$. We want to highlight that this term is different from zero when other types of reference systems are used, e.g. the one used in Chapter 4. The depth integration of a is then

$$-\frac{1}{\rho_f}\int_{z_b}^{\eta}\frac{\partial}{\partial x_1}p^f \, dx_3 = \frac{\partial}{\partial x_1}g_3\frac{H^2}{2} \tag{3.46}$$

The integral of term b in (3.43) presents a product between two quantities: the concentration c and the derivative of the fluid pressure respect direction x_1. It is possible to define, as for all the other terms integrated before where a product of two variables is present, a corrective coefficient α_{p_1} that allows to express the integral in terms of the depth average variables, namely

$$\alpha_{p_1} = \frac{\displaystyle\int_{z_b}^{\eta} c\frac{\partial}{\partial x_1}p^f \; dx_3}{HC\left(\dfrac{1}{H}\displaystyle\int_{z_b}^{\eta}\frac{\partial p^f}{\partial x_1}\; dx_3\right)} \tag{3.47}$$

Using this coefficient, the integration of b using the Leibniz rule gives

$$\int_{z_b}^{\eta}\frac{c}{\rho_f}\frac{\partial}{\partial x_1}p^f = \frac{\alpha_{p_1}C}{\rho_f}\left(\frac{\partial}{\partial x_1}\int_{z_b}^{\eta}p^f\; dx_3 - \left[p^f\right]_{\eta}\frac{\partial \eta}{\partial x_1} + \left[p^f\right]_{z_b}\frac{\partial z_b}{\partial x_1}\right)$$

Introducing the hydrostatic fluid pressure distribution (3.30) with the same boundary condition as before, the resulting expression is

$$\int_{z_b}^{\eta}\frac{c}{\rho_f}\frac{\partial}{\partial x_1}p^f\; dx_3 = -\alpha_{p_1}C\frac{\partial}{\partial x_1}g_3\frac{H^2}{2} \tag{3.48}$$

thus term II of (3.39) becomes

$$II = (1-\alpha_{p_1}C)\frac{\partial}{\partial x_1}g_3\frac{H^2}{2} \tag{3.49}$$

The term III is integrated in a similar way as II obtaining

$$\frac{(1-\alpha_{\tau_1}C)}{\rho_f}\left(\left[\tau_{31}^f\right]_{\eta} - \left[\tau_{31}^f\right]_{z_b}\right)$$

where

$$\alpha_{\tau_1} = \frac{\displaystyle\int_{z_b}^{\eta} c\frac{\partial}{\partial x_3}\tau_{31}^f\; dx_3}{HC\left(\dfrac{1}{H}\displaystyle\int_{z_b}^{\eta}\frac{\partial}{\partial x_3}\tau_{31}^f\; dx_3\right)} \tag{3.50}$$

Using the boundary condition concerning the fluid shear stresses at the bed (3.11), at the free-surface (3.13) and remembering that, for the shallow flow approximation, the terms τ_{11}^f and τ_{21}^f are negligible, the term III reduces to

$$III = -\frac{(1-\alpha_{\tau_1}C)}{\rho_f}r_{z_b}\tau_{1,z_b}^f \tag{3.51}$$

For the term IV of (3.39), its integral is

$$g_1 \int_{z_b}^{\eta} (1-c)\ dx_3 - \frac{1}{\rho_f} \int_{z_b}^{\eta} F_1^D\ dx_3$$

obtaining

$$IV = (1-C)\, g_1 H - \frac{1}{\rho_f} H \mathcal{F}_1^D \tag{3.52}$$

where

$$\mathcal{F}_i^D = \frac{1}{H} \int_{z_b}^{\eta} F_i^D\ dx_3 \tag{3.53}$$

is the depth average value of the drag force along x_1.

Assembling all the terms of the initial equation (3.39), namely the terms (3.42), (3.49), (3.51) and (3.52), the $2D$ depth averaged SF equation for the momentum of the fluid phase along x_1 direction becomes

$$\begin{aligned} &\frac{\partial}{\partial t}(1-\alpha_{cu_1} C) H U_1 + \frac{\partial}{\partial x_1}(1-\alpha_{cu_1 u_1} C) H U_1 U_1 + \frac{\partial}{\partial x_2}(1-\alpha_{cu_1 u_2} C) H U_1 U_2 = \\ &= (1-\alpha_{p_1} C)\, \frac{\partial}{\partial x_1} g_3 \frac{H^2}{2} - \frac{(1-\alpha_{\tau_1} C)}{\rho_f} r_{z_b} \tau^f_{1,z_b} - \frac{1}{\rho_f} H \mathcal{F}_1^D + \\ &\qquad + (1-C)\, g_1 H \end{aligned} \tag{3.54}$$

For the x_2 direction, the derivation is similar and the final result is

$$\begin{aligned} &\frac{\partial}{\partial t}(1-\alpha_{cu_2} C) H U_2 + \frac{\partial}{\partial x_1}(1-\alpha_{cu_1 u_2} C) H U_1 U_2 + \frac{\partial}{\partial x_2}(1-\alpha_{cu_2 u_2} C) H U_2 U_2 = \\ &= (1-\alpha_{p_2} C)\, \frac{\partial}{\partial x_2} g_3 \frac{H^2}{2} - \frac{(1-\alpha_{\tau_2} C)}{\rho_f} r_{z_b} \tau^f_{2,z_b} - \frac{1}{\rho_f} H \mathcal{F}_2^D + \\ &\qquad + (1-C)\, g_2 H \end{aligned} \tag{3.55}$$

In this equation the following corrective coefficients have been introduced

$$\alpha_{cu_2 u_2} = \frac{\int_{z_b}^{\eta} c u_2 u_2\ dz}{C H U_2 U_2} \tag{3.56}$$

$$\alpha_{p_2} = \frac{\displaystyle\int_{z_b}^{\eta} c\frac{\partial}{\partial x_2}p^f \; dx_3}{HC\left(\dfrac{1}{H}\displaystyle\int_{z_b}^{\eta}\frac{\partial p^f}{\partial x_2}\; dx_3\right)} \tag{3.57}$$

$$\alpha_{\tau_2} = \frac{\displaystyle\int_{z_b}^{\eta} c\frac{\partial}{\partial x_3}\tau_{32}^f \; dx_3}{HC\left(\dfrac{1}{H}\displaystyle\int_{z_b}^{\eta}\frac{\partial}{\partial x_3}\tau_{32}^f\; dx_3\right)} \tag{3.58}$$

The solid phase momentum on the x_1, x_2 plane

The $3D$ solid phase momentum equation along x_1 (2.34), derived in Chapter 2, is integrated in a similar way as for the fluid phase. The only term, that has a different treatment regards the integration of the solid pressure derivative

$$\int_{z_b}^{\eta}\frac{\partial}{\partial x_1}p^s \; dx_3 \tag{3.59}$$

The integral is evaluated, first of all, using the Leibniz rule obtaining

$$\frac{\partial}{\partial x_1}\int_{z_b}^{\eta} p^s \; dx_3 - [p^s]_{\eta}\frac{\partial \eta}{\partial x_1} + [p^s]_{z_b}\frac{\partial z_b}{\partial x_1}$$

Introducing now the expression for the hydrostatic solid pressure distribution presented in equation (3.35) and remembering that, for the reference system used the bed elevation derivative is null, the integral becomes

$$\rho' g_3 \frac{\partial}{\partial x_1}\left(\int_{z_b}^{\eta}\underbrace{\int_0^{x_3} c\; dx_3\; dx_3}_{a} - \int_{z_b}^{\eta} c_b z_b\; dx_3 - \int_{z_b}^{\eta} CH\; dx_3\right) \tag{3.60}$$

Term a can be divided in two integral and, since $c = c_b$ below the bed elevation, it becomes

$$\begin{aligned}\int_0^{x_3} c\; dx_3\; dx_3 &= \int_0^{z_b} c\; dx_3\; dx_3 + \int_{z_b}^{x_3} c\; dx_3\; dx_3 \\ &= c_b z_b + \int_{z_b}^{x_3} c\; dx_3\; dx_3\end{aligned}$$

Using this equation, expression (3.60) simplifies as

$$\rho' g_3 \frac{\partial}{\partial x_1} \left(\int_{z_b}^{\eta} \int_{z_b}^{x_3} c \; dx_3 \; dx_3 - \int_{z_b}^{\eta} CH \; dx_3 \right)$$

and, since CH is constant along x_3, it becomes

$$\rho' g_3 \frac{\partial}{\partial x_1} \left(\int_{z_b}^{\eta} \int_{z_b}^{x_3} c \; dx_3 \; dx_3 - CH^2 \right)$$

The problem arise when we have to evaluate the double integral, since the inner one is strictly related to the vertical concentration distribution. It is possible to introduce, also in this case, a corrective coefficient for the evaluation of the integral defined as

$$\alpha_c = 2 \frac{\int_{z_b}^{\eta} \int_{z_b}^{x_3} c \; dx_3 \; dx_3}{CH^2} \tag{3.61}$$

Using this coefficient, the depth integration of the solid pressure terms is

$$\int_{z_b}^{\eta} \frac{\partial}{\partial x_1} p^s \; dx_3 = -\frac{\partial}{\partial x_1} g_3 C \left(2 - \alpha_c\right) \rho' \frac{H^2}{2} \tag{3.62}$$

The derived $2D$ depth averaged shallow flow equation for the momentum of the solid phase along x_1 direction is

$$\begin{aligned} &\frac{\partial}{\partial t} \alpha_{cv_1} CHV_1 + \frac{\partial}{\partial x_1} \alpha_{cv_1 v_1} CHV_1 V_1 + \frac{\partial}{\partial x_2} \alpha_{cv_1 v_2} CHV_1 V_2 = \\ &= \frac{g_3}{\rho_s} \left(\rho' \frac{\partial}{\partial x_1} C \frac{H^2}{2} \left(2 - \alpha_c\right) + \rho_f \alpha_{p_1} C \frac{\partial}{\partial x_1} \frac{H^2}{2} \right) + \\ &\qquad - \frac{1}{\rho_s} r_{z_b} \left(\tau^s_{1,z_b} + \alpha_{\tau_1} C \tau^f_{1,z_b} \right) + \frac{1}{\rho_s} H \mathcal{F}^D_1 + + C g_1 H \end{aligned} \tag{3.63}$$

where the following corrective coefficients have been used

$$\alpha_{cv_1 v_1} = \frac{\int_{z_b}^{\eta} c u^s_1 u^s_1 \; dz}{CHV_1 V_2} \tag{3.64}$$

$$\alpha_{cv_1 v_2} = \frac{\int_{z_b}^{\eta} c u^s_1 u^s_2 \; dz}{CHV_1 V_2} \tag{3.65}$$

In the same way it is possible derive the averaged momentum for the x_2 direction starting from equation (2.34) with $i = 2$ obtaining the $2D$ vertical averaged shallow flow equation for the momentum of the solid phase along x_2 direction

$$\begin{aligned}
&\frac{\partial}{\partial t}\alpha_{cv_2} CHV_2 + \frac{\partial}{\partial x_1}\alpha_{cv_1v_2} CHV_1V_2 + \frac{\partial}{\partial x_2}\alpha_{cv_2v_2} CHV_2V_2 = \\
&= \frac{g_3}{\rho_s}\left(\rho' \frac{\partial}{\partial x_2} C\frac{H^2}{2}(2-\alpha_c) + \rho_f \alpha_{p_2} C\frac{\partial}{\partial x_2}\frac{H^2}{2}\right) + \\
&\qquad - \frac{1}{\rho_s} r_{z_b}\left(\tau^s_{2,z_b} + \alpha_{\tau_2} C\tau^f_{2,z_b}\right) + \frac{1}{\rho_s} H\mathcal{F}^D_2 + Cg_2 H
\end{aligned} \tag{3.66}$$

where the corrective coefficient

$$\alpha_{cv_2v_2} = \frac{\int_{z_b}^{\eta} cv_2v_2 \, dz}{CHV_2V_2} \tag{3.67}$$

has been used.

3.1.4 Final set of mobile bed motion equations and closure relations

The final set of equations describing the momentum balance in the x_1, x_2 directions are compose by the equations (3.54), (3.55) for the fluid phase and (3.63), (3.66) for the solid one. These equation plus the mass balance for fluid (3.21) and solid phase (3.24) are the set of Partial Differential Equations (PDEs) that describe the $2D$ depth averaged two-phase shallow flow over mobile bed.

$$
\begin{cases}
\dfrac{\partial}{\partial t}\left(1-C\right)H + \left(1-c_b\right)\dfrac{\partial z_b}{\partial t} + \dfrac{\partial}{\partial x_j}\left(1-\alpha_{cu_j}C\right)HU_j = 0 \\
\dfrac{\partial}{\partial t}\left(CH\right) + c_b\dfrac{\partial z_b}{\partial t} + \dfrac{\partial}{\partial x_j}\left(\alpha_{cv_j}CHV_j\right) = 0 \\
\dfrac{\partial}{\partial t}(1-\alpha_{cu_i}C)HU_i + \dfrac{\partial}{\partial x_j}(1-\alpha_{cu_iu_j}C)HU_iU_j = \\
\qquad = \left(1-\alpha_{p_i}C\right)\dfrac{\partial}{\partial x_i}g_3\dfrac{H^2}{2} - \dfrac{\left(1-\alpha_{\tau_i}C\right)}{\rho_f}r_{z_b}\tau^f_{i,z_b} + \\
\qquad\qquad -\dfrac{1}{\rho_f}H\mathcal{F}^D_i + \left(1-C\right)g_iH \\
\dfrac{\partial}{\partial t}\alpha_{cv_i}CHV_i + \dfrac{\partial}{\partial x_j}\alpha_{cv_iv_j}CHV_iV_j = \\
\qquad = \dfrac{g_3}{\rho_s}\left(\rho'\dfrac{\partial}{\partial x_i}C\dfrac{H^2}{2}\left(2-\alpha_c\right) + \rho_f\alpha_{p_i}C\dfrac{\partial}{\partial x_i}\dfrac{H^2}{2}\right) + \\
\qquad\qquad -\dfrac{r_{z_b}}{\rho_s}\left(\tau^s_{i,z_b} + \alpha_{\tau_i}C\tau^f_{i,z_b}\right) + \dfrac{1}{\rho_s}H\mathcal{F}^D_i + Cg_iH
\end{cases}
$$

where $i, j = 1, 2$. The unknowns of this system are: the two components of the fluid velocity U_i, the two components of the solid velocity V_i, the flow depth H, the bottom elevation z_b, the solid concentration C, the two components of the bottom shear stress for the fluid τ^f_{i,z_b} and for the solid phase τ^s_{i,z_b} and the two components of the drag force $\mathcal{F}^D_i$. In total the system is composed by six equations, while the unknowns are 13. Though, the number of unknowns are bigger since all the corrective coefficients are unknowns. For the evaluation of these coefficients, however, it is necessary the knowledge of the vertical distribution of the quantities. Since this is not still available, we assume that

$$\alpha_k = 1 \tag{3.68}$$

where k represent a generic corrective coefficient. With unitary coefficients, we assume that the distributions along the normal direction of the concentration c and the velocities $u_1^{f,s}, u_2^{f,s}$ are constant, i.e.

$$c = C; \qquad c = \phi; \qquad u_i^f = U_i; \qquad u_i^s = V_i$$

Since the equations are only six while the unknown variables are 13, it is necessary to define some closure relation. Typically, the hydrodynamic variables are taken as unknowns, so for this equations they are the four velocity components (U_i and V_i) the flow depth H and the bed elevation z_b. Instead, for the other quantities, we need to introduce some relations that connect them to the hydrodynamic variables.

The first closure relation needed is the one for the concentration C. The literature is full of such relations, mainly of empirical origin and obtained in conditions of equilibrium with respect to the hydrodynamic state (steady-state). For this reason the concentration obtained with these relations is also called *equilibrium concentration*. Generically, this relation is

$$C = \frac{q_s\left(|\mathbf{U}|, H\right)}{|\mathbf{U}| H} \tag{3.69}$$

where $|\mathbf{U}|$ in the module of the fluid velocity

$$|\mathbf{U}| = \sqrt{U_1^2 + U_2^2}$$

and $q_s\left(|\mathbf{U}|, H\right)$ is any sediment transport formula that can be found in the literature (see e.g. [66] for a possible list).

Other four closure relation are needed for the fluid and solid shear bed stresses. These types of closure are present in literature only for dilute suspension (see for example the works of Zhang and Prosperetti [68], Drew [21], Jackson [36] and Marchioro *et al.* [45]) and no general ones exist for hyperconcentrated flow or debris flow.

The last two closure relations are connected with the drag forces $\mathcal{F}_i^D$. As mentioned in the previous Chapters, a general structure of this term is

$$\mathcal{F}_i^D = C_D r^2 \rho_f \left(U_i - V_i\right)^2 \tag{3.70}$$

where r is the radius of the solid particle and C_D is the drag coefficient that depends on the regime of the flow. However a general formulation for C_D, in the case of debris flow, is still not present in the literature.

3.2 Fully two-phase free-surface fixed bed system

The derivation of the $2D$ shallow flow equations that describe the two-phase flow over fixed bed is performed in the same way as for the mobile bed ones. The main difference between the two derivations is in the lower extrema of integration that, in the fixed bed case, it is no more a function of time and space, but only of space, so the Leibniz rule for the time derivative produces a different result respect to the mobile bed condition, that is, for a generic function $f(\mathbf{x}, t)$

$$\int_{z_b(\mathbf{x})}^{\eta(\mathbf{x},t)} \frac{\partial}{\partial t} f(\mathbf{x}, t)\ dx_3 = \frac{\partial}{\partial t} \int_{z_b(\mathbf{x})}^{\eta(\mathbf{x},t)} f(\mathbf{x}, t)\ dx_3 - [f]_\eta \frac{\partial \eta}{\partial t} \tag{3.71}$$

Regarding the boundary conditions, they are the same as the mobile bed-case, so the depth integration could be developed in a similar way as before.

3.2.1 Continuity equations

The starting point for the fluid continuity equation is (2.14) and performing the vertical integration we end up with

$$\frac{\partial \eta}{\partial t} - \frac{\partial}{\partial t}\phi H + \frac{\partial}{\partial x_1}\left(1 - \alpha_{\varphi u_1}\phi\right) H U_1 + \frac{\partial}{\partial x_2}\left(1 - \alpha_{\varphi u_2}\phi\right) H U_2 = 0 \tag{3.72}$$

where ϕ is the depth averaged solid concentration in the flow field

$$\phi = \frac{1}{H}\int_{z_b}^{\eta} c\ dx_3 \tag{3.73}$$

and $\alpha_{\varphi u_1}$ and $\alpha_{\varphi u_2}$ are two corrective coefficients defined in the same way as in (3.22) and (3.23). All the other quantities have been defined in the previous

Section. Here we use the symbol ϕ to express the averaged concentration inside the flow field instead C since the concentration in the fixed bed has a different behavior than the one in the mobile bed. This difference will be explained briefly in Section 3.2.3, while in Chapter 4 a more exhaustive discussion is presented.

Equation (3.72) contains the term η that describe the free surface elevation. Since η is the sum of the bed elevation plus the flow depth, it is possible to rewrite the expression as

$$\frac{\partial}{\partial t}\left(1-\phi\right)H+\frac{\partial}{\partial x_1}\left(1-\alpha_{\varphi u_1}\phi\right)HU_1+\frac{\partial}{\partial x_2}\left(1-\alpha_{\varphi u_2}\phi\right)HU_2=0 \quad (3.74)$$

where we neglect the time derivative of z_b since it not depends on time.

Moving to the solid continuity equation (2.15), the depth averaged process produces

$$\frac{\partial}{\partial t}\phi H+\frac{\partial}{\partial x_1}\alpha_{\varphi v_1}\phi HV_1+\frac{\partial}{\partial x_2}\alpha_{\varphi v_2}\phi HV_2=0 \quad (3.75)$$

that is the $2D$ shallow flow equation for the solid mass balance over the fixed bed, where $\alpha_{\varphi v_1}$ and $\alpha_{\varphi v_2}$ are two corrective coefficients defined in the same way as (3.25) and (3.26).

3.2.2 Momentum equations

The depth integration of the momentum equation along the x_3 direction, does not change respect to the mobile bed case, so the expressions for the fluid and solid pressure are given by (3.30) and (3.35).

The depth integration of the momentum equations in the plane x_1, x_2 is performed in the same way and produce a similar results as the mobile bed. For the fluid phase the final equation is

$$\frac{\partial}{\partial t}(1-\alpha_{\varphi u_i}\phi)HU_i+\frac{\partial}{\partial x_j}(1-\alpha_{\varphi u_i u_j}\phi)HU_iU_j=-\frac{1}{\rho_f}H\mathcal{F}_i^D+(1-\phi)\,g_iH+ \\ +\left(1-\alpha_{p_i}\phi\right)\frac{\partial}{\partial x_i}g_3\frac{H^2}{2}-\frac{(1-\alpha_{\tau_i}\phi)}{\rho_f}r_{z_b}\tau^f_{i,z_b} \quad (3.76)$$

with $i,j=1,2$, while for the solid phase the resulting equation is

$$\frac{\partial}{\partial t}\alpha_{\varphi v_i}\phi H V_i+\frac{\partial}{\partial x_j}\alpha_{\varphi v_i v_j}\phi H V_i V_j=\frac{1}{\rho_s}H\mathcal{F}_i^D+\phi g_i H+ \\ +\frac{g_3}{\rho_s}\left(\rho'\frac{\partial}{\partial x_i}\phi\frac{H^2}{2}\left(2-\alpha_c\right)+\rho_f\alpha_p\phi\frac{\partial}{\partial x_i}\frac{H^2}{2}\right)-\frac{1}{\rho_s}r_{z_b}\left(\tau^s_{i,z_b}+\alpha_{\tau_i}\phi\tau^f_{i,z_b}\right) \tag{3.77}$$

with $i,j=1,2$. As for the continuity equations, also in the momentum equations we use the symbol ϕ for representing the solid depth average concentration.

3.2.3 Final set of fixed bed motion equations and closure relations

The final set of equations describing the fully two-phase fixed bed model is

$$\begin{cases}\dfrac{\partial\eta}{\partial t}-\dfrac{\partial}{\partial t}\phi H+\dfrac{\partial}{\partial x_j}\left(1-\alpha_{\varphi u_j}\phi\right)HU_j=0\\ \dfrac{\partial}{\partial t}\phi H+\dfrac{\partial}{\partial x_j}\alpha_{\varphi v_j}\phi H V_j=0\\ \dfrac{\partial}{\partial t}(1-\alpha_{\varphi u_i}\phi)HU_i+\dfrac{\partial}{\partial x_j}(1-\alpha_{\varphi u_i u_j}\phi)HU_iU_j=-\dfrac{1}{\rho_f}H\mathcal{F}_i^D+(1-\phi)\,g_iH+\\ \qquad+(1-\alpha_{p_i}\phi)\,\dfrac{\partial}{\partial x_i}g_3\dfrac{H^2}{2}-\dfrac{(1-\alpha_{\tau_i}\phi)}{\rho_f}r_{z_b}\tau^f_{i,z_b}\\ \dfrac{\partial}{\partial t}\alpha_{\varphi v_i}\phi H V_i+\dfrac{\partial}{\partial x_j}\alpha_{\varphi v_i v_j}\phi H V_i V_j=\dfrac{1}{\rho_s}H\mathcal{F}_i^D+\phi g_iH+\\ \qquad+\dfrac{g_3}{\rho_s}\left(\rho'\dfrac{\partial}{\partial x_i}\phi\dfrac{H^2}{2}\left(2-\alpha_c\right)+\rho_f\alpha_{p_i}\phi\dfrac{\partial}{\partial x_i}\dfrac{H^2}{2}\right)+\\ \qquad-\dfrac{r_{z_b}}{\rho_s}\left(\tau^s_{i,z_b}+\alpha_{\tau_i}\phi\tau^f_{i,z_b}\right)\end{cases}$$

with $i,j=1,2$. The number of equations are six, while the unknowns are 12. Comparing this model with the mobile bed one, we note that now there is one unknown less inasmuch the bed elevation does not change in time, so z_b is no more a variable of the problem. As for the mobile case, the hydrodynamic unknowns are the components of the fluid and solid velocities (U_i and V_i), the flow depth H and, conversely than before, the concentration ϕ.

The use of different symbols for describing the concentration in fixed bed and mobile bed systems derives from the processes involved in the generation of the concentration. In the mobile bed case, the concentration changes due to variations of the bed elevation so it is correlated with the local hydrodynamic, while in the fixed bed case the concentration is simply advected by the flow field so it become a variable of the problem. The closure relations, instead, define a relation between these hydrodynamic variables and the other unknowns, and in particular with the components of bed shear stresses and the drag forces. For this system, the closure relations needed are similar to the ones of the mobile bed case.

3.3 Isokinetic models

As said in Sections 3.1.4 and 3.2.3, in the literature there are still not complete and reliable closure relations valid for debris flow or hyperconcentrated flows, so we introduce an approximation widely used in the free-surface models (see e.g. [10],[13], [15] and [47]). The approximation is called isokinetic and it assumes equal solid and fluid velocities

$$u_i^f = u_i^s \tag{3.78}$$

where $i = 1, 2$. With this assumption, as a consequence, also the averaged velocities are equal

$$U_i = V_i \tag{3.79}$$

and the drag force is identically null.

With the isokinetic approximation, the number of unknowns is reduced and, as a consequence, the number of the equations needed for the description of the motion is smaller. Since we need less equations, a sensible choice is to use the simplest ones in order to simplify the model.

Usually, with the isokinetic approximation, the systems describing fixed or mobile bed are composed by mixture mass and momentum balances and by the solid mass equation. The mixture, as written in Chapter 1, is the

combination of the fluid and solid phases, and the equations describing its are the ones describing the fluid phase plus the equations for the solid phase. The presence of only the momentum balance equations for the mixture derives directly from the isokinetic assumptions. Since the fluid and solid velocities are equal, the momentum equations for the solid and fluid phases describe the same behaviors, so the equations for one of the two phases are redundant.

In the follow Section we derive the mixture and solid equations describing the isokinetic $2D$ two-phase free-surface flow over mobile and fixed bed.

3.3.1 Mobile bed isokinetic model

Regarding the mass conservations, since we want the simplest equation possible as said before, a good choice is to use the mass conservation of the mixture. The mixture, as written in Chapter 1, is the combination of the fluid and solid phases, and the equation describing its is the one describing the fluid phase plus the equation for the solid phase. Adding equation (3.21) with equation (3.24) and using the isokinetic approximation, the result is

$$\frac{\partial}{\partial t}\left(H + z_b\right) + \frac{\partial}{\partial x_1} HU_1 + \frac{\partial}{\partial x_2} HU_2 = 0 \tag{3.80}$$

and describe the mass conservation of the mixture. We highlight that, thanks to the equality of the velocities, the corrective coefficient α_{cu_i} is equal to α_{cv_i}

$$\alpha_{cv_i} = \frac{\int_{z_b}^{\eta} cv_i \; dz}{CHV_i} = \frac{\int_{z_b}^{\eta} cu_i \; dz}{CHU_i} = \alpha_{cu_i} \tag{3.81}$$

so they disappear from the equation.

The other mass conservation needed can be chosen between the fluid and the solid one. We chose the solid mass conservation (3.24) since it is composed by less terms than the fluid one. Using (3.79), it becomes

$$\frac{\partial}{\partial t}\left(CH\right) + c_b \frac{\partial z_b}{\partial t} + \frac{\partial}{\partial x_1}\left(\alpha_{cu_1} CHU_1\right) + \frac{\partial}{\partial x_2}\left(\alpha_{cu_2} CHU_2\right) = 0 \tag{3.82}$$

Also for the momentum equations a sensible choice is to use the mixture equations. These equations are derived, as for the mass conservation, adding

the equations for the solid phase (3.63) and (3.66) with the ones for the fluid phase (3.54) and (3.55). After some mathematical manipulation the final result is

$$\begin{aligned}
&\frac{\partial}{\partial t}\left(1+\alpha_{cu_i}C\Delta\right)HU_i+\frac{\partial}{\partial x_j}\left(1+\alpha_{cu_iu_j}C\Delta\right)HU_iU_j=\\
&=\frac{\partial}{\partial x_i}\left(1+\left(2-\alpha_c\right)C\Delta\right)g_3\frac{H^2}{2}+\\
&\qquad\qquad -r_{z_b}\frac{\tau^f_{i,z_b}+\tau^s_{i,z_b}}{\rho_f}+(1+C\Delta)g_iH
\end{aligned}\tag{3.83}$$

for $i=1,2$ where Δ is the relative submerged solid density defined as

$$\Delta=\frac{\rho_s-\rho_f}{\rho_f}\tag{3.84}$$

We highlight that this equation, respect to the fluid or solid momentum equation, is simplest since it is composed by less terms.

Other equations describing only the fluid or solid momentum are not needed. This derives from the assumption of equal fluid and solid velocity (3.79), so the momentum equations for the solid phases, the fluid phase and the mixture describe the same behaviors.

The final system of partial differential equations describing the motion of the isokinetic mixture for the mobile bed case is

$$\begin{cases}
\dfrac{\partial}{\partial t}\left(H+z_b\right)+HU_1+\dfrac{\partial}{\partial x_2}HU_2=0\\
\dfrac{\partial}{\partial t}\left(CH\right)+c_b\dfrac{\partial z_b}{\partial t}+\dfrac{\partial}{\partial x_1}\left(\alpha_{cu_1}CHU_1\right)+\dfrac{\partial}{\partial x_2}\left(\alpha_{cu_2}CHU_2\right)=0\\
\dfrac{\partial}{\partial t}\left(1+\alpha_{cu_i}C\Delta\right)HU_i+\dfrac{\partial}{\partial x_j}\left(1+\alpha_{cu_iu_j}C\Delta\right)HU_iU_j=\\
\qquad\qquad=\dfrac{\partial}{\partial x_i}\left(1+C\left(2-\alpha_c\right)\Delta\right)g_3\dfrac{H^2}{2}-r_{z_b}\dfrac{\tau_{i,z_b}}{\rho_f}+(1+C\Delta)g_iH
\end{cases}$$

for $i=1,2$, where τ_{i,z_b} is the total bed shear stress. With this model the number of equations are four: two mass balances and two momentum balances. The unknowns are now seven: the two components of the velocity U_i, the flow depth H, the bed elevation z_b, the solid volume concentration C and the components of the total bed shear stress τ_{i,z_b}. Also in this case

we assume unitary corrective coefficients. Now, the system needs to use only three closure relations. The first one is for the concentration C and it is the same as for the fully two-phase model (3.69).

The other closure relations needed are for the components of the total bed shear stress and in the literature exists lots of them. For example, we can use, for a hyperconcentrated flow, a relation like Strickler

$$\frac{\tau_{i,z_b}}{\rho_f} = g\frac{U_i\,|\mathbf{U}|}{k_s^2 H^{1/3}} \tag{3.85}$$

where k_s is the Strickler coefficient. For a debris flow, it is possible to use the relation derived by Bagnold (see [12] for more details)

$$\frac{\tau_{i,z_b}}{\rho_f} = \frac{25}{4}\frac{\rho_s}{\rho_f}\sin\phi_d\frac{\lambda^2}{Y^2}\,|\mathbf{U}|\,U_i \tag{3.86}$$

where ϕ_d is the dynamic friction angle of the sediment, Y is defined as

$$Y = \frac{h}{d\sqrt{a}} \tag{3.87}$$

with $a = 0.32$ for Takahashi (see [62]), d is the characteristic diameter of the solid particle, while λ is the linear concentration defined as

$$\lambda = \frac{C^{1/3}}{c_b^{1/3} - C^{1/3}} \tag{3.88}$$

A more complex relation, that we want to mention, is the one proposed by Armanini [8] where the bed shear stress is a weighted combination of the previous two expressions. This relation is valid for both hyperconcentrated flow, debris flow and also for classical sediment transport phenomena, however it is quite complicated to be implemented and fall outside the main scope of this thesis, so we do not discuss any more about its.

3.3.2 Fixed bed isokinetic model

For the fixed bed isokinetic model, the derivation is similar as for the mobile bed one, so the final set of PDEs is

$$\begin{cases} \dfrac{\partial \eta}{\partial t} + HU_1 + \dfrac{\partial}{\partial x_2} HU_2 = 0 \\ \dfrac{\partial}{\partial t}\phi H + \dfrac{\partial}{\partial x_1}\alpha_{\varphi u_1}\phi H u_1 + \dfrac{\partial}{\partial x_2}\alpha_{\varphi v_2}\phi H u_2 = 0 \\ \dfrac{\partial}{\partial t}\left(1 + \alpha_{\varphi u_i}\phi\Delta\right) HU_i + \dfrac{\partial}{\partial x_j}\left(1 + \alpha_{\varphi u_i u_j}\phi\Delta\right) HU_iU_j = \\ \qquad\qquad = \dfrac{\partial}{\partial x_i}\left(1 + \phi\left(2 - \alpha_c\right)\Delta\right) g_3 \dfrac{H^2}{2} - r_{z_b}\dfrac{\tau_{i,z_b}}{\rho_f} + (1 + \phi\Delta) g_i H \end{cases}$$

where the number of equations is four, while the unknowns are six, so two closure relations are needed. These closure relations are related to the bed shear stresses that can be expressed using a relation similar to the one used in the isokinetic mobile bed system, so equations (3.85) or (3.86), where it is necessary to swap the concentration C with ϕ.

3.4 Brief literature review

In the literature exists, as specified in the previous sections, two type of two-phase models: the first one is the *fully* two-phase model where the two phases (solid and fluid) can assume different velocities, while the second type is the *isokinetic* model where the fluid and solid velocities are equal. Among the paper dealing with the first type of model, notable to citation are the model proposed by Pitman and Le [49] and Greco *et al.* [30].

Pitman and Le [49], in they work, start from the $3D$ continuum equations (the ones derived in Chapter 1) and perform the depth integration ending up with a two-phase fixed bed model like the one derived in Section 3.2. As closure relations they assume an inviscid fluid (so $\tau^f_{i,z_b} = 0$) and a Mohr-Coulomb stress type for the solid phase. For the drag force they assume a linear dependency with the difference of velocity and a drag coefficient that depends on the concentration and flow type.

On the contrary, Greco *et al.* [30] derive the equations starting from the solid and fluid mass and momentum balance applied to a control volume. This model is similar to the mobile bed one derived here in Section 3.1, but it is valid only for low concentration. Greco *et al.* introduce also another partial differential equation describing the time variation of the bed elevation

$$\frac{\partial z_b}{\partial t} = D - E \tag{3.89}$$

where D is a generic deposition formula related with the settling velocity of the solid particles and E is a generic erosion expression strictly related to a sediment transport formula. This equation derives from a work of Armanini and Di Silvio [9] where they present a closure relations for the non-equilibrium concentration, thus the concentration becomes a variable of the problem.
As closure relation for the bed shear stresses they use a Chézy formulation

$$\frac{\tau_{i,z_b}}{\rho_f} = \frac{|\mathbf{U}|}{\chi^2} U_i$$

that is decompose in fluid and solid stresses

$$\frac{\tau_{i,z_b}}{\rho_f} = \frac{\tau^f_{i,z_b}}{\rho_f} + \frac{\tau^s_{i,z_b}}{\rho_s}$$

where the solid one is evaluated trough a Mohr-Coulomb relation as for Pitman and Le. For the drag force Greco *et al.* assume a quadratic dependency with the difference of velocities and a drag coefficient that depends on flow type.

The second type of shallow flow two-phase models is the isokinetic ones that can be classified essentially in two categories: the mobile bed models as derived in Section 3.3 and the models with a differential closure relation for the concentration in which a partial differential equation like to (3.89) is introduced. Among the first category we mentioned the model TRENT2D (see papers of Armanini *et al.* [10] and Rosatti and Begnudelli [53, 52]) that was developed for hyperconcentrated and debris flows. In the second categories we can cite the models proposed by Benkhaldoun *et al.* [13] and Cao *et al.* [15].

In literature, however, there are also lots of other $2D$ models, but them are developed only for low concentration regime, so they are suitable to simulate only bed load transport. This type of models are derived in a similar way as the isokinetic ones, but with the assumption of low concentration, so the terms containing the concentration in the mixture momentum equations are neglected (more details on this approximation are presented in Section 4.1). In this category we can cite the model of Murillo and García-Navarro [47].

Chapter 4

One-dimensional isokinetic modelling

The Chapter is devoted to the one-dimensional isokinetic modelling where the PDEs system describes a two-phase flow which properties change only in one direction. This one-dimensional model refers to purely one directional flow, so we do not speak about the section-averaged model. In real cases, a purely one directional flow is rarely, however the study of this flow type is fundamental for the development of numerical solvers in the framework of finite volume method with Godunov fluxes even for two dimensional application.

All the equations used in the following Sections derive from the $2D$ isokinetic models obtained in Section 3.3, where, as specified, the corrective coefficients are unitary. In previous Chapters the equations was derived using a reference system that are tangent to the bed with the x_3 direction normal to it. From now on, the reference system is different since we use as x_3 the vertical direction (the same direction of the gravity force but with opposite sign), while the other two directions (x_1 and x_2) are horizontal as specified in Figure 4.1. The switching from the boundary fitted reference system to the one with vertical x_3 direction is necessary since, in the mobile bed case, the bed elevation changes in time, so the slope are varying, thus the reference system has to change with it introducing lots of difficulties.

Using the reference systems with vertical x_3 direction, some modification on the PDEs systems derived in Section 3.3 have to been introduced:

1. the integration of the equations is performed on the vertical direction, therefore the vertical averaged variables are different from the normal depth averaged ones used in the previous Chapter. Also some corrective coefficients for the bed pressures and tangential stresses appears, but assuming them unitary no large errors are introduced (see Armanini *et al.* [10]);

2. for the shallow flow approximation, the velocity must be tangential to the bottom, so the velocity vector is

   $$\mathbf{U} = (U_1, U_2, W)$$

   where U_1 and U_2 are the velocity along the x_1 and x_2 directions, while W is the vertical velocity and it is related to the previous ones with

   $$\frac{W}{\sqrt{U_1^2 + U_2^2}} = \tan \alpha$$

   where α is the local bed slope;

3. since x_1 and x_2 directions are horizontal, the gravity acceleration is

   $$\mathbf{g} = (0, 0, -g)$$

   so the term

   $$g_i \left(1 + C\Delta\right) H$$

   with $i = 1, 2$ in the momentum equation vanishes. Instead, the term

   $$g \left(1 + C\Delta\right) H \frac{\partial z_b}{\partial x_i}$$

   where $i = 1, 2$, is present in the momentum equation as specified in Section 3.1.3. From a physical point of view, this term can be explained as the pressure that the bed exerts on the flow.

The two-dimensional isokinetic SF PDEs system with mobile bed is then

$$\begin{cases} \dfrac{\partial}{\partial t}\left(H+z_b\right)+\dfrac{\partial}{\partial x_j}HU_j=0 \\ \dfrac{\partial}{\partial t}\left(CH\right)+c_b\dfrac{\partial z_b}{\partial t}+\dfrac{\partial}{\partial x_j}CHU_j=0 \\ \dfrac{\partial}{\partial t}\left(1+C\Delta\right)HU_i+\dfrac{\partial}{\partial x_j}\left(1+C\Delta\right)HU_iU_j+\dfrac{\partial}{\partial x_i}\left(1+C\Delta\right)g\dfrac{H^2}{2}+ \\ \qquad +g\left(1+\Delta C\right)H\dfrac{\partial z_b}{\partial x_i}=-\dfrac{\tau_{i,z_b}}{\rho_f} \end{cases} \tag{4.1}$$

while in the fixed bed case is

$$\begin{cases} \dfrac{\partial}{\partial t}\left(H+z_b\right)+\dfrac{\partial}{\partial x_j}HU_j=0 \\ \dfrac{\partial}{\partial t}\phi H+\dfrac{\partial}{\partial x_j}\phi HU_j=0 \\ \dfrac{\partial}{\partial t}\left(1+\phi\Delta\right)HU_i+\dfrac{\partial}{\partial x_j}\left(1+\phi\Delta\right)HU_iU_j+\dfrac{\partial}{\partial x_i}\left(1+\phi\Delta\right)g\dfrac{H^2}{2}+ \\ \qquad +g\left(1+\Delta\phi\right)H\dfrac{\partial z_b}{\partial x_i}=-\dfrac{\tau_{i,z_b}}{\rho_f} \end{cases} \tag{4.2}$$

with $i=1,2$.

In this Chapter we speak about tree different classes of isokinetic $1D$ systems for fixed and mobile bed. All the systems presented derive from the previous two where, as said before, the common simplification made is to neglect all the derivative in the direction x_2

$$\frac{\partial}{\partial x_2}=0 \tag{4.3}$$

The other simplification made is to assume an unidirectional flow

$$\mathbf{U}=\left(U_1,0,W\right) \tag{4.4}$$

With these simplifications, for shake of clarity, we neglect the subscript 1 that indicate the x_1 direction since now is univocally defined.

The first class of systems, presented in Section 4.1, is the simplest one, since it describe only low concentrated flow. Then, in Section 4.2 we present

the class of models that describes hyperconcentrated flow or debris flow. Finally, in Section 4.3, we present the two-dimensional plane wave class. This class of models describes $2D$ problems but with a plane solution. We present this type of models among the one-dimensional ones, since the variations of the flow variables occurs only in one directions, so they can be assimilated to $1D$ problems. For this latter class of models, the assumption (4.4) is no more valid since velocity U_2 is present.

4.1 One-dimensional systems with low sediment concentration

When the concentration of the solid phase in the flow field, as find by Garegnani *et al.* [27], is less than 1%, the equations of motion can be simplified. In particular, it is possible to neglect the concentration in the momentum equation. This type of simplified equation is widely used in literature (see e.g. [39], [33], [22], [1] and [63] among many others), since the low concentration regime is the one that exist in the classical bed load transport phenomena. Following Garegnani *et al.* [27], the resulting system for the fixed bed is

$$\begin{cases} \dfrac{\partial}{\partial t}h + \dfrac{\partial}{\partial x}uh = 0 \\ \dfrac{\partial}{\partial t}uh + \dfrac{\partial}{\partial x}\left(hu^2 + g\dfrac{h^2}{2}\right) + gh\dfrac{\partial z_b}{\partial x} = -\dfrac{\tau_0}{\rho_f} \\ \dfrac{\partial}{\partial t}\varphi h + \dfrac{\partial}{\partial x}\varphi uh = 0 \\ \dfrac{\partial}{\partial t}z_b = 0 \end{cases} \tag{4.5}$$

where h is the flow depth, u is the flow velocity, z_b is the bed elevation, φ in the solid concentration inside the flow, g is the gravity acceleration, ρ_f is the fluid density and τ_0 is the bottom shear stress (see Figure 4.1a for a representation of the variables).

This system is composed by the well known shallow flow (SF) equations plus the advection of a passive scalar that is the solid phase concentration. Since φ is a quantity that is simply advected by the liquid phase, we call

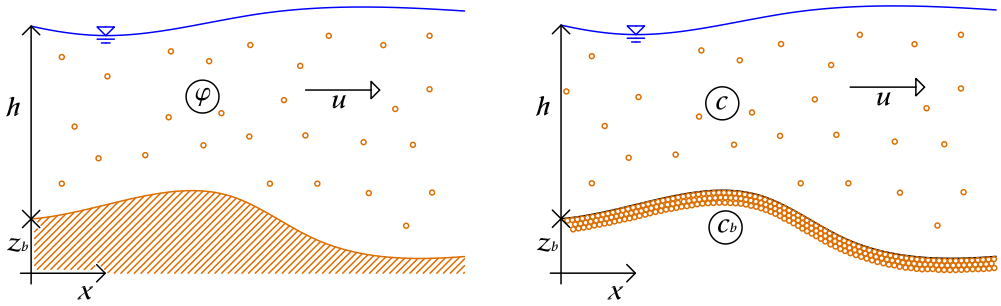

(a) Fixed-bed case. (b) Mobile-bed case.

Figure 4.1: Sketch with the indication of the variables for: (a) fixed-bed case, (b) mobile-bed case.

this concentration *transported concentration*. The last differential equation in system (4.5) describes the time invariance of the bed elevation. This equation is not strictly necessary, but allows a rigorous analytical investigation of problems involving discontinuities in the bed elevation (see the works of LeFloch and Thanh [42] and Rosatti and Begnudelli [51] among many others). In order to close the flow problem, an expression for the bed shear stress as a function of the flow depth and velocity must be provided. An expression derived from the uniform flow condition is commonly employed, for example the Gaukler relation, as specified in Section 3.3

$$\frac{\tau_0}{\rho_f} = \frac{gu^2}{K_s^2 h^{1/3}} \tag{4.6}$$

Moving to the mobile bed case, the approximations produce the following system

$$\begin{cases} \dfrac{\partial}{\partial t}h + \dfrac{\partial}{\partial x}uh = 0 \\ \dfrac{\partial}{\partial t}uh + \dfrac{\partial}{\partial x}\left(hu^2 + g\dfrac{h^2}{2}\right) + gh\dfrac{\partial z_b}{\partial x} = -\dfrac{\tau_0}{\rho_f} \\ c_b\dfrac{\partial z_b}{\partial t} + \dfrac{\partial}{\partial x}cuh = 0 \end{cases} \tag{4.7}$$

where c_b is the constant concentration inside the bed, c is the solid concentration inside the flow field and the other variables have the same meaning

as for fixed bed case (see Figure 4.1b for a representation of the variables). Also this system is composed by the well known SF equation, but this time the solid mass balance is the so-called Exner equation. This equation states that the bed elevation can change in time when a variation of solid discharge (cuh) occurs. The problem is solvable introducing two closure relations. The first one is for the bed shear stress τ_0 as for the fixed bed. The second regards the concentration i.e., as specified in Section 3.3, it is a relation between the local hydrodynamic variables and the concentration itself. This relation has mainly empirical origin and it is obtained in equilibrium conditions with the hydrodynamic variables (steady-state). For these reason we called *equilibrium concentration*. We want to remark that the concentration φ and c express the same physical quantity (the concentration of the solid phase inside the flow depth), however they are related to different physical phenomena: in the fixed-bed case, sediments are simply advected by the fluid phase, while in the mobile-bed case, besides the advection, the exchange of sediment with the bed plays a fundamental role in determining the actual value of the concentration.

As specified in Section 2.1, in a hyperconcentrated flow, the concentration is higher than 0.01, so these models are no more valid. However, we discuss about them since they are well studied, simple and easy to deal with thus they allows as, in Part II, to define a general procedure for the study of the complex phenomena that is the transition between fixed and mobile bed.

4.2 One-dimensional systems for high sediment concentration

The one-dimensional systems for high sediment concentration are a step of difficulty above the low concentration models derived in Section 4.1 and they are the base for an accurate description of an isokinetic hyperconcentrated two-phase free-surface flow.

Starting from (4.2) describing the $2D$ fixed bed isokinetic two-phase flow

and applying the simplification (4.4) the resulting system is

$$\begin{cases} \dfrac{\partial}{\partial t}\left(h+z_b\right)+\dfrac{\partial}{\partial x}uh=0 \\ \dfrac{\partial}{\partial t}\left(1+\varphi\Delta\right)uh+\dfrac{\partial}{\partial x}\left(1+\varphi\Delta\right)\left(hu^2+g\dfrac{h^2}{2}\right)+ \\ \qquad\qquad +\left(1+\varphi\Delta\right)gh\dfrac{\partial z_b}{\partial x}=-\dfrac{\tau_0}{\rho_f} \\ \dfrac{\partial}{\partial t}\varphi h+\dfrac{\partial}{\partial x}\varphi uh=0 \\ \dfrac{\partial}{\partial t}z_b=0 \end{cases} \tag{4.8}$$

where Δ is the constant relative submerged solid density defined as

$$\Delta=\frac{\rho_s-\rho_f}{\rho_f}$$

while the other variables are the same as the low concentration system. The equations constituting the system are mass and momentum balance of the mixture and the solid mass balance. The last equation, as for the low concentration system, is not necessary, but it covers a fundamental role for the correct description of discontinuous bed cases. The flow problem is resolvable when a closure relation for the total bed shear stress is introduced.

For the mobile bed case the resulting system is, indeed,

$$\begin{cases} \dfrac{\partial}{\partial t}\left(h+z_b\right)+\dfrac{\partial}{\partial x}uh=0 \\ \dfrac{\partial}{\partial t}\left(1+c\Delta\right)uh+\dfrac{\partial}{\partial x}\left(1+c\Delta\right)\left(hu^2+g\dfrac{h^2}{2}\right)+ \\ \qquad\qquad +\left(1+c\Delta\right)gh\dfrac{\partial z_b}{\partial x}=-\dfrac{\tau_0}{\rho_f} \\ c_b\dfrac{\partial z_b}{\partial t}+\dfrac{\partial}{\partial t}ch+\dfrac{\partial}{\partial x}cuh=0 \end{cases} \tag{4.9}$$

where the symbols are the same as before. The system is composed by the mixture mass and momentum balances plus the solid mass balance. Comparing this systems with the one developed under the low concentration approximation (4.7), the main difference, in addition to the presence of the concentration terms in the momentum equation, is the presence of the term

$\frac{\partial}{\partial t}ch$ in the solid mass balance that indicate the solid mass stored in the fluid column. With this term the variation of the bottom elevation occurs, not only due to a variation of the fluxes cuh, but also due to a increasing or decreasing of the solid mass stored in the fluid field. For solving this system, as for the previous mobile bed one, it is necessary to introduce two closure relation: one for the concentration c and one for the bed shear stress τ_0.

This type of systems has the advantage that describe not only debris flow, so flow with high value of sediment, but they represents also the classical bed load transport. The switch between a debris flow and the description of a river is possible simply changing the closure relations. For the debris flow case a granular-inertia relation, like the one proposed by Bagnold [12], is appropriated, while for the bed load transport an empirical relation like Gaukler-Strickler is adequate. As specified in Section 3.3, Armanini [8] proposes a more complex formulation which has validity all over the range of physical concentration. The use of this type of closure relation allow to simulate correctly most of the free-surface flow form low concentration up to debris-flow. However this formulation is very stiff to be introduced into numerical models, so, as said in the previous Chapter, we leave the use of this formulation to future works.

4.3 Two-dimensional plane-wave systems

The last systems that we consider are the two-dimensional plane-wave ones. As said before, these models describe $2D$ problems but with plane solutions. A plane solution is characterized by variations of the flow variables only in one directions, so they can be assimilated to $1D$ problem. These systems are the most interesting from a numerical point of view, since they are at the base of the Riemann solver for the $2D$ models. In fact they take into account not only the presence of the longitudinal velocity u, but also the transversal one (in the follow called v).

For the fixed bed case the PDEs system is

$$\begin{cases} \dfrac{\partial}{\partial t}\left(h+z_b\right)+\dfrac{\partial}{\partial x}uh=0 \\ \dfrac{\partial}{\partial t}\left(1+\varphi\Delta\right)uh+\dfrac{\partial}{\partial x}\left(1+\varphi\Delta\right)\left(hu^2+g\dfrac{h^2}{2}\right)+ \\ \qquad\qquad +\left(1+\varphi\Delta\right)gh\dfrac{\partial z_b}{\partial x}=-\dfrac{\tau_{0,x}}{\rho_f} \\ \dfrac{\partial}{\partial t}\left(1+\varphi\Delta\right)vh+\dfrac{\partial}{\partial x}\left(1+\varphi\Delta\right)huv=-\dfrac{\tau_{0,y}}{\rho_f} \\ \dfrac{\partial}{\partial t}\varphi h+\dfrac{\partial}{\partial x}\varphi uh=0 \\ \dfrac{\partial}{\partial t}z_b=0 \end{cases} \tag{4.10}$$

and it is composed by five equations: the mixture mass conservation, the momentum balance for the mixture along the normal (x) and transversal direction (y), the solid mass balance and, as for all the previous $1D$ fixed bed cases, the time invariance in time of bed elevation. For this systems the closure relations needed are the two bed shear stress, one for longitudinal direction $\tau_{0,x}$ and one for the transversal direction $\tau_{0,y}$.

For the mobile bed case, the relevant system is

$$\begin{cases} \dfrac{\partial}{\partial t}\left(h+z_b\right)+\dfrac{\partial}{\partial x}uh=0 \\ \dfrac{\partial}{\partial t}\left(1+c\Delta\right)uh+\dfrac{\partial}{\partial x}\left(1+c\Delta\right)\left(hu^2+g\dfrac{h^2}{2}\right)+ \\ \qquad\qquad +\left(1+c\Delta\right)gh\dfrac{\partial z_b}{\partial x}=-\dfrac{\tau_{0,x}}{\rho_f} \\ \dfrac{\partial}{\partial t}\left(1+c\Delta\right)vh+\dfrac{\partial}{\partial x}\left(1+c\Delta\right)huv=-\dfrac{\tau_{0,y}}{\rho_f} \\ c_b\dfrac{\partial z_b}{\partial t}+\dfrac{\partial}{\partial t}ch+\dfrac{\partial}{\partial x}cuh=0 \end{cases} \tag{4.11}$$

that is composed, as for the fixed one, by the mixture mass conservation, the longitudinal an transversal momentum equation for the mixture and the solid mass balance. The flow problem depicted by this system is solvable when two closure relations for the bed shear stresses and one for the concentration are introduced.

Regarding the closure relation for the concentration, the consideration done for the $1D$ high sediment concentration systems are still valid with the requirement to use the module of the velocity $|\mathbf{u}| = \sqrt{u^2 + v^2}$ in the transport formula

$$c = c\left(|\mathbf{u}|, h\right) = \frac{q_s\left(|\mathbf{u}|, h\right)}{|\mathbf{u}|\, h} \tag{4.12}$$

as for the $2D$ models presented in Chapter 3.1.4. Also for the bed shear stresses it is possible to use the previous relations once they are written in the same way as the $2D$ models.

Chapter 5

Eigenstructure of the one-dimensional models

This Chapter is devoted to the description of the mathematical features of the three different classes of one-dimensional free-surface two-phase systems derived in the Chapter 4.

Analyzing the eigenvalues and the associated eigenvectors, it is possible to understand the type (hyperbolic, parabolic or elliptic) of PDEs system we are dealing with. A system is hyperbolic if it has a full set of real eigenvalues and associated eigenvectors while in the other cases it is parabolic or elliptic. When the hyperbolicity is ensured, it is possible to define a Riemann Problem (RP) that is a particular initial value problem, associated to the PDEs system, where the initial condition consists in two piecewise constant states separated by a discontinuity. The solution of the RP is composed by a set of simple waves (rarefaction, shock or contact) with particular properties that derives from the eigenstructure of the PDEs system. As we will demonstrate in the following Sections, the fixed and mobile bed systems described in the previous Chapter are hyperbolic and the eigenstructure of each of them is composed by:

- the eigenvalues, i.e. the speed of the small perturbations and their dependency on the flow variables;
- the eigenvectors associated to each eigenvalues, that describe how the flow variables change across each wave;

- the nature of the characteristic fields, i.e. which type of waves an eigenvalue can develop (shock, rarefaction or contact);

- the Rankine-Hugoniot relations, that describe the discontinuous solutions that can occur.

All these properties are fundamental for the derivation of numerical finite volume method with Godunov fluxes since for each cell interface a RP occurs. The establishment of a RP on each cell interface will be crucial in the following Parts of the thesis where we use these properties for the solution of the transition between fixed and mobile bed.

Since the $1D$ fixed and mobile bed systems are well studied in the literature, only the major aspects used in the remainder of the thesis will be recalled hereafter. For a more exhaustive analysis of fixed bed systems with discontinuous bed, we refer the reader to the papers of Alcrudo and Benkhaldoun [2], LeFloch and Thanh [42] and Rosatti and Begnudelli [51], while for the mobile bed cases the papers are Fraccarollo and Capart [25], Morris and Williams [46] and Rosatti and Fraccarollo [54] among many others. Regarding the eigenstructure analysis methodology, we refer to the books of Toro [64] and LeVeque [43].

Since only the homogeneous part of the systems are necessary for the eigenstructure analysis, for the mobile bed cases it is fundamental to define the concentration closure relation. As written in the previous Chapter, the equilibrium concentration c is related to the local hydrodynamic (velocity u and flow depth h) via

$$c = c(u, h) \tag{5.1}$$

Here we have highlighted only the dependence on the dynamic quantities that affect the eigenstructure of the relevant system, while we have disregarded all the other quantities that characterize a given type of sediment (diameter, relative density etc.). The explicit expression of c is necessary only in the numerical application.

5.1 One-dimensional systems with low sediment concentration

The low concentration system for the fixed bed condition (4.5), derived in Section 4.1 can be written in compact form as

$$\frac{\partial}{\partial t}\mathbf{U}_f + \frac{\partial}{\partial x}\mathbf{F}_f + \mathbf{H}_f\frac{\partial \mathbf{W}_f}{\partial x} = \mathbf{S}_f \tag{5.2}$$

where the subscript f indicates the fixed bed case, $\mathbf{U}_f$ and $\mathbf{W}_f$ are the vectors of the conserved and primitive variables

$$\mathbf{U}_f = \begin{bmatrix} h \\ uh \\ \varphi h \\ z_b \end{bmatrix} \quad ; \quad \mathbf{W}_f = \begin{bmatrix} h \\ u \\ \varphi \\ z_b \end{bmatrix} \tag{5.3}$$

$\mathbf{F}_f$ and $\mathbf{H}_f$ are the conservative and non-conservative fluxes

$$\mathbf{F}_f = \begin{bmatrix} uh \\ u^2h + \frac{1}{2}gh^2 \\ \varphi uh \\ 0 \end{bmatrix} \quad ; \quad \mathbf{H}_f = \begin{bmatrix} 0 & 0 & 0 & 0 \\ 0 & 0 & 0 & gh \\ 0 & 0 & 0 & 0 \\ 0 & 0 & 0 & 0 \end{bmatrix} \tag{5.4}$$

while $\mathbf{S}_f$ are the source term

$$\mathbf{S}_f = \begin{bmatrix} 0 \\ -\dfrac{\tau_0}{\rho_f} \\ 0 \\ 0 \end{bmatrix} \tag{5.5}$$

The eigenstructure of this system can be obtained by analyzing the associated homogeneous quasi-linear form, that can be written as

$$\mathbf{J}_{\mathbf{U}_f}\frac{\partial \mathbf{W}_f}{\partial t} + \left(\mathbf{J}_{\mathbf{F}_f} + \mathbf{H}_f\right)\frac{\partial \mathbf{W}_f}{\partial x} = 0 \tag{5.6}$$

where

$$\mathbf{J}_{\mathbf{U}_f} = \frac{\partial \mathbf{U}_f}{\partial \mathbf{W}_f}; \qquad \mathbf{J}_{\mathbf{F}_f} = \frac{\partial \mathbf{F}_f}{\partial \mathbf{W}_f} \tag{5.7}$$

are respectively the Jacobian of the conserved variables and of the fluxes with respect to the primitive variable vector $\mathbf{W}_f$. Its characteristic polynomial, deriving from

$$\det\left|\mathbf{J}_{\mathbf{F}_f} + \mathbf{H}_f - \lambda \mathbf{J}_{\mathbf{U}_f}\right| = 0 \tag{5.8}$$

has four real and distinct eigenvalues

$$\begin{cases} \lambda_1 = u - \sqrt{gh} \\ \lambda_2 = u \\ \lambda_3 = u + \sqrt{gh} \\ \lambda_4 = 0 \end{cases} \tag{5.9}$$

It is important to notice that depending on the value of the Froude number $Fr = u/\sqrt{gh}$, if $Fr < 1$ (subcritical flow) two eigenvalues have the same sign as the velocity while one has an opposite sign. On the contrary, if $Fr > 1$ (supercritical flow), all the three nonnull eigenvalues have the same sign as the velocity.

The eigenvectors associated with the previous eigenvalues are

$$\begin{aligned} \mathbf{R}_1^{W_f} &= \begin{bmatrix} -\frac{1}{g}\sqrt{gh} \\ 1 \\ 0 \\ 0 \end{bmatrix} \quad ; \quad \mathbf{R}_2^{W_f} = \begin{bmatrix} 0 \\ 0 \\ 1 \\ 0 \end{bmatrix} \\ \mathbf{R}_3^{W_f} &= \begin{bmatrix} \frac{1}{g}\sqrt{gh} \\ 1 \\ 0 \\ 0 \end{bmatrix} \quad ; \quad \mathbf{R}_4^{W_f} = \begin{bmatrix} -g\frac{h}{gh-u^2} \\ g\frac{u}{gh-u^2} \\ 0 \\ 1 \end{bmatrix} \end{aligned} \tag{5.10}$$

Regarding the nature of the characteristic fields, those associated with λ_1 and λ_3 are Genuinely Non-Linear (GNL). A GNL field can develop rarefaction waves (i.e. continuous solutions) or shocks (i.e. discontinuous solutions). Moreover, considering the relevant Riemann Invariants (RI), we can state that both φ and z_b do not change across the waves of these fields. Thus the relevant possible shocks are described by the classical Rankine-Hugoniot

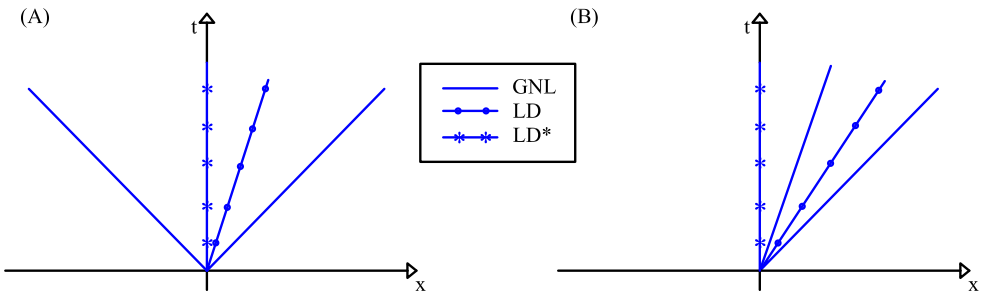

Figure 5.1: Possible wave patterns of a fixed-bed RP as a function of the Froude number of the flow near the origin - (A) subcritical flow, (B) supercritical flow. Velocity is assumed positive throughout.

(RH) relations, since these discontinuities occur over a flat bed.
The characteristic field associated with λ_2 is a classic Linearly Degenerate (LD) one across which only φ changes. In this case RI and RH relations give the same informations. Finally the field associated with $\lambda_4 = 0$ is a steady contact wave across which, in addition to h and u, the bed elevation also changes. This is a particular Linearly Degenerate (LD*) field across which, as demonstrated in [51], only the Generalized Rankine-Hugoniot (GRH) relations are valid. In compact form these relations can be written as:

$$\mathbf{F}^*_{fR} - \mathbf{F}^*_{fL} = \mathbf{D}_f \tag{5.11}$$

where $\mathbf{F}^*_{fR}, \mathbf{F}^*_{fL}$ are the fluxes respectively on the right and on the left of the wave while following [54], $\mathbf{D}^T_f = (0, D, 0, 0)$, where

$$D = -g\left(h_k - \frac{|z_R - z_L|}{2}\right)(z_R - z_L) \quad \text{with } k = \begin{cases} L & \text{if } z_L \leq z_R \\ R & \text{otherwise} \end{cases} \tag{5.12}$$

is the thrust term exerted by the bed step on the control volume used to obtain relations (5.11).

Finally, according to the features described above, the two possible wave patterns marking out a generic RP are reported in Figure 5.1 as a function of the Froude number of the flow near the origin.

Moving to the mobile bed case system (4.7) derived in Section 4.1, as the fixed bed one, it can be written in compact form as

$$\frac{\partial \mathbf{U}_m}{\partial t} + \frac{\partial}{\partial x}\mathbf{F}_m(\mathbf{U}_m) + \mathbf{H}_m \frac{\partial \mathbf{W}_m}{\partial x} = \mathbf{S}_m \tag{5.13}$$

where the subscript m indicates the mobile-bed case and

$$\mathbf{U}_m = \begin{bmatrix} h \\ uh \\ c_b z_b \end{bmatrix}; \qquad \mathbf{W}_m = \begin{bmatrix} h \\ u \\ z_b \end{bmatrix}; \qquad \mathbf{F}_m = \begin{bmatrix} uh \\ u^2 h + \frac{1}{2} g h^2 \\ cuh \end{bmatrix} \tag{5.14}$$

$$\mathbf{H}_m = \begin{bmatrix} 0 & 0 & 0 \\ 0 & 0 & gh \\ 0 & 0 & 0 \end{bmatrix}; \quad \mathbf{S}_m = \begin{bmatrix} 0 \\ -\dfrac{\tau_0}{\rho_f} \\ 0 \end{bmatrix} \tag{5.15}$$

The eigenstructure of this system can be obtained by analyzing the associated homogeneous quasi-linear form that can be written as

$$\mathbf{J}_{\mathbf{U}_m} \frac{\partial \mathbf{W}_m}{\partial t} + \left(\mathbf{J}_{\mathbf{F}_m} + \mathbf{H}_m \right) \frac{\partial \mathbf{W}_m}{\partial x} = 0 \tag{5.16}$$

where

$$\mathbf{J}_{\mathbf{U}_m} = \frac{\partial \mathbf{U}_m}{\partial \mathbf{W}_m}; \qquad \mathbf{J}_{\mathbf{F}_m} = \frac{\partial \mathbf{F}_m}{\partial \mathbf{W}_m} \tag{5.17}$$

are respectively the Jacobian of the conserved variables and of the fluxes with respect to the primitive variable vector $\mathbf{W}_m$. The relevant characteristic polynomial, deriving from

$$\det \left| \mathbf{J}_{\mathbf{F}_m} + \mathbf{H}_m - \lambda \mathbf{J}_{\mathbf{U}_m} \right| = 0 \tag{5.18}$$

is the following

$$\lambda^3 - 2u\lambda^2 - \left(gh - u^2 + \frac{gh}{c_b} \left(c + u \frac{\partial c}{\partial u} \right) \right) \lambda - \frac{ghu}{c_b} \left(h \frac{\partial c}{\partial h} - u \frac{\partial c}{\partial u} \right) = 0 \tag{5.19}$$

As demonstrated by several authors (e.g. [25] and [46]) when using different closure relations, the three solutions of the polynomial, λ_i with $i = 1, 3$, are real and distinct; two eigenvalues have the same sign of particle velocity u while one is opposite; the eigenvector associated to a generic eigenvalue λ_i is

$$\mathbf{R}_i^{W_m} = \begin{bmatrix} gh \\ -g(u - \lambda_i) \\ (u - \lambda_i)^2 - gh \end{bmatrix} \tag{5.20}$$

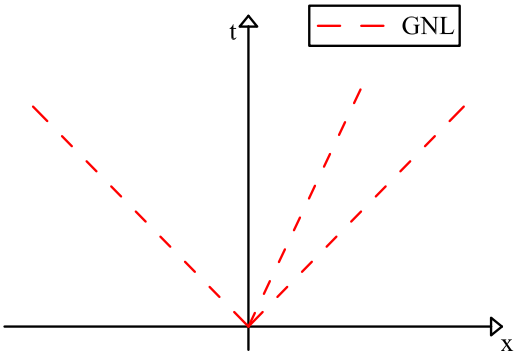

Figure 5.2: Wave patterns of a mobile-bed RP. Velocity is assumed positive throughout.

and the characteristic field associated to each eigenvalue is genuinely nonlinear except for the case of water at rest. Finally, since the system is nonconservative, the relations valid across any shock wave are the GRH relations

$$\mathbf{F}^*_{mR} - \mathbf{F}^*_{mL} - \mathbf{D}_m = S_s \left(\mathbf{U}^*_{mR} - \mathbf{U}^*_{mL}\right) \tag{5.21}$$

where S_s is the speed of the shock, $\mathbf{F}^*_{mR}, \mathbf{F}^*_{mL}$ and $\mathbf{U}^*_{mR}, \mathbf{U}^*_{mL}$ are the fluxes and the conserved variables respectively on the right and on the left of the shock wave and finally $\mathbf{D}^T_m = (0, D, 0)$, where D is given by equation (5.12).

Finally, according to the features described above, the possible wave pattern marking out a mobile-bed RP is reported in Figure 5.2 where the velocity is assumed positive everywhere.

5.2 One-dimensional systems for high sediment concentration

The eigenstructure analysis of the one-dimensional systems for high sediment concentration, derived in Section 4.2, is performed in the same way as in the previous Section.

Starting from the fixed bed system (4.8), its compact form is expressed

by an equation formally equal to (5.2) where in this case, the vectors are

$$\mathbf{U}_f = \begin{bmatrix} h + z_b \\ (1+\varphi\Delta)\, uh \\ \varphi h \\ z_b \end{bmatrix}; \quad \mathbf{F}_f = \begin{bmatrix} uh \\ (1+\varphi\Delta)\left(u^2 h + \frac{1}{2} g h^2\right) \\ \varphi uh \\ 0 \end{bmatrix} \tag{5.22}$$

$$\mathbf{H}_f = \begin{bmatrix} 0 & 0 & 0 & 0 \\ 0 & 0 & 0 & (1+\varphi\Delta)\, gh \\ 0 & 0 & 0 & 0 \\ 0 & 0 & 0 & 0 \end{bmatrix}; \qquad \mathbf{S}_f = \begin{bmatrix} 0 \\ -\dfrac{\tau_0}{\rho_f} \\ 0 \\ 0 \end{bmatrix}; \quad \mathbf{W}_f = \begin{bmatrix} h \\ u \\ \varphi \\ z_b \end{bmatrix} \tag{5.23}$$

The characteristic polynomial associated to this system has four real and distinct roots

$$\begin{cases} \lambda_1 = u - \sqrt{gh} \\ \lambda_2 = u \\ \lambda_3 = u + \sqrt{gh} \\ \lambda_4 = 0 \end{cases} \tag{5.24}$$

and thy are equal to the ones obtained for the low concentration systems (5.9). Moving to the eigenvectors, they are

$$\begin{aligned} \mathbf{R}_1^{W_f} &= \begin{bmatrix} -\dfrac{1}{g}\sqrt{gh} \\ 1 \\ 0 \\ 0 \end{bmatrix} \quad ; \quad \mathbf{R}_2^{W_f} = \begin{bmatrix} -h\dfrac{\Delta}{2\,(1+\varphi\Delta)} \\ 0 \\ 1 \\ 0 \end{bmatrix} \\ \mathbf{R}_3^{W_f} &= \begin{bmatrix} \dfrac{1}{g}\sqrt{gh} \\ 1 \\ 0 \\ 0 \end{bmatrix} \quad ; \quad \mathbf{R}_4^{W_f} = \begin{bmatrix} -g\dfrac{h}{gh - u^2} \\ g\dfrac{u}{gh - u^2} \\ 0 \\ 1 \end{bmatrix} \end{aligned} \tag{5.25}$$

and, compared with (5.10), only the second one is different.

Regarding the nature of the characteristic fields, they are the same as for the low concentration fixed bed case. The only difference is related to the

characteristic field associated with λ_2 that is a classic Linearly Degenerate (LD) one where, in this case, not only φ changes across it, but also the flow depth h changes its value. The variation of h across the λ_2 wave derives from the presence of an high sediment concentration inside the flow field that modify in a sensible way the characteristic of the flow itself.

The last difference between the eigenstructure of the complete 1D fixed bed system and the low concentration one is in the thrust term D exerted by the bed step on the control volume used to obtain relations (5.11) that is now, following [54],

$$D = -g\,(1+\varphi\Delta)\left(h_k - \frac{|z_R - z_L|}{2}\right)(z_R - z_L) \tag{5.26}$$

$$\text{with } k = \begin{cases} L & \text{if } z_L \le z_R \\ R & \text{otherwise} \end{cases}$$

The one-dimensional mobile bed system for high sediment concentration (4.9), in compact form, assume the same expression as (5.13) where, in this case,

$$\mathbf{U}_m = \begin{bmatrix} h + z_b \\ (1+c\Delta)\,uh \\ c_b z_b + ch \end{bmatrix}; \quad \mathbf{F}_m = \begin{bmatrix} uh \\ (1+c\Delta)\left(u^2 h + \frac{1}{2}gh^2\right) \\ cuh \end{bmatrix} \tag{5.27}$$

$$\mathbf{H}_m = \begin{bmatrix} 0 & 0 & 0 \\ 0 & 0 & (1+c\Delta)\,gh \\ 0 & 0 & 0 \end{bmatrix}; \quad \mathbf{S}_m = \begin{bmatrix} 0 \\ -\dfrac{\tau_0}{\rho_f} \\ 0 \end{bmatrix}; \quad \mathbf{W}_m = \begin{bmatrix} h \\ u \\ z_b \end{bmatrix} \tag{5.28}$$

As for the low concentration case, the relevant characteristic polynomial, is the following

$$a_3\lambda^3 + a_2\lambda^2 + a_1\lambda + a_0 = 0 \tag{5.29}$$

where the coefficients are

$$a_3 = (1+c\Delta)\left(h\frac{\partial c}{\partial h} - c_b + c\right) - (1+c_b\Delta)\,u\frac{\partial c}{\partial u}$$

$$a_2 = \frac{1}{2}gh\Delta\left(c_b - c\right)\frac{\partial c}{\partial u} + 2u\left(1+\Delta c\right)\left(c_b - c - h\frac{\partial c}{\partial h}\right) + \\ - u\left(1+\Delta c_b\right)\left(h\frac{\partial c}{\partial h} - 2u\frac{\partial c}{\partial u}\right)$$

$$a_1 = \left(1+c\Delta\right)\left(\left(gh-u^2\right)\left(c_b - c - h\frac{\partial c}{\partial h}\right) + ghu\frac{\partial c}{\partial u}\right) + \\ + \left(h\frac{\partial c}{\partial h} - u\frac{\partial c}{\partial u}\right)\left(u^2\left(1+c_b\Delta\right) + \frac{1}{2}gh\Delta\left(c_b - c\right)\right)$$

$$a_0 = ghu\left(1+c\Delta\right)\left(h\frac{\partial c}{\partial h} - u\frac{\partial c}{\partial u}\right)$$

Also in this case, when using different closure relations, the three solutions of the polynomial, λ_i with $i = 1, 3$, are real and distinct; two eigenvalues have the same sign of particle velocity u while one is opposite.

The eigenvector associated to a generic eigenvalue λ_i is

$$\mathbf{R}_i^{W_m} = \begin{bmatrix} h\lambda_i\left(c_b - c + \left(\lambda_i - u\right)\frac{\partial c}{\partial u}\right) \\ \lambda_i\left(u - \lambda_i\right)\left(h\frac{\partial c}{\partial h} - c_b + c\right) \\ h\left(u-\lambda_i\right)\left(h\frac{\partial c}{\partial h} - \left(u-\lambda_i\right)\frac{\partial c}{\partial u}\right) \end{bmatrix} \tag{5.30}$$

and the characteristic field associated to each eigenvalue is genuinely nonlinear. Finally, since the system is non-conservative, the relations valid across any shock wave are the GRH relations (5.21) with the following thrust term D

$$D = -g\left(1+c_k\Delta\right)\left(h_k - \frac{|z_R - z_L|}{2}\right)\left(z_R - z_L\right) \tag{5.31}$$

$$\text{with } k = \begin{cases} L & \text{if } z_L \le z_R \\ R & \text{otherwise} \end{cases}$$

A comparison between these eigenvalues, the ones of the low concentration mobile bed model and the fixed bed ones, it is possible if we introduce a closure relation. For this purpose the choice is to consider

$$c = c(u,h) = \beta\frac{u^2}{gh} = \beta Fr^2 \tag{5.32}$$

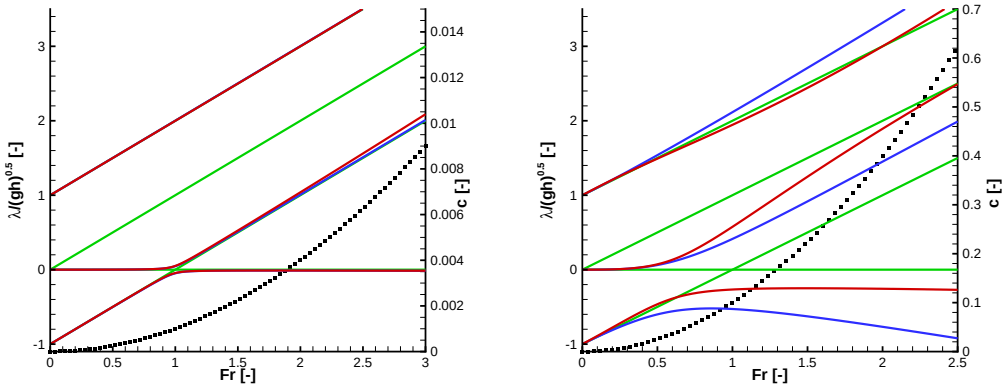

(a) Low transport capacity $\beta = 0.001$. (b) High transport capacity $\beta = 0.1$

Figure 5.3: Dimensionless eigenvalues for fixed bed (green), low concentration mobile bed (blue) and high concentration mobile bed (red): (a) low transport capacity case, (b) high transport capacity case. The parameters used are: $\Delta = 1.65$ and $c_b = 0.65$. Black dots represent the concentration.

where β is a semi-empirical non-dimensional constant, depending on sediment characteristics, and $g = 9.81 m/s^2$. The previous relation can be formally obtained from a Meyer-Peter and Müller sediment transport formula, assuming an expression for the bed shear stress of type $\tau_0/\rho_f = fu^2$, where the friction factor f depends on the diameter and the shape of the sediments. We refer the reader to the work of Rosatti and Fraccarollo [54] for details on this relation. Once the closure relation for the concentration has been defined, it is possible to represent the eigenvalues deriving from the characteristic polynomials (5.19), (5.29) and the eigenvalues for the fixed bed (5.25) on a dimensionless plot $\tilde{\lambda} = \frac{\lambda}{\sqrt{gh}}$ versus Fr reported in Figure 5.3. In this Figure it is possible to note that if the concentration is low (Figure 5.3a) all the systems have essentially the same eigenvalues, while when the concentration increase (Figure 5.3b), the eigenvalues of the two mobile bed systems become significantly different from each other and also from the fixed bed ones. As written before, we can notice that in the fixed bed case (green lines) one eigenvalue changes sign, while the ones for the mobile bed do not have this behavior.

5.3 Two-dimensional plane-wave systems

The last two systems that we analyze are the two-dimensional plane-wave systems derived in Section 4.3. The fixed bed case, defined by the set of equations (4.10), can be written in compact form as (5.2) where the vectors are now

$$\mathbf{U}_f = \begin{bmatrix} h + z_b \\ (1+\varphi\Delta)\, uh \\ (1+\varphi\Delta)\, vh \\ \varphi h \\ z_b \end{bmatrix}; \quad \mathbf{F}_f = \begin{bmatrix} uh \\ (1+\varphi\Delta)\left(u^2 h + \frac{1}{2} g h^2\right) \\ (1+\varphi\Delta)\, uvh \\ \varphi uh \\ 0 \end{bmatrix} \tag{5.33}$$

$$\mathbf{H}_f = \begin{bmatrix} 0 & 0 & 0 & 0 & 0 \\ 0 & 0 & 0 & (1+\varphi\Delta)\, gh & 0 \\ 0 & 0 & 0 & 0 & 0 \\ 0 & 0 & 0 & 0 & 0 \\ 0 & 0 & 0 & 0 & 0 \end{bmatrix}; \quad \mathbf{S}_f = \begin{bmatrix} 0 \\ -\dfrac{\tau_{0,x}}{\rho_f} \\ -\dfrac{\tau_{0,y}}{\rho_f} \\ 0 \\ 0 \end{bmatrix}; \quad \mathbf{W}_f = \begin{bmatrix} h \\ u \\ v \\ z_b \\ \varphi \end{bmatrix} \tag{5.34}$$

Analyzing the characteristic polynomial, it has five real roots

$$\begin{cases} \lambda_1 = u - \sqrt{gh} \\ \lambda_{2,3} = u \\ \lambda_4 = u + \sqrt{gh} \\ \lambda_5 = 0 \end{cases} \tag{5.35}$$

where all the property of the fixed bed low concentration systems are still valid.

The associated eigenvectors are instead

$$\mathbf{R}_1^{W_f} = \begin{bmatrix} -\frac{1}{g}\sqrt{gh} \\ 1 \\ 0 \\ 0 \\ 0 \end{bmatrix} \quad ; \quad \mathbf{R}_2^{W_f} = \begin{bmatrix} -h\frac{\Delta}{2\left(1+\varphi\Delta\right)} \\ 0 \\ 0 \\ 0 \\ 1 \end{bmatrix} \quad ; \quad \mathbf{R}_3^{W_f} = \begin{bmatrix} 0 \\ 0 \\ 1 \\ 0 \\ 0 \end{bmatrix}$$
$$\mathbf{R}_4^{W_f} = \begin{bmatrix} \frac{1}{g}\sqrt{gh} \\ 1 \\ 0 \\ 0 \\ 0 \end{bmatrix} \quad ; \quad \mathbf{R}_5^{W_f} = \begin{bmatrix} -g\frac{h}{gh-u^2} \\ g\frac{u}{gh-u^2} \\ 0 \\ 1 \\ 0 \end{bmatrix} \tag{5.36}$$

Regarding the nature of the characteristic fields, those associated with λ_1 and λ_4 are Genuinely Non-Linear (GNL). Moreover, considering the relevant Riemann Invariants (RI), we can state that both v, φ and z_b do not change across the waves of these fields. Thus the relevant possible shocks are described by the classical Rankine-Hugoniot (RH) relations, since these discontinuities occur over a flat bed. The characteristic field associated with λ_2 is a classic Linearly Degenerate (LD) one across which h and φ change (as for the pure $1D$ system). Also the characteristic field associated to λ_3 is LD and across its only v changes. In these two cases RI and RH relations give the same informations. Finally the field associated with $\lambda_5 = 0$ is a steady contact wave across which, in addition to h and u, the bed elevation also changes. This is a particular Linearly Degenerate (LD*) field across which, as demonstrated in [51], only the Generalized Rankine-Hugoniot (GRH) relations are valid.

The last model presented is the two-dimensional plane-wave mobile bed system (4.11). Written in compact form, it assumes the expression (5.13) where the terms are now

$$\mathbf{U}_m = \begin{bmatrix} h + z_b \\ \left(1+c\Delta\right)uh \\ \left(1+c\Delta\right)vh \\ c_b z_b + ch \end{bmatrix} ; \quad \mathbf{F}_m = \begin{bmatrix} uh \\ \left(1+c\Delta\right)\left(u^2h + \frac{1}{2}gh^2\right) \\ \left(1+c\Delta\right)uvh \\ cuh \end{bmatrix} \tag{5.37}$$

$$\mathbf{H}_m = \begin{bmatrix} 0 & 0 & 0 & 0 \\ 0 & 0 & 0 & (1+c\Delta)\, gh \\ 0 & 0 & 0 & 0 \\ 0 & 0 & 0 & 0 \end{bmatrix}; \quad \mathbf{S}_m = \begin{bmatrix} 0 \\ -\dfrac{\tau_{0,x}}{\rho_f} \\ -\dfrac{\tau_{0,y}}{\rho_f} \\ 0 \end{bmatrix}; \quad \mathbf{W}_m = \begin{bmatrix} h \\ u \\ v \\ z_b \end{bmatrix} \tag{5.38}$$

The characteristic polynomial of its linearized version (5.16) is the following

$$(\lambda - u)\left(a_3\lambda^3 + a_2\lambda^2 + a_1\lambda + a_0\right) = 0 \tag{5.39}$$

where the coefficients are

$$a_3 = (1+c\Delta)\left(h\frac{\partial c}{\partial h} - c_b + c\right) - (1+c_b\Delta)\left(u\frac{\partial c}{\partial u} + v\frac{\partial c}{\partial v}\right)$$

$$a_2 = \frac{1}{2}gh\Delta\,(c_b - c)\frac{\partial c}{\partial u} + 2u\,(1+c\Delta)\left(c_b - c - h\frac{\partial c}{\partial h}\right) + \\ - u\,(1+c_b\Delta)\left(h\frac{\partial c}{\partial h} - 2u\frac{\partial c}{\partial u} - 2v\frac{\partial c}{\partial v}\right)$$

$$a_1 = (1+c\Delta)\left(\left(gh - u^2\right)\left(c_b - c - h\frac{\partial c}{\partial h}\right) + ghu\frac{\partial c}{\partial u}\right) + \\ + \left(h\frac{\partial c}{\partial h} - u\frac{\partial c}{\partial u}\right)\left(u^2\,(1+c_b\Delta) + \frac{1}{2}gh\Delta\,(c_b - c)\right) + \\ + v\left(gh - u^2\right)\frac{\partial c}{\partial v}\,(1+c_b\Delta)$$

$$a_0 = ghu\,(1+c\Delta)\left(h\frac{\partial c}{\partial h} - u\frac{\partial c}{\partial u}\right)$$

These coefficients are different from the ones derived for the one-dimensional systems for high sediment concentration, due to the presence of the transversal velocity v. The roots of the third order polynomial, λ_i with $i = 1, 3$, when using different closure relations, are real and distinct and they degenerate to the ones of the pure $1D$ system when v is null. Two of these eigenvalues have the same sign of the velocity u while one is opposite.

The eigenvector associated to a generic eigenvalue λ_i is

$$\mathbf{R}_i^{W_m} = \begin{bmatrix} h\lambda_i \left((1+c\Delta) \left(c_b - c + (\lambda_i - u) \dfrac{\partial c}{\partial u} \right) + v \dfrac{\partial c}{\partial v} (1 + c_b \Delta) \right) \\ \lambda_i (\lambda_i - u) \left((1+c\Delta) \left(c_b - c - h \dfrac{\partial c}{\partial h} \right) + v \dfrac{\partial c}{\partial v} (1 + c_b \Delta) \right) \\ -v\lambda_i (1 + c_b \Delta) \left(h \dfrac{\partial c}{\partial h} + (\lambda_i - u) \dfrac{\partial c}{\partial u} \right) \\ h (u - \lambda_i) (1 + c\Delta) \left(h \dfrac{\partial c}{\partial h} + (\lambda_i - u) \dfrac{\partial c}{\partial u} \right) \end{bmatrix} \tag{5.40}$$

and the characteristic field associated to each eigenvalue is genuinely nonlinear except for the case of water at rest. Since the system is non-conservative, the relations valid across any shock wave are the GRH relations as for the $1D$ system for high sediment concentration.

The last solution of the characteristic polynomial (5.39) is

$$\lambda_4 = u \tag{5.41}$$

The associated eigenvector is

$$\mathbf{R}_4^{W_m} = \begin{bmatrix} h\Delta \dfrac{\partial c}{\partial v} \\ 0 \\ -2 (1 + c\Delta) - h\Delta \dfrac{\partial c}{\partial h} \\ 0 \end{bmatrix} \tag{5.42}$$

and the characteristic field is a classic linearly degenerate one where only h and v change. Across this wave, bot the RI and the classical RH condition are valid since no variation of the bed is admissible.

Part II

Transition from fixed bed to mobile bed: mathematical aspect

Chapter 6

Fixed and mobile-bed flows: possible coupled phenomena

In the previous Part we derive two different classes of systems: the fixed bed and the mobile bed one. As presented in Chapter 5, these two classes of systems have a different number of equations, a different number of unknowns and describe two different bed behaviors. However they refer to a common phenomena: a two-phase free-surface flow.

In this thesis, we are interested in modelling the transition across a fixed–mobile interface located at a given point of a flow field that not change in time. This condition occurs rather often in natural or partially anthropized environment. For example, a debris flow along its path in an alluvial fan can flow over a rigid bedrock in the upper part, while in the lower, sedimentation can occur with a significant increase in the bed level. Similarly, the same river can encounter both artificially paved and natural mobile-bed transects as in Figure 6.1. Careful modelling of the transition between fixed and mobile bed conditions is therefore an important task for obtaining reliable numerical simulations in flow situations involving this type of bed change. Moreover, it can become a crucial point in simulations addressed to disaster prevention and protection since the presence of artificial artifacts generates lots of these transitions.

However, in some situations the bed state can change dynamically. For example, a rigid surface can be placed at a given level under a layer of

Figure 6.1: Example of transition between mobile bed and fixed bed in Cismon creek.

sediments: the bed is initially in mobile condition, but if the erosion reaches the fixed surface, the bed becomes fixed. On the other hand, given a fixed-bed transect, if the concentration of sediments in the flowing mixture exceeds a threshold value (known as capacity transport concentration), a deposition occurs, the bed level increases and it becomes mobile. The dynamic changes of the bed state is left to further works.

In Section 6.1 a literature review about the fixed and mobile bed transition is presented, while in Section 6.2 a new approach for the coupling of the systems describing the two relevant bed states is described.

6.1 Literature review

In the literature, the problem of the transition between fixed and mobile bed condition is not well studied. In fact exists only a few papers about it and, in particular, notable to citation are the one of Struiksma [61] and the one of Rulot *et al.* [58]. Both of them use only the mobile bed systems where some suitable restrictions on the solid fluxes are imposed.

In the model proposed by Struiksma [61], the solid fluxes q_s are evaluated using a formulation like

$$q_s = \psi \left(\frac{z_b}{z_b^*} \right) q_s^* \tag{6.1}$$

where q_s^* is a sediment transport formula that can be found in the literature and $\psi \left(\frac{z_b}{z_b^*} \right)$ is an arbitrary regularization quantity, which is a function of the ratio between the actual bed elevation z_b and the fixed-bed elevation z_b^* in each point of the computational domain. This function ranges from 1, when the bed is far from the fixed level, to 0 when the bed is fixed. According to the author, this approach is limited to small scours for each time step, in order to avoid the computation of non-physical bed elevations.

The method proposed in Rulot *et al.* [58] is slightly different. In this case the solid fluxes are initially evaluated as if the bed was completely mobile (step 0 in Figure 6.2). Then, in a fixed-bed computational cell subjected to possible erosion, the outgoing flux, is forced to be equal to the ingoing flux to ensure that the solid mass balance does not change the bed elevation (step 1 in Figure 6.2). This flux modification requires that the mass balance of the downstream cell must be consistently updated.

Performing a critical review of this method we highlighted the following limit. Looking at the example in Figure 6.2, when the ingoing flux for the second fixed bed cell was modified, the outgoing flux must be changed in turn (step 2 in Figure 6.2) since no scour can happen. In this way, a cascade process interests the whole possible fixed-bed reach in a single time step independently of the actual length of the transect. This approach has two drawbacks: computational cost, connected to the sequential iterative procedure necessary to describe the cascade, and wrong computation of the sediment wave speed over the fixed-bed reach. In the example sketched in

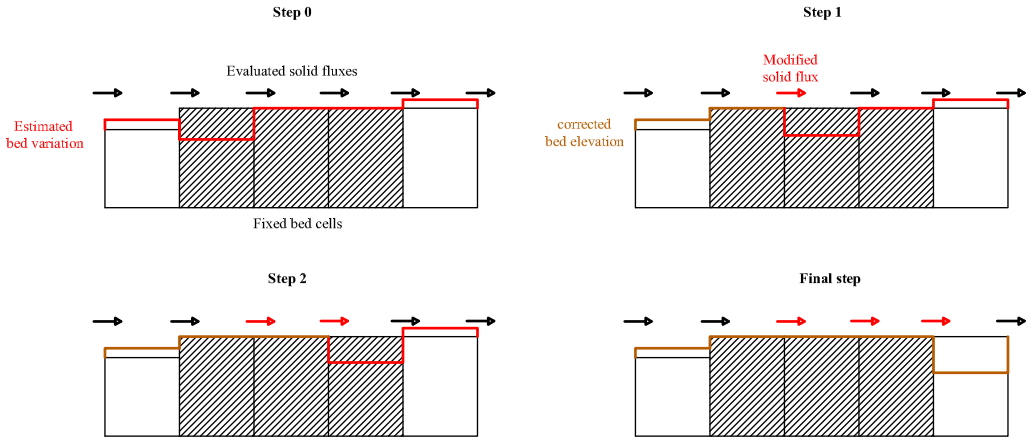

Figure 6.2: Example of a fixed-bed transect computation using the methodology developed by Rulot *et al.*.

Figure 6.2, the erosion process that potentially affect the first non erodible cell, are simply moved downstream in the closest mobile bed cell in only one time step.

A final remark for these two approaches is that both methods work only when the concentration of the solid phase is quite low and a low concentration model can be used.

6.2 A novel approach for the coupling of fixed and mobile bed systems

The transition between fixed and mobile bed can be analyzed using different sets of equations. This possibility is more physically based, i.e. it uses the set of equations for the fixed-bed situation where the bed is actually fixed, and the set of equations for the mobile-bed where the bed is actually mobile. In this case, at the interface between the fixed-and the mobile-bed conditions, an abrupt switch between the two systems occurs and appropriate treatment of this interface is therefore necessary. It is quite logical to conceive the possibility of describing what happens across the interface in terms of the development of Riemann Problems (RPs) since it is a initial-value problem in which the initial values of the variables are piecewise constant functions

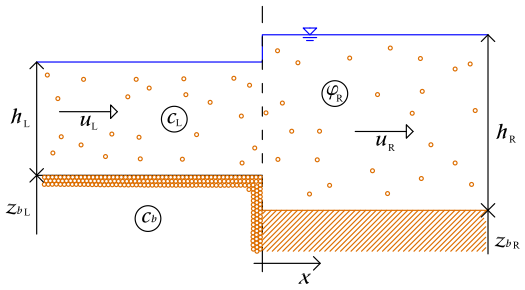

Figure 6.3: Sketch of a CRP describing the transition between mobile and fixed bed with the main variables involved.

with a single discontinuity located conventionally in the origin of the spatial axis. Nevertheless, these types of RPs present a new feature, in that not only the constant initial values of the variables change abruptly across the interface but also the relevant system of equations. We call this novel RP a Composite Riemann Problem (CRP). A sketch of a CRP describing the transition between mobile and fixed bed is presented in Figure 6.3 with the indication of the main variables involved. The solution of this challenging problem has intrinsic scientific importance but it becomes fundamental if, as in our case, we are interested in developing a finite-volume numerical method based on Godunov fluxes presented in Part III.

The key idea, introduced with this thesis and published in [57], is to merge the two original systems by means of a suitable weighting function, in order to obtain a new single system which is able to reproduce both the mobile-bed and the fixed-bed original conditions by simply acting on the weighting parameter. The introduction of a convenient differential equation for the weighting parameter makes it possible to obtain a single hyperbolic system valid on both sides of the discontinuity. Thus, it is possible to reduce a CRP to a classical RP, where its distinctive features can be analyzed by means of standard tools. In particular, the development of a standing contact wave can correctly describe the sharp transition between mobile and fixed bed conditions. This approach recalls some aspects of the work of Göz and Munz [29] in which a material interface, across which a sharp transition between two different gases occurs, is described by introducing a suitable flux weighting function and a convenient relevant differential equation which

allows the automatic switch of the fluxes across a contact wave.

The problem of coupling different sets of hyperbolic systems is in present in several fields of research [3, 4, 14, 28] and an overview can be found in Coquel [18]. However, these works develop a specific strategy strictly related to the problem involved, and they do not solve the Riemann problem at the interface where the systems change. We develop, in Chapter 7, a strategy to solve the coupling problem using a specific sets of equations: the fixed and the mobile bed systems. However, the strategy we present, for the solution of the CRP, is quite general and is actually not linked to the specific topic. For this reason the coupling methodology presented later on can be considered a possible alternative respect to others present in the literature where the only requirement needed is to have two systems related to the same physical problem.

Chapter 7

The Composite Riemann Problem: definition, solution and eigenstructure

In this Chapter we use the idea for the coupling different hyperbolic systems presented in Chapter 6, for the study of transition between the fixed and mobile bed. In order to derive a general methodology, we decide to start the dissertation about the transition between fixed an mobile bed using the systems for low sediment concentration. These systems of partial differential equations (PDEs) were obtained in Section 4.1 and for the fixed bed part of the problem, is (4.5) and reads

$$\begin{cases} \dfrac{\partial h}{\partial t} + \dfrac{\partial}{\partial x}(uh) = 0 \\ \dfrac{\partial}{\partial t}(uh) + \dfrac{\partial}{\partial x}\left(u^2 h + \dfrac{1}{2} g h^2\right) + gh\dfrac{\partial z_b}{\partial x} = -\dfrac{\tau_0}{\rho_w} \\ \dfrac{\partial}{\partial t}(\varphi h) + \dfrac{\partial}{\partial x}(\varphi uh) = 0 \\ \dfrac{\partial z_b}{\partial t} = 0 \end{cases} \tag{7.1}$$

while for the mobile part the system is (4.7)

$$\begin{cases} \dfrac{\partial h}{\partial t} + \dfrac{\partial}{\partial x}(uh) = 0 \\ \dfrac{\partial}{\partial t}(uh) + \dfrac{\partial}{\partial x}\left(u^2 h + \dfrac{1}{2}gh^2\right) + gh\dfrac{\partial z_b}{\partial x} = -\dfrac{\tau_0}{\rho_w} \\ \dfrac{\partial}{\partial t}(z_b) + \dfrac{\partial}{\partial x}\left(\dfrac{c}{c_b}uh\right) = 0 \end{cases} \tag{7.2}$$

where h is the flow depth, u is the velocity, z_b is the bottom elevation, φ the transported solid concentration pertaining to the fixed bed model, c is the solid equilibrium concentration pertaining to the mobile bed model, c_b is the constant sediment concentration in the bed, ρ_w is the water density, g is the constant gravity acceleration and τ_0 is the bed shear stress.

These systems are hyperbolic and the eigenstructures were analyzed in Section 5.1.

7.1 The Composite Riemann problem

A classical $1D$ RP is an initial-value problem in which an unique set of homogeneous equations holds throughout the flow field and the initial values of the variables are piecewise constant functions with a single discontinuity located conventionally in the origin of the spatial axis. Mathematically, it can be written as:

$$\begin{cases} \dfrac{\partial}{\partial t}\mathbf{U} + \dfrac{\partial}{\partial x}\mathbf{F}(\mathbf{U}) = 0 \\ \mathbf{U}(x,0) = \begin{cases} \mathbf{U}_L & \text{if} \quad x < 0 \\ \mathbf{U}_R & \text{if} \quad x > 0 \end{cases} \end{cases} \tag{7.3}$$

The RP that can be defined in the neighborhood of the fixed-mobile bed interface is somewhat different: as in the previous case the initial values of the variables are piecewise constant functions with a single discontinuity but the set of equations valid on the left and on the right of the discontinuity are different (see Figure 7.1). We called this novel type of RP as Composite Riemann Problem (CRP). Mathematically it can be described in the following

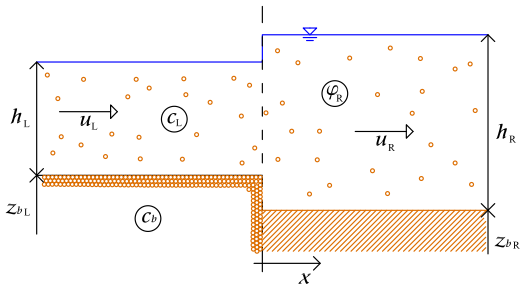

Figure 7.1: Sketch of the initial values of a Composite Riemann Problem with a mobile-bed condition on the left of the discontinuity and with a fixed-bed one on the right.

way:

$$\begin{cases} \dfrac{\partial \mathbf{U}_i}{\partial t} + \dfrac{\partial}{\partial x}\mathbf{F}_i(\mathbf{U}_i) + \mathbf{H}_i \dfrac{\partial \mathbf{W}_i}{\partial x} = 0 \\ \mathbf{U}_i\,(x,0) = \begin{cases} \mathbf{U}_{iL} \\ \mathbf{U}_{iR} \end{cases} \\ \text{where} \begin{cases} i = m \quad \text{if} \quad x < 0 \\ i = f \quad \text{if} \quad x > 0 \end{cases} \end{cases} \tag{7.4}$$

For $i = m$, the relevant set is given by the homogeneous part of system (7.2) while for $i = f$, the relevant system is the homogeneous part of system (7.1). The previous expression is valid for the case in which on the left of the discontinuity there is a mobile-bed condition and on the right a fixed-bed one. A simple swap of the indexes m and f gives the fixed-mobile case. It worth noticing that the two sets are characterized by a different number of differential equations.

Now some questions arise: is it possible to obtain CRP solutions? In the case, which are their properties? The rigorous answer to these questions is presented in Section 7.2. Here we focus on some intuitive features of the solutions that can be inferred from reasoning on the physics of the problem and on the relation that must hold across the fixed-mobile interface.

7.1.1 Expected features of the CRP solutions and the Generalized Rankine-Hugoniot relation

A CRP solution should be composed on the left by the set of waves associated with the negative eigenvalues of the left system and on the right by the set of waves associated with the positive eigenvalues of the right system. Across the origin, since it is assumed that the interface between the fixed- and mobile-bed conditions does not change its position in time, a stationary wave that guarantees the mass and momentum balance is expected. The relations that characterize this wave are the GRH relations which, following Rosatti and Fraccarollo [54], can be obtained by considering a control volume of infinitesimal width placed across the interface. Stationary mass and momentum balances for the liquid phase and mass balance for the solid phase written in integral form for the given control volume provide the following expressions for the mobile–fixed case:

$$\begin{cases} [uh]^*_{fR} - [uh]^*_{mL} = 0 \\ \left[u^2h + \frac{1}{2}gh^2\right]^*_{fR} - \left[u^2h + \frac{1}{2}gh^2\right]^*_{mL} = D \\ [\varphi uh]^*_{fR} - [cuh]^*_{mL} = 0 \end{cases} \tag{7.5}$$

where the star values refer to the constant states on the left and on the right of the standing wave, while D is is, as specified in Section5.1, the thrust term exerted by the bed step on the control volume

$$D = -g\left(h_k - \frac{|z_R - z_L|}{2}\right)(z_R - z_L) \quad \text{with } k = \begin{cases} L & \text{if } z_L \leq z_R \\ R & \text{otherwise} \end{cases} \tag{7.6}$$

The indication of the subscript m, f is actually useless, since the meaning of h and u is the same in both bed conditions, while φ and c are defined only in their respective cases. Therefore, it will not be used any longer. For the fixed–mobile case, only the last equation changes with a swap in the subscripts. It is worth noting that while the first two equations are standard, the third, concerning the solid mass balance, provides the connection between the transported concentration φ and the equilibrium concentration c: the fluxes of solid mass across the discontinuity must be equal independently from the form in which the sediment is conveyed. Moreover, considering the

water flux is the same (first equation), the constancy of solid mass through the discontinuity is reduced to an equality between the equilibrium and the transported concentrations, $c = \varphi$.

7.2 The CRP solution strategy: the Composite PDEs system

As we stated in Section 6.2, the strategy to obtain the solution to the CRP is based on the key idea of merging the two original systems by means of a suitable weighting function, in order to obtain a single system able to reproduce both the mobile-and the fixed-bed original conditions simply by changing the value of the weighting parameter. Nevertheless, it is not possible to do this in a straightforward manner because, as already indicated in Section 7.1, the number of variables (and obviously of equations) is different in the two bed situations. As a result, the first step is to introduce a new appropriate equation in the mobile-bed system, in order to balance the number of equations. In fact, comparing both the primitive variable vector of this bed case, $\mathbf{W}_m^T = \begin{bmatrix} h & u & z_b \end{bmatrix}$, with the corresponding fixed-bed case, $\mathbf{W}_f^T = \begin{bmatrix} h & u & \varphi & z_b \end{bmatrix}$, and the relevant systems, namely equations (7.2) and (7.1), it is clear that a suitable equation involving the variable φ should be added to the mobile-bed system. Obviously in mobile-bed conditions φ does not represent the concentration of the solid phase at all, but simply a dummy variable that does not affect the overall flow. A differential equation stating that the dummy product φh does not change in time can be introduced in system (7.2), giving rise to

$$\begin{cases} \dfrac{\partial h}{\partial t} + \dfrac{\partial}{\partial x}(uh) = 0 \\ \dfrac{\partial}{\partial t}(uh) + \dfrac{\partial}{\partial x}\left(u^2 h + \dfrac{1}{2} g h^2\right) + gh\dfrac{\partial z_b}{\partial x} = -\dfrac{\tau_0}{\rho_f} \\ \dfrac{\partial z_b}{\partial t} + \dfrac{\partial}{\partial x}\left(\dfrac{c}{c_b} uh\right) = 0 \\ \dfrac{\partial}{\partial t}(\varphi h) = 0 \end{cases} \tag{7.7}$$

This system resembles now system (7.1) since both of them have the same number and types of equations (namely mass and momentum balance of the water, mass balance of the solid phase and time invariance of one property) and unknowns.

In order to compose the two sets of PDEs, now we introduce the variable $\alpha(x)$ which describes the state of the bed as a function of the space

$$\alpha(x) = \begin{cases} 0 & \text{if} \quad \textit{fixed-bed} \\ 1 & \text{if} \quad \textit{mobile-bed} \end{cases} \tag{7.8}$$

We called this function *erodibility*. It must be stressed that in the CRP the switch between mobile-and fixed-bed conditions occurs only in a given position of the space and do not change in time. For this reason, the erodibility is not a function of time. In principle, a more general relation could be used for α, but in this case the physical justification for the choice and the relevant mathematical consequences fall far outside the scope of this Part where the mathematical description of how to combine two different systems of PDEs is presented. We therefore restrict our analysis to the case expressed by equation (7.8).

The Composite PDEs system can be derived adding system (7.1) multiplied by $(1-\alpha)$ to system (7.2) multiplied by α

$$\begin{cases} \dfrac{\partial h}{\partial t} + \dfrac{\partial (uh)}{\partial x} = 0 \\ \dfrac{\partial}{\partial t}(uh) + \dfrac{\partial}{\partial x}\left(u^2 h + \dfrac{1}{2}gh^2\right) + gh\dfrac{\partial z_b}{\partial x} = -\dfrac{\tau_0}{\rho_w} \\ \dfrac{\partial}{\partial t}((1-\alpha)\varphi h + \alpha z_b) + (1-\alpha)\dfrac{\partial}{\partial x}(\varphi uh) + \alpha\dfrac{\partial}{\partial x}\left(\frac{c}{c_b}uh\right) = 0 \\ \dfrac{\partial}{\partial t}(\alpha\varphi h + (1-\alpha)z_b) = 0 \end{cases} \tag{7.9}$$

Here α has been shifted inside the time derivatives because it does not depend on time. In this way a single standard PDE system has been obtained and it is straightforward to check that it converges to system (7.1) using $\alpha = 0$ and to system (7.2) using $\alpha = 1$.

Nevertheless, the introduction of the erodibility function is not enough to describe the development of the CRP in a proper manner. In fact, the

previous partially nonconservative system does not allow the development of a standing wave, located in the origin, which is able to describe the flow associated with the discontinuity in $\alpha(x)$. This limit can be overcome by using the same strategy used by Le Roux [41], who introduced a differential equation stating the time invariance of the bed elevation, in order to describe fixed-bed SW flows over a discontinuity of the topography. In the present case, the equation of the time invariance of the erodibility can be introduced

$$\frac{\partial \alpha}{\partial t} = 0 \tag{7.10}$$

With the addition of this equation, the system (7.9) admits a steady contact wave that is expected to adequately describe the transition across the two bed conditions. An important manipulation can now be introduced: the functions $(1-\alpha)$ and α in the third equation can be brought inside the spatial partial derivative. In fact, both the functions are piecewise constant and so, since their derivatives are null everywhere except in the discontinuity point, the following equivalence holds

$$(1-\alpha)\frac{\partial}{\partial x}(\varphi u h) + \alpha \frac{\partial}{\partial x}\left(\frac{c}{c_b} u h\right) = \frac{\partial}{\partial x}\left[\left((1-\alpha)\varphi + \alpha\frac{c}{c_b}\right) u h\right] \tag{7.11}$$

The inclusion of the function α and $(1-\alpha)$ in the spatial derivatives of system (7.9) can be justified also in the following way.

The system composed by system (7.9) plus equation (7.10), can be formally written in compact form as

$$\frac{\partial \mathbf{U}}{\partial t} + \frac{\partial \mathbf{F}'}{\partial x} + \mathcal{H}\frac{\partial \mathbf{U}}{\partial x} = \mathbf{S} \tag{7.12}$$

where

$$\mathbf{U} = \begin{bmatrix} h \\ uh \\ \varphi h + z_b \\ \alpha\varphi h + (1-\alpha) z_b \\ \alpha \end{bmatrix}; \qquad \mathbf{F}' = \begin{bmatrix} uh \\ u^2 h + \frac{1}{2} g h^2 \\ \varphi u h \\ 0 \\ 0 \end{bmatrix} \tag{7.13}$$

while $\mathcal{H} = \mathbf{H}' \partial \mathbf{W} / \partial \mathbf{U}$ where

$$\mathbf{W}^T = [h, u, z_b, \varphi, \alpha] \tag{7.14}$$

is the vector of the primitive variables and

$$\mathbf{S}^T = [0, -\tau_0/\rho_f, 0, 0, 0] \tag{7.15}$$

is the source term. It is not strictly necessary to know the actual expressions of $\mathbf{H}'$ and of $\partial\mathbf{W}/\partial\mathbf{U}$ so they are not reported. The only important thing is to guess that in $\mathcal{H}$ some terms depends on α. System (7.9) is composed by a conservative part, namely $\partial\mathbf{F}'/\ \partial x$, and a non-conservative part, namely $\mathcal{H}\partial\mathbf{U}/\partial x$. Following the theory developed by Dal Maso *et al.* [20], the relation that must hold across the steady wave of the fixed-mobile interface is:

$$\int_0^1 \mathbf{f}(\Phi(s; \mathbf{U}_L^*, \mathbf{U}_R^*))\frac{\partial\mathbf{\Phi}}{\partial s}(s; \mathbf{U}_L^*, \mathbf{U}_R^*)ds = 0. \tag{7.16}$$

where

$$\mathbf{f} = \frac{\partial\mathbf{F}'}{\partial\mathbf{U}} + \mathcal{H} \tag{7.17}$$

$\mathbf{\Phi}(s; \mathbf{U}_L^*, \mathbf{U}_R^*)$, called family of paths, is a Lipschitz map $\mathbf{\Phi} : [0,1] \times \mathbb{R}^m \times \mathbb{R}^m \to \mathbb{R}^m$ satisfying some properties of consistency and regularity and $\mathbf{U}_L^*$, $\mathbf{U}_R^*$ are the constant values of the conserved variables on the left and on the right of the wave. The Jacobian part of $\mathbf{f}$ gives rise to a path-independent value of the integral while the truly nonconservative one leads to a path-dependent term:

$$\mathbf{F}_R'^* - \mathbf{F}_L'^* + \int_0^1 \mathcal{H}(\Phi(s; \mathbf{U}_L^*, \mathbf{U}_R^*))\frac{\partial\mathbf{\Phi}}{\partial s}(s; \mathbf{U}_L^*, \mathbf{U}_R^*)ds = 0. \tag{7.18}$$

In particular, the integral depends on the path connecting the left and right values of α. In the present case the path connecting the two states cannot be chosen arbitrarily but, in order to be physically correct, it must follow the one described by the GRH relations of equation (7.5). Looking at these expressions, it is straightforward to notice that they don't depend on α. So the integral of the nonconservative term must be independent from the path relevant to the variable α. This condition can be achieved rewriting the nonconservative fluxes of the third equation of system (7.9) in a conservative form, i.e. bringing inside the spatial derivative the terms depending on α as expressed by equation (7.11).

Considering the previous operation, the final form of the CPDEs system is then made up of system (7.9), where it is useful to add the fourth equation of (7.9) to the third, plus equation (7.10)

$$\begin{cases} \dfrac{\partial h}{\partial t} + \dfrac{\partial (uh)}{\partial x} = 0 \\ \dfrac{\partial}{\partial t}(uh) + \dfrac{\partial}{\partial x}\left(u^2 h + \dfrac{1}{2} g h^2\right) + gh\dfrac{\partial z_b}{\partial x} = -\dfrac{\tau_0}{\rho_f} \\ \dfrac{\partial}{\partial t}(\varphi h + z_b) + \dfrac{\partial}{\partial x}\left[\left(\varphi(1-\alpha) + \alpha\dfrac{c}{c_b}\right) uh\right] = 0 \\ \dfrac{\partial}{\partial t}(\alpha\varphi h + (1-\alpha) z_b) = 0 \\ \dfrac{\partial \alpha}{\partial t} = 0 \end{cases} \tag{7.19}$$

In compact form, the previous system becomes

$$\frac{\partial \mathbf{U}}{\partial t} + \frac{\partial \mathbf{F}}{\partial x} + \mathbf{H}\frac{\partial \mathbf{W}}{\partial x} = \mathbf{S} \tag{7.20}$$

where

$$\mathbf{U} = \begin{bmatrix} h \\ uh \\ \varphi h + z_b \\ \alpha\varphi h + (1-\alpha) z_b \\ \alpha \end{bmatrix}; \qquad \mathbf{F} = \begin{bmatrix} uh \\ u^2 h + \dfrac{1}{2} g h^2 \\ \left(\varphi(1-\alpha) + \alpha\frac{c}{c_b}\right) uh \\ 0 \\ 0 \end{bmatrix} \tag{7.21}$$

$$\mathbf{H} = \begin{bmatrix} 0 & 0 & 0 & 0 & 0 \\ 0 & 0 & gh & 0 & 0 \\ 0 & 0 & 0 & 0 & 0 \\ 0 & 0 & 0 & 0 & 0 \\ 0 & 0 & 0 & 0 & 0 \end{bmatrix}; \qquad \mathbf{W} = \begin{bmatrix} h \\ u \\ z_b \\ \varphi \\ \alpha \end{bmatrix}; \qquad \mathbf{S} = \begin{bmatrix} 0 \\ -\tau_0/\rho_f \\ 0 \\ 0 \\ 0 \end{bmatrix} \tag{7.22}$$

7.3 Eigenstructure and shock relations of the CPDEs

In order to study the eigenstructure of the CPDEs system (7.19), its homogeneous part can be rewritten in the following quasi-liner form:

$$\mathbf{J_U}\frac{\partial \mathbf{W}}{\partial t} + (\mathbf{J_F} + \mathbf{H})\frac{\partial \mathbf{W}}{\partial x} = 0 \tag{7.23}$$

where

$$\mathbf{J_U} = \frac{\partial \mathbf{U}}{\partial \mathbf{W}}; \qquad \mathbf{J_F} = \frac{\partial \mathbf{F}}{\partial \mathbf{W}} \tag{7.24}$$

are respectively the Jacobian of the conserved variables and of the fluxes respect to the primitive variable vector $\mathbf{W}$ defined in equation (7.22). Their detailed expression is

$$\mathbf{J}_U = \begin{bmatrix} 1 & 0 & 0 & 0 & 0 \\ u & h & 0 & 0 & 0 \\ \varphi & 0 & c_b & h & 0 \\ \alpha\varphi & 0 & c_b\,(1-\alpha) & h\alpha & h\varphi - z_b c_b \\ 0 & 0 & 0 & 0 & 1 \end{bmatrix} \tag{7.25}$$

$$\mathbf{J}_F = \begin{bmatrix} u & h & 0 & 0 \\ u^2 + gh & 2hu & 0 & 0 \\ u\varphi\,(1-\alpha) + u\alpha\left(c + h\frac{\partial c}{\partial h}\right) & h\varphi\,(1-\alpha) + h\alpha\left(c + u\frac{\partial c}{\partial u}\right) & 0 & 0 \\ 0 & 0 & 0 & 0 \\ 0 & 0 & 0 & 0 \end{bmatrix} \tag{7.26}$$

The relevant characteristic polynomial, obtained from

$$\det\left|\mathbf{J_F} + \mathbf{H} - \lambda \mathbf{J_U}\right| = 0 \tag{7.27}$$

is the following

$$\lambda^2 \left(a_3\lambda^3 + a_2\lambda^2 + a_1\lambda + a_0\right) = 0 \tag{7.28}$$

where the coefficient of the polynomial are

$$a_3 = c_b \left(1 - 2\alpha\right) \tag{7.29}$$

$$a_2 = uc_b \left(6\alpha - \alpha^2 - 3\right) \tag{7.30}$$

$$a_1 = \left(2u^2c_b + gh\left(c - \varphi + u\frac{\partial c}{\partial u}\right)\right)\alpha^2 + \left(gh\left(\varphi + 2c_b\right) - 6c_bu^2\right)\alpha + \\ + c_b\left(3u^2 - gh\right) \tag{7.31}$$

$$a_0 = u\left(gh\left(\varphi + c_b + h\frac{\partial c}{\partial h} - u\frac{\partial c}{\partial u}\right) - u^2c_b\right)\alpha^2 + \\ - u\left(gh\left(\varphi + 2c_b\right) - 2c_bu^2\right)\alpha - uc_b\left(u^2 - gh\right) \tag{7.32}$$

It is useful to note that since a_i depends only on velocity, depth and erodibility parameter (it must be noted that the terms depending on φ can be cancelled in each polynomial coefficient both if $\alpha = 0$ and if $\alpha = 1$), the eigenvalues also depend on these variables only

$$\lambda_i = \lambda_i(h, u, \alpha) \tag{7.33}$$

Moreover, two eigenvalues are identically null, namely

$$\lambda_i = 0 \quad \text{for} \quad i = 4, 5$$

so the problem is not strictly hyperbolic. The other three eigenvalues, λ_i for $i = 1, 3$, derive from the solution of the third order polynomial present in equation (7.28), namely

$$a_3\lambda^3 + a_2\lambda^2 + a_1\lambda + a_0 = 0$$

With $\alpha = 0$ the previous polynomial collapse to

$$(u - \lambda)\left(\lambda^2 - 2u\lambda + u^2 - gh\right) = 0 \tag{7.34}$$

with roots

$$\lambda_1 = u + \sqrt{gh}; \quad \lambda_2 = u; \quad \lambda_3 = u - \sqrt{gh} \tag{7.35}$$

These eigenvalues are equal to the first three eigenvalues of the fixed bed case (see equation (5.9)). Also $\lambda_4 = 0$ is equal to the corresponding eigenvalue of the fixed bed case while λ_5 is obviously present only in the CPDE case. Analogously, with $\alpha = 1$ we checked that the resulting third order polynomial is equal to the one obtained in the mobile bed case, expressed by equation (5.19). As a result, in this bed condition, the first three eigenvalues of the CPDEs system are equal to the corresponding values in the mobile-bed case. The last two eigenvalues are obviously present only in the composite problem.

The eigenvectors related to system (7.19) are given by

$$\left(\mathbf{J_F} + \mathbf{H}\right)\mathbf{R}_i^W = \lambda_i \mathbf{J_U}\mathbf{R}_i^W \tag{7.36}$$

The general expression of $\mathbf{R}_i^W$ for $i = 1, 4$ is

$$\mathbf{R}_i^W = \begin{bmatrix} gh^2\left(\lambda_i - u\left(1-\alpha\right)\right) \\ -gh\left(u - \lambda_i\right)\left(\lambda_i - u\left(1-\alpha\right)\right) \\ h\left(\lambda_i - u\left(1-\alpha\right)\right)\left(\left(u-\lambda_i\right)^2 - gh\right) \\ -\lambda_i\left(\left(u-\lambda_i\right)^2 - gh\right) + \dfrac{gh\alpha}{c_b}\left[\lambda_i\left(c-\varphi\right) + u\left(h\dfrac{\partial c}{\partial h} - \left(u-\lambda_i\right)\dfrac{\partial c}{\partial u}\right)\right] \\ 0 \end{bmatrix} \tag{7.37}$$

while for $\lambda_5 = 0$, since the system is not strictly hyperbolic, the relevant

eigenvalue has one degree of freedom

$$\mathbf{R}_5^W = \begin{bmatrix} -gh\left(\xi\left(1-\alpha\right)+c-\varphi\right) \\ gu\left(\xi\left(1-\alpha\right)+c-\varphi\right) \\ \left(gh-u^2\right)\left(\xi\left(1-\alpha\right)+c-\varphi\right) \\ gh\xi\alpha\dfrac{\partial c}{\partial h} - g\xi u\alpha\dfrac{\partial c}{\partial u} \\ gh\alpha\dfrac{\partial c}{\partial h} - gu\alpha\dfrac{\partial c}{\partial u} \end{bmatrix} \tag{7.38}$$

where ξ is an arbitrary constant. It is important to notice that the eigenvectors associated to the null eigenvalues $\lambda_{4,5}$ are independent. In the following, we will indicate with $R_{i,j}^W$ the j-th component of the i-th eigenvector.

Carrying out some simple manipulations it is possible to verify the consistency of the CPDEs eigenvectors with the pure fixed- or mobile-bed eigenvectors. In particular, with $\alpha = 0$ the first four components of the first four CPDE eigenvectors coincide with the eigenvector components obtained from the pure fixed-bed system with discontinuous topography reported in equation (5.10), namely

$$R_{i,j}^{W_f} = R_{i,j}^W \text{ with } i,j = 1,4$$

while $R_{i,5}^W$ with $i = 1,4$ is identically null. In the mobile-bed sate, with $\alpha = 1$, the first three components of the first three CPDE eigenvectors are equal to the eigenvector components obtained from the pure mobile-bed system expressed by equation (5.20), namely

$$R_{i,j}^{W_m} = R_{i,j}^W \text{ with } i,j = 1,3$$

while $R_{i,4}^W$ with $i = 1,3$ is always non-null and $R_{i,5}^W$ with $i = 1,3$ is identically null.

The nature of the characteristic fields can be determined by analyzing the quantity $G = \nabla^W \lambda_i \cdot \mathbf{R}_i^W$, where the gradient of λ_i is calculated respect the primitive variable vector. Considering equation (7.33), the previous dot product becomes

$$G = \frac{d\lambda_i}{dh}\mathbf{R}_{i,1}^W + \frac{d\lambda_i}{du}\mathbf{R}_{i,2}^W + \frac{d\lambda_i}{d\alpha}\mathbf{R}_{i,5}^W \tag{7.39}$$

λ_1		λ_2		λ_3	
$\alpha = 0$	$\alpha = 1$	$\alpha = 0$	$\alpha = 1$	$\alpha = 0$	$\alpha = 1$
GNL	GNL	LD	GNL	GNL	GNL
φ, z_b, α	α	h, u, z_b, α	α	φ, z_b, α	α

$\lambda_4 = 0$		$\lambda_5 = 0$	
$\alpha = 0$	$\alpha = 1$	$\xi = 0$	$\xi \neq 0$
LD*	LD*	LD*	LD*
φ, α	h, u, z_b, α	φ	-

Table 7.1: Summary of the possible characteristic fields with indication of the variables that remain constant across each wave of that field. Meanings of the symbols: GNL = genuinely nonlinear field; LD = classical linearly degenerate field; LD* = linearly degenerate field with λ independent from U. Finally ξ is a degree of freedom of the fifth field

and, as a result, the nature of each characteristic field depends on the first two components and on the last one of the relevant eigenvector. Other features of the waves can be obtained analyzing the RI associated with each eigenvalue, namely

$$\frac{dW_j}{R^W_{i,j}} = \kappa_i \quad \text{with} \quad i, j = 1, 5 \tag{7.40}$$

where κ_i indicates a generic constant. It is important to recall that if the j-th component of the i-th eigenvector is null, namely $R^W_{i,j} = 0$, the relevant variable W_j remains constant across each possible wave type of the i-th field while if $R^W_{i,j} \neq 0$, then $Wj \neq const$. A summary of the possible fields for the CPDEs system along with their main properties is reported in Table **7.1**.

A series of useful observations can be made.

Regarding the first four fields, since $R^W_{i,5} = 0$ for $i = 1, 4$, they are characterized by $W_5 = \alpha = const$, namely the state of the bed does not change across these waves. So these waves are pure fixed-bed or pure mobile-bed:

- for $\alpha = 0$ and $i = 1, 4$, then $R^W_{i,1}$ and $R^W_{i,2}$ become equal to the corresponding values of the fixed-bed eigenvector, while $R^W_{i,5} = 0$. Therefore,

thanks to (7.39), we can say that the nature of these characteristic fields of the CPDEs system, in fixed-bed state, is equal to that obtained in the pure fixed-bed case (see Section 5.1);

- for $\alpha = 1$ and $i = 1, 3$, the relevant characteristic fields have the same nature as the pure mobile-bed fields (see Section 5.1). In the fourth field, all the component of $\mathbf{R}_4^W$ are null except the fourth and therefore across this wave only φ changes. Actually this wave is not important because the quantity φ has no physical meaning in mobile-bed conditions.

Therefore we can conclude that the CPDEs system reproduce correctly both the pure fixed or mobile bed models if no transition is present.

Regarding the last wave $\lambda_5 = 0$, the corresponding field is linearly degenerate with eigenvalue independent from $\mathbf{U}$. Moreover, since $R^W_{5,5} \neq 0$, α must change across this wave. In other words, the fifth characteristic field describes the fixed–mobile transition. Recalling that this eigenvector presents a degree of freedom ξ (see equation (7.38)), it can be noted (Table 7.1) that if $\xi \neq 0$ all the variables can change across the wave, while if $\xi = 0$, φ must remain constant while the other three variables can change. Obviously, the choice $\xi \neq 0$ is more general, since it includes $\varphi = const$ as a particular case and for this reason is preferable.

Genuinely nonlinear fields can develop shocks. In these cases, since system (7.19) is nonconservative, the following GRH relations must hold

$$\mathbf{F}^*_R - \mathbf{F}^*_L - \mathbf{D} = S_s \left(U^*_R - \mathbf{U}^*_L\right) \tag{7.41}$$

where S_s is the speed of the shock, $\mathbf{F}^*_R, \mathbf{F}^*_L$ and $\mathbf{U}^*_R, \mathbf{U}^*_L$ are the fluxes and the conserved variables respectively on the right and on the left of the shock wave and finally $\mathbf{D}^T = (0, D, 0, 0, 0)$, where D is given by equation (7.6). Considering Table 7.1, we can notice that if $\alpha = 0$, since z_b is constant across λ_1 and λ_3 fields, the term D is null and the GRH relations degenerates to standard RH ones where the first tree relation are equal to the RH relations for the pure fixed-bed case while the last two are trivial relations. If $\alpha = 1$, the first three GRH relations are equal to the GRH ones for the pure mobile-bed case, equation (5.21), while the last two relations are trivial.

Regarding the linearly degenerate fields, the contact wave associated to λ_2 with $\alpha = 0$ is nothing but a classical contact wave over flat bed. On the contrary, the relations valid across λ_4 are the GRH ones with null wave speed

$$\begin{cases} \mathbf{F}_R^* - \mathbf{F}_L^* = \mathbf{D} & \text{if } \alpha = 0 \\ \mathbf{F}_R^* - \mathbf{F}_L^* = 0 & \text{if } \alpha = 1 \end{cases}$$

while the ones valid across the contact wave associated to λ_5 are

$$\begin{cases} \mathbf{F}_{R,0}^* - \mathbf{F}_{L,1}^* = \mathbf{D} & \text{mobile-fixed transition} \\ \mathbf{F}_{R,1}^* - \mathbf{F}_{L,0}^* = \mathbf{D} & \text{fixed-mobile transition} \end{cases} \tag{7.42}$$

where the second subscript refers to the bed state at which the fluxes must be evaluates. The first three equations of these vectorial expressions are nothing but equation (7.5) while the last two are trivial relations. It is important to notice that these equations provide a relation between φ on the fixed-bed side and con the mobile-bed side. Nevertheless, no constraint that links φ on both sides of the transition is present. Moreover, considering that with the choice $\xi \neq 0$, φ can change, we conclude that the value of the transported concentration on the mobile-bed side is completely arbitrary. So, it is possible to consider an initial value $\varphi = 0$ in all the transects characterized by mobile bed and we are sure that this condition is in any case compatible with any condition present on the fixed bed side of a transition. Moreover, considering the last equation of system (7.7), we can conclude that the null value is maintained in time.

7.4 Classes of solutions of the CRP

As we noticed in Section (7.2), the solution of a CRP, defined by equation (7.4), is composed by a suitable combination of the waves whose features have been presented in the previous Section. Solutions can be conveniently grouped in classes characterized by some common peculiarities. For simplicity, from now on, we suppose that the velocity in a neighborhood of the origin is always positive for times $t > 0$. If the velocity is negative, the proposed classification is still valid but must be applied specularly respect what we present here.

The type of waves generated by the CRP that travel the left and the right part of the flow field must be consistent with the possible waves admitted by the relevant bed state. The first feature that can be used to make the classification is the sequence of bed states from left to right of the origin. Two categories can be identified:

- FB-MB: flow with fixed to mobile bed transition;
- MB-FB: flow with mobile to fixed bed transition.

Another key feature, peculiar of the fixed-bed condition, is the change of sign in one eigenvalue as a function of the Froude number (see Section 5.1 for details). Therefore, the second feature that must be used for the classification is the nature of the flow (super or subcritical) in the neighborhood of the origin on the fixed-bed side.

As a result there are four different categories:

- FBsub-MB: transition from subcritical flow over fixed bed to mobile-bed condition;
- FBsup-MB: transition from supercritical flow over fixed bed to mobile-bed condition;
- MB-FBsub: transition from mobile-bed condition to subcritical flow over fixed bed;
- MB-FBsup: transition from mobile-bed condition to supercritical flow over fixed bed.

The wave-pattern associated to each category, reported in Figure 7.2, is then composed by parts of wave pattern of pure fixed- or mobile-bed RPs (see Figures 5.1 and 5.2) plus a LD* wave in the origin. Analysis of the peculiarity of each class demonstrates that:

FBsub-MB The solutions of this class are composed, from left to right, by a λ_1 GNL fixed-bed wave, a λ_5 LD* contact followed by two λ_2, λ_3 GNL mobile-bed waves.

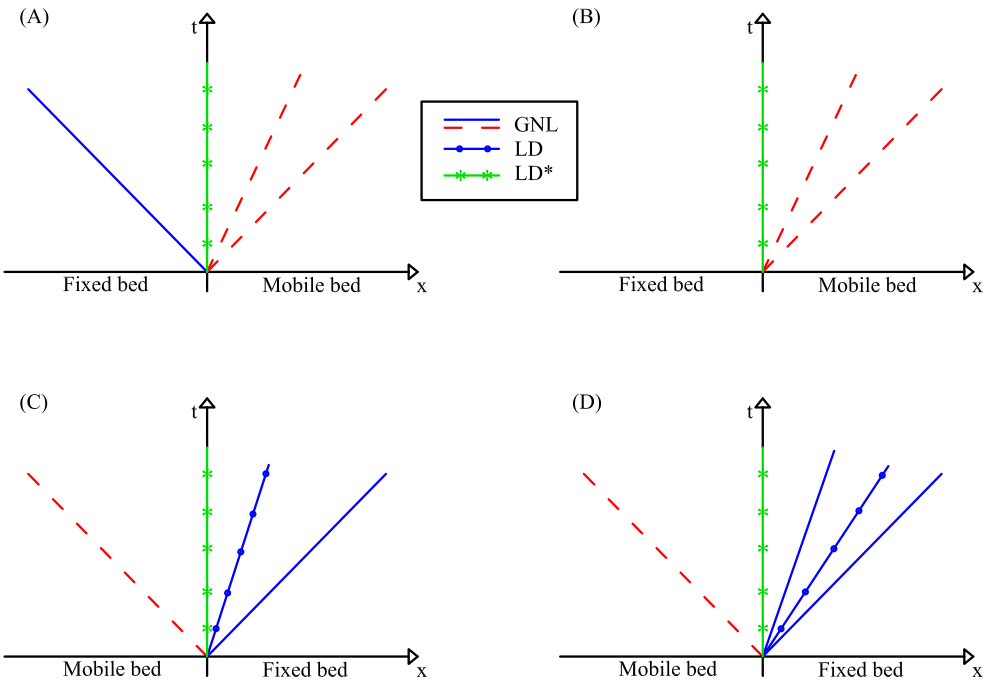

Figure 7.2: The four different classes of CRP solutions for positive velocity in the neighborhood of the origin: (a) FBsub-MB, (b) FBsup-MB, (c) MB-FBsub, (d)MB-FBsup. Dashed lines represent mobile-bed fields, solid lines fixed-bed ones. GNL represent genuinely nonlinear fields, LD classical linearly degenerate fields and LD* linearly degenerate fields with λ independent from $\mathbf{U}$.

FBsup-MB This class is characterized by the absence of waves on the left of the origin, a λ_5 LD* contact in the origin followed by two λ_2, λ_3 GNL mobile-bed waves.

MB-FBsub The solutions of this class are composed by a λ_1 GNL mobile-bed wave, a λ_5 LD* contact, a LD λ_2 contact and finally by a λ_3 GNL fixed-bed wave.

MB-FBsup In this case the solutions are composed by a λ_1 GNL mobile-bed wave, a λ_5 LD* contact, a LD λ_2 contact and two λ_1, λ_3 GNL fixed-bed waves.

Some final observation must be made:

1. The proposed classification exclude the extreme case in which the sign of the velocity changes across the origin.

2. As highlighted in the presentation of the models, in pure fixed-bed conditions, resonant cases may occur (see Section 5.1). On the other hand, in pure mobile-bed conditions, resonance cannot occur (Section5.1). With fixed-mobile transition, resonance can occur if a sonic rarefaction on the fixed-bed side overlap the bed step wave.

3. The MB-FBsup class shows the peculiar feature that infinite wave patterns connecting given left and right initial conditions can be found. In fact, the supercritical condition of the fixed-bed side presents a complete wave pattern of a standard RP over flat bed, which permits the linking of the initial right condition to any condition arising from the central contact wave. On the other hand, since there is no constraint deriving from the right side, any suitable couple of λ_1 GNL mobile-bed wave and λ_5 LD* contact can be chosen starting from the left initial value. These fortuitous conditions lead to the non-uniqueness of the CRP solution in this case. An example of two possible exact solutions associated with the same initial values are reported in Figure 7.3. It must be noted that all the waves considered in the example are entropic. More effort is needed to clarify this point but, since it is an extreme case with a low probability of occurrence in practical applications, we leave this topic for a future in-deep analysis.

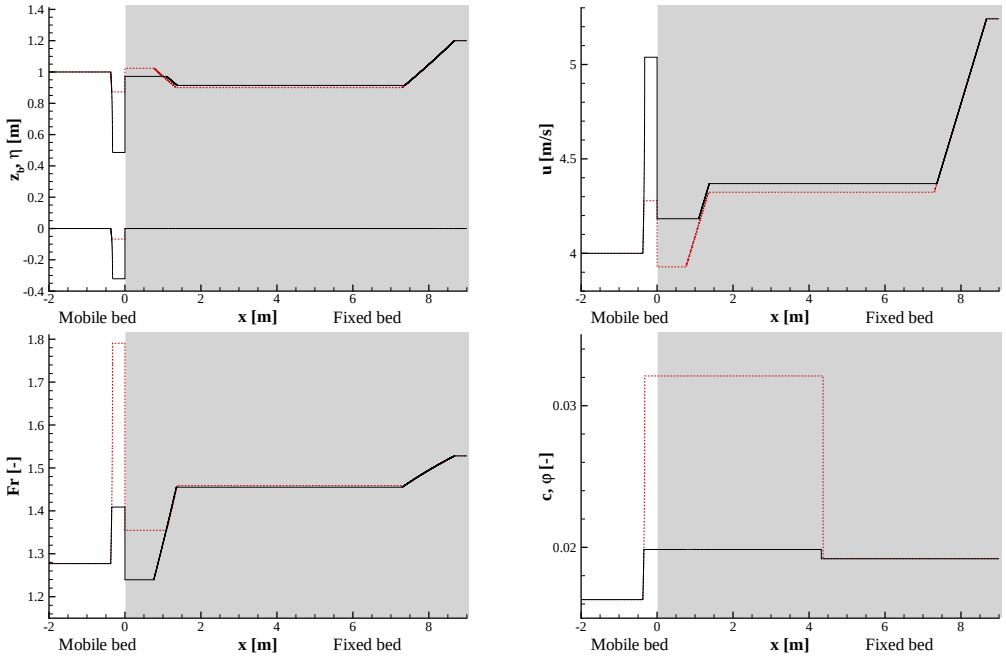

Figure 7.3: Example of two possible exact solutions of a RP of MB-FBsup type. All the waves are entropy satisfying.

Chapter 8

Application of the CRP procedure to high sediment cases

The strategy for coupling different PDEs systems developed in Chapter 7 can be applied, as specified in Chapter 6, to different sets of equations related to the same physical problem. In this Chapter we apply this strategy in order to couple the fixed and the mobile bed systems in cases of high sediment concentration. Although the coupling procedure is the same, the complexity of the systems obtained is gradually increasing, in particular the eigenstructure analysis becomes more and more complicated.

Firstly we present the Composite PDEs system for the one-dimensional high concentration system in Section 8.1, while in Section 8.2 the two-dimensional plane wave CPDEs is derived.

8.1 CPDEs system for one-dimensional case

The one-dimensional two-phase free-surface flow over fixed bed for high sediment concentration described by the system (4.8) derived in Chapter 4.2 reads

$$\begin{cases} \dfrac{\partial}{\partial t}\left(h+z_b\right)+\dfrac{\partial}{\partial x}uh=0 \\ \dfrac{\partial}{\partial t}\varphi h+\dfrac{\partial}{\partial x}\varphi uh=0 \\ \dfrac{\partial}{\partial t}\left(1+\varphi\Delta\right)uh+\dfrac{\partial}{\partial x}\left(1+\varphi\Delta\right)\left(hu^2+g\dfrac{h^2}{2}\right)+ \\ \qquad\qquad +\left(1+\varphi\Delta\right)gh\dfrac{\partial z_b}{\partial x}=-\dfrac{\tau_0}{\rho_f} \\ \dfrac{\partial}{\partial t}z_b=0 \end{cases} \tag{8.1}$$

where h is the flow depth, u is the flow velocity, z_b is the bed elevation, $\Delta=\frac{\rho_s-\rho_f}{\rho_f}$ is the constant relative submerged solid density, φ in the solid concentration inside the flow, g is the constant gravity acceleration, ρ_f is the fluid density and τ_0 is the bed shear stress. For the mobile bed, the system (4.9) is

$$\begin{cases} \dfrac{\partial}{\partial t}\left(h+z_b\right)+\dfrac{\partial}{\partial x}uh=0 \\ c_b\dfrac{\partial z_b}{\partial t}+\dfrac{\partial}{\partial t}ch+\dfrac{\partial}{\partial x}cuh=0 \\ \dfrac{\partial}{\partial t}\left(1+c\Delta\right)uh+\dfrac{\partial}{\partial x}\left(1+c\Delta\right)\left(hu^2+g\dfrac{h^2}{2}\right)+ \\ \qquad\qquad +\left(1+c\Delta\right)gh\dfrac{\partial z_b}{\partial x}=-\dfrac{\tau_0}{\rho_f} \end{cases} \tag{8.2}$$

where c_b is the constant concentration inside the bed, c is the solid concentration inside the flow field and the other variables have the same meaning as for fixed bed case.

The eigenstructure of both systems has been analyzed in Chapter 5.2, where we demonstrated their hyperbolicity.

Following the procedure developed in the previous Chapter, the first step for the coupling is to check systems (8.1) and (8.2) in order to find if some

additional variables and associated equations are needed. Comparing the primitive vector of the two systems, i.e. $\mathbf{W}_f^T = \begin{bmatrix} h & u & \varphi & z_b \end{bmatrix}$ and $\mathbf{W}_m^T = \begin{bmatrix} h & u & z_b \end{bmatrix}$, the missing variable in the latter vector is φ. This variable, as states in Section 7.2, is a dummy variable for the mobile bed part of the problem, so it does not affect the flow. A suitable equation involving this dummy variable is

$$\frac{\partial}{\partial t}\varphi h = 0 \tag{8.3}$$

Introducing this equations in the mobile bed system, we obtain

$$\begin{cases} \dfrac{\partial}{\partial t}\left(h + z_b\right) + \dfrac{\partial}{\partial x} uh = 0 \\ c_b \dfrac{\partial z_b}{\partial t} + \dfrac{\partial}{\partial t} ch + \dfrac{\partial}{\partial x} cuh = 0 \\ \dfrac{\partial}{\partial t}\left(1 + c\Delta\right) uh + \dfrac{\partial}{\partial x}\left(1 + c\Delta\right)\left(hu^2 + g\dfrac{h^2}{2}\right) + \\ \qquad\qquad + \left(1 + c\Delta\right) gh\dfrac{\partial z_b}{\partial x} = -\dfrac{\tau_0}{\rho_f} \\ \dfrac{\partial}{\partial t}\varphi h = 0 \end{cases} \tag{8.4}$$

It is composed by the same number (four) and type (mixture and solid mass conservations, mixture momentum balance and invariance of one property) of equations. Using the erodibility function (7.8) and its associated equation (7.10), and following the approach developed in Section 7.2, the final CPDEs that describe the transition between fixed and mobile bed valid for high concentration regime, is

$$\begin{cases} \dfrac{\partial}{\partial t}\left(h + z_b\right) + \dfrac{\partial}{\partial x} uh = 0 \\ \dfrac{\partial}{\partial t}\left(c_b z_b + \varphi h + \alpha ch\right) + \dfrac{\partial}{\partial x}\left(\delta uh\right) = 0 \\ \dfrac{\partial}{\partial t}\left(1 + \delta\Delta\right) uh + \dfrac{\partial}{\partial x}\left(1 + \delta\Delta\right)\left(u^2 h + g\dfrac{h^2}{2}\right) + \\ \qquad\qquad + \left(1 + \delta\Delta\right) gh\dfrac{\partial z_b}{\partial x} = -\dfrac{\tau_0}{\rho_f} \\ \dfrac{\partial}{\partial t}\left(\left(1 - \alpha\right) c_b z_b + \alpha\varphi h\right) = 0 \\ \dfrac{\partial}{\partial t}\alpha = 0 \end{cases} \tag{8.5}$$

where $\delta = (\alpha c + (1-\alpha)\,\varphi)$. It is straightforward to check that this system converges to system (8.1) using $\alpha = 0$ and to system (8.2) using $\alpha = 1$.

The system (8.5) can be written in compact form as

$$\frac{\partial \mathbf{U}}{\partial t} + \frac{\partial \mathbf{F}}{\partial x} + \mathbf{H}\frac{\partial \mathbf{W}}{\partial x} = \mathbf{S} \tag{8.6}$$

where $\mathbf{U}$ and $\mathbf{W}$ are the vectors of the conserved and primitive variables

$$\mathbf{U} = \begin{bmatrix} h + z_b \\ c_b z_b + \varphi h + \alpha c h \\ (1 + \delta\Delta)\, uh \\ (1-\alpha)\, c_b z_b + \alpha\varphi h \\ \alpha \end{bmatrix}; \qquad \mathbf{W} = \begin{bmatrix} h \\ u \\ z_b \\ \varphi \\ \alpha \end{bmatrix} \tag{8.7}$$

$\mathbf{F}$ and $\mathbf{H}$ are the conservative and non-conservative fluxes

$$\mathbf{H} = \begin{bmatrix} 0 & 0 & 0 & 0 & 0 \\ 0 & 0 & 0 & 0 & 0 \\ 0 & 0 & (1+\delta\Delta)\, gh & 0 & 0 \\ 0 & 0 & 0 & 0 & 0 \\ 0 & 0 & 0 & 0 & 0 \end{bmatrix}; \qquad \mathbf{F} = \begin{bmatrix} uh \\ \delta uh \\ (1+\delta\Delta)\left(u^2 h + g\dfrac{h^2}{2}\right) \\ 0 \\ 0 \end{bmatrix} \tag{8.8}$$

while $\mathbf{S}$ is the source term

$$\mathbf{S} = \begin{bmatrix} 0 \\ 0 \\ -\tau_0/\rho_f \\ 0 \\ 0 \end{bmatrix} \tag{8.9}$$

8.1.1 Eigenstructure and shock relation of the CPDEs

The eigenstructure of system (8.5) can be determined analyzing its linearized homogeneous form that reads

$$\mathbf{J_U}\frac{\partial \mathbf{W}}{\partial t} + (\mathbf{J_F} + \mathbf{H})\frac{\partial \mathbf{W}}{\partial x} = 0 \tag{8.10}$$

where

$$\mathbf{J_U} = \frac{\partial \mathbf{U}}{\partial \mathbf{W}}; \qquad \mathbf{J_F} = \frac{\partial \mathbf{F}}{\partial \mathbf{W}} \tag{8.11}$$

are respectively the Jacobian of the conserved variables and of the fluxes respect to the primitive variable vector $\mathbf{W}$ defined in equations (8.7) and (8.8). Their detailed expressions are

$$\mathbf{J}_U = \begin{bmatrix} 1 & 0 & 1 & 0 & 0 \\ \varphi + \alpha c + h\alpha\frac{\partial c}{\partial h} & h\alpha\frac{\partial c}{\partial u} & c_b & h & hc \\ u\left(1 + \delta\Delta + h\Delta\alpha\frac{\partial c}{\partial h}\right) & h\left(1 + \delta\Delta + u\Delta\alpha\frac{\partial c}{\partial u}\right) & 0 & hu\Delta\left(1-\alpha\right) & hu\Delta\left(c-\varphi\right) \\ \alpha\varphi & 0 & c_b\left(1-\alpha\right) & h\alpha & h\varphi - zc_b \\ 0 & 0 & 0 & 0 & 1 \end{bmatrix} \tag{8.12}$$

$$\mathbf{J}_F = \begin{bmatrix} u & h & 0 & 0 & 0 \\ u\left(\delta + h\alpha\frac{\partial c}{\partial h}\right) & h\left(\delta + u\alpha\frac{\partial c}{\partial u}\right) & 0 & hu\left(1-\alpha\right) & hu\left(c-\varphi\right) \\ \left(gh+u^2\right)\left(1+\delta\Delta\right) + \Delta\alpha\frac{\partial c}{\partial h}\Phi & 2hu\left(1+\delta\Delta\right) + \Delta\alpha\frac{\partial c}{\partial u}\Phi & 0 & \Phi\Delta\left(1-\alpha\right) & \Phi\Delta\left(c-\varphi\right) \\ 0 & 0 & 0 & 0 & 0 \\ 0 & 0 & 0 & 0 & 0 \end{bmatrix} \tag{8.13}$$

where $\Phi = \left(\frac{1}{2}gh^2 + hu^2\right)$.

Evaluating the relevant characteristic polynomial we obtain

$$\lambda^2\left(a_3\lambda^3 + a_2\lambda^2 + a_1\lambda + a_0\right) = 0 \tag{8.14}$$

where the expression of the four coefficients a_i with $i = 0, \ldots, 3$ will be not reported due to their complexity and length. An important aspect is that

these coefficients depend only on variables u, h and α, as for the simplified system (7.33). Two null eigenvalues are present

$$\lambda_i = 0 \quad \text{for} \quad i = 4, 5$$

so the problem is not strictly hyperbolic, while the other three eigenvalues derive from the solution of the third order polynomial. Imposing $\alpha = 0$ in this polynomial, the three roots are the ones associate to the fixed bed system (8.1) and presented in Section 5.2. On the contrary, using $\alpha = 1$, the characteristic polynomial associate to the mobile bed system (8.2) is obtained.

The eigenvectors related to system (8.5) are given by equation (7.36). For the same reason as the polynomial coefficients, the general expression of $\mathbf{R}_i^W$ for $i = 1, 3$ is not reported. Here we present only the two eigenvectors associated to the two null eigenvalues ($\lambda_{4,5} = 0$) that read

$$\mathbf{R}_4^W = \begin{bmatrix} gh\,(\alpha - 1) \\ -gu\,(\alpha - 1) \\ -(\alpha - 1)\,(gh - u^2) \\ gh\alpha\dfrac{\partial c}{\partial h} - gu\alpha\dfrac{\partial c}{\partial u} \\ 0 \end{bmatrix} \tag{8.15}$$

$$\mathbf{R}_5^W = \begin{bmatrix} -gh\,(\xi\,(1 - \alpha) + c - \varphi) \\ gu\,(\xi\,(1 - \alpha) + c - \varphi) \\ (gh - u^2)\,(\xi\,(1 - \alpha) + c - \varphi) \\ gh\xi\alpha\dfrac{\partial c}{\partial h} - g\xi u\alpha\dfrac{\partial c}{\partial u} \\ gh\alpha\dfrac{\partial c}{\partial h} - gu\alpha\dfrac{\partial c}{\partial u} \end{bmatrix} \tag{8.16}$$

where ξ is an arbitrary constant. It is important to notice that the eigenvectors associated to the null eigenvalues $\lambda_{4,5}$ are independent. All the properties related to the eigenvectors and associated characteristic fields highlighted in Section 7.3 are still valid also for the CPDEs system (8.5), so we refer to that Section for more details.

As specified in the previous Chapter, genuinely nonlinear fields can develop shocks. In these cases, since system (8.5) is nonconservative, the following GRH relations hold

$$\mathbf{F}^*_{\mathbf{R}} - \mathbf{F}^*_{\mathbf{L}} - \mathbf{D} = S_s \left(\mathbf{U}^*_{\mathbf{R}} - \mathbf{U}^*_{\mathbf{L}} \right) \tag{8.17}$$

where S_s is the speed of the shock, $\mathbf{F}^*_R, \mathbf{F}^*_L$ and $\mathbf{U}^*_R, \mathbf{U}^*_L$ are the fluxes and the conserved variables respectively on the right and on the left of the shock wave and finally $\mathbf{D}^T = (0, 0, D, 0, 0)$. Following Rosatti and Fraccarollo [54] it is possible to determinate the expression of D obtaining

$$D = -g \left(1 + \alpha_k c_k \Delta + (1 - \alpha_k) \varphi_k \Delta\right) \left(h_k - \frac{|z_R - z_L|}{2} \right) (z_R - z_L) \tag{8.18}$$

$$\text{with } k = \begin{cases} L & \text{if } z_L \leq z_R \\ R & \text{otherwise} \end{cases}$$

All the other properties, included the classes of solutions, are the same as the CPDEs system for low sediment concentration, so we refer to Sections 7.3 and 7.4 for all the details.

8.2 CPDEs for two-dimensional plane wave case

The two-phase free-surface flow over fixed bed with the plane wave is described by the system (4.10) derived in Chapter 4.3 and reads

$$\begin{cases} \dfrac{\partial}{\partial t}\left(h+z_b\right)+\dfrac{\partial}{\partial x}uh=0 \\ \dfrac{\partial}{\partial t}\varphi h+\dfrac{\partial}{\partial x}\varphi uh=0 \\ \dfrac{\partial}{\partial t}\left(1+\varphi\Delta\right)uh+\dfrac{\partial}{\partial x}\left(1+\varphi\Delta\right)\left(hu^2+g\dfrac{h^2}{2}\right)+ \\ \qquad\qquad +\left(1+\varphi\Delta\right)gh\dfrac{\partial z_b}{\partial x}=-\dfrac{\tau_{0,x}}{\rho_f} \\ \dfrac{\partial}{\partial t}\left(1+\varphi\Delta\right)vh+\dfrac{\partial}{\partial x}\left(1+\varphi\Delta\right)uvh=-\dfrac{\tau_{0,y}}{\rho_f} \\ \dfrac{\partial}{\partial t}z_b=0 \end{cases} \tag{8.19}$$

The mobile bed the system (4.11) is

$$\begin{cases} \dfrac{\partial}{\partial t}\left(h+z_b\right)+\dfrac{\partial}{\partial x}uh=0 \\ c_b\dfrac{\partial z_b}{\partial t}+\dfrac{\partial}{\partial t}ch+\dfrac{\partial}{\partial x}cuh=0 \\ \dfrac{\partial}{\partial t}\left(1+c\Delta\right)uh+\dfrac{\partial}{\partial x}\left(1+c\Delta\right)\left(hu^2+g\dfrac{h^2}{2}\right)+ \\ \qquad\qquad +\left(1+c\Delta\right)gh\dfrac{\partial z_b}{\partial x}=-\dfrac{\tau_{0,x}}{\rho_f} \\ \dfrac{\partial}{\partial t}\left(1+c\Delta\right)vh+\dfrac{\partial}{\partial x}\left(1+c\Delta\right)huv=-\dfrac{\tau_{0,y}}{\rho_f} \end{cases} \tag{8.20}$$

The eigenstructure of both systems has been analyzed in Section 5.3, where we demonstrate their hyperbolicity.

Following the coupling procedure developed in Chapter 7, as first step we compare the two initial systems in order to find if some additional variables and associated equations are needed. Comparing the primitive vector of the two systems, i.e. $\mathbf{W}_f^T=\begin{bmatrix}h & u & v & z_b & \varphi\end{bmatrix}$ and $\mathbf{W}_m^T=\begin{bmatrix}h & u & v & z_b\end{bmatrix}$ the

mobile bed system has one variable less and, also in this case, the missing variable is φ so, as performed in Section 7.2, the dummy variable φ and a suitable equation involving this dummy variable

$$\frac{\partial}{\partial t}\varphi h = 0 \tag{8.21}$$

are introduced in the mobile bed system obtaining

$$\begin{cases} \dfrac{\partial}{\partial t}\left(h + z_b\right) + \dfrac{\partial}{\partial x} uh = 0 \\ c_b \dfrac{\partial z_b}{\partial t} + \dfrac{\partial}{\partial t} ch + \dfrac{\partial}{\partial x} cuh = 0 \\ \dfrac{\partial}{\partial t}\left(1 + c\Delta\right) uh + \dfrac{\partial}{\partial x}\left(1 + c\Delta\right)\left(hu^2 + g\dfrac{h^2}{2}\right) + \\ \qquad + \left(1 + c\Delta\right) gh\dfrac{\partial z_b}{\partial x} = -\dfrac{\tau_{0,x}}{\rho_f} \\ \dfrac{\partial}{\partial t}\left(1 + c\Delta\right) vh + \dfrac{\partial}{\partial x}\left(1 + c\Delta\right) huv = -\dfrac{\tau_{0,y}}{\rho_f} \\ \dfrac{\partial}{\partial t}\varphi h = 0 \end{cases} \tag{8.22}$$

and it is composed by the same number (five) and type (mixture and solid mass conservation, mixture momentum balance along longitudinal and transversal direction and invariance of one property) of equations. Introducing the erodibility function (7.8) and the associated differential equation (7.10), and following the same approach as before, the final CPDEs system with plane

wave is

$$\begin{cases} \dfrac{\partial}{\partial t}\left(h+z_b\right)+\dfrac{\partial}{\partial x}uh=0 \\ \dfrac{\partial}{\partial t}\left(c_b z_b+\varphi h+\alpha c h\right)+\dfrac{\partial}{\partial x}\left(\delta uh\right)=0 \\ \dfrac{\partial}{\partial t}\left(1+\delta\Delta\right)uh+\dfrac{\partial}{\partial x}\left(1+\delta\Delta\right)\left(u^2h+g\dfrac{h^2}{2}\right)+ \\ \qquad +\left(1+\delta\Delta\right)gh\dfrac{\partial z_b}{\partial x}=-\dfrac{\tau_{0,x}}{\rho_f} \\ \dfrac{\partial}{\partial t}\left(1+\delta\Delta\right)vh+\dfrac{\partial}{\partial x}\left(1+\delta\Delta\right)uvh=-\dfrac{\tau_{0,y}}{\rho_f} \\ \dfrac{\partial}{\partial t}\left(\left(1-\alpha\right)c_b z_b+\alpha\varphi h\right)=0 \\ \dfrac{\partial}{\partial t}\alpha=0 \end{cases} \tag{8.23}$$

It is straightforward to check that this system converges to system (8.19) using $\alpha=0$ and to system (8.20) using $\alpha=1$.

In compact form it reads

$$\frac{\partial \mathbf{U}}{\partial t}+\frac{\partial \mathbf{F}}{\partial x}+\mathbf{H}\frac{\partial \mathbf{W}}{\partial x}=\mathbf{S} \tag{8.24}$$

where $\mathbf{U}$ and $\mathbf{W}$ are the vectors of the conserved and primitive variables

$$\mathbf{U}=\begin{bmatrix} h+z \\ \alpha c h+\varphi h+c_b z_b \\ \left(1+\delta\Delta\right)uh \\ \left(1+\delta\Delta\right)vh \\ \alpha\varphi h+\left(1-\alpha\right)c_b z_b \\ \alpha \end{bmatrix}; \qquad \mathbf{W}=\begin{bmatrix} h \\ u \\ v \\ z_b \\ \varphi \\ \alpha \end{bmatrix} \tag{8.25}$$

$\mathbf{F}$ and $\mathbf{H}$ are the conservative and non-conservative fluxes

$$\mathbf{H}=\begin{bmatrix} 0 & 0 & 0 & 0 & 0 & 0 \\ 0 & 0 & 0 & 0 & 0 & 0 \\ 0 & 0 & 0 & \left(1+\delta\Delta\right)gh & 0 & 0 \\ 0 & 0 & 0 & 0 & 0 & 0 \\ 0 & 0 & 0 & 0 & 0 & 0 \\ 0 & 0 & 0 & 0 & 0 & 0 \end{bmatrix}; \quad \mathbf{F}=\begin{bmatrix} uh \\ \delta uh \\ \left(1+\delta\Delta\right)\left(u^2h+g\frac{h^2}{2}\right) \\ \left(1+\delta\Delta\right)uvh \\ 0 \\ 0 \end{bmatrix} \tag{8.26}$$

while $\mathbf{S}$ is the source term

$$\mathbf{S} = \begin{bmatrix} 0 \\ 0 \\ -\tau_{0,x}/\rho_f \\ -\tau_{0,y}/\rho_f \\ 0 \\ 0 \end{bmatrix} \tag{8.27}$$

8.2.1 Eigenstructure and shock relation for the CPDEs

The eigenstructure of system (8.23) can be determined analyzing its linearized homogeneous form that reads

$$\mathbf{J_U}\frac{\partial \mathbf{W}}{\partial t} + (\mathbf{J_F} + \mathbf{H})\frac{\partial \mathbf{W}}{\partial x} = 0 \tag{8.28}$$

where

$$\mathbf{J_U} = \frac{\partial \mathbf{U}}{\partial \mathbf{W}}; \qquad \mathbf{J_F} = \frac{\partial \mathbf{F}}{\partial \mathbf{W}} \tag{8.29}$$

are respectively the Jacobian of the conserved variables and of the fluxes respect to the primitive variable vector $\mathbf{W}$ defined in equations (8.25) and (8.26). Their detailed expressions are

$$\mathbf{J_U} = \begin{bmatrix} 1 & 0 & 0 \\ \varphi + \alpha c + h\alpha\frac{\partial c}{\partial h} & h\alpha\frac{\partial c}{\partial u} & h\alpha\frac{\partial c}{\partial v} \\ u\left(1 + \delta\Delta + h\Delta\alpha\frac{\partial c}{\partial h}\right) & h\left(1 + \delta\Delta + u\Delta\alpha\frac{\partial c}{\partial u}\right) & hu\Delta\alpha\frac{\partial c}{\partial v} \\ v\left(1 + \delta\Delta + h\Delta\alpha\frac{\partial c}{\partial h}\right) & hv\Delta\alpha\frac{\partial c}{\partial u} & h\left(1 + \delta\Delta + v\Delta\alpha\frac{\partial c}{\partial v}\right) \\ \alpha\varphi & 0 & 0 \\ 0 & 0 & 0 \end{bmatrix}$$

$$\begin{bmatrix} 1 & 0 & 0 \\ c_b & h & hc \\ 0 & hu\Delta\,(1-\alpha) & hu\Delta\,(c-\varphi) \\ 0 & hv\Delta\,(1-\alpha) & hv\Delta\,(c-\varphi) \\ c_b\,(1-\alpha) & h\alpha & h\varphi - zc_b \\ 0 & 0 & 1 \end{bmatrix} \tag{8.30}$$

and

$$\mathbf{J_F} = \begin{bmatrix} u & h & & \\ u\left(\delta + h\alpha\frac{\partial c}{\partial h}\right) & h\left(\delta + u\alpha\frac{\partial c}{\partial u}\right) & & \\ \left(gh + u^2\right)\left(1 + \delta\Delta\right) + \Phi\Delta\alpha\frac{\partial c}{\partial h} & 2hu\left(1 + \delta\Delta\right) + \Phi\Delta\alpha\frac{\partial c}{\partial u} & & \\ uv\left(1 + \delta\Delta + h\Delta\alpha\frac{\partial c}{\partial h}\right) & hv\left(1 + \delta\Delta\varphi + u\Delta\alpha\frac{\partial c}{\partial u}\right) & & \\ 0 & 0 & & \\ 0 & 0 & & \end{bmatrix}$$
$$\begin{bmatrix} 0 & 0 & 0 & 0 \\ hu\alpha\frac{\partial c}{\partial v} & 0 & hu - hu\alpha & huc - hu\varphi \\ \Phi\Delta\alpha\frac{\partial c}{\partial v} & 0 & \Phi\Delta\left(1 - \alpha\right) & \Phi\Delta\left(c - \varphi\right) \\ hu\left(1 + \delta\Delta + v\Delta\alpha\frac{\partial c}{\partial v}\right) & 0 & huv\Delta\left(1 - \alpha\right) & huv\Delta\left(c - \varphi\right) \\ 0 & 0 & 0 & 0 \\ 0 & 0 & 0 & 0 \end{bmatrix} \tag{8.31}$$

The characteristic polynomial is

$$\lambda^2\left(u - \lambda\right)\left(a_3\lambda^3 + a_2\lambda^2 + a_1\lambda + a_0\right) = 0 \tag{8.32}$$

where a_i with $i = 0, \ldots, 3$ are four coefficients (not written in this thesis due to their complexity and length) that depend only on variables u, v, h and α. It is important to highlight the presence of two null eigenvalues

$$\lambda_i = 0 \quad \text{for} \quad i = 4, 5 \tag{8.33}$$

so the problem is not strictly hyperbolic. One eigenvalue is always

$$\lambda_6 = u \tag{8.34}$$

while the other three eigenvalues derive from the solution of the third order polynomial

$$\left(a_3\lambda^3 + a_2\lambda^2 + a_1\lambda + a_0\right) = 0 \tag{8.35}$$

Imposing $\alpha = 0$ or $\alpha = 1$ this polynomial reduces to the one associated to the fixed and mobile bed case respectively derived in Section 5.3.

The eigenvectors related to system (8.23) can be obtained form equation (7.36). For the same reason of the polynomial coefficients, the general expression of $\mathbf{R}_i^W$ for $i = 1, 3$ is not reported. The eigenvectors associated to the two null eigenvalues ($\lambda_{4,5} = 0$) are

$$\mathbf{R}_4^W = \begin{bmatrix} gh\,(\alpha - 1) \\ -gu\,(\alpha - 1) \\ 0 \\ -\,(\alpha - 1)\,(gh - u^2) \\ gh\alpha\dfrac{\partial c}{\partial h} - gu\alpha\dfrac{\partial c}{\partial u} \\ 0 \end{bmatrix} \tag{8.36}$$

$$\mathbf{R}_5^W = \begin{bmatrix} -gh\,(\xi\,(1 - \alpha) + c - \varphi) \\ gu\,(\xi\,(1 - \alpha) + c - \varphi) \\ 0 \\ (gh - u^2)\,(\xi\,(1 - \alpha) + c - \varphi) \\ gh\xi\alpha\dfrac{\partial c}{\partial h} - g\xi u\alpha\dfrac{\partial c}{\partial u} \\ gh\alpha\dfrac{\partial c}{\partial h} - gu\alpha\dfrac{\partial c}{\partial u} \end{bmatrix} \tag{8.37}$$

where ξ is an arbitrary constant (as for the previous cases). It is important to notice that the eigenvectors associated to the null eigenvalues $\lambda_{4,5}$ are independent. The last eigenvector presented here is associated to $\lambda_6 = u$ and it is

$$\mathbf{R}_6^W = \begin{bmatrix} \Delta\alpha h\dfrac{\partial c}{\partial v} \\ 0 \\ \Delta\alpha\left(\varphi - 2c - h\dfrac{\partial c}{\partial h}\right) - \Delta\varphi - 2 \\ 0 \\ -\Delta\alpha\varphi\dfrac{\partial c}{\partial v} \\ 0 \end{bmatrix} \tag{8.38}$$

All the properties related to the eigenvectors $\mathbf{R}_i^W$ with $i = 1, \ldots, 5$ and their associated characteristic fields highlighted in Section 8.1.1 are still valid also

λ_1		λ_2		λ_3	
$\alpha = 0$	$\alpha = 1$	$\alpha = 0$	$\alpha = 1$	$\alpha = 0$	$\alpha = 1$
GNL	GNL	LD	GNL	GNL	GNL
φ, z_b, v, α	α	h, u, z_b, v, α	α	φ, z_b, v, α	α

$\lambda_4 = 0$		$\lambda_5 = 0$		$\lambda_6 = u$	
$\alpha = 0$	$\alpha = 1$	$\xi = 0$	$\xi \neq 0$	$\alpha = 0$	$\alpha = 1$
LD*	LD*	LD*	LD*	LD	LD
φ, v, α	h, u, z_b, v, α	φ, v	v	$h, u, z_b, \varphi, \alpha$	u, z_b, α

Table 8.1: Summary of the possible characteristic fields with indication of the variables that remain constant across each wave of that field. Meanings of the symbols: GNL = genuinely nonlinear field; LD = classical linearly degenerate field; LD* = linearly degenerate field with λ independent from $\mathbf{U}$. Finally ξ is a degree of freedom of the fifth field

for the CPDEs system (8.23) but, in this case, there is one more component in each eigenvectors, related to the velocity v, that does not affect the dissertation done before. Regarding the eigenvector $\mathbf{R}_6^W$, the associated characteristic field is a classical linearly degenerate one where α, u and z_b does not change. Some important property related to the eigenvectors and associated characteristic fields are summarized in Table 8.1.

Since system (8.23) is nonconservative, the relation valid across shocks associated to GNL fields is following GRH relation

$$\mathbf{F}_{\mathbf{R}}^* - \mathbf{F}_{\mathbf{L}}^* - \mathbf{D} = S_s \left(\mathbf{U}_{\mathbf{R}}^* - \mathbf{U}_{\mathbf{L}}^* \right) \tag{8.39}$$

where S_s is the speed of the shock, $\mathbf{F}_R^*, \mathbf{F}_L^*$ and $\mathbf{U}_R^*, \mathbf{U}_L^*$ are the fluxes and the conserved variables respectively on the right and on the left of the shock wave and finally $\mathbf{D}^T = (0, 0, D, 0, 0, 0)$ where D is defined by equation (8.18).

The classes of solutions of the CRP are similar to the one presented for the simplified model (Section 7.4). The only difference is in the presence of the contact wave λ_6 in all the categories as reported in Figure 8.1 where the wave pattern associated to each categories is presented. Nevertheless,

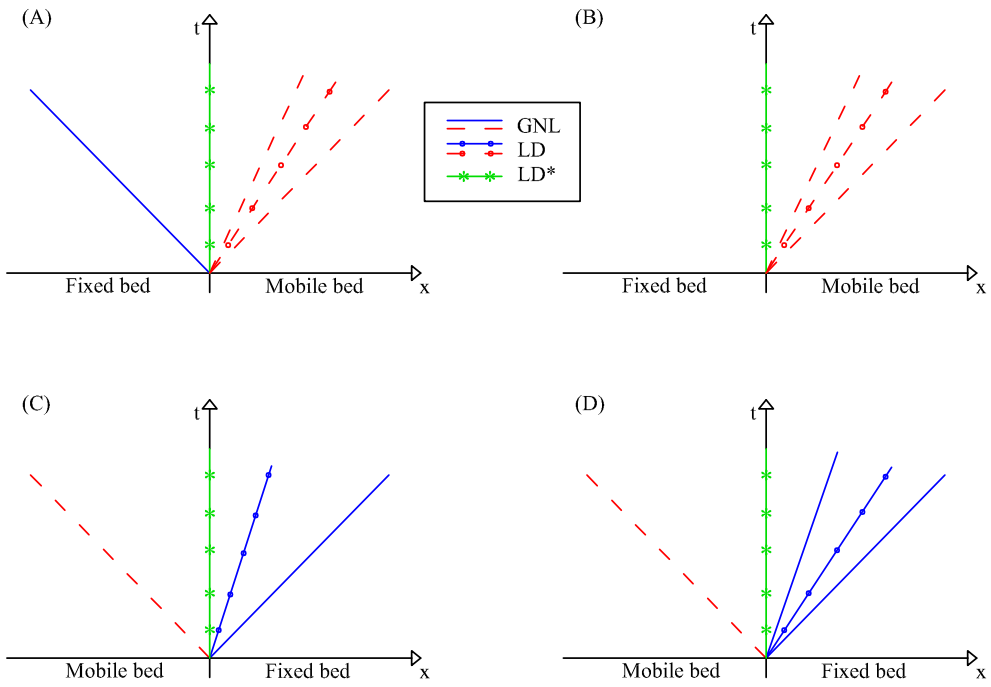

Figure 8.1: The four different classes of CRP solutions for positive velocity in the neighborhood of the origin: (a) FBsub-MB, (b) FBsup-MB, (c) MB-FBsub, (d)MB-FBsup. Dashed lines represent mobile-bed fields, solid lines fixed-bed ones. GNL represent genuinely nonlinear fields, LD classical linearly degenerate fields and LD* linearly degenerate fields with λ independent from $\mathbf{U}$.

the existence of this additional wave does not modify all the characteristics highlighted in Section 7.4.

Part III

Transition from fixed bed to mobile bed: numerical aspect

Chapter 9

Numerical Riemann solvers

The homogeneous part of generic PDEs system (as the composite systems developed in Part II) can be written, in compact form, as

$$\frac{\partial \mathbf{U}}{\partial t} + \frac{\partial \mathbf{F}}{\partial x} + \mathbf{H}\frac{\partial \mathbf{W}}{\partial x} = 0 \tag{9.1}$$

where $\mathbf{U}$ and $\mathbf{W}$ are the vectors of conservative and primitive variables, while $\mathbf{F}$ and $\mathbf{H}$ represents the conservative and non conservative fluxes respectively. In the framework of finite volume method the classical update formula for equation (9.1) is

$$\mathbf{U}_i^{n+1} = \mathbf{U}_i^n - \frac{\Delta t}{\Delta x}\left(\mathbf{F}_{i+1/2}^- - \mathbf{F}_{i-1/2}^+\right) \tag{9.2}$$

where Δt is the time step integration, Δx is the space discretization, the superscript n refers to the time step $n\Delta t$, the subscript i refers to cell i which center is located at $i\Delta x$, $\mathbf{F}_{i+1/2}^-$ is the outgoing flux on the right border of cell i, while $\mathbf{F}_{i-1/2}^+$ is the incoming flux evaluated on the left side of cell i. Since we want to use the Godunov method, the evaluation of $\mathbf{F}_{i-1/2}^-$ and $\mathbf{F}_{i+1/2}^+$ is performed solving a Riemann problem (RP) with appropriated and numerical solvers. We highlight that, since equation (9.1) contains both conservative and non conservative fluxes, the $\mathbf{F}_{i-1/2}^-$ and $\mathbf{F}_{i+1/2}^+$ can be different, so the numerical solver must take into account both conservative and non-conservative terms.

In this Chapter we present three different Riemann solvers used to solve the CPDEs systems derived in the previous Chapters. In particular, in Section 9.1 a modified version of the LHLL solver is presented, in Section 9.2 the

Closure Independent Generalized Roe solver is introduced and the Extended Multiple Averages strategy is developed, while in Section 9.3 a new version of the Universal Osher solver is presented. Finally, in Section 9.4, a comparison between the three different Riemann solvers is performed.

In the following Sections, we focus our attention on the homogeneous part of the CPDEs system for high sediment concentration (8.5) developed in Section 8.1 that reads

$$\begin{cases} \dfrac{\partial}{\partial t}\left(h+z_b\right)+\dfrac{\partial}{\partial x}uh=0 \\ \dfrac{\partial}{\partial t}\left(c_b z_b+\varphi h+\alpha c h\right)+\dfrac{\partial}{\partial x}\left(\delta uh\right)=0 \\ \dfrac{\partial}{\partial t}\left(1+\delta\Delta\right)uh+\dfrac{\partial}{\partial x}\left(1+\delta\Delta\right)\left(u^2h+g\dfrac{h^2}{2}\right)+\left(1+\delta\Delta\right)gh\dfrac{\partial z_b}{\partial x}=0 \\ \dfrac{\partial}{\partial t}\left(\left(1-\alpha\right)c_b z_b+\alpha\varphi h\right)=0 \\ \dfrac{\partial}{\partial t}\alpha=0 \end{cases} \tag{9.3}$$

where $\delta=\left(\alpha c+\left(1-\alpha\right)\varphi\right)$, while the associated CRP problem can be written in the following form

$$\begin{cases} \dfrac{\partial \mathbf{U}}{\partial t}+\dfrac{\partial \mathbf{F}}{\partial x}+\mathbf{H}\dfrac{\partial \mathbf{W}}{\partial x}=0 \\ \mathbf{U}\left(x,0\right)=\begin{cases} \mathbf{U}_L & \text{if} \quad x<0 \\ \mathbf{U}_R & \text{if} \quad x>0 \end{cases} \end{cases} \tag{9.4}$$

where $\mathbf{U}$, $\mathbf{W}$, $\mathbf{F}$ and $\mathbf{H}$ are defines in equations (8.7) and (8.8). The extensions to the CPDEs model for low sediment concentration (7.19) and to the CPDEs with plane wave (8.23) are not reported since they are quite straightforward.

9.1 The LHLL solver

The LHLL Riemann solver developed by Fraccarollo *et al.* [26] is an extension of the HLL Riemann solver of Harten *et al.* [31]. The general expression, for

the left and right intercell fluxes, using the LHLL is

$$\mathbf{F}_{LHLL}^{L,R} = \mathbf{F}^{HLL} - \frac{S_{L,R}}{S_R - S_L} g\overline{h\left(1+\delta\Delta\right)}\left(z_R - z_L\right) \tag{9.5}$$

where L and R are respectively the left and the right initial values of Riemann's problem,

$$S_L = \min\left(\lambda_{L,\min}, \lambda_{R,\min}\right)$$
$$S_R = \max\left(\lambda_{L,\max}, \lambda_{R,\max}\right)$$

are respectively the minimum and maximum of the eigenvalues λ evaluated with left and right initial values, $\overline{h\left(1+\delta\Delta\right)}$ is the arithmetic mean of $h\left(1+\delta\Delta\right)$

$$\overline{h\left(1+\delta\Delta\right)} = \frac{h_L\left(1+\delta_L\Delta\right) + h_R\left(1+\delta_R\Delta\right)}{2}$$

and $\mathbf{F}^{HLL}$ is the flux evaluated using the HLL solver

$$\mathbf{F}^{HLL} = \begin{cases} \mathbf{F}_L & \text{if } S_L > 0 \\ \mathbf{F}_R & \text{if } S_R < 0 \\ \dfrac{S_R\mathbf{F}_L - S_L\mathbf{F}_R + S_L S_R\left(\mathbf{U}_R - \mathbf{U}_L\right)}{S_R - S_L} & \text{otherwise} \end{cases}$$

The drawback of its simplicity is the highly numerical diffusion peculiar of this type of Riemann solver where only some features of the RP are used. In order to avoid the diffusion on the last two equations of systems (9.3), so the ones where the fluxes are null, a simple superimposition of zero value can be applied

$$F_4^{LHLL} = 0 \tag{9.6}$$
$$F_5^{LHLL} = 0 \tag{9.7}$$

where the subscripts 4 and 5 indicate the fourth and fifth element of the flux vector $\mathbf{F}^{LHLL}$. The superimposition of these null fluxes is necessary since the function α can assume, as specified in Chapter 7, only value 0 or 1, thus the diffusion must be neglected. However performing a numerical simulation (see the blue dots in Figure 9.1) for the transition between mobile and fixed bed,

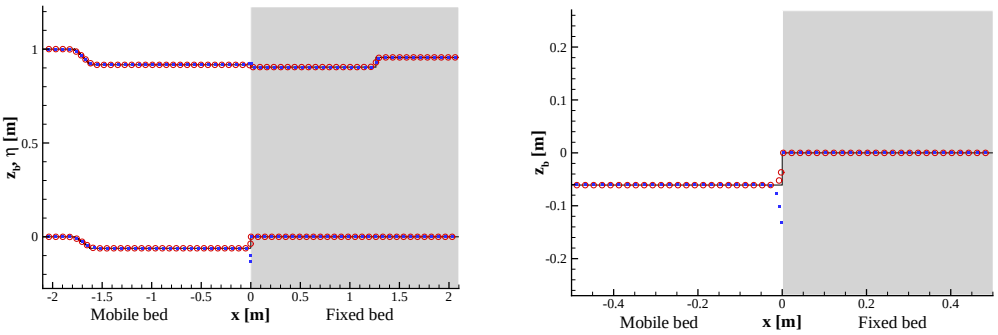

Figure 9.1: Comparison between analytical (solid line) and numerical solutions obtained with LHLL without (blue dots) and with (red circles) F_2 correction for the transition between mobile and fixed bed case. On the left subfigure: free surface η and bed elevation z_b; on the right: detail of the bottom elevation near the interface.

we highlight the development of incorrect solutions near the interface between mobile and fixed bed. The initial data for the simulation are $h_L = 1\ m$, $h_R = 1.2\ m$, $u_L = 1\ m/s$, $u_R = 2\ m/s$, $z_{b,L} = 0\ m$, $z_{b,R} = 0\ m$, $\varphi_L = 0$, $\varphi_R = 0$ and $\alpha_L = 1$, $\alpha_R = 0$. As closure relation for the concentration we used equation (5.32) with $\beta = 0.5$. Other parameters are $c_b = 0.6$, $\Delta = 1.65$, spatial discretization $\Delta x = 0.005\ m$, simulation time $t = 1\ s$ and Courant number $CFL = 0.9$.

The key idea to solve the problem is to try to estimate the numerical diffusion associated to the solid mass conservation from one of the equations of the system. In particular here we focus on the fourth equation that reads

$$\frac{\partial}{\partial t}\left((1-\alpha)\, c_b z_b + \alpha\varphi h\right) = 0 \tag{9.8}$$

Since the LHLL solver is quite diffusive we can imagine that the real equation solved is

$$\frac{\partial}{\partial t}\left((1-\alpha)\, c_b z_b + \alpha\varphi h\right) = D_{num} \tag{9.9}$$

where D_{num} is the numerical diffusion associated to the fourth equation. Since the second equation of system (9.3), as described in Chapter 8, derives from the weighted sum of the fixed and mobile bed solid mass balance and

then it is added to the fourth one, we can imagine that also the second equation contains the same diffusion term as the fourth one as

$$\frac{\partial}{\partial t}\left(\alpha ch + c_b z_b + \varphi h\right) + \frac{\partial}{\partial x}\left(\alpha cuh + (1-\alpha)\,\varphi uh\right) = D_{num} \tag{9.10}$$

Knowing the general structure of equations (9.9) and (9.10) it is possible to obtain a better estimation of the numerical flux for the second equation in the following way

$$F_2^{LHLL,*} = F_2^{LHLL} - F_4^{LHLL} \tag{9.11}$$

where $F_2^{LHLL,*}$ is a new estimation of the solid flux. At this point it is possible to nullify F_4. Schematically the procedure to follow is:

1. evaluate the numerical fluxes using the classical LHLL solver (9.5);
2. estimate the *corrected* solid mass flux $F_2^{LHLL,*}$ with equation (9.11);
3. nullify F_4 and F_5.

Performing the same numerical simulation presented in Figure 9.1, following this new procedure the solution obtained (red circles) is now a good approximation of the analytical one (solid black line in the same Figure) since only some diffusion is present.

9.2 The Closure Independent Generalized Roe solver

An effective numerical scheme for the system (9.3), which is partially non-conservative, as said before, is the Generalized Roe (GR) method originally introduced in [55] and extended to a general closure relations in [52] (the Closure Independent GR). In particular, here we will exploit and improve the Multiple Averages (MAs) approach introduced in this last paper in order to obtain in a rather straightforward way the matrices needed in the GR scheme. For sake of completeness, here we will only briefly summarize the method and we address the reader to the original papers for details.

In the GR method, the approximated solution of (9.4) is obtained from the exact solution of the following linear problem:

$$\begin{cases} \dfrac{\partial \mathbf{U}}{\partial t} + \mathcal{A}\left(\mathbf{U}_L, \mathbf{U}_R\right) \dfrac{\partial \mathbf{U}}{\partial x} = 0 \\ \mathbf{U}\left(x, 0\right) = \begin{cases} \mathbf{U}_L & \text{if} \quad x < 0 \\ \mathbf{U}_R & \text{if} \quad x > 0 \end{cases} \end{cases} \tag{9.12}$$

where $\mathcal{A}$ is a suitable constant matrix whose values depend on the left and right states. In order to obtain a good matrix, it must satisfy the following three conditions:

1. the linear problem (9.12) must tend smoothly to the linearized version of (9.4)

$$\mathcal{A}\left(\mathbf{U}_L, \mathbf{U}_R\right) \rightarrow \frac{\partial \mathbf{F}}{\partial \mathbf{U}} + \mathbf{H}\frac{\partial \mathbf{W}}{\partial \mathbf{U}} \quad \text{smoothly as} \quad \mathbf{U}_L \rightarrow \mathbf{U}_R \tag{9.13}$$

2. the matrix $\mathcal{A}\left(\mathbf{U}_L, \mathbf{U}_R\right)$ must have a complete set of real eigenvalues and associated eigenvectors;

3. the integral of the approximate solution over a space-time interval must be equal to the integral of the exact solution over the same interval

$$\mathcal{A}\left(\mathbf{U}_L, \mathbf{U}_R\right)\left(\mathbf{U}_R - \mathbf{U}_L\right) = \left(\mathbf{F}_R - \mathbf{F}_L\right) - \mathbf{D} \tag{9.14}$$

where D is defined by equation (8.18).

Considering that it is useful to rewrite the matrix $\mathcal{A}\left(\mathbf{U}_L, \mathbf{U}_R\right)$ as a function of the primitive variables in the following way

$$\mathcal{A}\left(\mathbf{U}_L, \mathbf{U}_R\right) = \left[\mathbf{A}\left(\mathbf{W}_L, \mathbf{W}_R\right) + \mathbf{H}\left(\mathbf{W}_L, \mathbf{W}_R\right)\right] \mathbf{B}^{-1}\left(\mathbf{W}_L, \mathbf{W}_R\right) \tag{9.15}$$

where $\mathbf{A}, \mathbf{H}, \mathbf{B}$ are suitable unknown matrices function of the primitive variables, the previous three conditions become

$$\mathbf{B}\left(\mathbf{W}_L, \mathbf{W}_R\right)\left(\mathbf{W}_R - \mathbf{W}_L\right) = \mathbf{U}_R - \mathbf{U}_L \tag{9.16a}$$

$$\mathbf{A}\left(\mathbf{W}_L, \mathbf{W}_R\right)\left(\mathbf{W}_R - \mathbf{W}_L\right) = \mathbf{F}_R - \mathbf{F}_L \tag{9.16b}$$

$$\mathbf{H}\left(\mathbf{W}_L, \mathbf{W}_R\right)\left(\mathbf{W}_R - \mathbf{W}_L\right) = -\mathbf{D} \tag{9.16c}$$

The MAs procedure allows to determine the matrices satisfying the previous constraints in the following way

$$\mathbf{B}\left(\mathbf{W}_L, \mathbf{W}_R\right) = \mathbf{J}_U(\dddot{\mathbf{M}}) \tag{9.17a}$$

$$\mathbf{A}\left(\mathbf{W}_L, \mathbf{W}_R\right) = \mathbf{J}_F(\dddot{\mathbf{M}}) \tag{9.17b}$$

$$\mathbf{H}\left(\mathbf{W}_L, \mathbf{W}_R\right) = \mathbf{H}(\dddot{\mathbf{M}}) \tag{9.17c}$$

where $\mathbf{J}_U$ and $\mathbf{J}_F$ are respectively the Jacobians of the conserved variables and of the fluxes evaluated respect the primitive variables (detailed expression are reported in Section 8.1.1) while $\dddot{\mathbf{M}}$ is a suitable set of primitive variable averages. Following the procedure presented in [52] it is possible to determine the required set.

Firstly, we consider the introduce the algebraic average state

$$\widetilde{u} = \frac{u_L + u_R}{2}; \quad \widetilde{h} = \frac{h_L + h_R}{2}; \quad \widetilde{\varphi} = \frac{\varphi_L + \varphi_R}{2} \tag{9.18}$$

while, in order to avoid problems with the inversion of matrix $\mathbf{B}$, the following average for the erodibility parameter has been used

$$\widetilde{\alpha} = \frac{k_1\alpha_L + k_2\alpha_R}{k_1 + k_2} \tag{9.19}$$

where k_1 and k_2 are two distinct parameters, function of the left and right initial conditions. A possible choice is to use the following value

$$\begin{cases} \begin{cases} k_1 = 1 \\ k_2 = 0 \end{cases} & \text{if } \widetilde{u} > 0 \\ \begin{cases} k_1 = 0 \\ k_2 = 1 \end{cases} & \text{otherwise} \end{cases} \tag{9.20}$$

that is an upwind method for the erodibility parameter.

If we insert these averaged values in the general expression of $\mathbf{J}_U$, two of the relations of equation (9.16a) are satisfied (i.e. the ones related to the first and the fifth rows of the matrix). In order to satisfy the fourth equation we have to introduce an unknown average in $\mathbf{J}_U$ and then solve the linear equation deriving from equation (9.16a). In this case we have considered as unknown the non linear variable $\widehat{\varphi h - z_b c_b}$. Highlighting only the fourth row

of $\mathbf{J}_U(\dddot{\mathbf{M}})$, the linear equation to be solved reads

$$\begin{bmatrix} 0 & 0 & 0 & 0 & 0 \\ 0 & 0 & 0 & 0 & 0 \\ 0 & 0 & 0 & 0 & 0 \\ \tilde{\alpha}\tilde{\varphi} & 0 & c_b - \tilde{\alpha}c_b & \tilde{h}\tilde{\alpha} & \widehat{\varphi h - z_b c_b} \\ 0 & 0 & 0 & 0 & 0 \end{bmatrix} \Delta\mathbf{W} - \Delta\mathbf{U}_4 = 0 \tag{9.21}$$

where $\Delta\mathbf{W} = \mathbf{W}_R - \mathbf{W}_L$ and $\Delta\mathbf{U}_4 = \mathbf{U}_4^R - \mathbf{U}_4^L$ in which $\mathbf{U}_4$ is the conserved variables vector where only the fourth row is non null (i.e. $\mathbf{U}_4^T = [0, 0, 0, \alpha c h + c_b z_b + \varphi h, 0]$). The result of this linear equation is

$$\widehat{\varphi h - z_b c_b} = \frac{\varphi_R k_1 h_R + \varphi_L k_2 h_L}{k_1 + k_2} - c_b \frac{k_1 z_R + k_2 z_L}{k_1 + k_2}$$

that is the unknown average value that satisfy equation (9.16a). We highlight that this average value satisfy also the differential consistency (9.13).

In a similar way it is possible to solve the second equation

$$\begin{bmatrix} 0 & 0 & 0 & 0 & 0 \\ \tilde{\varphi} + \tilde{\alpha}c_m + \widehat{h\alpha}c_h & \widehat{h\alpha}c_u & c_b & \tilde{h} & \breve{h}c_m \\ 0 & 0 & 0 & 0 & 0 \\ 0 & 0 & 0 & 0 & 0 \\ 0 & 0 & 0 & 0 & 0 \end{bmatrix} \Delta\mathbf{W} - \Delta\mathbf{U}_2 = 0 \tag{9.22}$$

in which $\mathbf{U}_2$ refers to the conserved variables vector where only the second row is non null,

$$\breve{h} = \frac{k_1 h_L + k_2 h_R}{k_1 + k_2} \tag{9.23}$$

is a-priori defined average state,

$$c_m = c\left(\widetilde{u}, \widetilde{h}\right);\ c_h = \left.\frac{\partial c}{\partial h}\right|_{\left(\widetilde{u},\widetilde{h}\right)};\ c_u = \left.\frac{\partial c}{\partial u}\right|_{\left(\widetilde{u},\widetilde{h}\right)} \tag{9.24}$$

that are univocally determined when a proper closure relation for the concentration is defined, while the unknown average value is

$$\widehat{h\alpha} = \frac{\alpha_L c_L h_L - \alpha_R c_R h_R - (\alpha_L h_L - \alpha_R h_R)\, c_m}{(h_L - h_R)\, c_h + (u_L - u_R)\, c_u} \tag{9.25}$$

The third equation, derived from (9.16a), is the most complicated one and the application of the MAs procedure is quite difficult, since lot of non-linear products are present but only one unknown average can be defined. In order to overcome this problem, we developed the Extended Multiple Averages procedure (EMAs).

9.2.1 A novel Extended Multiple Averages procedure

With the MAs procedure, as said before, it is possible to obtain only one unknown average for each equation derived from the integral consistency (equations (9.16a), (9.16b) and (9.16c)), while all the other average values have to be defined. When in the Jacobian matrix, used as starting point in the MAs strategy, there are lots of non-linear products, the choice of the unknown average and the known ones becomes crucial, since if we impose in an arbitrary way the known averages, often enough we obtain as result an unknown that is not an average, but a difference of terms, so it does not satisfy the differential consistency (9.13).

The key idea for the EMAs is to take advantage of the linearity of the Jacobian matrix respect to the algebraic sum. For example, when a conserved variable can be decomposed in the sum of n terms, it is possible to split the conserved vector as

$$\mathbf{U} = \sum_{i=1}^{n} \mathbf{U}^i \tag{9.26}$$

where $\mathbf{U}^i$ is the vector of conserved variable containing one of the term of the decomposition. For each of these vectors the Jacobian matrixes respect to the primitive are evaluated

$$\mathbf{J}_{U^i} = \frac{\partial \mathbf{U}^i}{\partial \mathbf{W}} \tag{9.27}$$

and using the linearity of the Jacobian the following relation can be written

$$\mathbf{J}_U = \sum_{i=1}^{n} \mathbf{J}_{U^i} \tag{9.28}$$

With equations (9.26) and (9.28), the integral consistency (9.16a) becomes

$$\sum_{i=1}^{n} \mathbf{J}_{U^i}(\dddot{\mathbf{M}}) \left(\mathbf{W}_R - \mathbf{W}_L\right) = \sum_{i=1}^{n} \mathbf{U}_R^i - \sum_{i=1}^{n} \mathbf{U}_L^i \tag{9.29}$$

that can be decomposed in n equations

$$\mathbf{J}_{U^i}(\dddot{\mathbf{M}}) \left(\mathbf{W}_R - \mathbf{W}_L\right) = \mathbf{U}_R^i - \mathbf{U}_L^i \tag{9.30}$$

with $i = 1, \ldots, n$. The same procedure can be applied also to the flux components ending up with

$$\mathbf{J}_{F^i}(\dddot{\mathbf{M}}) \left(\mathbf{W}_R - \mathbf{W}_L\right) = \mathbf{F}_R^i - \mathbf{F}_L^i \tag{9.31}$$

where $i = 1, \ldots, n_F$ and n_F is the number of terms in which the flux vector is decomposed.

With this decomposition strategy the complexity of each equation is drastically reduced, namely the number of non-linear terms in each equation is limited. In this way, the choice of the known averages is more simple, since for a linear term the arithmetic mean is a sensible choice, while one of the non-linear terms becomes the unknown average and the other can be imposed as multiplication of linear terms. Using the EMAs strategy, the possibility to obtained unknown averages that satisfy the differential consistency (9.13) is greater than the classical MAs.

In the following section we apply the EMAs strategy tThe third equation, derived from (9.16a) (the one not solved before with the MAs), showing the capability of this new methodology.

9.2.2 Application of the EMAs

The third conserved variable of systems (9.3) is

$$U_3 = \left(1 + \left(\alpha c + \left(1 - \alpha\right) \varphi\right) \Delta\right) uh \tag{9.32}$$

and can be decomposed in four different terms

$$U_3 = U_3' + U_3'' + U_3''' + U_3'''' \tag{9.33}$$

where

$$
\begin{aligned}
U_3' &= uh \\
U_3'' &= \varphi \Delta uh \\
U_3'''' &= -\alpha\varphi\Delta uh \\
U_3'''' &= \alpha c \Delta uh
\end{aligned}
$$

For each component, as said before, it is possible to evaluate the Jacobian matrix respect to the primitive variables $\mathbf{W}$ (we remember that we are focusing only on the third row of the conserved vector $\mathbf{U}$, so the other elements can be assumed null)

$$
\mathbf{J}_{U_3} = \mathbf{J}_{U_3'} + \mathbf{J}_{U_3''} + \mathbf{J}_{U_3'''} + \mathbf{J}_{U_3''''} \tag{9.34}
$$

where, for example

$$
\mathbf{J}_{U_3''} = \frac{\partial \mathbf{U}_3''}{\partial \mathbf{W}} = \begin{bmatrix} 0 & 0 & 0 & 0 & 0 \\ 0 & 0 & 0 & 0 & 0 \\ u\Delta\varphi & h\Delta\varphi & 0 & hu\Delta & 0 \\ 0 & 0 & 0 & 0 & 0 \\ 0 & 0 & 0 & 0 & 0 \end{bmatrix}
$$

and $\mathbf{U}_3''$ is the conserved vector where only the U_3'' term is present on the third row. Using this splitting of the conserved variables it is possible to obtain, from the integral consistency (9.16a) as specified before, four simplest conditions that must be fulfilled

$$
\mathbf{J}_{U_3'}(\dddot{\mathbf{M}})\,(\mathbf{W}_R - \mathbf{W}_L) = \mathbf{U}_{3R}' - \mathbf{U}_{3L}' \tag{9.35a}
$$

$$
\mathbf{J}_{U_3''}(\dddot{\mathbf{M}})\,(\mathbf{W}_R - \mathbf{W}_L) = \mathbf{U}_{3R}'' - \mathbf{U}_{3L}'' \tag{9.35b}
$$

$$
\mathbf{J}_{U_3'''}(\dddot{\mathbf{M}})\,(\mathbf{W}_R - \mathbf{W}_L) = \mathbf{U}_{3R}''' - \mathbf{U}_{3L}''' \tag{9.35c}
$$

$$
\mathbf{J}_{U_3''''}(\dddot{\mathbf{M}})\,(\mathbf{W}_R - \mathbf{W}_L) = \mathbf{U}_{3R}'''' - \mathbf{U}_{3L}'''' \tag{9.35d}
$$

Introducing a new average value

$$
\widetilde{hu} = \frac{k_2 h_L u_L + k_1 h_R u_R}{k_1 + k_2} \tag{9.36}
$$

the matrix $\mathbf{J}_{U_3}(\dddot{\mathbf{M}})$ becomes

$$\mathbf{J}_{U_3}(\dddot{\mathbf{M}}) = \begin{bmatrix} 0 & 0 & 0 & 0 & 0 \\ 0 & 0 & 0 & 0 & 0 \\ \tilde{u}\tilde{\zeta} + \widehat{uh\alpha}\Delta c_h & \tilde{h}\tilde{\zeta} + \widehat{uh\alpha}\Delta c_u & 0 & \widehat{hu}\,(1-\tilde{\alpha})\,\Delta & \Delta\left(c_m\widetilde{hu} - \widehat{\varphi hu}\right) \\ 0 & 0 & 0 & 0 & 0 \\ 0 & 0 & 0 & 0 & 0 \end{bmatrix}$$

where $\tilde{\zeta} = (1 + (\tilde{\alpha}c_m + (1-\tilde{\alpha})\,\tilde{\varphi})\,\Delta)$, while the unknown average values obtained are

$$\widehat{hu} = \frac{h_L u_L + h_R u_R}{2} \tag{9.37}$$

$$\widehat{\varphi hu} = \frac{k_2\varphi_L h_L u_L + k_1\varphi_R h_R u_R}{k_1 + k_2} \tag{9.38}$$

$$\widehat{uh\alpha} = \frac{\alpha_L c_L h_L u_L - \alpha_R c_R h_R u_R - (\alpha_L h_L u_L - \alpha_R h_R u_R)\,c_m}{c_h\,(h_L - h_R) + c_u\,(u_L - u_R)} \tag{9.39}$$

We highlight that using the EMAs we obtain three unknown averages, while if we used the MAs strategy only one of these terms can be obtained, while the other two must be imposed.

Assembling together all the elements of the matrix $\mathbf{J}_U(\dddot{\mathbf{M}})$ obtained, the result is

$$\mathbf{J}_U(\dddot{\mathbf{M}}) = \begin{bmatrix} 1 & 0 & 1 & & \\ \tilde{\varphi} + \tilde{\alpha}c_m + \widehat{h\alpha}c_h & \widehat{h\alpha}c_u & c_b & & \\ \tilde{u}\tilde{\zeta} + \widehat{uh\alpha}\Delta c_h & \tilde{h}\tilde{\zeta} + \widehat{uh\alpha}\Delta c_u & 0 & & \\ \tilde{\alpha}\tilde{\varphi} & 0 & c_b - \tilde{\alpha}c_b & & \\ 0 & 0 & 0 & & \end{bmatrix}$$

$$\begin{bmatrix} 0 & 0 \\ \tilde{h} & \breve{h}c_m \\ \widehat{hu}\,(1-\tilde{\alpha})\,\Delta & \Delta\left(c_m\widetilde{hu} - \widehat{\varphi hu}\right) \\ \tilde{h}\tilde{\alpha} & \widehat{\varphi h - z_b c_b} \\ 0 & 1 \end{bmatrix} \tag{9.40}$$

Analogous procedure can be applied to obtain matrix $\mathbf{A}$. As known average variables to by introduced in $\mathbf{J}_F$, we use

$$\widetilde{u} = \frac{u_L + u_R}{2}; \quad \widetilde{h} = \frac{h_L + h_R}{2}; \quad \widetilde{\varphi} = \frac{\varphi_L + \varphi_R}{2}; \quad \breve{\alpha} = \frac{\alpha_L + \alpha_R}{2}$$

and, applying the EMAs strategy explained before, we obtain

$$\mathbf{J}_F(\ddot{\mathbf{M}}) = \begin{bmatrix} \tilde{u} & \tilde{h} & 0 & 0 & 0 \\ \tilde{u}\tilde{\varphi}\left(1-\breve{\alpha}\right) + \breve{\alpha}\tilde{u}c_m + \widehat{uh\alpha}c_h & \tilde{h}\tilde{\varphi}\left(1-\breve{\alpha}\right) + \breve{\alpha}\tilde{h}c_m + \widehat{uh\alpha}c_u & 0 & \widehat{hu}\left(1-\breve{\alpha}\right) & -\widetilde{uh\varphi} + \widehat{huc_m} \\ \left(\widehat{u^2} + g\tilde{h}\right)\breve{\zeta} + \widehat{\Phi\alpha}\Delta c_h & \left(2\tilde{u}\tilde{h}\right)\breve{\zeta} + \widehat{\Phi\alpha}\Delta c_u & 0 & \Delta\widehat{\Phi}\left(1-\breve{\alpha}\right) & \widehat{\Phi}\Delta c_m - \Delta\widehat{\Phi\varphi} \\ 0 & 0 & 0 & 0 & 0 \\ 0 & 0 & 0 & 0 & 0 \end{bmatrix} \tag{9.41}$$

where the unknown averages are

$$\widehat{\Phi} = \left(\frac{1}{2}g\frac{h_R^2 + h_L^2}{2} + \frac{u_R^2 h_R + u_L^2 h_L}{2}\right) \tag{9.42}$$

$$\widehat{\Phi\varphi} = \left(\frac{1}{2}g\frac{h_R^2\varphi_R + h_L^2\varphi_L}{2} + \frac{u_R^2 h_R\varphi_R + u_L^2 h_L\varphi_L}{2}\right) \tag{9.43}$$

$$\widehat{\Phi\alpha} = \frac{\alpha_L c_L\Phi_L - \alpha_R c_R\Phi_R - \left(\alpha_L\Phi_L - \alpha_R\Phi_R\right)c_m}{\left(h_L - h_R\right)c_h + \left(u_L - u_R\right)c_u} \tag{9.44}$$

$$\widehat{u^2} = \frac{u_L^2 + u_R^2}{2} \tag{9.45}$$

$$\widetilde{uh\varphi} = \frac{h_R u_R\varphi_R + h_L u_L\varphi_L}{2} \tag{9.46}$$

in which

$$\Phi = \left(hu^2 + g\frac{h^2}{2}\right)$$

and

$$\breve{\zeta} = 1 + \left(\breve{\alpha}c_m + \left(1-\breve{\alpha}\right)\tilde{\varphi}\right)\Delta$$

We highlight that all the unknown averages satisfy the differential consistency (9.13).

Finally, from relation (9.16c) it is straightforward to obtain the expression for $\mathbf{H}$, where the only non-null term is:

$$\mathbf{H}_{3,3}(\dddot{\mathbf{M}}) = -g\left(1+\delta_k\Delta\right)\left(h_k - \frac{|z_R - z_L|}{2}\right) \quad \text{with } k = \begin{cases} L & \text{if } z_L \leq z_R \\ R & \text{otherwise} \end{cases} \tag{9.47}$$

The GR fluxes are then

$$\mathbf{F}^- = \mathbf{F}_L + \mathcal{A}^-\left(\mathbf{U}_R - \mathbf{U}_L\right) \quad ; \quad \mathbf{F}^+ = \mathbf{F}_R - \mathcal{A}^+\left(\mathbf{U}_R - \mathbf{U}_L\right) \tag{9.48}$$

where

$$\mathcal{A}^{\pm} = \mathcal{R}\boldsymbol{\Lambda}^{\pm}\mathcal{R}^{-1} \tag{9.49}$$

and $\mathcal{R}$ is the matrix of the right eigenvalues of $\mathcal{A}$,

$$\boldsymbol{\Lambda}^{\pm} = \Lambda^{\pm}_{ii} = \frac{1}{2}\left(\lambda^i \pm \left|\lambda^i\right|\right) \tag{9.50}$$

is the diagonal matrix of the eigenvalues of $\mathcal{A}$ where

$$\mathcal{A} = \left[\mathbf{J}_F(\dddot{\mathbf{M}}) + \mathbf{H}(\dddot{\mathbf{M}})\right]\left[\mathbf{J}_U(\dddot{\mathbf{M}})\right]^{-1}$$

9.3 The Universal Osher solver

The Osher Solomon solver that was developed by Osher and Solomon [48] for conservative systems, so systems where the matrix $\mathbf{H}$ is identically null. This Riemann solver is based on the assumption that it is possible to split the flux in positive part and negative one

$$\mathbf{F}\left(\mathbf{U}\right) = \mathbf{F}^-\left(\mathbf{U}\right) + \mathbf{F}^+\left(\mathbf{U}\right) \tag{9.51}$$

and on the existence of

$$\frac{\partial \mathbf{F}^-}{\partial \mathbf{U}} = \mathbf{A}^-_U \quad ; \quad \frac{\partial \mathbf{F}^+}{\partial \mathbf{U}} = \mathbf{A}^+_U \tag{9.52}$$

Given the left value $\mathbf{U}_L$ and the right one $\mathbf{U}_R$ of any Riemann problem, the Osher flux is evaluated using

$$\mathbf{F}_{i+\frac{1}{2}} = \mathbf{F}^+(\mathbf{U}_L) + \mathbf{F}^-(\mathbf{U}_R) \tag{9.53}$$

and, with the integral relation of $\mathbf{A}^+$ and $\mathbf{A}^-$ namely

$$\int_{\mathbf{U}_L}^{\mathbf{U}_R} \mathbf{A}_U^+ \, \mathrm{d}\mathbf{U} = \mathbf{F}^+(\mathbf{U}_R) - \mathbf{F}^+(\mathbf{U}_L) \tag{9.54}$$

$$\int_{\mathbf{U}_L}^{\mathbf{U}_R} \mathbf{A}_U^- \, \mathrm{d}\mathbf{U} = \mathbf{F}^-(\mathbf{U}_R) - \mathbf{F}^-(\mathbf{U}_L) \tag{9.55}$$

the Osher flux (9.53) becomes

$$\mathbf{F}_{i+\frac{1}{2}} = \frac{1}{2}(\mathbf{F}_L + \mathbf{F}_R) - \frac{1}{2}\int_{\mathbf{U}_L}^{\mathbf{U}_R} |\mathbf{A}_U| \, \mathrm{d}\mathbf{U} \tag{9.56}$$

where $|\mathbf{A}_U| = \mathbf{A}_U^+ - \mathbf{A}_U^- = \mathcal{R}\,|\mathbf{\Lambda}|\,\mathcal{R}^{-1}$, $\mathcal{R}$ is the matrix of the right eigenvectors of $\mathbf{A}_U$ and $|\mathbf{\Lambda}| = \mathbf{\Lambda}^+ - \mathbf{\Lambda}^-$. The first term of the flux is the central part of the fluxes, while the integral represents the so called numerical viscosity. The critical point of this solver is to chose the integral path in order to solve the integral itself. The strategy used in the Osher-Solomon approach is to select a particular integration path based on the eigenstructure of the problem, so as to been able to solve the integral in an explicit form. For this purpose the Osher-Solomon solver divides the path $I(\mathbf{U})$ that connect $\mathbf{U}_L$ and $\mathbf{U}_R$ in m disjointed partial paths $I_k(\mathbf{U})$ with $k = 1, \ldots, m$. Each of these partial paths connect two states called $\mathbf{U}_{\frac{k-1}{m}}$ and $\mathbf{U}_{\frac{k}{m}}$ and are tangential to the associated right eigenvector $\mathbf{R}_k(\mathbf{U})$. The fundamental aspect is that all the intermediate states $\mathbf{U}_k$ have to be known. This implies that we have to solve the Riemann problem in an approximated way (e.g. using only simple wave patterns) and then use these solutions to solve the integral in the (9.56). This leads to a complicated and expensive numerical solver.

To overcome the necessity to know all the intermediate states, Dumbser and Toro [23] developed the Universal Osher (UO) solver using the explicit form of the integral path in the phase-space (we refer to the original paper for more details on it) ending up with

$$\mathbf{F}_{i+\frac{1}{2}} = \frac{1}{2}(\mathbf{F}_L + \mathbf{F}_R) - \frac{1}{2}\int_0^1 |\mathbf{A}_U(\mathbf{\Psi}(\mathbf{U}_L, \mathbf{U}_R; s))| \frac{\partial \mathbf{\Psi}}{\partial s} \, \mathrm{d}s \tag{9.57}$$

where $\mathbf{\Psi}(s)$ is the path that links the left state $\mathbf{U}_L$ with the right one $\mathbf{U}_R$ in the phase-space. This path is a Lipschitz continuous function defined in the interval $s \in [0,1]$ with $\mathbf{\Psi}(0) = \mathbf{U}_L$ and $\mathbf{\Psi}(1) = \mathbf{U}_R$. In this way it is possible to use every type of path, detaching from the necessity to know all the intermediate states.

They also extended the UO solver to the case of fully non-conservative systems (i.e. systems where the conserved fluxes vector $\mathbf{F}$ is null) (see the original work of Dumbser and Toro [24] for more details) using the theory of Dal Maso *et al.* [20] about the non-conservative products. With this theory the compatibility condition on the fluxes becomes

$$\mathbf{D}^-_{i+\frac{1}{2}} - \mathbf{D}^+_{i+\frac{1}{2}} = \int_0^1 \mathbf{H}\left(\mathbf{\Psi}\left(\mathbf{U}_L, \mathbf{U}_R; s\right)\right) \frac{\partial \mathbf{\Psi}}{\partial s}\, \mathrm{d}s \tag{9.58}$$

where $\mathbf{D}^-_{i+\frac{1}{2}}$ and $\mathbf{D}^+_{i+\frac{1}{2}}$ are the fluxes evaluated respectively at the left and right side of the initial discontinuity and $\mathbf{D}$ is the matrix of nonconservative fluxes. From this definition, the authors define the fluxes for the Universal Osher solver in the following way

$$\mathbf{D}^+_{i+\frac{1}{2}} = -\frac{1}{2}\int_0^1 \left(\mathbf{H}\left(\mathbf{\Psi}\left(\mathbf{U}_L, \mathbf{U}_R; s\right)\right) + \left|\mathbf{H}\left(\mathbf{\Psi}\left(\mathbf{U}_L, \mathbf{U}_R; s\right)\right)\right|\right) \frac{\partial \mathbf{\Psi}}{\partial s}\, \mathrm{d}s \tag{9.59}$$

$$\mathbf{D}^-_{i+\frac{1}{2}} = \frac{1}{2}\int_0^1 \left(\mathbf{H}\left(\mathbf{\Psi}\left(\mathbf{U}_L, \mathbf{U}_R; s\right)\right) - \left|\mathbf{H}\left(\mathbf{\Psi}\left(\mathbf{U}_L, \mathbf{U}_R; s\right)\right)\right|\right) \frac{\partial \mathbf{\Psi}}{\partial s}\, \mathrm{d}s \tag{9.60}$$

A second key-point of the Universal Osher solver introduced by Dumbser and Toro [23, 24] is the use of the simplest path to connect the left and the right state. They propose to use a straight-line segment path

$$\mathbf{\Psi}\left(\mathbf{U}_L, \mathbf{U}_R; s\right) = \mathbf{U}_L + s\left(\mathbf{U}_R - \mathbf{U}_L\right) \tag{9.61}$$

This assumption is used in lots of paper and among which we can cite Castro Diaz *at al.* [16] where they say: "*...when there are no clear indication about the correct family of paths to be chosen, the family of straight segments is a sensible choice...*".

Using the straight line path the Universal Osher solver for a fully non-

conservative systems becomes the follow

$$\mathbf{D}^{\pm}_{i+\frac{1}{2}} = -\left(\pm\frac{1}{2}\left(\int_0^1 \mathbf{H}\left(\mathbf{\Psi}\left(\mathbf{U}_L,\mathbf{U}_R;s\right)\right)\,\mathrm{d}s \pm \int_0^1 \left|\mathbf{H}\left(\mathbf{\Psi}\left(\mathbf{U}_L,\mathbf{U}_R;s\right)\right)\right|\,\mathrm{d}s\right)\right)\left(\mathbf{U}_R-\mathbf{U}_L\right) \quad (9.62)$$

This leads to a versatile and general scheme that could be used over a great number of hyperbolic problems since the Universal Osher use the liner path, and needs only the eigenstructure of the problem.

9.3.1 The Universal Osher solver for partially non-conservative system

The general structure of generic hyperbolic PDEs system (e.g. the CPDEs system (9.3)) is composed both form conservative and non-conservative terms, therefore the UO solvers reported before could not be applied directly, but it is necessary to combine them together. In quasi-linear form, a generic PDEs system can be written as

$$\frac{\partial \mathbf{U}}{\partial t} + \mathcal{A}_U(\mathbf{U})\frac{\partial \mathbf{U}}{\partial x} = 0 \quad (9.63)$$

where

$$\mathcal{A}_U(\mathbf{U}) = \mathbf{A}_U\left(\mathbf{U}\right) + \mathbf{H}\left(\mathbf{U}\right) \quad (9.64)$$

and

$$\mathbf{A}_U\left(\mathbf{U}\right) = \frac{\partial \mathbf{F}}{\partial \mathbf{U}} \quad (9.65)$$

Since $\mathcal{A}_U(\mathbf{U})$ is composed by a conservative $\mathbf{A}_U$ and a non-conservative $\mathbf{H}$ part and the Osher scheme assumes a splitting of the fluxes, for the evaluation of the fluxes $\mathbf{F}^{\pm}_{i+\frac{1}{2}}$ is possible to split the fluxes in the conservative and the non-conservative one as

$$\mathbf{F}^{\pm}_{i+\frac{1}{2}} = \mathbf{F}_{i+\frac{1}{2}} + \mathbf{D}^{\pm}_{i+\frac{1}{2}} \quad (9.66)$$

where $\mathbf{F}_{i+\frac{1}{2}}$ is described by equation (9.57) and $\mathbf{D}^{\pm}_{i+\frac{1}{2}}$ with the equations (9.59) and (9.60). With this statement we end up with

$$\mathbf{F}^{\pm}_{i+\frac{1}{2}} = \frac{1}{2}\left(\mathbf{F}_L + \mathbf{F}_R\right) - \frac{1}{2}\int_0^1 \left|\mathbf{A}_U\left(\mathbf{\Psi}\left(s\right)\right)\right| \frac{\partial \mathbf{\Psi}}{\partial s}\,\mathrm{d}s + \\ - \frac{1}{2}\int_0^1 \left|\mathbf{H}\left(\mathbf{\Psi}\left(s\right)\right)\right| \frac{\partial \mathbf{\Psi}}{\partial s}\,\mathrm{d}s - \left(\pm\frac{1}{2}\int_0^1 \mathbf{H}\left(\mathbf{\Psi}\left(s\right)\right) \frac{\partial \mathbf{\Psi}}{\partial s}\,\mathrm{d}s\right) \quad (9.67)$$

For the sake of clarity from now on we neglect the dependency from $\mathbf{U}_L$ and $\mathbf{U}_R$ in the path $\mathbf{\Psi}$. It is also possible to add the absolute value matrixes of the conservative and the non-conservative fluxes

$$\left|\mathcal{A}_U\right| = \left|\mathbf{A}_U\right| + \left|\mathbf{H}\right| \quad (9.68)$$

obtaining the Universal Osher solver for a generic hyperbolic system containing conservative and non-conservative fluxes

$$\mathbf{F}^{\pm}_{i+\frac{1}{2}} = \frac{1}{2}\left(\mathbf{F}_L + \mathbf{F}_R\right) - \frac{1}{2}\int_0^1 \left|\mathcal{A}_U\left(\mathbf{\Psi}\left(s\right)\right)\right| \frac{\partial \mathbf{\Psi}}{\partial s}\,\mathrm{d}s \\ - \left(\pm\frac{1}{2}\int_0^1 \mathbf{H}\left(\mathbf{\Psi}\left(s\right)\right) \frac{\partial \mathbf{\Psi}}{\partial s}\,\mathrm{d}s\right) \quad (9.69)$$

We can easily check that for a conservative system ($\mathbf{H} = 0$ and $\left|\mathcal{A}_U\right| = \left|\mathbf{A}_U\right|$) the solver becomes exactly the conservative one (9.57). Also the compatibility condition that reads

$$\mathbf{F}^{-}_{i+\frac{1}{2}} - \mathbf{F}^{+}_{i+\frac{1}{2}} = \int_0^1 \mathbf{H}\left(\mathbf{\Psi}\left(s\right)\right) \frac{\partial \mathbf{\Psi}}{\partial s}\,\mathrm{d}s \quad (9.70)$$

as for the non-conservative system (9.58), can be easily proved.

9.3.2 A new Universal Osher solver with Primitive reconstitution

The UO for partially non-conservative systems was developed starting form an hyperbolic PDEs system where the fluxes are written using the conservative variables, so in equation (9.69) the path integral is performed using the conserved variables $\mathbf{U}$. However, for a generic hyperbolic PDEs system,

is not always possible to write the fluxes in term of conservative variables, indeed in the CPDEs system (9.3) the flux terms are written in term of primitive variables (i.e. $\mathbf{F} = \mathbf{F}(\mathbf{W})$ and $\mathbf{H} = \mathbf{H}(\mathbf{W})$). In quasi linear form the system is

$$\frac{\partial \mathbf{U}}{\partial t} + \mathcal{A}_W \frac{\partial \mathbf{U}}{\partial x} = 0 \tag{9.71}$$

where

$$\mathcal{A}_W(\mathbf{W}) = \left(\mathbf{J}_{\mathbf{F}}\left(\mathbf{W}\right) + \mathbf{H}\left(\mathbf{W}\right)\right) \mathbf{J}_U\left(\mathbf{W}\right)^{-1} \tag{9.72}$$

Comparing the two linear forms (9.63) and (9.71) we can notice that they are similar except for the definition of the matrix $\mathcal{A}_W$. Since the UO solver is associated to the linear form of the problem, a change of $\mathcal{A}$ matrix can be done, therefore we can use $\mathcal{A}_W$ in equation (9.69) instead $\mathcal{A}_U$. This lead, after some manipulations, to the following expression for the fluxes

$$\begin{aligned}\mathbf{F}^{\pm}_{i+\frac{1}{2}} = \frac{1}{2}\left(\mathbf{F}_L + \mathbf{F}_R\right) - \frac{1}{2}\int_0^1 \left|\mathcal{A}_W\left(\mathbf{\Psi}\left(s\right)\right)\right| \frac{\partial \mathbf{\Psi}}{\partial s}\,\mathrm{d}s \\ - \left(\pm\frac{1}{2}\int_0^1 \mathbf{H}\left(\mathbf{\Psi}\left(s\right)\right) \mathbf{J}_U^{-1}\left(\mathbf{\Psi}\left(s\right)\right) \frac{\partial \mathbf{\Psi}}{\partial s}\,\mathrm{d}s\right)\end{aligned} \tag{9.73}$$

where $\left|\mathcal{A}_W\right| = \mathcal{R}_W \left|\mathbf{\Lambda}\right| \mathcal{R}_W^{-1}$, $\mathcal{R}_W$ is the matrix of the right eigenvectors of $\mathcal{A}_W$. This simple extension has the disadvantage that the path integral is defined for the conserved variables, while the matrixes $\mathbf{J}_F$, $\mathbf{J}_U$ and $\mathbf{H}$ are functions of the primitive ones. Therefore, the integration along the path needs a change of variable from the conserved variable to the primitive ones. For the CPDEs system (9.3), the switch from conserved variables to primitive ones is quite complicated and lead to a non-liner system that must be solved several time during the numerical solution of the integrals. In order to overcome this problem, our idea is to change the path integration from the conserved variables to the primitive ones. Starting from the flux definition (9.73) we can substitute the path with the original definition of the integral and then

making a change of variable from conserved to primitive ending up with

$$\mathbf{F}^{\pm}_{i+\frac{1}{2}} = \frac{1}{2}\left(\mathbf{F}_L + \mathbf{F}_R\right) - \frac{1}{2}\int_{\mathbf{W}_L}^{\mathbf{W}_R} \left|\mathcal{A}_W\right| \frac{\partial \mathbf{U}}{\partial \mathbf{W}}\,\mathrm{d}\mathbf{W} - \left(\pm\frac{1}{2}\int_{\mathbf{W}_L}^{\mathbf{W}_R} \mathbf{H}\mathbf{J}_U^{-1}\frac{\partial \mathbf{U}}{\partial \mathbf{W}}\,\mathrm{d}\mathbf{W}\right) \quad (9.74)$$

and, remembering the definition of $\mathbf{J}_U$, we obtain

$$\mathbf{F}^{\pm}_{i+\frac{1}{2}} = \frac{1}{2}\left(\mathbf{F}_L + \mathbf{F}_R\right) - \frac{1}{2}\int_{\mathbf{W}_L}^{\mathbf{W}_R} \left|\mathcal{A}_W\right| \mathbf{J}_U\,\mathrm{d}\mathbf{W} - \left(\pm\frac{1}{2}\int_{\mathbf{W}_L}^{\mathbf{W}_R} \mathbf{H}\,\mathrm{d}\mathbf{W}\right) \quad (9.75)$$

At this point it is possible to re-introduce the path integral in phase-space but, this time, written using the primitive variable. In this way a new Universal Osher solver with Primitive variable (UOP) is obtained

$$\mathbf{F}^{\pm}_{i+\frac{1}{2}} = \frac{1}{2}\left(\mathbf{F}_L + \mathbf{F}_R\right) - \frac{1}{2}\int_0^1 \left|\mathcal{A}_W\left(\mathbf{\Psi}_P\left(s\right)\right)\right| \mathbf{B}\left(\mathbf{\Psi}_P\left(s\right)\right)\frac{\partial \mathbf{\Psi}_P}{\partial s}\,\mathrm{d}s - \left(\pm\frac{1}{2}\int_0^1 \mathbf{H}\left(\mathbf{\Psi}_P\left(s\right)\right)\frac{\partial \mathbf{\Psi}_P}{\partial s}\,\mathrm{d}s\right) \quad (9.76)$$

where $\mathbf{\Psi}_P\left(s;\mathbf{W}_L,\mathbf{W}_R\right)$ is the path in primitive variable connecting the left values $\mathbf{W}_L$ and the right ones $\mathbf{W}_R$. The the first term of the UOP is the central part of the fluxes, the first integral represents the so called numerical viscosity that derives from the conservative and non-conservative fluxes, while the second integral is strictly connected with the non-conservative fluxes.

To understand better the meaning of the last integral in the UOP solver, we need to refer to the theory developed by Dal Maso *et al.* [20] about the non-conservative product. Following them, the weak solution of (9.71) across a discontinuity must satisfy

$$\int_0^1 \left(-S_S\mathbf{J}_U\left(\mathbf{\Psi}_P\left(s\right)\right) + \mathbf{J}_F\left(\mathbf{\Psi}_P\left(s\right)\right) + \mathbf{H}\left(\mathbf{\Psi}_P\left(s\right)\right)\right)\frac{\partial \mathbf{\Psi}_P\left(s\right)}{\partial s}\,\mathrm{d}s = 0 \quad (9.77)$$

where S_S is the speed of the travelling discontinuity. After some manipulation and remembering the definition of $\mathbf{J}_F$ and $\mathbf{J}_B$ we end up with

$$S_S\left(\mathbf{U}_R - \mathbf{U}_L\right) = \mathbf{F}_R - \mathbf{F}_L + \int_0^1 \mathbf{H}\left(\mathbf{\Psi}_P\left(s\right)\right)\frac{\partial \mathbf{\Psi}_P}{\partial s}\,\mathrm{d}s \quad (9.78)$$

Comparing this equation with the GRH condition (5.21) that reads

$$S_S\left(\mathbf{U}_R - \mathbf{U}_L\right) = \mathbf{F}_R - \mathbf{F}_L - \mathbf{D}$$

we notice that, from a physical point of view, the integral of the non-conservative term is nothing more than the pressure exerted by the bed step on fluid

$$\int_0^1 \mathbf{H}\left(\mathbf{\Psi}_P\left(s\right)\right) \frac{\partial \mathbf{\Psi}_P}{\partial s}\, \mathrm{d}s = -\mathbf{D} \tag{9.79}$$

With this equation, the choice of the path $\mathbf{\Psi}_P$ is no more arbitrary, but it is strictly related to the value of $\mathbf{D}$. Cozzolino *et al.* [19] derive a path satisfying this relation, but its expression is quite complicated to be used since is composed by a discontinuous function. However we can overcame the problem simply using directly the expression of $\mathbf{D}$ in the UOP solver (9.76) obtaining

$$\mathbf{F}^{\pm}_{i+\frac{1}{2}} = \frac{1}{2}\left(\mathbf{F}_L + \mathbf{F}_R\right) - \frac{1}{2}\int_0^1 \left|\mathcal{A}_W\left(\mathbf{\Psi}_P\left(s\right)\right)\right| \mathbf{B}\left(\mathbf{\Psi}_P\left(s\right)\right) \frac{\partial \mathbf{\Psi}_P}{\partial s}\, \mathrm{d}s \pm \frac{1}{2}\mathbf{D} \tag{9.80}$$

At this point, no constrains exist for the path integral of the numerical viscosity, so we can maintain the universality of the solver, as the UO, using the segment linear path

$$\mathbf{\Psi}_P\left(\mathbf{W}_L, \mathbf{W}_R; s\right) = \mathbf{W}_L + s\left(\mathbf{W}_R - \mathbf{W}_L\right) \tag{9.81}$$

In this way the final version of the UOP is

$$\mathbf{F}^{\pm}_{i+\frac{1}{2}} = \frac{1}{2}\left(\mathbf{F}_L + \mathbf{F}_R\right) - \frac{1}{2}\left(\int_0^1 \left|\mathcal{A}_W\left(\mathbf{\Psi}_P\left(s\right)\right)\right| \mathbf{B}\left(\mathbf{\Psi}_P\left(s\right)\right)\, \mathrm{d}s\right)\left(\mathbf{W}_R - \mathbf{W}_L\right) \pm \frac{1}{2}\mathbf{D} \tag{9.82}$$

The last difficult in this approach is the evaluation the integral. Since a closed form is not always available, it is possible to use some numerical method (e.g. trapezoidal rules, midpoint rules, ...) among which a good accuracy is obtained using the Gauss-Legendre (GL) quadrature rule with

three points (as demonstrate by Dumbser and Toro [23, 24]). Using the three point GL rule in the UOP solver (9.82) we obtain

$$\mathbf{F}^{\pm}_{i+\frac{1}{2}} = \frac{1}{2}\left(\mathbf{F}_L + \mathbf{F}_R\right) - \frac{1}{2}\sum_{i=1}^{3}\left(\omega_i \left|\mathcal{A}_W\left(\mathbf{\Psi}_P\left(s_i\right)\right)\right| \mathbf{B}\left(\mathbf{\Psi}_P\left(s_i\right)\right)\right)\left(\mathbf{W}_R - \mathbf{W}_L\right) \pm \frac{1}{2}\mathbf{D} \tag{9.83}$$

where s_i is the position and ω_i is the weight and for the three point integration, in the domain $[0;1]$, are

$$s_{1,3} = \frac{1}{2} \pm \frac{\sqrt{15}}{10},\ s_2 = \frac{1}{2} \qquad \omega_{1,3} = \frac{5}{18},\ \omega_2 = \frac{8}{18} \tag{9.84}$$

9.4 Comparison between the three numerical Riemann solver

In this Section we present a brief comparison between the three different Riemann solvers introduced and developed in this Chapter. We compare essentially three aspects: the mathematical and numerical implementation, the computational cost and the accuracy of the solution.

The LHLL Riemann solver, as specified in Section 9.1, is composed essentially by equation (9.5) where the required terms are the conserved fluxes $\mathbf{F}$, the conserved variables $\mathbf{U}$ and the maximum and minimum eigenvalues $\lambda_{\text{max,min}}$. Since the evaluation of all these variables are quite simple (the only difficult could arise in the determination of the eigenvalues), we can state that the implementation cost is very low. Also the computational cost is very low since equation (9.5) is composed only by simple numerical operation (i.e. algebraic sums and multiplications).
For the Closure Independent GR (CIGR) solver, on the contrary, the mathematical and numerical implementation is quite costly since we need to obtain the Roe constant matrix $\mathcal{A}\left(\dddot{\mathbf{M}}\right)$. As specified in Section 9.2, the development of the EMAs approach allow to obtain this matrix in a easier way than the

Case	Side	α	h $[m]$	u $[m/s]$	z_b $[m]$	φ $[-]$
Fixed-mobile	L	0	1.0	1.0	0.0	0.01
	R	1	1.2	2.0	0.0	0.0
Mobile-Fixed	L	1	1.0	1.0	0.0	0.0
	R	0	1.2	2.0	0.0	0.0

Table 9.1: Initial values used for the fixed to mobile bed transition, and mobile to fixed bed transition RPs test case.

MAs, however some mathematical efforts are needed. Regarding the computational cost, it is bigger than the LHLL, since the complete set of eigenvalues and associated eigenvectors of matrix $\mathcal{A}\left(\ddot{\mathbf{M}}\right)$ has to be determined for each cell of the computational domain.
The implementation of the UOP solver is more complicated than the LHLL one since it is necessary the evaluation of the eigenvalues and associated eigenvectors of the PDEs system. However, it is easier than the CIGR since the matrix $\mathcal{A}_W$ derives directly, as specified in Section 9.3, from the linearization of the system. Nevertheless, from a computational point of view, the UOP is the most expensive, since as written in equation (9.83), is necessary to evaluate the $|\mathcal{A}_W| = \mathcal{R}_W |\mathbf{\Lambda}| \mathcal{R}_W^{-1}$ three times (one for each point of the GL) for each cell of the computational domain. Compared to the CIGR solver, the cost of the UOP is two time more.

For the evaluation of the accuracy of the solution, we show two different numerical simulation of RP: one for the transition from fixed to mobile bed case and one for the transition from mobile to fixed bed. The initial data for the different simulation is reported in Table 9.1. As closure relation for the concentration we use equation (5.32) with $\beta = 0.5$. The common parameters of the simulations are $c_b = 0.6$, $\Delta = 1.65$, spatial discretization $\Delta x = 0.005\, m$ and simulation time $t = 1\ s$ and Courant number $CFL = 0.9$.

In Figure (9.2) is shown the transition from fixed to mobile bed case. The solutions obtained from the three numerical Riemann solvers are in good agreement with the analytical one. Nevertheless, looking more in detail the bed elevation near the transition (the right subfigure), some differences between the three numerical solvers arise. In particular the LHLL solver

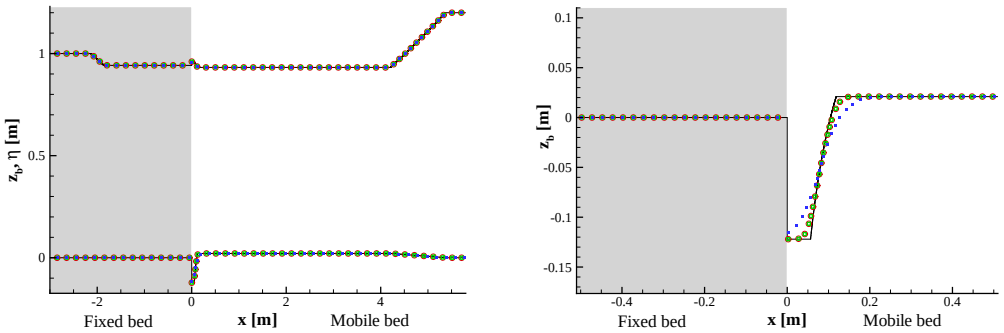

Figure 9.2: Comparison between analytical (solid line) and numerical solutions obtained with LHLL (blue dots), CIGR (red dots) and UOP (green dots) numerical solvers for the transition between fixed and mobile bed case. On the left subfigure: free surface η and bed elevation z_b; on the right: details of the bottom elevation near the interface.

is quite diffusive in the mobile bed part, while the UOP and the CIGR solvers reproduce exactly the analytical solution. We highlight that for all the Riemann solvers, no spurious erosions or depositions occur in the fixed-bed side.

In Figure (9.3) is shown the transition from mobile to fixed bed case. As for the previous case, the solutions obtained from the three numerical Riemann solvers are in good agreement with the analytical one. Looking more in detail the bed elevation near the transition (the right subfigure), we highlight that the LHLL solver is quite diffusive in the mobile bed part, the UOP solver present, in the first cell of the mobile-bed side, a small spike that anyhow, does not affect the overall goodness of the method, while the CIGR reproduces in a correct way the analitical solution. We emphasize that also for this case, all the Riemann solvers produce no spurious erosions or depositions in the fixed-bed side.

From these comparisons, we can state that, looking at the accuracy of the solution the best numerical RP solver is the CIGR, followed by the UOP, while the worst is the LHLL due to its high numerical diffusion.

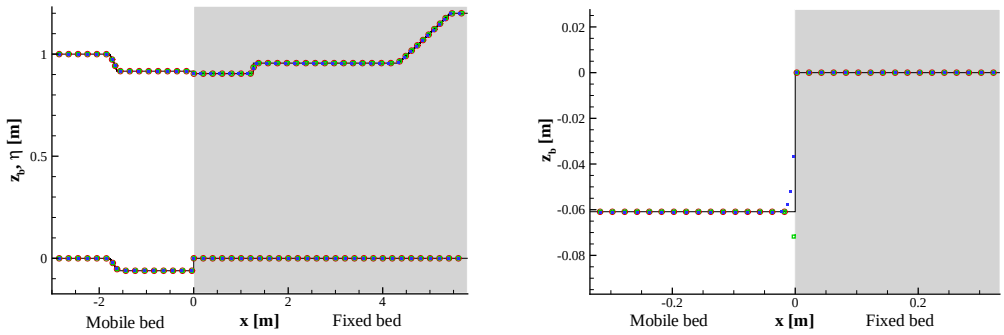

Figure 9.3: Comparison between analytical (solid line) and numerical solutions obtained with LHLL (blue dots), CIGR (red dots) and UOP (green dots) numerical solvers for the transition between mobile and fixed bed case. On the left subfigure: free surface η and bed elevation z_b; on the right: detail of the bottom elevation near the interface.

Chapter 10

Numerical applications of the CRP

In this Chapter, we present in Section 10.1 a set of Riemann problems describing the transition between fixed and mobile bed for all the three CPDEs systems developed (i.e. the low sediment concentration model in Section 10.1.1, high sediment concentration model in Section 10.1.2 and the plane-wave model in Section 10.1.3). In Section 10.2 a realistic application for the transition between fixed an mobile bed are presented.

In all the numerical applications presented, the following closure relation for the concentration has been considered

$$c(u,h) = \beta \frac{u^2}{gh} \tag{10.1}$$

where β is a semi-empirical non-dimensional constant, depending on sediment characteristics, and $g = 9.81\ m/s^2$. More details on this closure relation are written in Chapter 5.

The numerical scheme implemented is second-order accuracy achieved with a MUSCL-type method. A second order version of the update formula shown in equation (9.2) can be straightforwardly obtained following Armanini *et al.* [10], where a minmod slope limiter is used to reconstruct the variables in the nonconservative half step. As numerical Riemann solver we choose to use the CIGR since, as highlighted in Section 9.4, it produces, compared

with the UOP and the LHLL, the more accurate solution at the interface between fixed and mobile bed.

10.1 Riemann problems

In this Section we present some numerical tests aimed at validating the capability of the CIGR scheme to solve correctly and accurately any CRP. In particular, we will compare numerical solutions with exact solutions obtained by solving an inverse problem [25, 54]. This procedure is based on the fact that knowing the left state of a wave it is possible to obtain the right state by using the relevant wave relation. Therefore, given a left initial state and assumed a wave pattern, moving through the wave sequence, it is possible to reconstruct the right initial state.

10.1.1 CPDEs model for low sediment concentration

First of all we present two tests regarding a pure fixed-bed and mobile-bed case, in order to show that the scheme is able to solve standard RPs. Then, to demonstrate the capabilities in fixed–mobile cases, we present four tests, each one belonging to a different class introduced in Section 7.4. The last case analyzes the behavior of the scheme in case of resonant problems. In all the simulation we used $c_b = 0.6$, a Courant number equal to 0.9, the space was discretized with cells of width $\Delta x = 0.001\ m$ and the ending time is $t = 1\ s$. In addition, the free-surface elevation $\eta = h + z_b$ is shown in the plots instead of the flow depth h. The test cases presented in this Section were achieved using a first order scheme, with the exception of the resonant cases where the second order schema, as specified before, were used.

Pure fixed-bed and mobile-bed cases

The initial conditions used for these two test cases are shown in Table 10.1, while the value of the transport parameter is $\beta = 0.5$.

Comparison between analytical and numerical solutions is shown in Figure 10.1: the numerical scheme correctly reproduces the wave pattern, with

Type	Side	α	$h\ [m]$	$u\ [m/s]$	$z_b\ [m]$	$\varphi\ [-]$
Fixed	L	0	5.0	0.0	0.0	0.01
Fixed	R	0	1.86	0.80	0.0	0.01
Mobile	L	1	5.0	0.0	0.0	0.01
Mobile	R	1	2.90	0.59	0.36	0.017

Table 10.1: Initial values used for the pure fixed-bed and the pure mobile-bed RP test case.

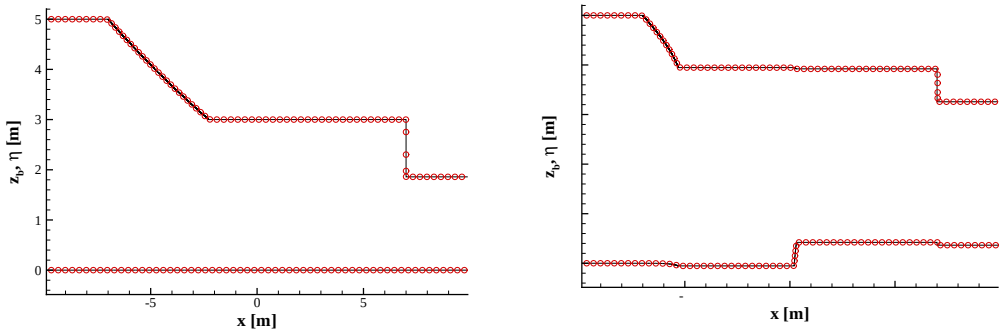

Figure 10.1: Comparison between analytical (solid line) and numerical (circles) solutions of the free surface η and the bed level z_b for the pure fixed-bed (on the left) and the pure mobile-bed (on the right) RP test case.

the same accuracy that can be obtained by using the CIGR approach applied to the pure fixed-bed and mobile-bed PDEs systems. In other words, the numerical solution of a CRP converges correctly to the exact solution of a standard RP if the erodibility function is constant.

FBsub-MB test case

This test case belongs to the class characterized by a transition from fixed-to mobile-bed conditions with a subcritical nature of the flow near the left side of the origin. The relevant wave pattern is described in case (A) of Figure 7.2. The initial conditions are: $h_L = 3.0\ m$, $h_R = 1.356\ m$, $u_L = 1.0\ m/s$, $u_R = 0.617\ m/s$, $z_{bL} = 0.0\ m$, $z_{bR} = -0.114\ m$, $\varphi_L = 0.01$, $\varphi_R = 0.0$, $\beta = 0.05$. The comparison between numerical and analytical solution is

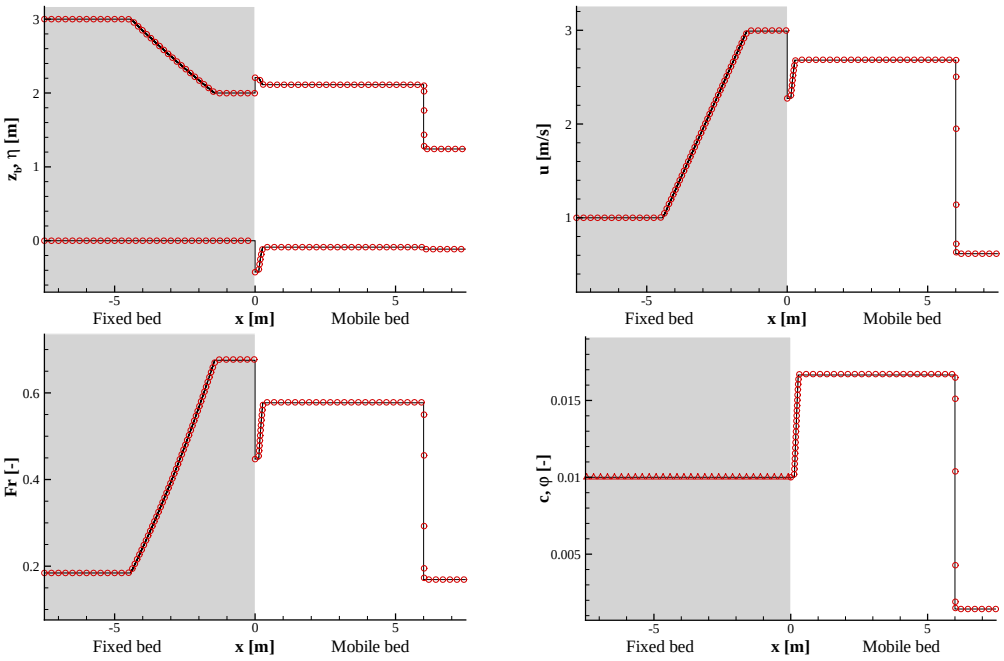

Figure 10.2: Comparison between analytical (solid line) and numerical (circles) solutions of the FBsub-MB test case. Clockwise from upper left subfigure: free surface η and bed level z_b, velocity u, Froude number $u/\sqrt{gh}$, equilibrium and transported concentrations φ, c.

presented in Figure 10.2. All the waves are correctly reproduced with the expected high accuracy. In particular, the shift between the transported and the equilibrium concentration is exact ($\varphi = c$, see Chapter 7) as well as the bed step, where no spurious erosions or depositions occur in the fixed-bed side (see Figure 10.3).

FBsup-MB test case

This second test belongs to the class characterized by a transition from fixed- to mobile-bed conditions, with a supercritical nature of the flow near the left side of the origin. The relevant wave pattern is described in case (B) of Figure 7.2. The initial conditions are:$h_L = 1.0\ m$, $h_R = 0.452\ m$, $u_L = 4.0\ m/s$, $u_R = 2.321\ m/s$, $z_{bL} = 0.0\ m$, $z_{bR} = 0.098\ m$, $\varphi_L = 0.01$, $\varphi R = 0.0$, $\beta = 0.01$. The comparison between numerical and analytical solution is

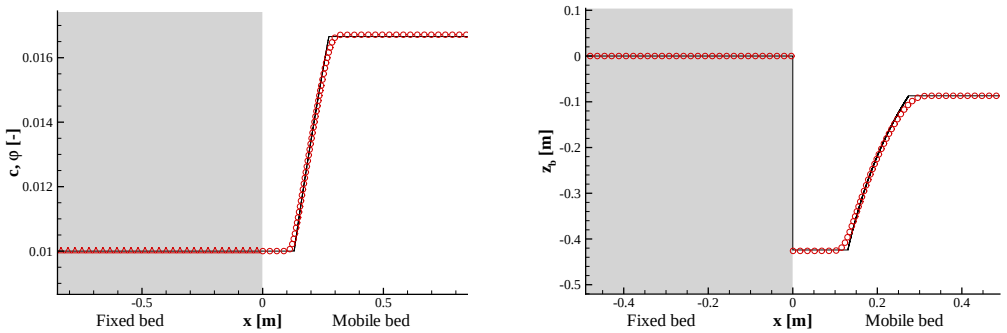

Figure 10.3: Details of the behavior of the concentration (on the left) and of the bottom elevation (on the right) near the interface between fixed and mobile bed for the FBsub-MB test case.

presented in Figure 10.4. As expected, on the left there is no wave, while on the mobile part there is a rarefaction followed by a shock. Also in this case, the agreement with the analytic solution is very good.

MB-FBsub test case

The third test belongs to the class characterized by a transition from mobile- to fixed-bed conditions, with a subcritical nature of the flow near the right side of the origin. The relevant wave pattern is described in case (C) of Figure 7.2. The initial conditions are: $h_L = 3.0\ m$, $h_R = 1.087\ m$, $u_L = 1.0\ m/s$, $u_R = 0.806\ m/s$, $z_{bL} = 0.0\ m$, $z_{bR} = 0.1\ m$, $\varphi_L = 0.0$, $\varphi_R = 0.02$, $\beta = 0.01$. The comparison between numerical and analytical solution is presented in Figure.10.5, where the agreement is similar to the previous cases.

MB-FBsup test case

The last test belongs to the class characterized by a transition from mobile-to fixed-bed conditions, with a supercritical nature of the flow near the right side of the origin. The relevant wave pattern is described in case (D) of Figure 7.2. The initial conditions are: $h_L = 1.0\ m$, $h_R = 1.2\ m$, $u_L = 4.0\ m/s$, $u_R = 5.242\ m/s$, $z_{bL} = 0.0\ m$, $z_{bR} = 0.0\ m$, $\varphi_L = 0.0$, $\varphi_R = 0.019$, $\beta = 0.01$. Since in this class there are infinite solutions relevant to a given couple of left

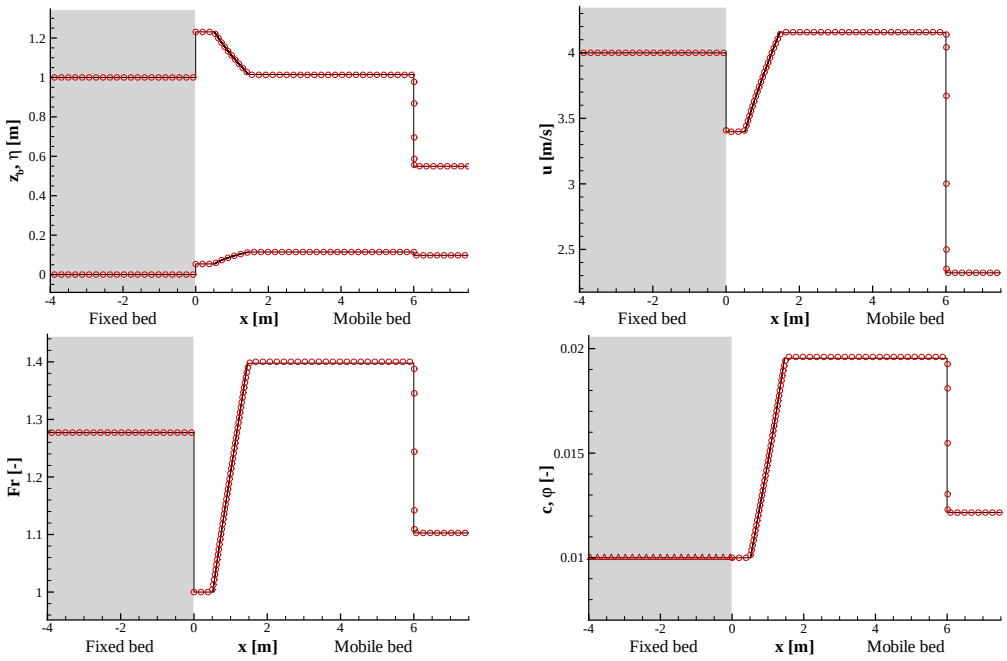

Figure 10.4: Comparison between analytical (solid line) and numerical (circles) solutions of the FBsup-MB test case. Clockwise from upper left subfigure: free surface η and bed level z_b, velocity u, Froude number $u/\sqrt{gh}$, equilibrium and transported concentrations φ, c.

and right initial values, this time the comparison was performed between the numerical solution and the analytical solution consistent with the numerical results. In other words, Figure 10.6 asserts that the numerical solution is a good approximation of one of the possible solutions to the CRP. The reason why the numerical scheme chooses a specific solution is an open question. However, Figure 10.7 indicates the absence of spurious erosions or depositions in the fixed-bed side.

Resonant test cases

As explained in Section 7.4, resonance occurs if a rarefaction on the fixed-bed side has a sonic point. The problem is extremely interesting from a pure mathematical point of view, but it has less meaning for practical purposes since it is characterized by extreme conditions.

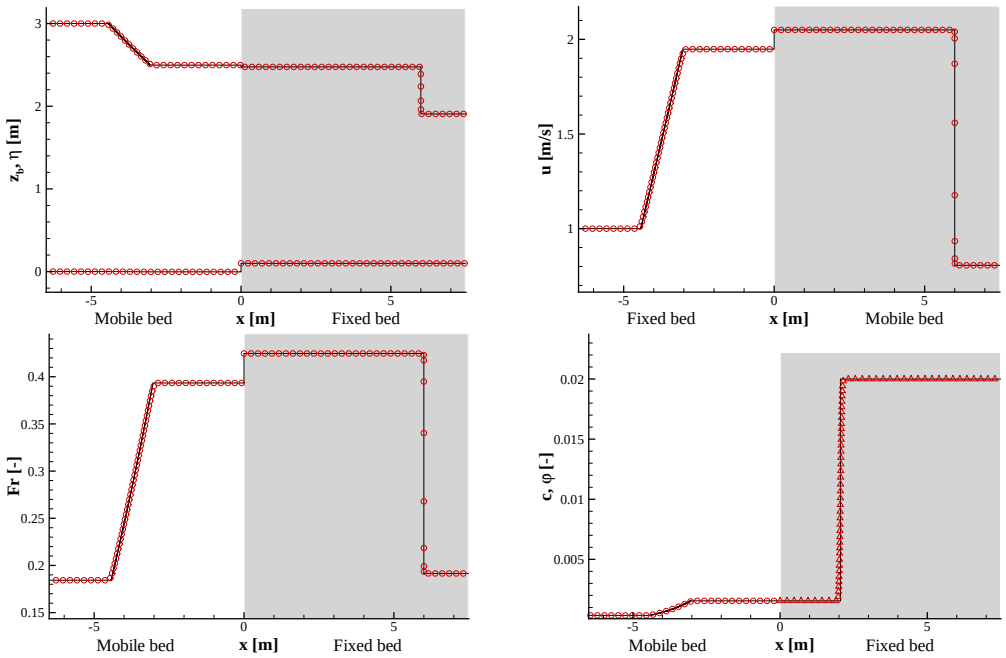

Figure 10.5: Comparison between analytical (solid line) and numerical (circles) solutions of the MB-FBsub test case. Clockwise from upper left subfigure: free surface η and bed level z_b, velocity u, Froude number $u/\sqrt{gh}$, equilibrium and transported concentrations φ, c.

The performance of the first and second order scheme in case of resonance has been analyzed considering both a mobile-fixed and a fixed-mobile transition. Figure 10.8 shows the first case. The initial conditions are: $h_L = 5.0\ m$, $h_R = 0.1\ m$, $u_L = 0.0\ m/s$, $u_R = 1.86\ m/s$, $z_{bL} = 0.0\ m$, $z_{bR} = 0.0\ m$, $\varphi_L = 0.00$, $\varphi_R = 6.74 \times 10^{-3}$, $\beta = 0.01$. In this case, resonance appears on the right side, where a sonic rarefaction characterizes the solution on the fixed-bed side. It can be noted that the second order scheme reproduces correctly the analytical solution, while, as expected, the first order is affected by the classical entropy glitch.

Figure 10.9 shows the second case. The initial conditions are: $h_L = 3.0\ m$, $h_R = 2.0\ m$, $u_L = 0.0\ m/s$, $u_R = 7.13\ m/s$, $z_{bL} = 0.0\ m$, $z_{bR} = 0.12\ m$, $\varphi_L = 0.01$, $\varphi R = 0.0$, $\beta = 0.01$. Here, the deviation of the numerical results with respect to the exact solution is more significant. In particular, in the first order solution, the glitch in the central wave actually affects the left

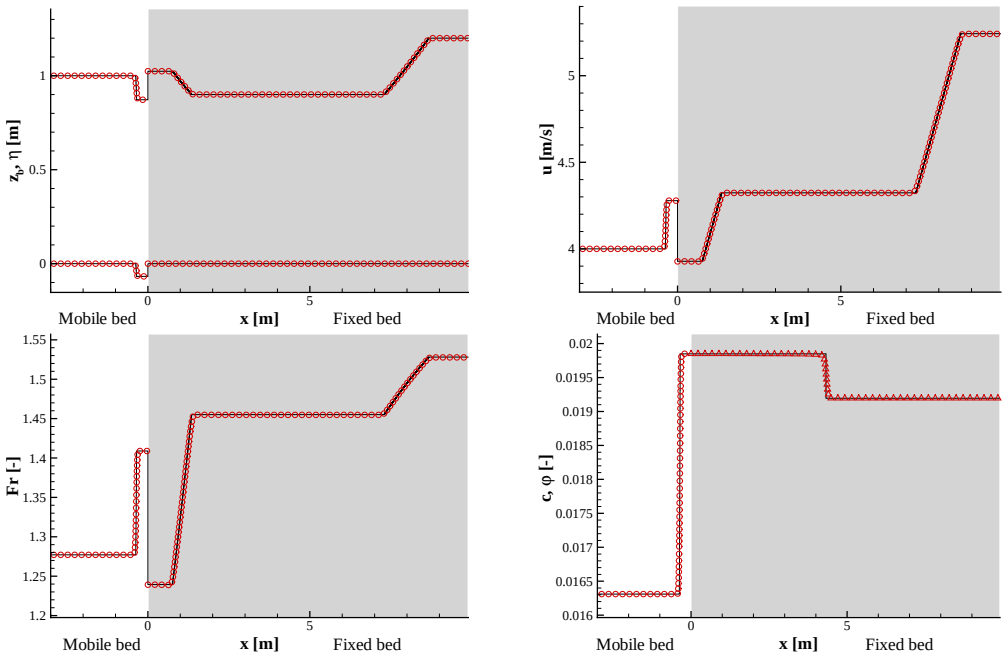

Figure 10.6: Comparison between analytical (solid line) and numerical (circles) solutions of the MB-FBsup test case. Clockwise from upper left subfigure: free surface η and bed level z_b, velocity u, Froude number $u/\sqrt{gh}$, equilibrium and transported concentrations φ, c.

rarefaction and both the right waves as well. Moreover, there is a significant spike in the first cell of the mobile-bed side. On the contrary, the second order approach has a good behavior, except in the first cell of the mobile-bed side where a spike, by far smaller than in the first order case, is present. Anyhow, the other waves are not affected by this local error.

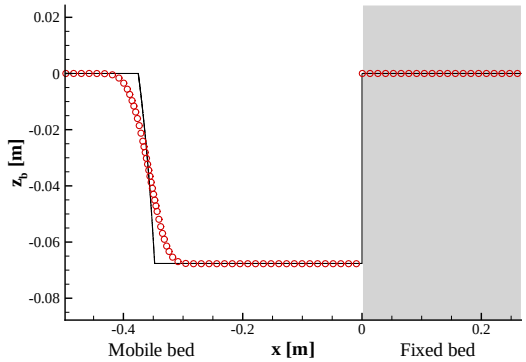

Figure 10.7: Details of the bottom elevation near the interface between fixed and mobile bed for the MB-FBsup test case.

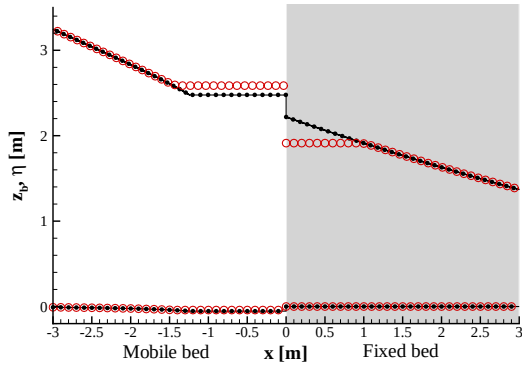

Figure 10.8: Comparison of the exact solution (solid line) with the first order solution (red circles) and the second order one (black dots) for a resonant case relevant to a mobile-fixed transition.

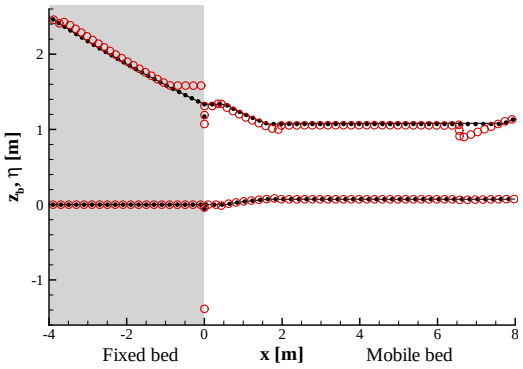

Figure 10.9: Comparison of the exact solution (solid line) with the first order solution (circles) and the second order one (dots) for a resonant case relevant to a fixed-mobile transition.

10.1.2 CPDEs model for high sediment concentration

In this Sections we present the CRP problems related the one-dimensional high sediment concentration CPDEs obtained in Section 8.1. Here, four CRP tests, each one belonging to a different class introduced in Section 7.4 are shown. In all the simulation we used $c_b = 0.6$, $\Delta = 1.65$, a Courant number equal to 0.9, the space was discretized with cells of width $\Delta x = 0.005\ m$ and the ending time is $t = 1\ s$. In addition, the free-surface elevation $\eta = h + z_b$ is shown in the plots instead of the flow depth h.

FBsub-MB test case

This test case belongs to the class characterized by a transition from fixed-to mobile-bed conditions with a subcritical nature of the flow near the left side of the origin. The relevant wave pattern is described in case (A) of Figure 7.2. The initial conditions are: $h_L = 3.5\ m$, $h_R = 2.453\ m$, $u_L = 1.0\ m/s$, $u_R = 3.374\ m/s$, $z_{bL} = 0.0\ m$, $z_{bR} = 0.547\ m$, $\varphi_L = 0.2$, $\varphi_R = 0.0$, $\beta = 1.0$. The comparison between numerical and analytical solution is presented in Figure 10.10. All the waves are correctly reproduced with the expected high accuracy. In particular, the shift between the transported and the equilibrium concentration is exact ($\varphi = c$) as well as the bed step, where no spurious erosions or depositions occur in the fixed-bed side (see Figure 10.11).

FBsup-MB test case

This second test belongs to the class characterized by a transition from fixed-to mobile-bed conditions, with a supercritical nature of the flow near the left side of the origin. The relevant wave pattern is described in case (B) of Figure 7.2. The initial conditions are:$h_L = 1.0\ m$, $h_R = 0.166\ m$, $u_L = 4.0\ m/s$, $u_R = 0.807\ m/s$, $z_{bL} = 0.0\ m$, $z_{bR} = 0.178\ m$, $\varphi_L = 0.1$, $\varphi_R = 0.0$, $\beta = 0.1$. The comparison between numerical and analytical solution is presented in Figure 10.12. As expected, on the left there is no wave, while on the mobile part there is a rarefaction followed by a shock. Also in this case, the agreement with the analytic solution is good.

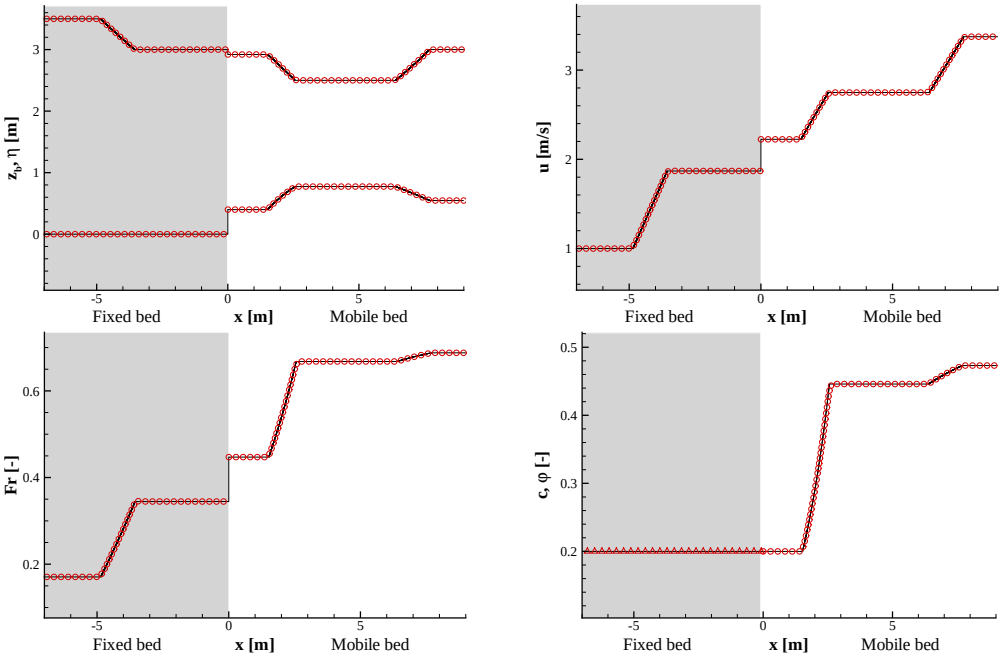

Figure 10.10: Comparison between analytical (solid line) and numerical (circles) solutions of the FBsub-MB test case. Clockwise from upper left subfigure: free surface η and bed level z_b, velocity u, Froude number $u/\sqrt{gh}$, equilibrium and transported concentrations φ, c.

MB-FBsub test case

The third test belongs to the class characterized by a transition from mobile- to fixed-bed conditions, with a subcritical nature of the flow near the right side of the origin. The relevant wave pattern is described in case (C) of Figure 7.2. The initial conditions are: $h_L = 3.0\ m$, $h_R = 2.3\ m$, $u_L = 1.0\ m/s$, $u_R = 3.6\ m/s$, $z_{bL} = 0.0\ m$, $z_{bR} = 0.0\ m$, $\varphi_L = 0.0$, $\varphi_R = 0.167$, $\beta = 0.5$. The comparison between numerical and analytical solution is presented in Figure.10.13, where the agreement is similar to the previous cases. Figure 10.14 indicates the absence of spurious erosions or depositions in the fixed-bed side.

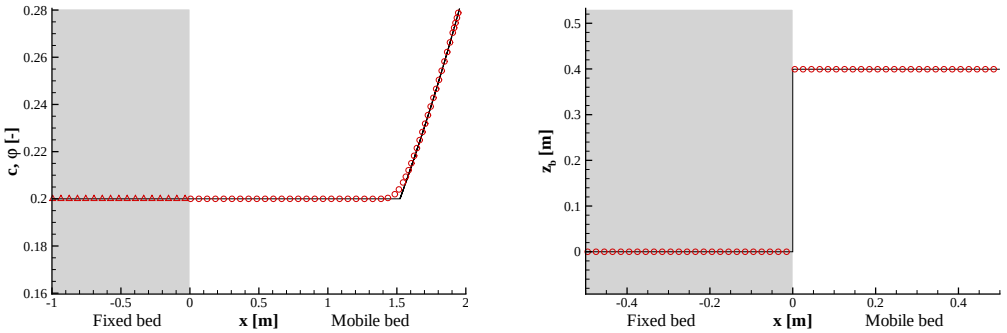

Figure 10.11: Details of the behavior of the concentration (on the left) and of the bottom elevation (on the right) near the interface between fixed and mobile bed for the FBsub-MB test case.

MB-FBsup test case

The last test belongs to the class characterized by a transition from mobile-to fixed-bed conditions, with a supercritical nature of the flow near the right side of the origin. The relevant wave pattern is described in case (D) of Figure 7.2. The initial conditions are: $h_L = 1.0\ m$, $h_R = 1.2\ m$, $u_L = 4.0\ m/s$, $u_R = 5.242\ m/s$, $z_{bL} = 0.0\ m$, $z_{bR} = 0.0\ m$, $\varphi_L = 0.0$, $\varphi_R = 0.019$, $\beta = 0.01$. Since in this class there are infinite solutions relevant to a given couple of left and right initial values, this time the comparison was performed between the numerical solution and the analytical solution consistent with the numerical results. In other words, Figure 10.15 asserts that the numerical solution is a good approximation of one of the possible solutions to the CRP. Only a very small overshoot is present in the transported concentration φ near the contact wave in the fixed bed part.

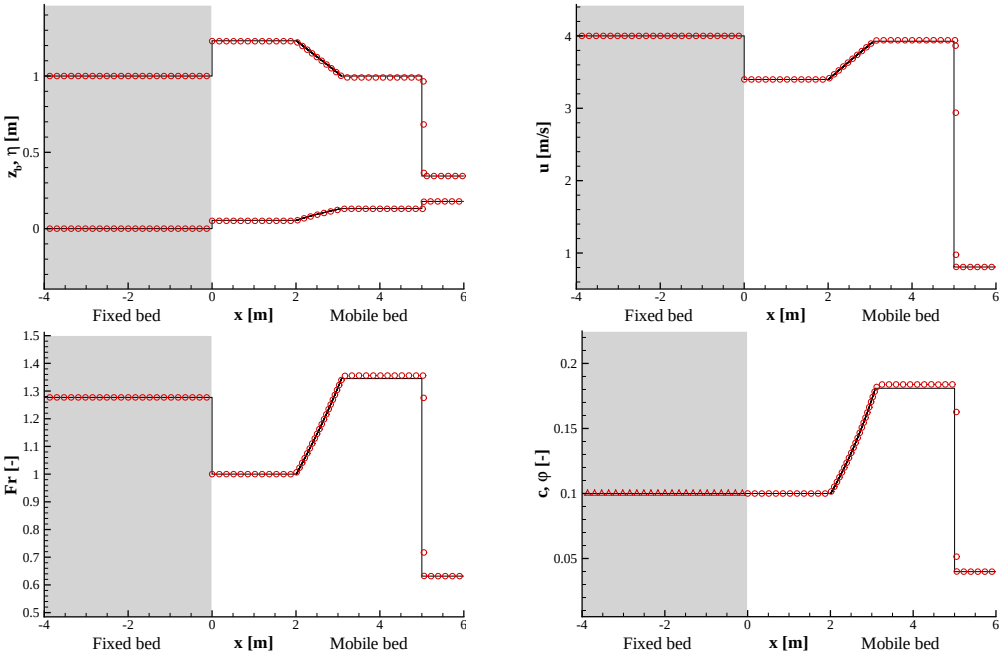

Figure 10.12: Comparison between analytical (solid line) and numerical (circles) solutions of the FBsup-MB test case. Clockwise from upper left subfigure: free surface η and bed level z_b, velocity u, Froude number $u/\sqrt{gh}$, equilibrium and transported concentrations φ, c.

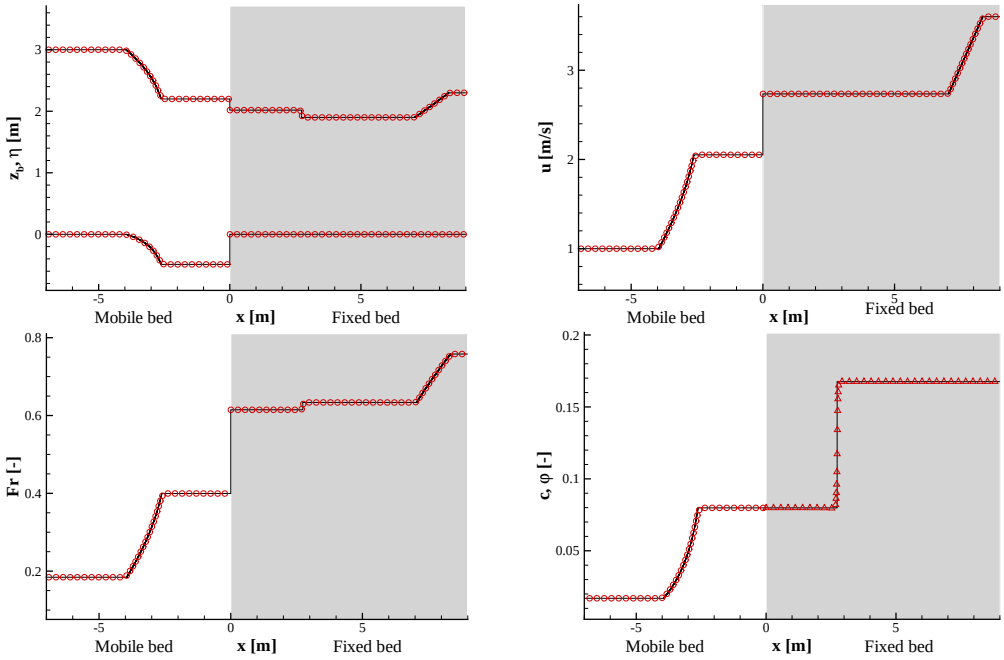

Figure 10.13: Comparison between analytical (solid line) and numerical (circles) solutions of the MB-FBsub test case. Clockwise from upper left subfigure: free surface η and bed level z_b, velocity u, Froude number $u/\sqrt{gh}$, equilibrium and transported concentrations φ, c.

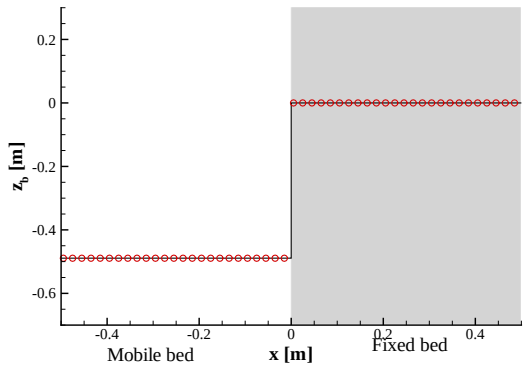

Figure 10.14: Details of the bottom elevation near the interface between fixed and mobile bed for the MB-FBsub test case.

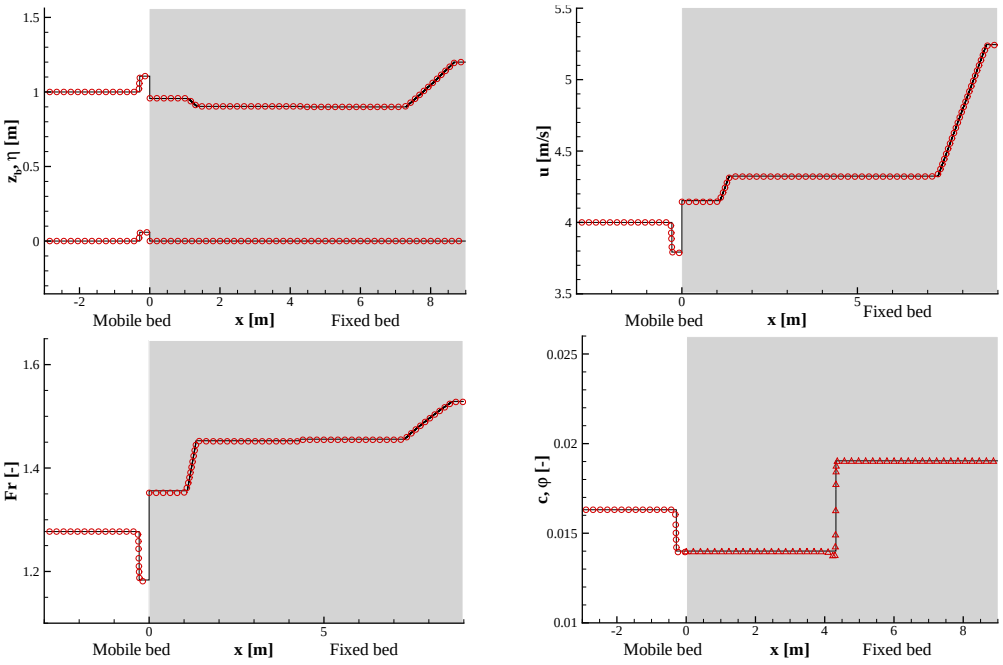

Figure 10.15: Comparison between analytical (solid line) and numerical (circles) solutions of the MB-FBsup test case. Clockwise from upper left subfigure: free surface η and bed level z_b, velocity u, Froude number $u/\sqrt{gh}$, equilibrium and transported concentrations φ, c.

10.1.3 CPDEs plane-wave model

In this Sections we present the CRP problems related the two-dimensional plane wave high sediment concentration CPDEs obtained in Section 8.2. Here, four CRP tests, each one belonging to a different class introduced in Section 7.4 are shown. In all the simulation we used $c_b = 0.65$, $\Delta = 1.65$, a Courant number equal to 0.9, the space was discretized with cells of width $\Delta x = 0.01\ m$ and the ending time is $t = 1\ s$. In addition, the free-surface elevation $\eta = h + z_b$ is shown in the plots instead of the flow depth h.

FBsub-MB test case

This test case belongs to the class characterized by a transition from fixed-to mobile-bed conditions with a subcritical nature of the flow near the left side of the origin. The relevant wave pattern is described in case (A) of Figure 8.1. The initial conditions are: $h_L = 2.0\ m$, $h_R = 0.919\ m$, $u_L = 1.0\ m/s$, $u_R = 2.173\ m/s$, $v_L = 0.5\ m/s$, $v_R = 0.87\ m/s$, $z_{bL} = 0.0\ m$, $z_{bR} = 0.682\ m$, $\varphi_L = 0.2$, $\varphi_R = 0.0$, $\beta = 0.5$. The comparison between numerical and analytical solution is presented in Figure 10.16. All the waves are correctly reproduced with the expected high accuracy. In particular, the shift between the transported and the equilibrium concentration is exact ($\varphi = c$) as well as the bed step, where no spurious erosions or depositions occur in the fixed-bed side (see Figure 10.17).

FBsup-MB test case

The second test belongs to the class characterized by a transition from fixed-to mobile-bed conditions, with a supercritical nature of the flow near the left side of the origin. The relevant wave pattern is described in case (B) of Figure 8.1. The initial conditions are:$h_L = 1.0\ m$, $h_R = 0.156\ m$, $u_L = 4.0\ m/s$, $u_R = 0.690\ m/s$, $v_L = 0.1\ m/s$, $v_R = 0.551\ m/s$, $z_{bL} = 0.0\ m$, $z_{bR} = 0.174\ m$, $\varphi_L = 0.1$, $\varphi_R = 0.0$, $\beta = 0.1$. The comparison between numerical and analytical solution is presented in Figure 10.18. As expected, on the left there is no wave, while on the mobile part there is a rarefaction followed by

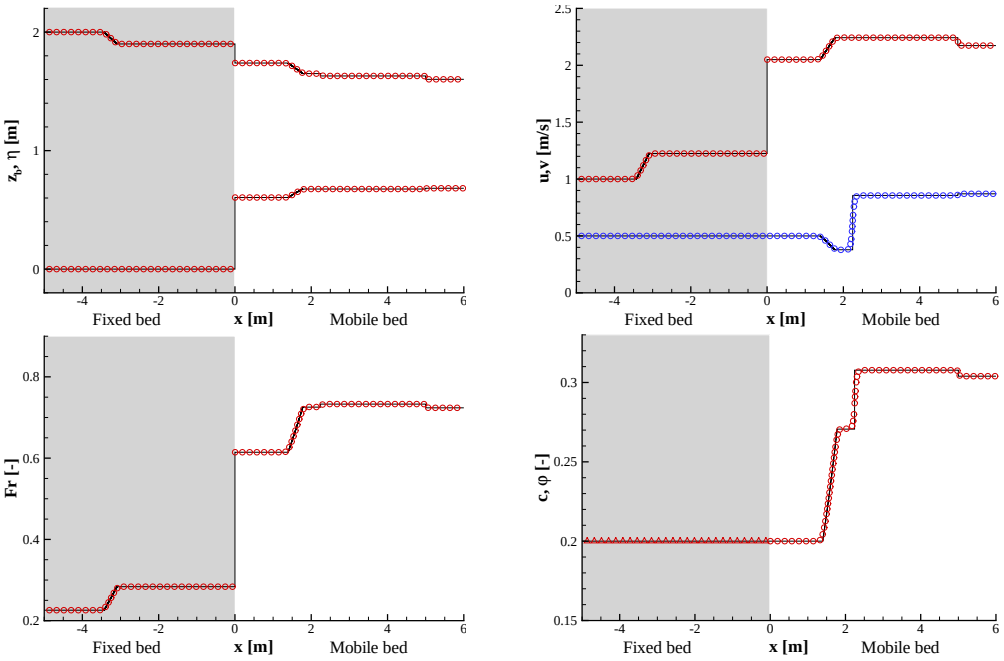

Figure 10.16: Comparison between analytical (solid line) and numerical (circles) solutions of the FBsub-MB test case. Clockwise from upper left subfigure: free surface η and bed level z_b, velocities u (red) and v (blue), Froude number $u/\sqrt{gh}$, equilibrium and transported concentrations φ, c.

the contact wave associated to v and then a shock. Also in this case, the agreement with the analytic solution is good.

MB-FBsub test case

The third test belongs to the class characterized by a transition from mobile- to fixed-bed conditions, with a subcritical nature of the flow near the right side of the origin. The relevant wave pattern is described in case (C) of Figure 8.1. The initial conditions are: $h_L = 3.0\ m$, $h_R = 1.299\ m$, $u_L = 1.0\ m/s$, $u_R = 1.411\ m/s$, $v_L = 0.1\ m/s$, $v_R = 1.0\ m/s$, $z_{bL} = 0.0\ m$, $z_{bR} = 0.0\ m$, $\varphi_L = 0.0$, $\varphi_R = 0.255$, $\beta = 0.1$. The comparison between numerical and analytical solution is presented in Figure.10.19, where the agreement is similar to the previous cases. Figure 10.20 indicates the absence of spurious erosions or depositions in the fixed-bed side.

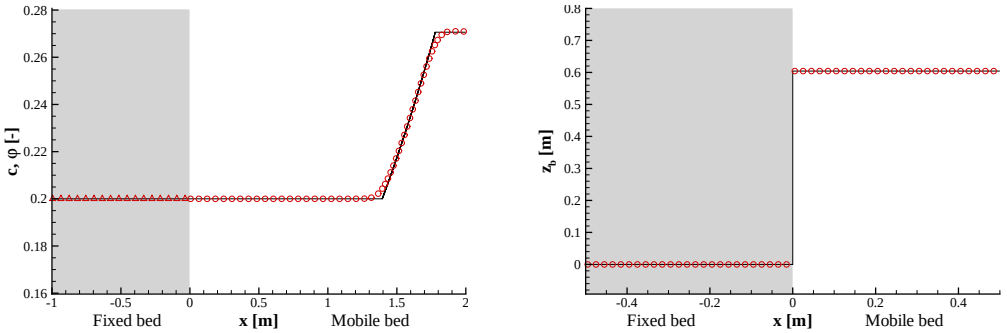

Figure 10.17: Details of the behavior of the concentration (on the left) and of the bottom elevation (on the right) near the interface between fixed and mobile bed for the FBsub-MB test case.

MB-FBsup test case

The last test belongs to the class characterized by a transition from mobile-to fixed-bed conditions, with a supercritical nature of the flow near the right side of the origin. The relevant wave pattern is described in case (D) of Figure 8.1. The initial conditions are: $h_L = 1.0\ m$, $h_R = 1.2\ m$, $u_L = 4.0\ m/s$, $u_R = 5.242\ m/s$, $v_L = 0.0\ m/s$, $v_R = 0.5\ m/s$, $z_{bL} = 0.0\ m$, $z_{bR} = 0.0\ m$, $\varphi_L = 0.0$, $\varphi_R = 0.019$, $\beta = 0.01$. Since in this class there are infinite solutions relevant to a given couple of left and right initial values, this time the comparison was performed between the numerical solution and the analytical solution consistent with the numerical results. In other words, Figure 10.21 asserts that the numerical solution is a good approximation of one of the possible solutions to the CRP. Only a small overshoot is localized in the transported concentration φ near the contact wave in the fixed bed part.

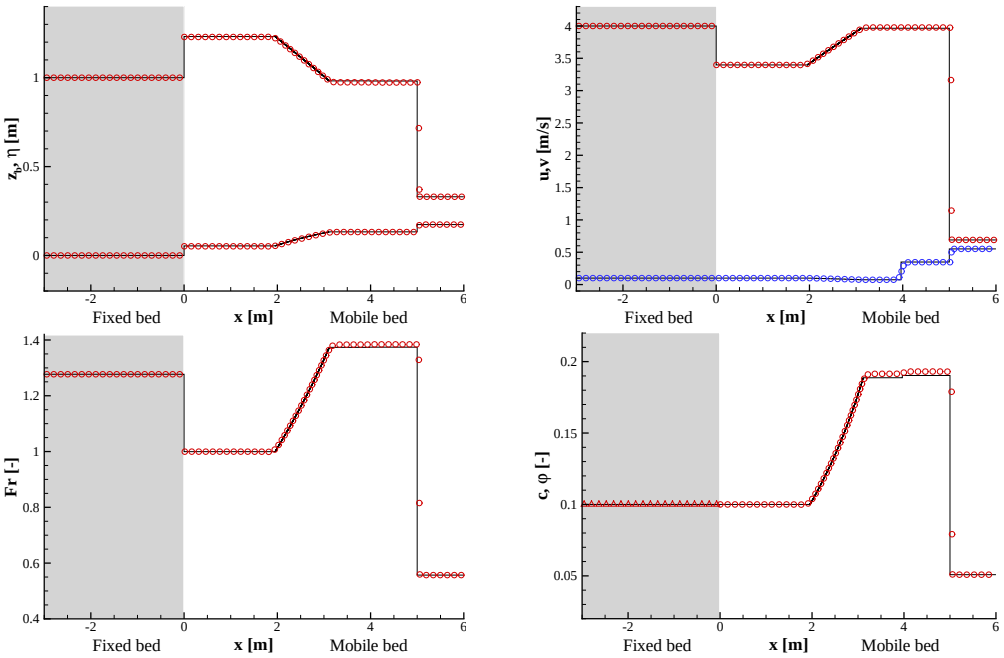

Figure 10.18: Comparison between analytical (solid line) and numerical (circles) solutions of the FBsup-MB test case. Clockwise from upper left subfigure: free surface η and bed level z_b, velocities u (red) and v (blue), Froude number $u/\sqrt{gh}$, equilibrium and transported concentrations φ, c.

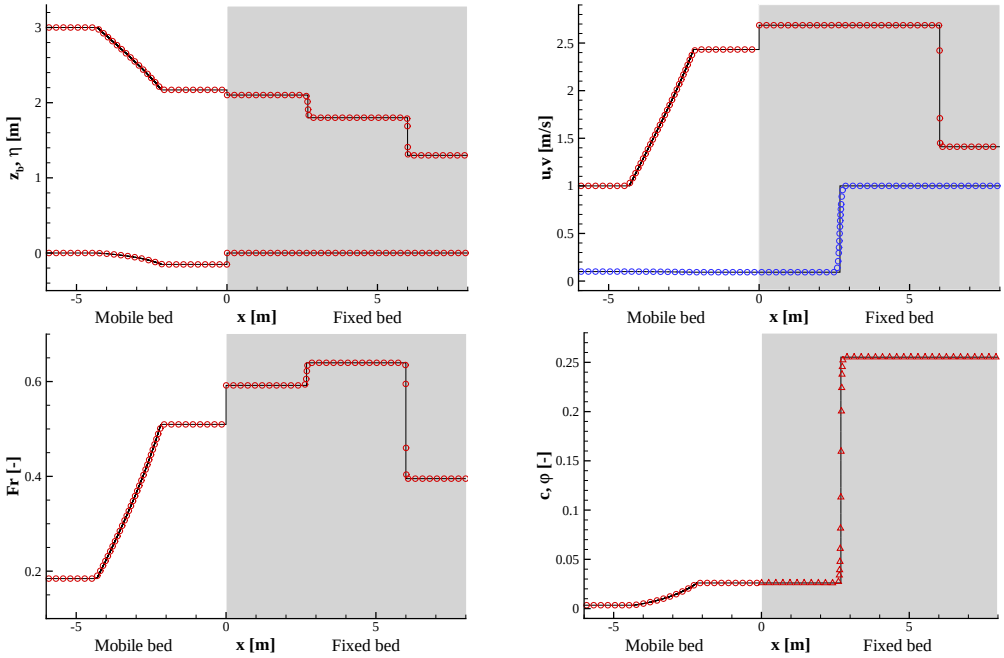

Figure 10.19: Comparison between analytical (solid line) and numerical (circles) solutions of the MB-FBsub test case. Clockwise from upper left subfigure: free surface η and bed level z_b, velocities u (red) and v (blue), Froude number $u/\sqrt{gh}$, equilibrium and transported concentrations φ, c.

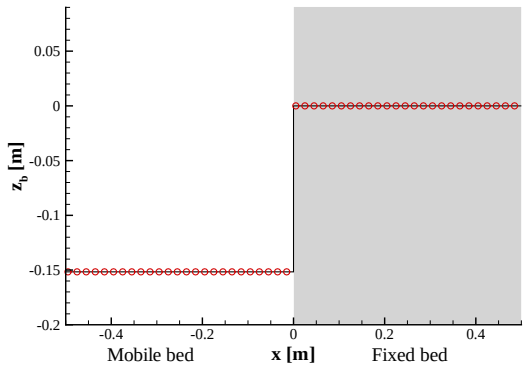

Figure 10.20: Details of the bottom elevation near the interface between fixed and mobile bed for the MB-FBsub test case.

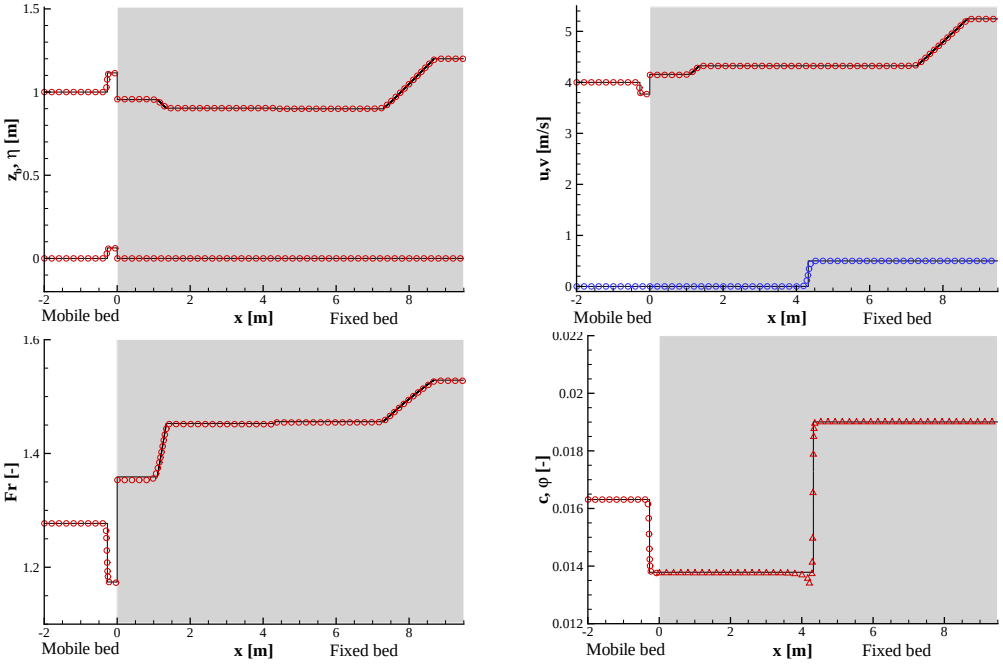

Figure 10.21: Comparison between analytical (solid line) and numerical (circles) solutions of the MB-FBsup test case. Clockwise from upper left subfigure: free surface η and bed level z_b, velocities u (red) and v (blue), Froude number $u/\sqrt{gh}$, equilibrium and transported concentrations φ, c.

10.2 Realistic application

For the simulation of realistic applications it is necessary to solve not only the homogeneous part of equation (8.5), but also the source term. The source term has been evaluated using a classical operator-splitting approach. The first step is to solve the homogeneous problem obtaining $\tilde{\mathbf{U}}_i^{n+1}$ at time $t = (n+1)\,\Delta t$. This solution is then used as initial value for the ordinary differential equation

$$\frac{d\mathbf{U}}{dt} = \mathbf{S} \tag{10.2}$$

This equation is solved using the implicit Euler method in order to have no integration time step restriction

$$\mathbf{U}_i^{n+1} = \tilde{\mathbf{U}}_i^{n+1} + \Delta t \mathbf{S}_i^{n+1} \tag{10.3}$$

The primitive variables $\mathbf{W}$ are then obtained solving the non liner system (10.3). More details can be found in Armanini *et al.* [10].

10.2.1 Trench evolution

As realistic test case we present the evolution of a trench dug in an channel with uniform flow in which, in the middle, there is a fixed bed transect. The model used is the one-dimensional CPDEs system for high sediment transport since the phenomena is 1D. For the bed shear stress we use the closure relation (3.85) with $Ks = 25\ m^{1/3}s^{-1}$, while for the concentration the relation is the same as before where $\beta = 2.31$. The initial uniform flow has the following properties: total discharge for unit width $q = 1.0\ m^2/s$, bed slope $i_f = 0.1\%$, solid concentration $c = \varphi = 0.02$. With these data we obtain $h = 2.275\ m$ and $u = 0.439\ m/s$. In this uniform flow, in the upper the mobile bed transect a trench is present. Since in the trench the water depth is higher and consequently the velocity is lower, the equilibrium concentration c, respect to the rest of the channel, is lower (see Figure 10.22).

We expect that the trench, during the flow, moves downstream, approaches the fixed bed transect and then, after some time, it reappears in the

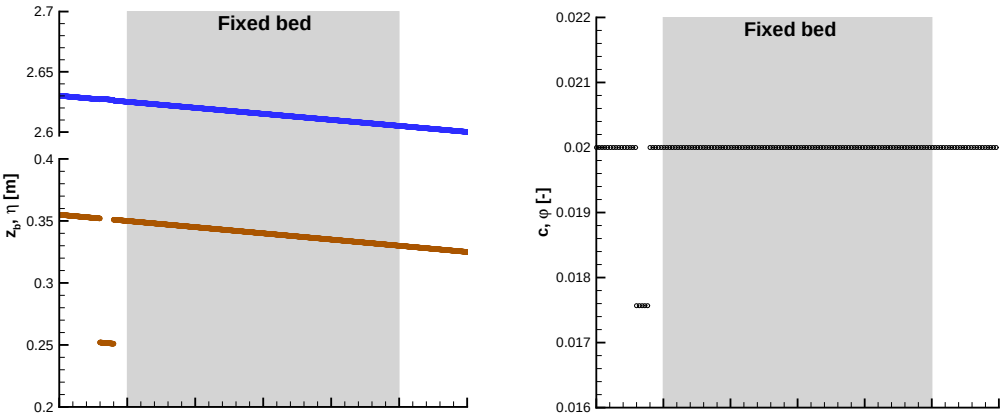

Figure 10.22: Initial condition of the trench. On the left the free surface and the bottom elevation, on the right the concentration.

downstream mobile bed transect. We highlight that, with the approach proposed by Rulot *et al.* [58] the trench, when approach the fixed bed transect, is instantaneously transfered in the downstream mobile bed, as depicted in Section 6.1, producing a wrong estimation of the evolution speed.

Looking at the Figures 10.23, 10.24 and 10.25, we notice that the model developed reproduces, in a correct way, what we expected. In particular 10.23 shows the trench approaching the fixed bed transect. then, in Figure 10.24, we highlight the presence of the lower concentration wave that is advected by the flow field in the fixed bed transect. When this wave approach the downstream mobile bed transect (Figure 10.25), it is as a boundary condition for the flow, so the local hydrodynamic changes in order to adapt to the solid concentration arriving from upstream. When the concentration wave is completely outside the fixed bed transect (Figure 10.26), the trench is fully recreated and then moves downstream. We highlight that the trench, moving downstream, changes its shape due to the bed shear stress and, as a consequence, also the equilibrium concentration changes according to it.

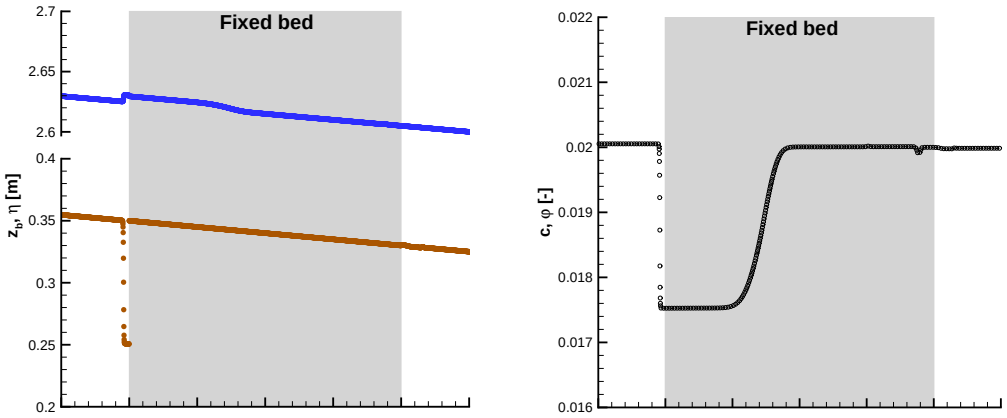

Figure 10.23: Evolution of a trench: approaching the fixed bed transect. On the left the free surface and the bottom elevation, on the right the concentration.

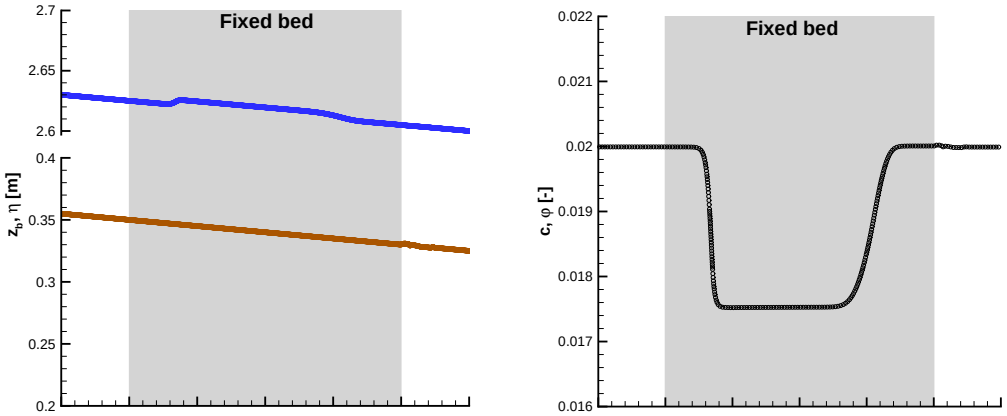

Figure 10.24: Evolution of a trench: inside the fixed bed transect. On the left the free surface and the bottom elevation, on the right the concentration.

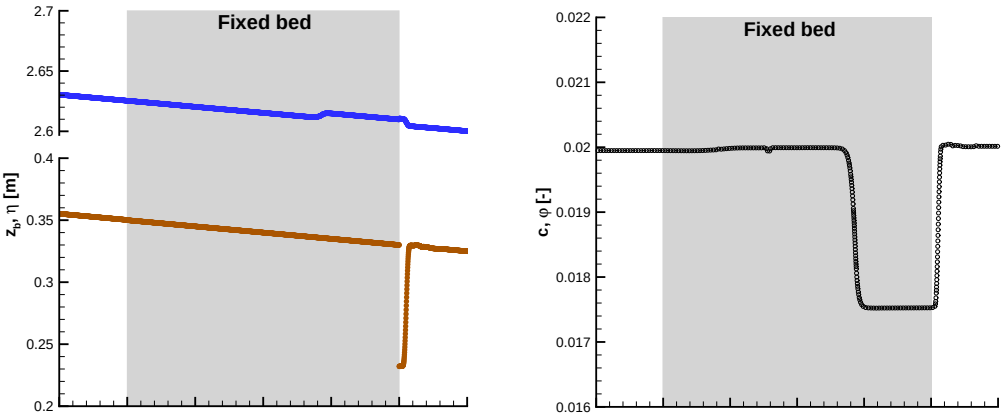

Figure 10.25: Evolution of a trench: approaching the downstream mobile bed transect. On the left the free surface and the bottom elevation, on the right the concentration.

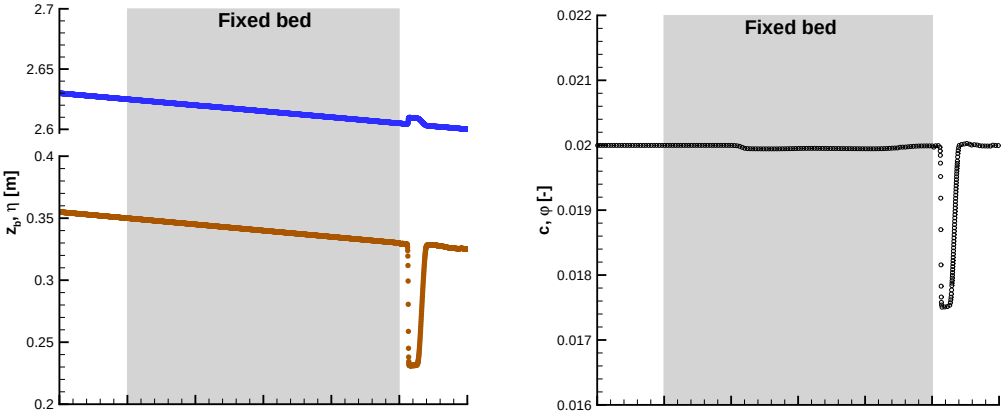

Figure 10.26: Evolution of a trench: trench moving in the downstream mobile bed transect. On the left the free surface and the bottom elevation, on the right the concentration.

Conclusions

In the first Part of the thesis, a review of the literature about of the three-dimensional continuum motion equations for the liquid-granular mixture flow was carried out. Then, after the introduction of the shallow flow hypothesis, the two-dimensional depth averaged fully two-phase free-surface shallow flow systems for high sediment concentration over fixed and mobile bed are derived. A particular attention was carried out in the depth average process where the presence of lots of corrective coefficients was highlighted. A brief literature review has been done comparing the models obtained with the ones presented in literature. The isokinetic two-dimensional models are also derived since, in the literature there are still not complete and reliable closure relations valid for debris flow or hyperconcentrated flow. Finally the one-dimensional isokinetic models both for low and high sediment concentration over fixed and mobile bed was obtained and their eigenstructure was analyzed.

In the second Part, the mathematical description of coupling two different hyperbolic systems is investigated. A general solution strategy, using the two-phase free-surface flows with low solid concentration, across a sharp transition in the bed conditions was developed by introducing the Composite Riemann Problem, a new type of RP in which not only the initial constant values of the variables but also the system of equations changes from left to right of a discontinuity. The possibility of solving a CRP was obtained by reducing the original problem to a classical RP associated with a single composite system, made up of a suitable weighted combination of the original fixed-bed and mobile-bed systems plus an additional differential equation for the weighting parameter, namely the erodibility function. Consistency of the

CPDEs system, i.e. reduction to the pure fixed-bed or to the pure mobile-bed system as a function of the erodibility value, was carefully checked. Moreover, the features of the CRP waves and solutions were analyzed in detail by using standard theoretical tools and a classification of the possible wave patterns was presented. The application of this coupling strategy was then applied to the high sediment concentration cases showing the versatility of method developed.

In the last Part of the thesis, three different Riemann solvers (LHLL, Closure Independent Generalized Roe and Universal Osher) were analyzed and improved. In particular the LHLL solver was modified in order to adapt it to the transition between fixed and mobile bed. An Extended Multiple Average strategy, an improvement of the MAs, was developed for the CIGR solver allowing to obtain in an easier way the Roe constant matrix satisfying the differential and integral condition. The UO solver was extended to the case of partially nonconservative hyperbolic systems where non-conservative fluxes are evaluated directly without a path integral. Also a new path integral strategy in primitive variables was introduced. The three numerical Riemann solver was tested and compared highlighting pros and cons of each. A second-order finite volume scheme was then developed, which was systematically validated by comparing the computed solutions with those obtained through an inverse procedure. As expected, when applied to problems that fall within the physical range of applicability of the relevant mathematical model, the numerical method has an overall high accuracy and it is exactly well-balanced across any discontinuous wave, in particular across the standing contact wave which describes the transition from mobile to fixed-bed conditions. Finally, a realistic test case regarding the evolution of a trench over partially non-erodible bed was presented, proving the capabilities of both the mathematical approach and the numerical scheme.

The future developments of the work presented in this thesis are firstly the implementation in a two dimensional numerical model of the CRP, secondly the possibility of considering dynamic fixed-mobile transitions and finally the extension of this approach to the fully two-phase models. In this way the barrier between mobile-bed and fixed-bed models may be broken down and

a single model may be applied in any bed condition.

Bibliography

[1] J. D. Abad, G. C. Buscaglia, and M. H. Garcia. 2D stream hydrodynamic, sediment transport and bed morphology model for engineering applications. *Hydrological Processes*, 22(10):1443–1459, 2008.

[2] F. Alcrudo and F. Benkhaldoun. Exact solutions to the Riemann problem of the shallow water equations with a bottom step. *Computers & Fluids*, 30(6):643–671, 2001.

[3] A. Ambroso, C. Chalons, F. Coquel, E. Godlewski, F. Lagoutière, P.-A. Raviart, and N. Seguin. Coupling of general Lagrangian systems. *Mathematics of Computation*, 77(262):909–941, 2008.

[4] A. Ambroso, J.-M. Hérard, and O. Hurisse. A method to couple HEM and HRM two-phase flow models. *Computers & Fluids*, 38(4):738 – 756, 2009.

[5] T. B. Anderson and R. Jackson. Fluid mechanical description of fluidized beds. Equations of motion. *Industrial & Engineering Chemistry Fundamentals*, 6(4):527–539, 1967.

[6] A. Armanini. *Principi di idraulica fluviale*. Editoriale Bios, second edition, 2005.

[7] A. Armanini. Granular flows driven by gravity. *Journal of Hydraulic Research*, 51(2):111–120, 2013.

[8] A. Armanini. Closure relations for mobile bed debris flows in a wide range of slopes and concentrations. *Advances in Water Resources*, In press, 2014.

[9] A. Armanini and G. Di Silvio. A one-dimensional model for the transport of a sediment mixture in non-equilibrium conditions. *Journal of Hydraulic Research*, 26(3):275–292, 1988.

[10] A. Armanini, L. Fraccarollo, and G. Rosatti. Two-dimensional simulation of debris flows in erodible channels. *Computers & Geosciences*, 35(5):993–1006, 2009.

[11] A. Armanini, M. Larcher, E. Nucci, and M. Dumbser. Submerged granular channel flows driven by gravity. *Advances in Water Resources*, 63:1–10, 2014.

[12] R. A. Bagnold. Experiments on a gravity-free dispersion of large solid spheres in a Newtonian fluid under shear. *Proceedings of the Royal Society of London A: Mathematical, Physical and Engineering Sciences*, 225(1160):49–63, 1954.

[13] F. Benkhaldoun, I. Elmahi, S. Sari, and M. Seaid. An unstructured finite-volume method for coupled models of suspended sediment and bed load transport in shallow-water flows. *International Journal for Numerical Methods in Fluids*, 72(9):967–993, 2013.

[14] B. Boutin, C. Chalons, and P.-A. Raviart. Existence result for the coupling problem of two scalar conservation laws with riemann initial data. *Mathematical Models and Methods in Applied Sciences*, 20(10):1859–1898, 2010.

[15] Z. Cao, G. Pender, and P. A. Carling. Shallow water hydrodynamic models for hyperconcentrated sediment-laden floods over erodible bed. *Advances in W*, 29(4):546–557, 2006.

[16] M. J. Castro Díaz, E. D. Fernández-Nieto, T. Morales de Luna, G. Narbona-Reina, and C. Parés. A HLLC scheme for nonconservative hyperbolic problems. Application to turbidity currents with sediment transport. *ESAIM: Mathematical Modelling and Numerical Analysis*, 47(1):1–32, 2013.

[17] S. Chapman and T. G. Cowling. *The mathematical theory of non-uniform gases: An account of the kinetic theory of viscosity, thermal conduction and diffusion in gases*. Cambridge Mathematical Library. Cambridge University Press, third edition, February 1991.

[18] F. Coquel. Coupling of nonlinear hyperbolic systems: A journey from mathematical to numerical issues. In E. Vázquez-Cendón, A. Hidalgo, P. García-Navarro, and L. Cea, editors, *Numerical Methods for Hyperbolic Equations: Theory and Applications*, pages 21–35. Taylor & Francis, 2013.

[19] L. Cozzolino, R. Della Morte, C. Covelli, G. Del Giudice, and D. Pianese. Numerical solution of the discontinuous-bottom Shallow-water Equations with hydrostatic pressure distribution at the step. *Advances in Water Resources*, 34(11):1413–1426, 2011.

[20] G. Dal Maso, P. G. LeFloch, and F. Murat. Definition and weak stability of nonconservative products. *Journal de Mathmatiques Pures et Appliquées*, 74(6):483–548, 1995.

[21] D. A. Drew. Mathematical modeling of two-phase flow. *Annual Review of Fluid Mechanics*, 15:261–291, 1983.

[22] B. M. Duc, T. Wenka, and W. Rodi. Numerical modeling of bed deformation in laboratory channels. *Journal of Hydraulic Engineering*, 130(9):894–904, 2004.

[23] M. Dumbser and E. F. Toro. On universal Osher type schemes for general nonlinear hyperbolic conservation laws. *Communications in Computational Physics*, 10(3):635–671, 2011.

[24] M. Dumbser and E. F. Toro. A simple extension of the Osher Riemann solver to non-conservative hyperbolic systems. *Journal of Scientific Computing*, 48(1-3):70–88, 2011.

[25] L. Fraccarollo and H. Capart. Riemann wave description of erosional dam-break flows. *Journal of Fluid Mechanics*, 406:183–228, 2002.

[26] L. Fraccarollo, H. Capart, and Y. Zech. A Godunov method for the computationof erosional shallow water transient. *International Journal for Numerical Methods in Fluids*, 41(9):951–976, 2003.

[27] G. Garegnani, G. Rosatti, and L. Bonaventura. On the range of validity of the Exner-based models for mobile-bed river flow simulations. *Journal of Hydraulic Research*, 51(4):380–391, 2013.

[28] E. Godlewski, K.-C. Le Thanh, and P.-A. Raviart. The numerical interface coupling of nonlinear hyperbolic systems of conservation laws: II. The case of systems. *ESAIM: Mathematical Modelling and Numerical Analysis*, 39(4):649–692, 2005.

[29] M. F. Göz and C.-D. Munz. Approximate Riemann solvers for fluid flow with material interfaces. In E. F. Toro and J. F. Clarke, editors, *Numerical Methods for Wave Propagation*, volume 47 of *Fluid Mechanics and Its Applications*, pages 211–235. Springer Netherlands, 1998.

[30] M. Greco, M. Iervolino, A. Leopardi, and A. Vacca. A two-phase model for fast geomorphic shallow flows. *International Journal of Sediment Research*, 27(4):409–425, 2012.

[31] A. Harten, P. D. Lax, and B. van Leer. On upstream differencing and Godunov-type schemes for hyperbolic conservation laws. *SIAM Review*, 25(1):35–61, 1983.

[32] D. P. Hill. *The computer simulation of dispersed two-phase flows*. PhD thesis, Imperial College of Science, Technology and Medicine. Department of Mechanical Engineering, London, UK, July 1998.

[33] J. D. Hudson and P. K. Sweby. Formulations for numerically approximating hyperbolic systems governing sediment transport. *Journal of Scientific Computing*, 19(1-3):225–252, 2003.

[34] R. M. Iverson. The physics of debris flows. *Reviews of Geophysics*, 35(3):245296, 1997.

[35] R. Jackson. Locally averaged equations of motion for a mixture of identical spherical particles and a newtonian fluid. *Chemical Engineering Science*, 52(15):2457–2469, 1997.

[36] R. Jackson. *The dynamics of fluidized particles*. Cambridge monographs on mechanics. Cambridge University Press, 2000.

[37] J. T. Jenkins and S. B. Savage. A theory for the rapid flow of identical, smooth, nearly elastic, spherical particles. *Journal of Fluid Mechanics*, 130:187–202, 1983.

[38] D. D. Joseph and T. S. Lundgren. Ensemble averaged and mixture theory equations for incompressible fluid-particle suspensions. *International Journal of Multiphase Flow*, 16(1):35–42, 1990.

[39] A. A. Kassem and M. H. Chaudhry. Numerical modeling of bed evolution in channel bends. *Journal of Hydraulic Engineering*, 128(5):507–514, 2002.

[40] M. Larcher, L. Fraccarollo, A. Armanini, and H. Capart. Set of measurement data from flume experiments on steady uniform debris flows. *Journal of Hydraulic Research*, 45(Supplement 1):59–71, 2007.

[41] A. Y. Le Roux. Discrétisation des termes sources raides dans les problemes hyperboliques. In *Systemes hyperboliques: Nouveaux schémas et nouvelles applications*. Ecoles CEA-EDF-INRIA problemes non lineaires appliqués, INRIA Rocquencourt (France), 1996.

[42] P. G. LeFloch and M. D. Thanh. The Riemann problem for the shallow water equations with discontinuous topography. *Communications in Mathematical Sciences*, 5(4):865–885, 2007.

[43] R. J. LeVeque. *Numerical methods for conservation laws*. Lectures in Mathematics. ETH Zürich. Birkhauser, second edition, 1992.

[44] H. Li and X. Cai. Some characteristics of debris flow in mountain areas of Western China. In *Internationales Symposion INTERPRAEVENT 1988 - GRAZ*, 1988.

[45] M. Marchioro, M. A. Tanksley, and A. Prosperetti. Mixture pressure and stress in disperse two-phase flow. *International Journal of Multiphase Flow*, 25(6-7):1395–1429, 1999.

[46] P. H. Morris and D. J. Williams. Relative celerities of mobile bed flows with finite solids concentrations. *Journal of Hydraulic Engineering*, 122(6):311–315, 1996.

[47] J. M. Murillo and P. García-Navarro. An Exner-based coupled model for two-dimensional transient flow over erodible bed. *Journal of Computational Physics*, 229(23):8704–8732, 2010.

[48] S. Osher and F. Solomon. Upwind difference schemes for hyperbolic system of conservation laws. *Mathematics of Computation*, 38(158):339–374, 1982.

[49] E. B. Pitman and L. Le. A two-fluid model for avalanche and debris flows. *Philosophical Transactions of the Royal Society A*, 363(1832):1573–1601, 2005.

[50] F. Reif. *Fundamentals of statistical and thermal physics*. McGraw-Hill Higher Education, June 1965.

[51] G. Rosatti and L. Begnudelli. The Riemann problem for the one-dimensional, free-surface shallow water equations with a bed step: Theoretical analysis and numerical simulations. *Journal of Computational Physics*, 229(3):760–787, 2010.

[52] G. Rosatti and L. Begnudelli. A closure-independent Generalized Roe solver for free-surface, two-phase flows over mobile bed. *Journal of Computational Physics*, 25:362–383, 2013.

[53] G. Rosatti and L. Begnudelli. Two-dimensional simulation of debris flows over mobile bed: enhancing the TRENT2D model by using a well-balanced generalized Roe-type solver. *Computers & Fluids*, 71:179–195, 2013.

[54] G. Rosatti and L. Fraccarollo. A well-balanced approach for flows over mobile-bed with high sediment-transport. *Journal of Computational Physics*, 220(1):312–338, 2006.

[55] G. Rosatti, J. M. Murillo, and L. Fraccarollo. Generalized Roe schemes for 1D two-phase, free-surface flows over a mobile bed. *Journal of Computational Physics*, 227(24):10058–10077, 2006.

[56] G. Rosatti, N. Zorzi, L. Begnudelli, and A. Armanini. Evaluation of the TRENT2D model capabilities to reproduce and forecast debris-flow deposition patterns through a back analysis of a real event. In *Engineering Geology for Society and Territory - Volume 2*, pages 1629–1633. Springer International Publishing, 2015.

[57] G. Rosatti and D. Zugliani. Modelling the transition between fixed and mobile bed conditions in two-phase free-surface flows: The Composite Riemann Problem and its numerical solution. *Journal of Computational Physics*, 285:Journal of Computational Physics, 2015.

[58] F. Rulot, B. J. Dewals, S. Erpicum, P. Archambeau, and M. Pirotton. Modelling sediment transport over partially non-erodible bottoms. *International Journal for Numerical Methods in Fluids*, 70(2):186–199, 2012.

[59] S. B. Savage. The mechanics of rapid granular flows. *Advances in Applied Mechanics*, 24:289–366, 1984.

[60] L. M. Stancanelli, G. Rosatti, L. Begnudelli, A. Armanini, and E. Foti. Single or two-phase modelling of debris-flow? A systematic comparison of the two approaches applied to a real debris flow in Giampilieri village (Italy). In *Landslice Science and Practice, Second World Landslide Forum Putting Science into Practice* , volume 3, pages 277–283. Springer, 2013.

[61] N. Struiksma. Mathematical modelling of bedload transport over non-erodible layers. In *1st IAHR symposium on River, Coastal and Estuarine Morphodynamics (RCEM)*, volume 1, pages 89–98, 1999.

[62] T. Takahashi. Mechanical characteristics of debris flow. *Journal of the Hydraulics Division*, 104(8):1153–1169, 1978.

[63] P. A. Tassi, S. Rhebergen, C. A. Vionnet, and O. Bokhove. A discontinuous Galerkin finite element model for river bed evolution under shallow flows. *Computer Methods in Applied Mechanics and Engineering*, 197(33-40):2930–2947, 2008.

[64] E. F. Toro. *Riemann solvers and numerical methods for fluid dynamics: A practical introduction*. Springer, third edition, 2009.

[65] C. Truesdell. *Rational thermodynamics*. Springer-Verlag, 2nd edition edition, 1984.

[66] W. Wu. *Computational River Dynamics*. Taylor & Francis, 2007.

[67] D. Z. Zhang and A. Prosperetti. Averaged equations for inviscid disperse two-phase flow. *Journal of Fluid Mechanics*, 267:185–219, 1994.

[68] D. Z. Zhang and A. Prosperetti. Momentum and energy equations for disperse two-phase flows and their closure for dilute suspensions. *International Journal of Multiphase Flow*, 23(3):425–453, 1997.

[69] N. Zorzi, L. Begnudelli, and G. Rosatti. Reconstruction of Val Molinara 2010 debris flow and validation of the hazard mapping methodology. In *European Geosciences Union General Assembly 2013*, 2013.